Spring August 2014

VISUALIZING AND CONTROLLING CHARGE TRANSPORT IN CONJUGATED POLYMER NETWORKS AND FILMS

Andrew Davis
University of Massachusetts - Amherst

VISUALIZING AND CONTROLLING CHARGE TRANSPORT IN CONJUGATED POLYMER NETWORKS AND FILMS

A Dissertation Presented

by

ANDREW R. DAVIS

Submitted to the Graduate School of the
University of Massachusetts Amherst in partial fulfillment
of the requirements for the degree of

DOCTOR OF PHILOSOPHY

May 2014

Polymer Science and Engineering

VISUALIZING AND CONTROLLING CHARGE TRANSPORT IN CONJUGATED POLYMER NETWORKS AND FILMS

A Dissertation Presented

by

ANDREW R. DAVIS

Approved as to style and content by:

_____
Kenneth R. Carter, Chair

_____
James J. Watkins, Member

_____
Paul M. Lahti, Member

_____
David A Hoagland, Department Head
Polymer Science and Engineering

DEDICATION

To my loving family

ACKNOWLEDGMENTS

I would first and foremost like to thank Professor Ken Carter for being a mentor and guiding me through my graduate school career. Without him, I'm certain the journey would have been immeasurably more difficult and frustrating. I am extremely grateful for all the scientific insight he has provided in Conte and the connections he has helped me make during conferences and travel. Ken's trust in me as a student, and the freedom he provided me in my academic pursuits, were immeasurably valuable. Whether I was proposing a collaboration on a wild new project or asking for some time to pursue popular science writing, Ken always let me steer my own ship and never discouraged me.

I would also like to thank my other committee members Professors Jim Watkins and Paul Lahti for providing valuable input on my work during my time in Polymer Science. Jim always kept me grounded in the practical aspects and feasible applications of what was at times very fundamental blue-skies research. Paul's experience with similar research topics as my own ran both wide and deep, and his expertise was invaluable. Paul's inspiration is clearly evident in Chapter 5 of this dissertation which overlaps strongly with his ongoing work (look for the citations!).

Professors Janice Hudgings and Kathy Aidala of Mt. Holyoke College, along with their students Lorelle, Achyut, Amy, Pawana, and Morgen, are particularly deserving of thanks. A random, one-off joint experiment turned into a very exciting and successful two year collaboration which I am very sad to be leaving behind. Their trust in continuing with a project that didn't always have a light at the end of tunnel was greatly appreciated. I'd like to thank all of them for many hours of wrestling with difficult ideas and experiments that none of us understood when we started and for supporting truly interdisciplinary research.

The members of the Carter Group, both past and present, have been fantastic companions during my years in Massachusetts: Damla, Burcin, Janet, Joe, Nick, Sam, Mikhail, Yinyong, Jaewon, Jared, Soeun, Yiliang, Kara, Isaac, Jacob, Jin, Fatma, and Charlotte. Joe and Janet in particular are still having strong effects on me years after their departures. Janet's no-nonsense approach to lab work and Joe's methods of exploring scientific ideas shaped who I am at the bench, and I greatly enjoyed our friendship outside of Conte. I cannot think of anyone better to have had as lab-mates for my formative years in the Carter Group. Jared and Mikhail deserve special mention as well. Mikhail's dedication, Jared's humor, and both of their scientific abilities have been sources of inspiration and encouragement during my time with them. I cannot wait to hear about their undoubted future successes.

I'd like to thank all of my teachers along the way who have fostered a love of science, especially the professors of the Polymer Science and Engineering department. It's because of them that I will always be proud of my PSE degree. Professors Al Crosby, who supported me as a wide-eyed summer student, and Bryan Coughlin, who has had any number of encouraging conversations with me, deserve special thanks for their support, as does Greg Dabkowski for passing on his love of outreach. I am also deep in debt to the staff of this department for enabling it (and me) to run so reliably and efficiently. Lisa Groth has been invaluable as a resource and a friendly face every day, cutting through bureaucracy and red tape so easily and dependably and making my time here that much simpler and more enjoyable.

A range of Amherst friends deserve deep thanks as well, starting with my fellow classmates of 2009. The adventures of classes, cumulative exams, and trying to eat all the department pizza provided to us is not a journey undertaken lightly, and I'm glad to have taken it with them. Cathy, Travis, Katie, Ray, and Isaac have earned themselves specific and eternal

shout outs for their friendships. There will always be a movie, board game, and glass of something strong waiting for them wherever I am.

An enormous thank you to my parents and brother for being supportive of my science habit throughout my life as it has pulled me farther and farther from home. Without their love and support, I would not be who I am today. A sheynem hartsiken dank, from the newest family doctor.

And finally, the deepest unending thanks to Neith. Her support, humor, and love have sustained me whether from 300 miles away in Ithaca or from across the breakfast table. I could not have made it this far without her. Her presence throughout years of classes, research, and travel has been a lasting and comforting one, and she gives me the strength to do anything.

ABSTRACT

VISUALIZAING AND CONTROLLING CHARGE TRANSPORT IN CONJUGATED POLYMER NETWORKS AND FILMS

MAY 2014

ANDREW R. DAVIS,

B.S., UNIVERSITY OF VIRGINIA

M.S., UNIVERSITY OF MASSACHUSETTS AMHERST

Ph.D., UNIVERSITY OF MASSACHUSETTS AMHERST

Directed by: Professor Kenneth R. Carter

The desire for more commercially feasible flexible electronic plastics has led to the development of increasingly complex conjugated polymer architectures and device geometries. Through these efforts, tremendous advances have been made in the design and performance of electronic devices fabricated with solution-processable semiconducting polymers. However, none of these materials have yet reached commercial maturity, so the opportunity for their further exploration from both a fundamental science and an application-driven point of view motivates this dissertation.

Chapter 1 presents a background introduction to many of the concepts, ideas, and existing research necessary to set the context of this dissertation's work. The first component of this work (Chapters 2-6) investigates thiol-ene cross-linked conjugated polymer networks. By installing vinyl functionalities in poly(fluorene) molecules at chain ends (Chapters 2 and 3) and along the polymer backbone (Chapters 4 and 5), the polymers can be rapidly and efficiently cross-linked by photo-reaction with thiol cross-linkers into highly tunable semiconducting polymer networks. It is shown that the thiol-ene cross-linking reaction allows for a new molecular handle on modifying interchain electronic communication via network density, which

is visualized using characteristic and unambiguous photoemission from low-energy fluorenone species. Light emitting diodes fabricated using these networks as an emissive layer show enhanced color stability compared to as-spun counterparts, and the robustness of the networks allows for solution processing of multiple stratified emissive layers for controlling color emission. Furthermore, the highly efficient thiol-ene cross-linking reaction is shown to work as an effective means for grafting poly(fluorene)s onto functionalized surfaces.

This work's second component in Chapter 7 details the direct visualization of charge carrier density in polymeric thin film transistors using Modulation-Amplified Reflectance Spectroscopy (MARS) measurements. Owing to the unique changes in optical behavior following the formation of a charged state within the conjugated polymer film, optical spectroscopy coupled to a CCD camera offers a powerful visualization tool for observing and mapping charges across large areas as they interact with electrodes, defects, and film morphologies in active devices. The MARS technique illuminates the spatial distribution of carriers in electronic polymer films, allowing direct spatial visualization of charge density and film defects.

Finally, a brief concluding comment on this work and an outlook for the field in general is presented in Chapter 8.

TABLE OF CONTENTS

Page

LIST OF TABLES

LIST OF FIGURES

LIST OF EQUATIONS

CHAPTER 1

CONJUGATED POLYMERS AND CHARGE TRANSPORT IN ORGANIC MOLECULES

The overall inspiration and goal of the research presented here is to take advantage of the inherent polymeric nature of conjugated polymers to enable new ways of thinking about, using, and designing conjugated polymers for fundamental research and applied uses. More specifically, this dissertation is focused on using discrete, controllable molecular architectures to investigate how molecular connectivity in conjugated polymer thin films and networks affects their semiconducting properties. At the time of writing, those issues have not been the topic of any systemic investigations with conjugated polymers despite being a unique property and variable inherent to covalently bound polymer semiconductors in contrast to their inorganic counterparts. Both interchain connectivity within networks as well as surface-binding connectivity in grafted systems will be discussed. Additionally, the optical changes characteristic of electronic charges and excited states in a semiconducting polymers will be leveraged to visualize electronic phenomena in these molecules.

A general introduction is presented in this chapter to give a brief overview of the context and background for some of the concepts necessary to understand the work presented in this dissertation. Each chapter additionally contains a more specific introduction for those particular topics.

1.1 Introduction to Conjugated Polymers

Semiconductivity was strictly the domain of metals and inorganic materials for effectively half a century following the invention of the transistor at Bell Labs in the early 20th century.(*1*) However, by the end of the century, a new class of materials was proven to possess semiconducting and current-carrying capabilities: conjugated organic molecules. While arguably

known since the late 1800s with the electropolymerization of aniline into an ill-defined insoluble blue powder which was likely polyaniline,(*2*) the promise of conjugated polymers as wholly new semiconducting materials was cemented by the awarding of the 2000 Nobel Prize in Chemistry to Alan Heeger, Alan MacDiarmid, and Hideki Shirakawa for their work on conjugated polacetylenes in 1970s.(*3-6*) The number of publications on conjugated polymers, now numbering over 2000 new publication annually, has steadily increased every year since their award, and major electronics companies have begun pursuing the commercialization of organic electronic devices, displays, and solar cells with over 3000 organizations in 2013 pursuing organic electronics.(*7*)

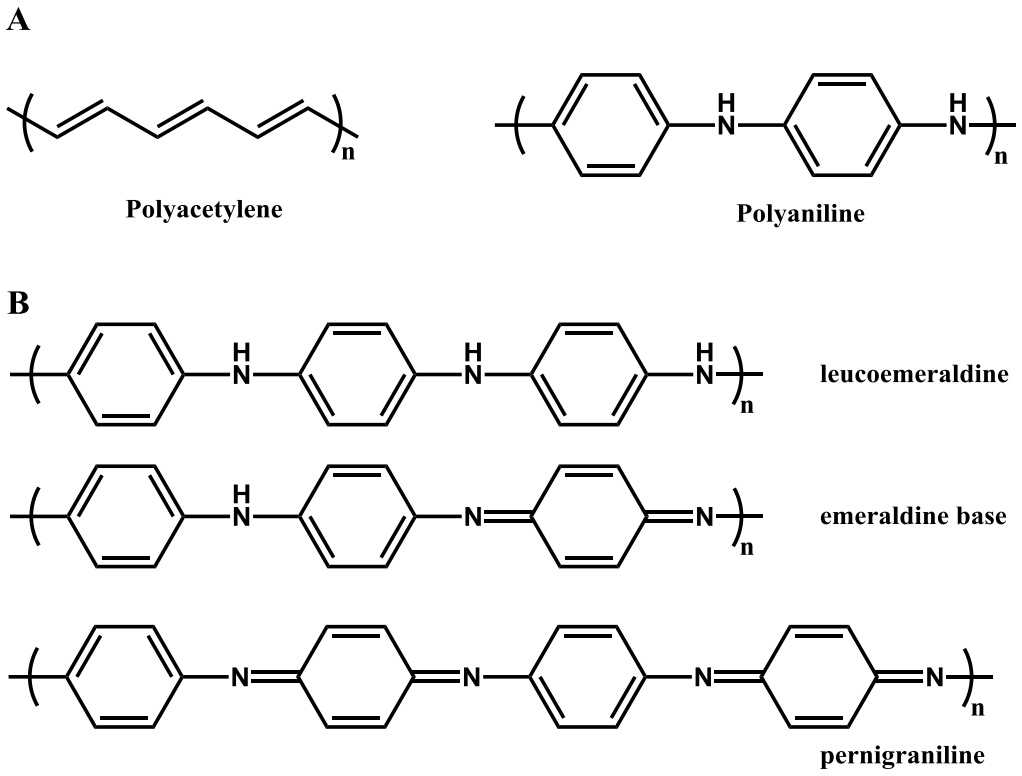

Figure 1.1: (A) Example of historically important conjugated polymers polyacetylene and polyaniline. (B) Structures of polyaniline in variously doped forms.

The polymers mentioned above – polyacetylene and polyaniline – are shown in Figure 1.1 as structures typical of conjugated polymers. The basic working principle of conjugated

polymers as semiconducting materials is the delocalization of electronic charge through the covalently bonded polymer backbone, which is in marked contrast to the band-theory of inorganic semiconductors.(*8, 9*) This delocalization is most commonly accomplished through alternating saturated and unsaturated carbon-carbon bonds which leads to extended, overlapping π-orbitals, however a number of additional motifs involving heteroatoms and non-covalent interactions (e.g., coordination of organic molecules with metallic species) have been similarly explored.(*10*) Despite not adhering to the traditional band model of semiconductivity, hole transport in conjugated polymers is often described as occurring through the "valence band"-like highest occupied molecular orbital (HOMO) energy levels, while electrons are transported through the "conduction band"-like lowest unoccupied molecular orbital (LUMO) energy levels.

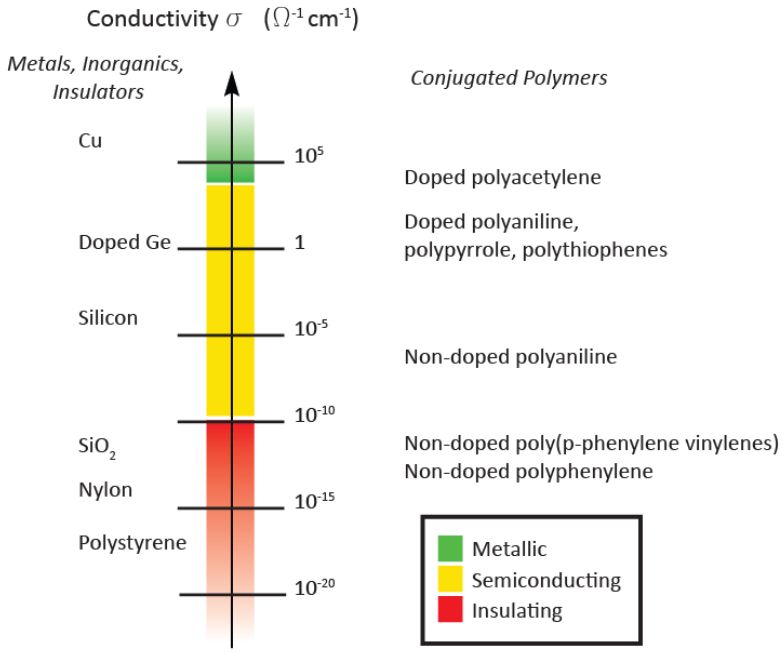

Figure 1.2: Rough comparison of the conductivities of conjugated polymers with conventional conductors, semiconductors, and insulators. Adapted with permission from Moliton and Hiorns, *Polym. Int.*, 53, 1397-1412 (2004). Copyright 2004 Society of Chemical Industry.(*8*)

Figure 1.2 shows a selection of approximate conductivities for typical electronic and insulating systems. Like inorganic semiconductors, conjugated polymers can be chemically

doped to achieve a wide range of conductivity and energy levels. By far polyaniline, first identified and described in the 1980s by the research group of MacDiarmid from the Nobel-winning trio, remains the most common example of this behavior. Through acidic doping of the conjugated backbone, semiconducting polyaniline can be reversibly converted to a more conductive form, illustrated in Figure 1.1B.(*11*) Colloquially referred to as the leucoemeraldine and emeraldine base forms of polyaniline, respectively, the chemical changes associated with this doping can be more broadly defined as the conversion between non-degenerative benzoid and quinoid bonding arrangements. These two states are further discussed in Sections 1.6 and 1.7, but it is worthwhile here to note that similar conversions have been observed in a range of conjugated polymers other than polyaniline, including polythiophenes and polypyrroles.(*8*)

1.2 Device Applications of Conjugated Polymers

The semiconducting nature of conjugated polymers allows for their use in any conventional semiconducting application with few exceptions.(*8*) Some conjugated polymer and organic small molecules have seen limited commercialization, and widespread development of cheap, flexible polymer electronics is an attractive goal. But even without widespread commercialization, many of these devices serve important roles in advancing the fundamental understanding of how optoelectronic phenomena behave in these materials in varying electronic architectures.

Polymer light emitting diodes (PLEDs) and photovoltaics (PVs) both rely on a vertical stack of thin organic films sandwiched between two electrodes, where one is generally a low work function metal (e.g. Ca or Al) and the other is a transparent conductive electrode (e.g. indium tin oxide) to allow for light to transmit in or out of the device. In a simplistic view, PLEDs and PVs operate via similar but opposite charge transport modes under an applied voltage. In

PLEDs holes and electrons are injected from each electrode which then meet, recombine as excitons, and relax via emission of light. In PVs incident light induces the formation of an exciton, which then dissociates into holes and electrons that are extracted by each electrode. In both cases, one or more semiconducting organic layers are vertically sandwiched between the two electrodes.

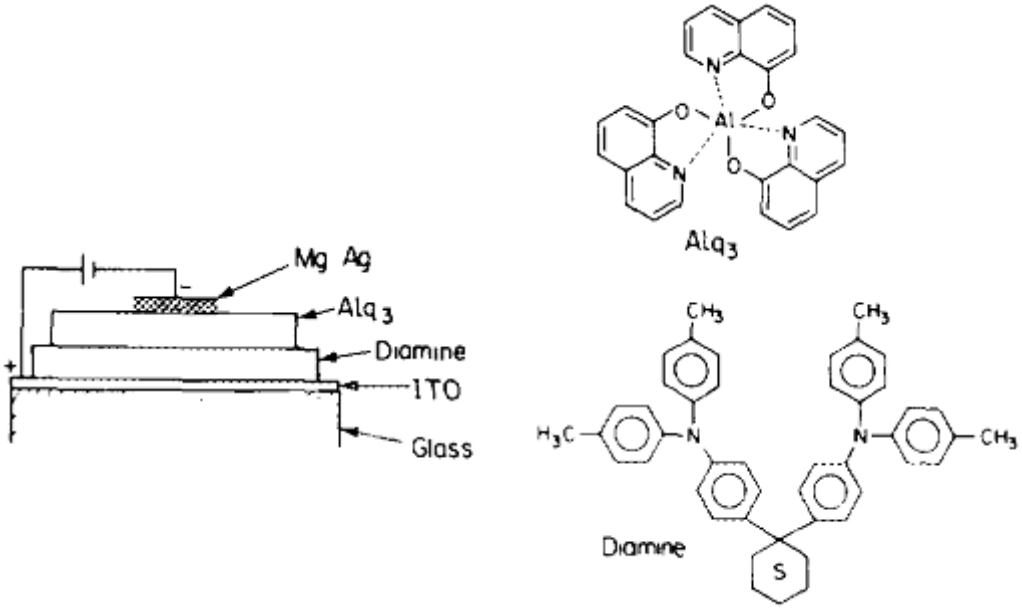

Figure 1.3: Typical multilayer structure for organic and polymeric light emitting diodes. Reprinted with permission from Tang and VanSlyke, *Appl. Phys. Lett.*, 51, 913-915 (1987). Copyright 1987, AIP Publishing LLC.(*12*)

For organic LEDs (including polymers), while electroluminescent behavior was known nearly since the discovery of organic semiconductors, the critical work of Tang and VanSlyke introduced multiple organic layers which pushed unrealistic operating conditions (driving voltages in excess of 100V) to much more reasonable values with orders of magnitude improvements in brightness and efficiency.(*12*) The design of hole/electron transport and blocking layers, shown in Figure 1.3, led to orders of magnitude improvements in brightness and luminous efficiency. These layers serve to transport their respective charges, funneling them into the emissive layer where subsequent charge blocking layers ensure holes and electrons

recombine and emit light in the desired luminescent layer. Both PLEDs and polymeric PVs benefit from multiple layers dedicated to specific electronic tasks. In PVs, similar layers lead to significant improvements in the extraction of charges. In PVs, there is often an additional desire for interdigitation-like contact between dedicated hole and electron transporting layers on the order of the photo-generated exciton diffusion length (generally on the order of 10 nm) to increase the interfacial area between those layers, thus extracting more current.(*13*)

Conjugated polymers can also serve as the active semiconducting layer in thin film transistors (TFT), identical in operation to their inorganic TFT counterparts.(*10, 13*) In these devices, illustrated in Figure 1.4, a thin semiconducting organic layer is deposited on a dielectric-coated conductive gate electrode. Application of a voltage to the gate electrode (V_G) induces capacitor-like charges to form along a thin sheet at the interface between the semiconducting polymer film and dielectric insulator. Source and drain electrodes in contact with the organic semiconductor layer can then be biased with a drain voltage V_D to drive current through the device. Thus the gate voltage acts as a switch to amplify (or turn off) current and charge flow between the source and drain electrodes.

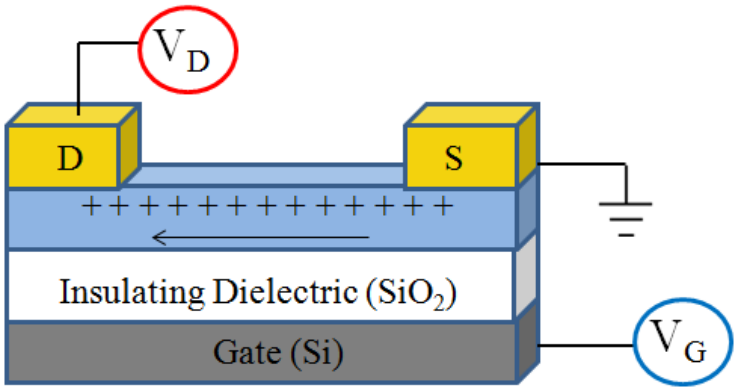

Figure 1.4: Schematic illustration of a thin film transistor, with semiconducting polymer layer shown in blue.

These two device architectures – the vertical stack of PLEDs and PVs and the horizontal transport of TFTs – will be important in the following chapters of this work. However, an even

wider range of device applications exist for conjugated polymers, including electrochromic devices, fluorescent and electronic sensors, organic lasers, and thermoelectric materials.(*14*)

The above examples of devices and applications for CPs make their versatility clear. However, as of 2014, strikingly few of these polymeric devices have been successfully commercialized. The reasons for this are simple: performance and reliability. The underlying challenges are numerous, charge mobility in conjugated polymers approaches that of amorphous silicon in only the extreme best cases, and mobilities are more commonly orders of magnitude lower than in silicon.(*13*) Positively charged holes are generally more stable than electrons due to deeper, redox-resistant energy levels of the highest occupied molecular orbital (where they reside) as well as by typical organic chemistry arguments of carbocation versus carbanion stability on hydrocarbon scaffolds.(*16*) This significantly limits device architectures (particularly those relying on p-n junctions or electron transport). Furthermore, the environmental stability and longevity of these materials is historically unreliable. For LEDs, a minimum of 10,000 hours of operation is typically required. In the case of PVs, the industry standard is 25 years of operation is required. While some polymers show adequate lifetime, many of the best performing polymers begin to lose their properties within minutes of operation. The contrasting success of inorganic semiconductor devices, which superficially operate in an identical manner, is an obvious indication that problems remain to be solved for electronic polymer devices. Understanding and controlling these effects is one overarching goal of this dissertation.

1.3 Effects of Morphology and Polymer Architecture on Electronic Properties

Despite their weaknesses, conjugated polymers offer a remarkable advantage over inorganic semiconductors: solution processibility. A conjugated polymer backbone is generally

insoluble on its own, but non-conjugated side-chains can easily be incorporated as solubilizing components. Throughout many years of study, a nearly inexhaustible range of side-chains have been investigated, from alkyl to hydrophilic to zwitterionic, with structures ranging from linear to branched to cyclic to dendritic. This has allowed for CP processing from polar, non-polar, organic, aqueous, and orthogonal solvents as desired.(*13, 17-20*)

One reason so many solubilizing side-chains have been studied is their dramatic effect on solid state morphology and charge transport. A quintessential example is the hexyl side-chain of poly(3-hexylthiophene) (P3HT). P3HT has become a benchmark material in polymer-based TFTs and PVs with its easily characterized semi-crystalline nature and relatively high hole mobility. Numerous studies have examined the role of side chains other than the hexyl group on poly(thiophene)s by varying the alkyl length, branching, and regularity.(*21-23*) Perhaps unintuitively, shorter linear alkyl side-chains have occasionally been reported to result in worse electronic performance despite presumably denser chain packing and interaction. With the same conjugated poly(thiophene) backbone, varying the side-chain architecture can demonstrably affect UV-vis absorption,(*21*) carrier mobility,(*24*) and even the HOMO and LUMO energy levels.(*22*) The hexyl group is often reported to provide the most marked performance improvements in alkylated poly(thiophene)s, such that P3HT remains the benchmark poly(thiophene) system, but it is not at all challenging to find conflicting reports about which side-chain configurations perform the best in identical devices. (*21, 25*) Poly(thiophene) is mentioned here due to its popularity in the literature, but these general concerns have been observed in effectively all conjugated polymers in which solubilizing side-chains are employed, such as in poly(fluorene)s which are particularly relevant to this dissertation.(*26*)

With conflicting performance reports, it follows that processing conditions themselves can also affect the morphology and performance of chemically identical polymers. A wide range

of processing conditions all have influence on the final conjugated polymer morphology and device performance: processing solvent, polymer concentration, thermal annealing, vapor annealing, etc. (*27-33*) A few examples from widely extensive literature illustrate how organic solar cells fabricated from identical conjugated materials performed with over double the efficiency when spin-coated from dichlorobenzene at short vs. long coating times,(*30*) and the π-π* transition energy in thin films of alkoxy-functionalized poly(phenylene vinylene) dramatically increased when processed from a high vapor pressure solvent compared to one with low vapor pressure.(*28*) Understanding processing conditions is clearly a critical concern when designing conjugated polymer-based application.

1.4 Cross-Linking Conjugated Polymer Thin Films

A particular draw of conjugated polymers is their solution processibility; however, the advantage of solubility is simultaneously a disadvantage. As described in section 1.2, the most efficient semiconducting devices are designed with multiple stacked layers, such as dedicated hole transport, electron transport, and emissive layers in PLEDs. In these designs, fully solution-processed devices require orthogonal solvents for the deposition of each layer in order to prevent disruption of any previously coated films. Realistically, this constraint allows for only two or maybe three layers, and even then specially designed and synthesized polymers are necessary to achieve orthogonal solubilities.

Cross-linking has been one approach to solve the difficulties of solution processing multiple layers of fully soluble materials. By using soluble cross-linkable polymers, a thin semiconducting polymer film can be deposited from solution, cross-linked to an insoluble state, and then subsequent films can be processed from the same initial solvent. Researchers have

studied both thermal curing and photo curing routes to achieve robust cross-linked conjugated polymer films.(*34-41*)

In addition to their solvent-processing benefits, cross-linked conjugated polymer films offer some control over undesirable changes in morphology over time which can lead to degraded performance. An early example particularly relevant to the work in following chapters was reported by Klärner and co-workers.(*35*) In their work, cross-linked poly(fluorene) demonstrated superb color stability compared to an un-cross-linked counterpart which was shown to evolve an undesirable low-energy green photoemission following annealing. This control over morphological and optoelectronic stability is elaborated further in Chapter 2, as are previously explored thermal and photo-initiated cross-linking routes.

Curiously, no studies to date examine correlations between network connectivity and charge transport in cross-linked conjugated polymers achieved by any chemistry. As discussed in Section 1.3, similar aspects of molecular architecture and processing are known to have significant effects on the optoelectronic properties of conjugated polymers. Thus, one goal of this dissertation is to explore the relationships of architecture and performance in cross-linked systems using the highly efficient and selective thiol-ene reaction.

1.5 Thiol-Ene Cross-Linking for Network Formation

Thiol-ene and thiol-yne chemistry, in which a thiol reacts with an unsaturated carbon-carbon bond to form a new thio-ether bond, have been known in some form since 1905.(*42*) In the subsequent century, thiol-ene chemistry has been applied to biological systems and hydrogels, drug design, three-dimensional photolithography, particle ligand and surface modification, fabrication of high glass transition temperature and low stress networks, and functionalization of countless polymers.(*43-46*)

This wide range of applied chemistry is in no small part due to the remarkable ease, efficiency, and selectivity of the thiol-ene reaction. In recent years, these properties have earned the reaction a seat at the table with similar vaunted reactions termed “click chemistry”. Particularly noteworthy is the photo-initiated thiol-ene click reaction. In this reaction, exposure to UV radiation (particularly low wavelength 254 nm emission) initiates the thiol-ene reaction by homolytic cleavage of the S-H bond to form a thiyl radical which then adds to an unsaturated carbon-carbon bond via radical chemistry.(*47*) Thiol-ene reactions can thus be accomplished without the need of a dedicated photo initiator. Furthermore, the reaction mechanism is known to proceed even in the presence of oxygen, leading to particularly facile reaction without the need for rigorous atmospheric control.(*45*)

A general reaction scheme for the radical thiol-ene reaction is illustrated in Figure 1.5. In this reaction, photo generation of the thiyl radical (either by self-initiation or by reaction with an added photoinitiator) proceeds to form a new thio-ether bond by selectively reacting with an unsaturated carbon-carbon bond. This carbon-carbon bond can either by internal or terminal in the reacting “ene”. The resulting carbon-centered radical on the newly formed species extracts a proton from a free thiol, and the cycle begins anew.

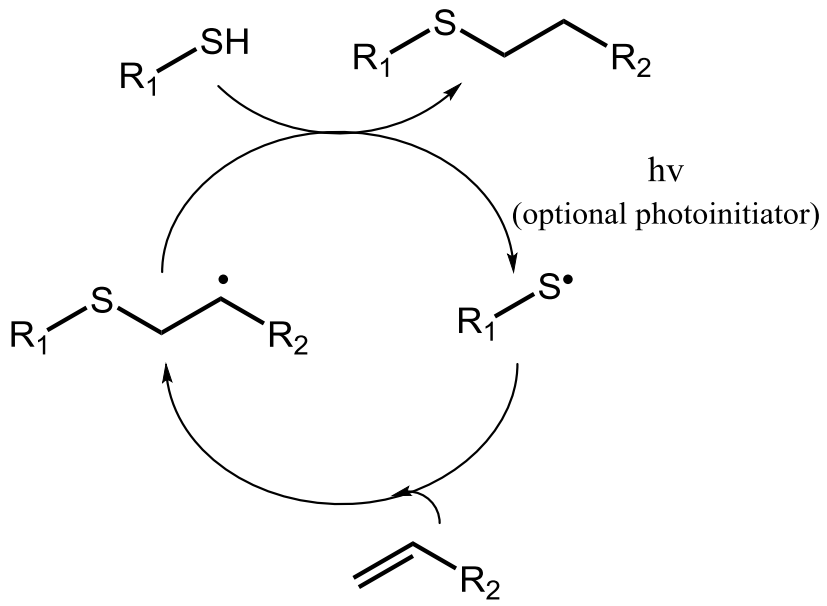

Figure 1.5: Reaction cycle for photoinitiated radical thiol-ene click reaction.

A number of studies have investigated the effects of varying monomer structure, functionality, and the thiol to "ene" ratio on the reactivity and final properties of thiol-ene cross-linked networks.(*45, 48, 49*) The structure of the unsaturated ene is most commonly varied due to synthetic convenience, and a broad summary of these results are shown in Figure 1.6. Generally fewer reports exist regarding variable thiol structure on curing and network properties. However, in general alkyl thiols are more reactive than thiol acetates which are in turn more reactive than aromatic thiols.(*46*) This owes to the relative stability of the electrophilic thiyl radical. The general trends for the reactivity of enes is intuitive given the radical reaction illustrated in Figure 1.5 and the electrophilic nature of the thiyl radical: electron donating groups increase reactivity while electron withdrawing groups decreases reactivity. Also intuitively, higher functionality enes (hence denser networks) on cyclic or tethered architectures yield more rigid networks with higher glass transition temperatures and larger elastic modulii than lower functionality, linear enes.

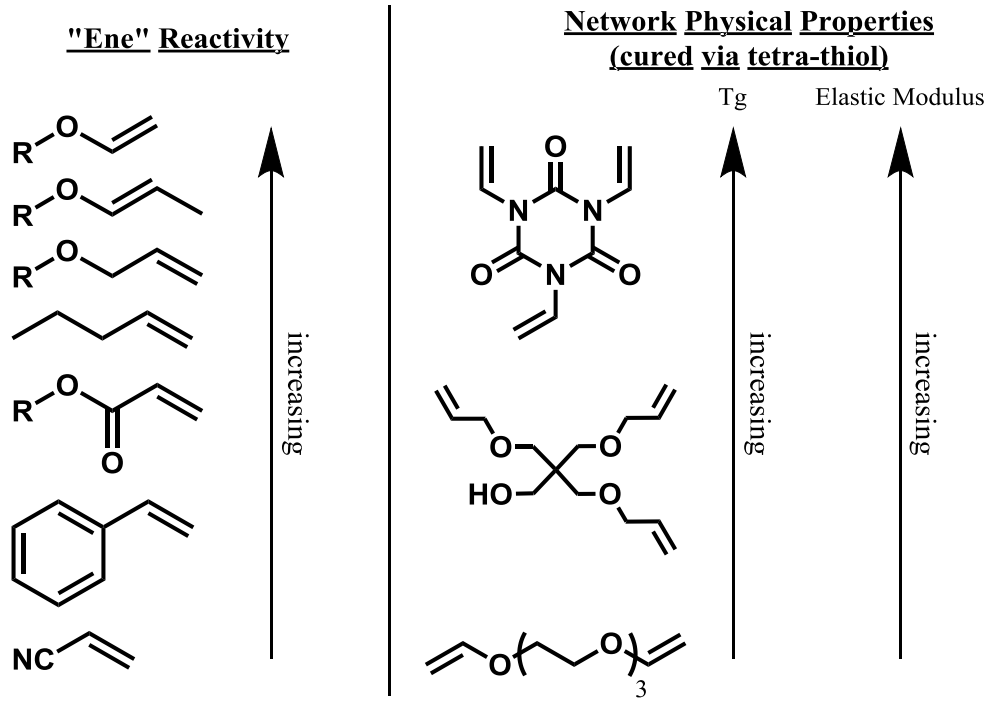

Figure 1.6: General summary of reactivity and network property trends for thiol-ene molecules and networks fabricated from "ene" monomers of varying architecture. Trend data from References (*48, 49*).

In the vast array of thiol-ene and conjugated polymer literature to date, exactly two reports outside the work of this dissertation have investigated the thiol-ene reaction as applied to conjugated polymers.(*50, 51*) Both of these studies have reacted a mono-functional thiol with the internal "ene" of phenylene-vinylene and phenylene-ethynylene type polymers, leading to a reduction in overall conjugation length and resulting in higher energy band gaps. While providing an interesting handle to tune optoelectronics, these reactions do not result in cross-linked networks given the mono-functionality of the investigated thiols.

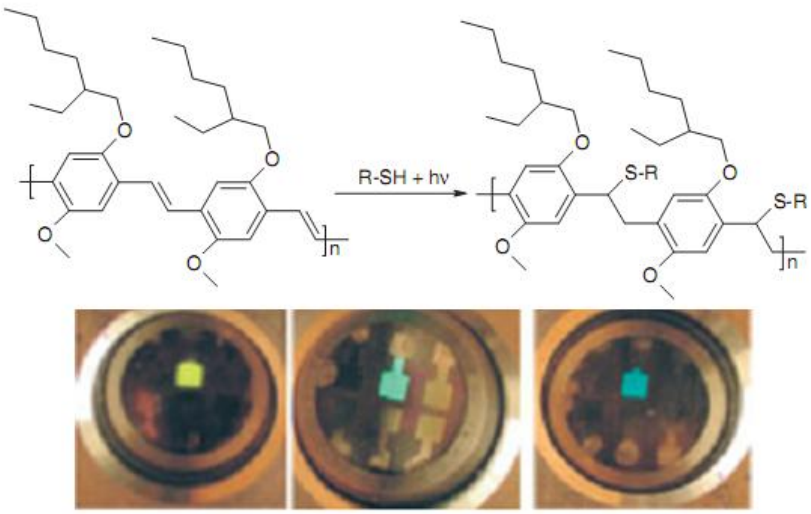

Figure 1.7: Example of thiol-ene chemistry used to modify the emissive properties of conjugated poly(phenylene vinylene) by reaction with an internal alkene. Reprinted with permission from Pogantsch and co-workers, *Adv. Func. Mater.*, 15, 403-409 (2005). Copyright 2005 Wiley-VCH.

1.6 Charge Transport in Organic Semiconductors

Semiconducting polymer devices have seen only a fraction of the operational success as their inorganic counterparts, as mentioned in Section 1.2. One of the most significant differences between organic and inorganic semiconductors is the mechanism of charge formation and transport. In conjugated polymers, charges exist as discretely localized species existing as an inseparable coupling of charge and structural deformation of the polymer backbone.

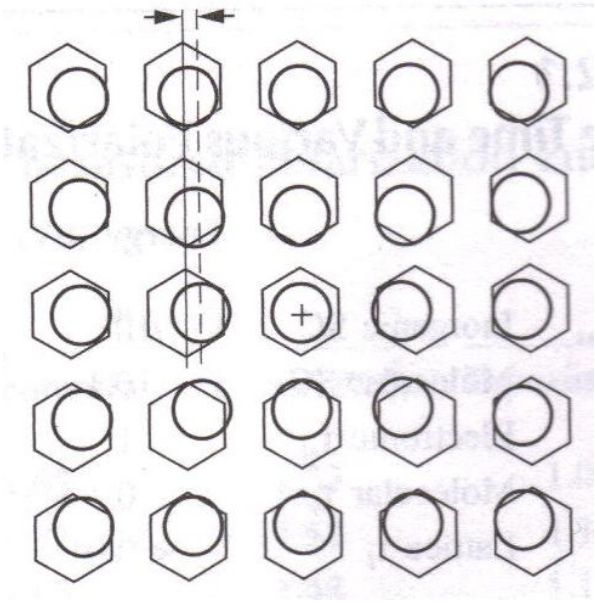

Figure 1.8: Illustration of a charged state in a conjugated organic matrix, where hexagons represent the carbon-carbon σ-bonding of an aromatic benzene-like ring, and circles represent their respective delocalized π-electron cloud. Republished with permission of CRC Press, from "Charge Transport in Oligomers" in *Organic Field-Effect Transistors*, Gilles Horowitz, CRC Press 2007(*9*); permission conveyed through Copyright Clearance Center, Inc.

Unsurprisingly, such a localized inhomogeneous phenomenon of charge formation does not fit well with the classical band theory of charge transport in crystalline inorganic semiconductors which relies on a multitude of overlapping indistinct atomic interactions.(*52*) In contrast, a single charged state in conjugated polymers greatly polarizes the electron clouds of its neighbors, illustrated in Figure 1.8 (hence the term "polaron"). A number of alternative models for organic charge transport have been explored in the literature.(*9*) The most prominent of these are Marcus-like theories which rely on the ease of polarization and reorganization of the semiconductor matrix(*53*) and various hopping theories(*54, 55*) which describe charge transport through more disorganized materials as the intermolecular interactions between localized but separated band-like states.

The specific details, advantages, and shortcomings of these models are not particularly relevant to this dissertation and can be found in the references cited above. However, the fact

that they all agree on slow, localized charges accompanied by structural changes in the polymer backbone is indeed important for some of the work presented here. These mechanisms of charge transport, which are qualitatively different than the highly mobile, highly delocalized holes and electrons in inorganic semiconductors, are a fundamental reason why the performance of organic semiconductors is so different than their inorganic counterparts.

1.7 Optically Imaging Charged States in Organic Semiconductor Thin Films

A unique advantage of the low mobility and localized, backbone-altering structure of charged states in conjugated polymers is their distinct, spectroscopically-obervable effect on the optical behavior of charge-carrying molecules. This contrasts to tedious non-optical tools like Kelvin probe force microscopy in which electric fields and charge distributions are mapped across an active device surface using an electrically charged probe tip.(*56, 57*) Specifically, researchers have taken advantage of changes in light transmission or absorption when a conjugated polymer goes from the neutral "benzoid" structure to the charge-carrying "quinoid" structure (Figure 1.9A). These molecular configurations were briefly discussed in Section 1.1 in regard to polyaniline, but any conjugated polymer built on a cyclic aromatic monomer undergoes similar changes. This transition has been deliberately accomplished via both chemical doping shown in Figure 1.9B(*58*) as well as by electric field-induced charge formation (e.g., field-effect transistors or capacitors) shown in Figure 1.9C.(*59*)

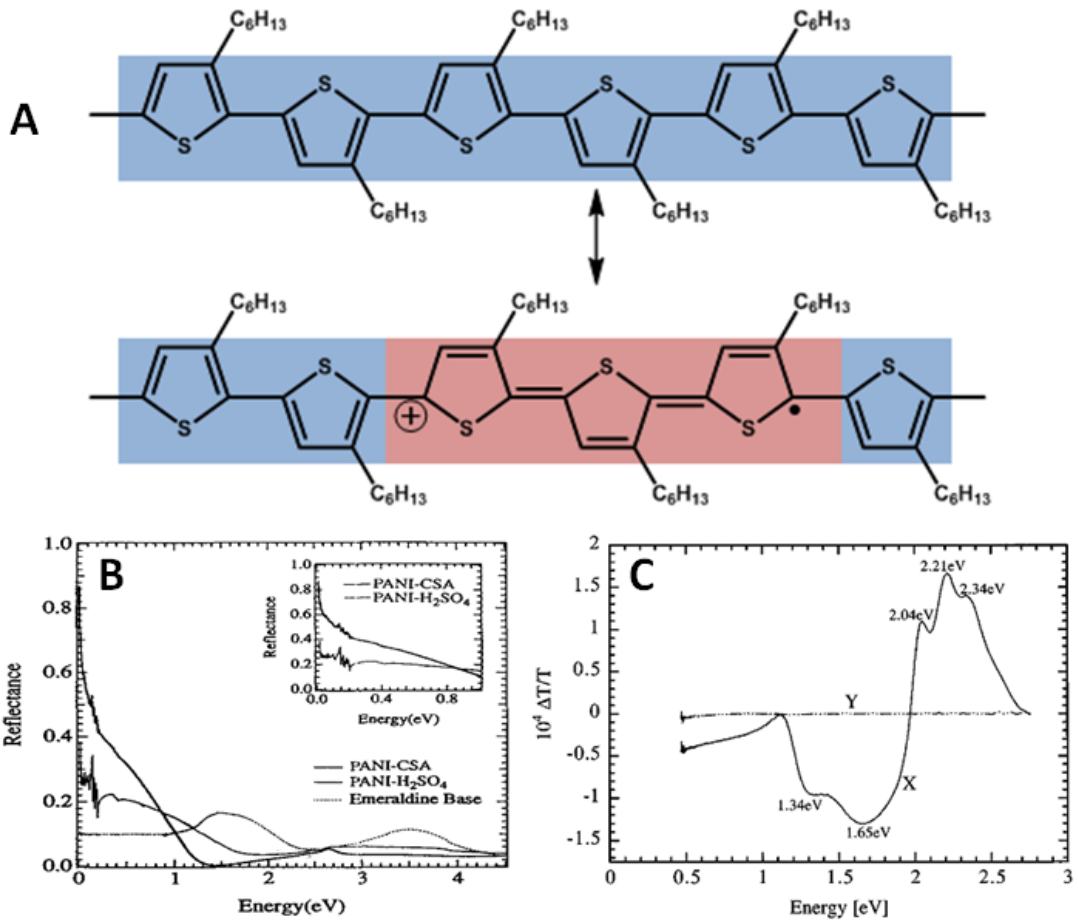

Figure 1.9: (A) Illustration of the neutral benzoid and charge-carrying quinoid molecular bonding configurations in example conjugated polymer poly(3-hexylthiophene). (B) Spectroscopic identification of the chemically-induced benzoid and quinoid forms of polyaniline. Reprinted *Synthetic Metals*, vol. 72, Lee, Heeger, Cao, "Reflectance spectra of polyaniline", pp. 25-24, Copyright 1995, with permission from Elsevier.(*58*) (C) Differential optical transmission spectroscopy showing the difference between the electric field-induced benzoid and quinoid states in poly(3-hexylthiophene). Reprinted figure reproduced from Brown and co-workers in *Physical Review B, 63, p. 125204 (2001).* Copyright 2001 by the American Physical Society.(*59*)

Following successful spectroscopic identification of the charge carrying states shown in Figure 1.9B and C, a handful of researchers have shown interest in using optical spectroscopy techniques to identify more complicated charge transport behavior in conjugated molecules and even spatially visualize distributions of charges. Such direct mapping techniques are experimentally complex and effectively impossible in non-organic systems where charged states are highly mobile, dynamic, and energetically indistinct.

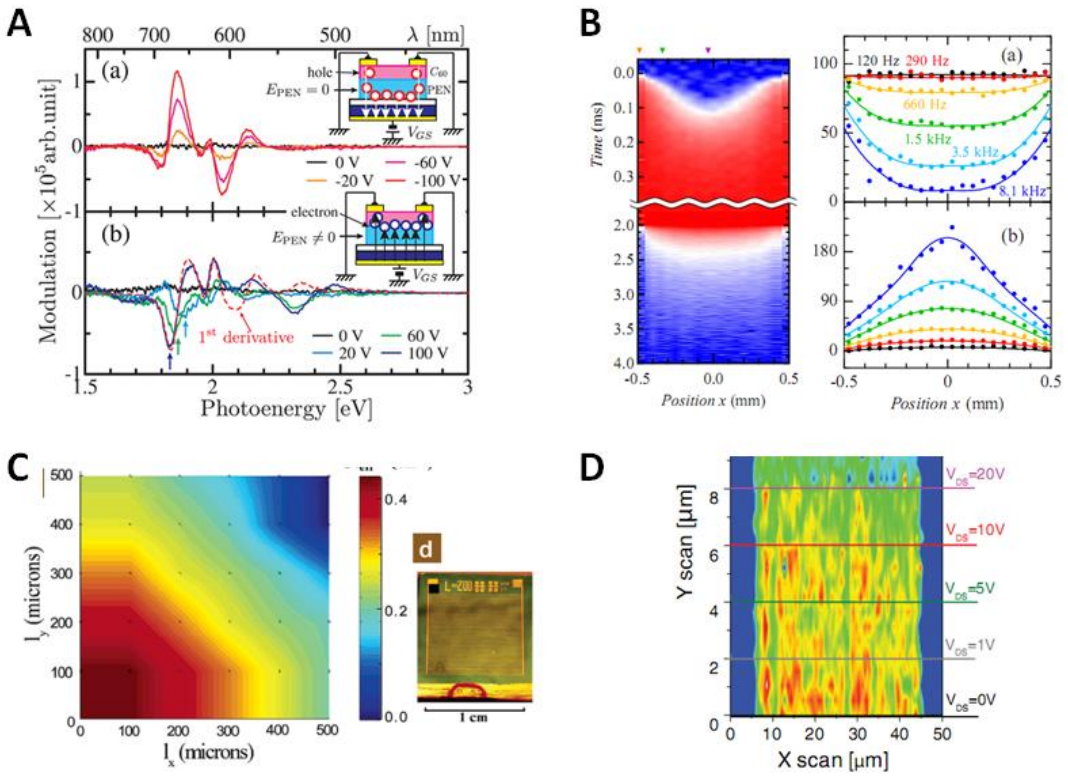

Figure 1.10: Examples of organic charge carrier imaging from published literature. Charges have been spectroscopically mapped for small molecules such as C_{60} fullerenes and pentacene (A,B,D), as well as conjugated polymers such as poly(3-hexylthiophene) (C). Figure A reprinted with permission from Zhang, *Appl. Phys. Lett.*, 100, p. 103301 (2012). Copyright 2012, AIP Publishing LLC. Figure B reprinted with permission from Matsui, *Appl. Phys. Lett.*, 95, p. 223301 (2009). Copyright 2009, AIP Publishing LLC. Figure C reprinted with permission from Li, *Nano Lett.*, 6, 224-228 (2006). Copyright 2006 American Chemical Society. Figure D reprinted with permission from Sciascia, *Adv. Mater.*, 23, 5086-5090 (2011). Copyright 2011 Wiley-VCH.(*60-63*)

Figure 1.10 shows some of the few literature reports on mapping and imaging charge carriers in conjugated molecules. Various reports have visualized electronic phenomena in organic semiconductors: both hole and electron accumulation has been spectroscopically resolved due to their different changes in structure and therefore optical absorption (Figure 1.10A),(*60*) time resolved carrier flow(*61*) and large grain-dominated trap sites(*62*) have been observed in pentacene thin films (Figure 1.10B, D), and carrier distributions in P3HT have been mapped between two perpendicular electrodes (Figure 1.10 C).(*63*) Figure 1.10 is representative of the organic charge visualization field in that most reported studies have focused on

conjugated small molecules or oligomers such as C_{60} fullerenes and pentacene, with some modest work on polymeric systems.(64-66)

While a great deal has been learned from these techniques, they present disadvantages. A number of these and related studies have employed highly focused laser probes with small spot-sizes, in which the probe laser must be rastered across the area of interest to generate a one- or two-dimensional mapping of charge phenomena.(*62, 63*) Such methods are time-consuming, particularly over large areas, and disadvantageous in high-throughput metrology applications. Many of these same studies also depend on measuring the differential *transmission* of an optical probe, requiring at minimum a semi-transparent device substrate and layer stack.(*62*) Such devices are often not comparable to the most commonly employed device architectures built on opaque substrates (metals and inorganics). Similarly difficult architectural concerns arise in studies using the differential optics resulting from a piezo-like dielectric layer which responds to changes in electric field correlating to changes in carrier density.(*61*) While remarkably clever, it is difficult to translate these measurements to more practical, widespread device architectures.

There are no theoretical constraints on why more conventional non-transmissive device architectures (such as the ubiquitous Si/SiO_2 gate/dielectric pair) cannot be used in optical visualization studies, nor why a small probe size of a laser is required for an optical probe. For these reasons, another goal of this dissertation is to develop a more robust, wide-area, rapid tool for the visualization of the unique optical changes that occur in semiconducting organic materials when carrying charge. These advantages could conceivably allow for more general insight into important phenomena occurring across the entire electronic polymer device as the whole area could ideally be imaged simultaneously on common device architecture.

1.8 Outline of the Dissertation

The introduction presented in this chapter offered the background concepts and work necessary to understand the goals and approaches of the research described in this dissertation, whose focus is on the visualization and control of charge transport in conjugated polymers. A brief history of conjugated polymers was presented, placing them in context with other semiconducting materials and applications. This was followed by additional details on the processing of these materials which has been known to affect their behavior and an overview of thiol-ene click chemistry as a tool for fabrication cross-linked networks. A more detailed description of the mechanism of charge transport in conjugated polymers was then presented to provide a sense of how those mechanisms might be controlled and observed.

Chapters 2-5 describe the synthesis, characterization, and thiol-ene network-forming capabilities of alkene-functionalized poly(fluorene)s. The effect of these networks' architecture is then observed on the polymers' electronic properties, and charge transport is abstractly visualized by careful observation and measurement of fluorescent behavior. Chapter 6 expands the thiol-ene reaction in poly(fluorene)s to surface grafting applications. Chapter 7 demonstrates the direct spatial visualization of charged states in polymeric thin film transistors using modulation-amplified reflectance spectroscopy. Finally, Chapter 8 offers a brief summary and outlook following the results of this dissertation.

1.9 References

1. W. Shockley (1948). *U.S. Patent No. 2,569,347*. Washington, DC: U.S. Patent and Trandemark Office.

2. H. Letheby, XXIX. - On the production of a blue substance by the electrolysis of sulphate of aniline, *J. Chem. Soc.* **15**, 161-163 (1862).

3. H. Shirakawa, E. J. Louis, A. G. MacDiarmid, C. K. Chiang, A. J. Heeger, Synthesis of electrically conducting organic polymers: halogen derivatives of polyacetylene, (CH)x, *J. Chem. Soc., Chem. Comm.* 578-580 (1977).

4. H. Shirakawa, S. Ikeda, Infrared Spectra of Poly(acetylene), *Polym. J.* **2**, 231-244 (1971).

5. H. Shirakawa, T. Ito, S. Ikeda, Raman Scattering and Electronic Spectra of Poly(acetylene), *Polym. J.* **4**, 460-462 (1973).

6. T. Ito, H. Shirakawa, S. Ikeda, Polymerization and Formation of Polyacetylene Film, *J. Polym. Sci. A: Polym. Chem.* **12**, 11-20 (1974).

7. R. Das, P. Harrop, "Printed, Organic & Flexible Electronics: Forecasts, Players & Opportunities 2013-2023" (IDTechEx, 2013).

8. A. Moliton, R. C. Hiorns, Review of electronic and optical properties of semiconducting π-conjugated polymers: applications in optoelectronics, *Polym. Int.* **53**, 1397-1412 (2004).

9. G. Horowitz, in *Organic Field-Effect Transistors,* Z. Bao, J. Locklin, Eds. (CRC Press, Boca Raton, FL, 2007).

10. A. Facchetti, π-Conjugated Polymers for Organic Electronics and Photovoltaic Cell Applications, *Chem. Mater.* **23**, 733-758 (2011).

11. J.-C. Chiang, A. G. MacDiarmid, 'Polyanilin': Protonic acid doping of the emeraldine form to the metallic regime, *Synth. Met.* **13**, 193-205 (1986).

12. C. W. Tang, S. A. VanSlyke, Organic electroluminescent diodes, *Appl. Phys. Lett.* **51**, 913-915 (1987).

13. C. Brabec, V. Dyakonov, U. Scherf, *Organic Photovoltaics - Materials, Deice Physics, and Manufacturing Technologies*. (John Wiley & Sons, Hoboken, NJ, 2008).

14. F. So. *Organic electronics: materials, processing, devices, and applications.* CRC Press, Boca Raton, FL, 2010).

15. Z. Bao, J. Locklin, *Organic Field-Effect Transistors*. (CRC Press, Boca Raton, FL, 2007).

16. S. Ege, *Organic Chemistry Structure and Reactivity*. (Houghton Mifflin Company, New York, 2004).

17. J. van Herrikhuyzen, A. Syamakumari, A. P. H. J. Schenning, E. W. Meijer, Synthesis of n-type perylene bisimide derivatives and their orthogonal self-assembly with p-type oligo(p-phenylene vinylene)s, *J. Am. Chem. Soc.* **126**, 10021-10027 (2004).

18. S. Sax, N. Rugen-Penkalla, A. Neuhold, S. Schuh, E. Zojer, E. J. W. List, K. Müllen, Efficient blue-light-emitting polymer heterostructure devices: the fabrication of multilayer structures from orthogonal solvents, *Adv. Mater.* **22**, 2087-2091 (2010).

19. Z. A. Page, V. V. Duzhko, T. Emrick, Conjugated Thiophene-Containing Polymer Zwitterions: Direct Synthesis and Thin Film Electronic Properties, *Macromolecules* **46**, 344-351 (2013).

20. S. Allard, M. Forster, B. Souharce, H. Thiem, U. Scherf, Organic semiconductors for solution-processable field-effect transistors (OFETs), *Angew. Chem. Int. Ed.* **47**, 4070-4098 (2008).

21. A. Babel, S. a. Jenekhe, Alkyl chain length dependence of the field-effect carrier mobility in regioregular poly(3-alkylthiophene)s, *Synth. Met.* **148**, 169-173 (2005).

22. B. Friedel, C. R. McNeill, N. C. Greenham, Influence of Alkyl Side-Chain Length on the Performance of Poly(3-alkylthiophene)/Polyfluorene All-Polymer Solar Cells, *Chem. Mater.* **22**, 3389-3398 (2010).

23. R. J. Kline, D. M. Delongchamp, D. A. Fischer, E. K. Lin, L. J. Richter, M. L. Chabinyc, M. F. Toney, M. Heeney, I. McCulloch, Critical Role of Side-Chain Attachment Density on the Order and Device Performance of Polythiophenes, *Macromolecules* **40**, 7960-7965 (2007).

24. V. Ho, B. W. Boudouris, R. A. Segalman, Tuning Polythiophene Crystallization through Systematic Side Chain Functionalization, *Macromolecules* **43**, 7895-7899 (2010).

25. Y. D. Park, D. H. Kim, Y. Jang, J. H. Cho, M. Hwang, H. S. Lee, J. A. Lim, K. Cho, Effect of side chain length on molecular ordering and field-effect mobility in poly(3-alkylthiophene) transistors, *Org. Elec.* **7**, 514-520 (2006).

26. U. Scherf, D. Neher, in *Advances in Polymer Science*. (Springer, New York, 2008), vol. 212.

27. T.-Q. Nguyen, R. C. Kwong, M. E. Thompson, B. J. Schwartz, Improving the performance of conjugated polymer-based devices by control of interchain interactions and polymer film morphology, *Appl. Phys. Lett.* **76**, 2454 (2000).

28. B. J. Schwartz, Conjugated polymers as molecular materials: how chain conformation and film morphology influence energy transfer and interchain interactions, *Ann. Rev. Phys. Chem.* **54**, 141-172 (2003).

29. J.-F. Chang, B. Sun, D. W. Breiby, M. M. Nielsen, T. I. Sölling, M. Giles, I. McCulloch, H. Sirringhaus, Enhanced Mobility of Poly(3-hexylthiophene) Transistors by Spin-Coating from High-Boiling-Point Solvents, *Chem. Mater.* **16**, 4772-4776 (2004).

30. D. H. Kim, Y. Jang, Y. D. Park, K. Cho, Controlled one-dimensional nanostructures in poly(3-hexylthiophene) thin film for high-performance organic field-effect transistors, J. P*hys. Chem. B* **110**, 15763-15768 (2006).

31. H. Jia, S. Gowrisanker, G. K. Pant, R. M. Wallace, B. E. Gnade, Effect of poly (3-hexylthiophene) film thickness on organic thin film transistor properties, *J. Vac. Sci. Tech. A* **24**, 1228 (2006).

32. G. Li , Y. Yao, H. Yang, V. Shrotriya, G. Yang, Y. Yang, "Solvent Annealing" Effect in Polymer Solar Cells Based on Poly(3-hexylthiophene) and Methanofullerenes, *Adv. Func. Mater.* **17**, 1636-1644 (2007).

33. M. Campoy-Quiles *et al.*, Morphology evolution via self-organization and lateral and vertical diffusion in polymer:fullerene solar cell blends. *Nature Mater.* **7**, 158-164 (2008).

34. J. P. Chen, G. Klaerner, J. Lee, D. Markiewicz, V. Y. Lee, R. D. Miller, J. C. Scott, Efficient, blue light-emitting diodes using cross-linked layers of polymeric arylamine and fluorene, *Synth. Met.* 129-135 (1999).

35. G. Klärner, J.-I. Lee, V. Y. Lee, E. Chan, J.-P. Chen, A. Nelson, D. Markiewicz, R. Siemens, J. C. Scott, R. D. Miller, Cross-linkable Polymers Based on Dialkylfluorenes, *Chem. Mater.* **11**, 1800-1805 (1999).

36. L. D. Bozano, K. R. Carter, V. Y. Lee, R. D. Miller, R. Dipietro, J. C. Campbell, Electroluminescent devices based on cross-linked polymer blends *J. Appl. Phys.* **94**, (2003).

37. H. Sun, Z. E. Liu, Y. Hu, L. Wang, D. Ma, X. Jing, F. Wang, Crosslinkable Poly(p-phenylenevinylene) Derivative, *J. Polym. Sci. A: Polym. Chem.* **42**, 2124-2129 (2004).

38. G. K. Paul, J. Mwaura, A. A. Argun, P. Taranekar, J. R. Reynolds, Cross-Linked Hyperbranched Arylamine Polymers as Hole-Transporting Materials for Polymer LEDs, *Macromolecules* **39**, 7789-7792 (2006).

39. B. B. Ma, B. J. Kim, D. A. Poulsen, S. J. Pastine, J. M. J. Fre, Multifunctional Crosslinkable Iridium Complexes as Hole Transporting / Electron Blocking and Emitting Materials for Solution-Processed Multilayer Organic Light-Emitting Diodes, *Adv. Func. Mater.,* **19**, 1024-1031 (2009).

40. E. Scheler, I. Bauer, P. Strohrigl, Synthesis and Photopatterning of Fluorene Based Reactive Mesogens, *Macromolecular Symposia,* **254,** 203-209 (2007).

41. M. S. Bayerl, T. Braig, O. Nuyken, D. C. Mu, M. Groß, K. Meerholz, Crosslinkable hole-transport materials for preparation of multilayer organic light emitting devices by spin-coating, *Macromolecular Rapid Comm.* **20**, 224-228 (1999).

42. T. Posner, Beiträge zur Kenntniss der ungesättigten Verbindungen. II. Ueber die Addition von Mercaptanen an ungesättigte Kohlenwasserstoffe, *Berichte der deutschen chemischen Gesellschaft* **38**, 646 (1905).

43. R. K. Iha, K. L. Wooley, A. M. Nystrom, D. J. Burke, M. J. Kade, C. J. Hawker, Applications of Orthogonal "Click" Chemistries in the Synthesis of Functional Soft Materials, *Chem. Rev.* **109**, 5620-5686 (Nov, 2009).

44. A. B. Lowe, Thiol-ene "click" reactions and recent applications in polymer and materials synthesis *Polym. Chem.* **1**, 17-36 (Mar, 2010).

45. C. E. Hoyle, C. N. Bowman, Thiol-Ene Click Chemistry, *Angew. Chem. Int. Ed.* **49**, 1540-1573 (2010).

46. C. E. Hoyle, A. B. Lowe, C. N. Bowman, Thiol-click chemistry: a multifaceted toolbox for small molecule and polymer synthesis, *Chem. Soc. Rev.* **39**, 1355-1387 (2010).

47. N. B. Cramer, J. P. Scott, C. N. Bowman, Photopolymerizations of Thiol-Ene Polymers without Photoinitiators, *Macromolecules* **35**, 5361-5365 (2002).

48. C. R. Morgan, F. Magnotta, A. D. Ketley, Thiol / Ene Photocurable Polymers, *J. Polym. Sci. A: Polym. Chem.* **15**, 627-645 (1977).

49. Q. Li, H. Zhou, C. E. Hoyle, The effect of thiol and ene structures on thiol–ene networks: Photopolymerization, physical, mechanical and optical properties, *Polymer* **50**, 2237-2245 (2009).

50. A. Pogantsch, S. Rentenberger, G. Langer, J. Keplinger, W. Kern, E. Zojer, Tuning the Electroluminescence Color in Polymer Light-Emitting Devices Using the Thiol-Ene Photoreaction, *Adv. Func. Mater.* **15**, 403-409 (2005).

51. B. Kiskan, J. Weber, Versatile Postmodification of Conjugated Microporous Polymers Using Thiol-yne Chemistry, *ACS Macro Letters* **1**, 37-40 (2012).

52. M. Shur, *Physics of Semiconductor Devices*. (Prentice-Hall, Inc., Englewood Cliffs, NJ, 1990).

53. J.-L. Brédas, D. Beljonne, V. Coropceanu, J. Cornil, Charge-Transfer and Energy-Transfer Processes in π-Conjugated Oligomers and Polymers: A Molecular Picture, *Chem. Rev.* **104**, 4971-5004 (2004).

54. W. D. Gill, Drift mobilities in amorphous charge-transfer complexes of trinitrofluorene and poly-n-vinylcarbazole, *J. Appl. Phys.* **43**, 5033 (1972).

55. H. Bässler, Charge Transport in Disordered Organic Photoconductors a Monte Carlo Simulation Study, *Physica Status Solidi B* **175**, 15-56 (1993).

56. L. Bürgi, T. J. Richards, R. H. Friend, H. Sirringhaus, Close look at charge carrier injection in polymer field-effect transistors, *J. Appl. Phys.* **94**, 6129 (2003).

57. L. S. C. Pingree, O. G. Reid, D. S. Ginger, Electrical Scanning Probe Microscopy on Active Organic Electronic Devices, *Adv. Mater.* **21**, 19-28 (2009).

58. K. Lee, A. J. Heeger, Y. Cao, Reflectance spectra of polyaniline, *Synth. Met.* **72**, 25-34 (1995).

59. P. Brown, H. Sirringhaus, M. Harrison, M. Shkunov, R. Friend, Optical spectroscopy of field-induced charge in self-organized high mobility poly(3-hexylthiophene), *Phys. Rev. B* **63**, 125204 (2001).

60. L. Zhang, D. Taguchi, T. Manaka, M. Iwamoto, Direct probing of selective electron and hole accumulation processes along the channel of an ambipolar double-layer field-effect transistor by optical modulation spectroscopy, *Appl. Phys. Lett.* **100**, 103301 (2012).

61. H. Matsui, T. Hasegawa, Visualization of accumulated charge density in operating organic thin-film transistors, *Appl. Phys. Lett.* **95**, 223301 (2009).

62. C. Sciascia, N. Martino, T. Schuettfort, B. Watts, G. Grancini, M. R. Antognazza, M. Zavelani-Rossi, C. R. McNeill, M. Caironi, Sub-Micrometer Charge Modulation Microscopy of a High Mobility Polymeric n-Channel Field-Effect Transistor, *Adv. Mater.* **23**, 5086-5090 (2011).

63. Z. Q. Li, G. M. Wang, N. Sai, D. Moses, M. C. Martin, M. Di Ventra, A. J. Heeger, D. N. Basov, Infrared imaging of the nanometer-thick accumulation layer in organic field-effect transistors, *Nano Lett.* **6**, 224-228 (2006).

64. T. Manaka, E. Lim, R. Tamura, M. Iwamoto, *Nature Photonics* **1**, 581 (2007).

65. T. Manaka, S. Kawashima, M. Iwamoto, *Appl. Phys. Lett.* **97**, 113302 (2010).

66. N. M. Gabor, J. C. W. Song, Q. Ma, N. L. Nair, T. Taychatanapat, K. Watanabe, T. Taniguchi, L. S. Levitov, P. Jarillo-Herrero, *Science* **334**, 648 (2011).

CHAPTER 2

SEMICONDUCTING POLYMER NETWORKS VIA THIOL-ENE PHOTO-CLICK CHEMISTRY*

2.1 Introduction

Cross-linking semiconducting polymers into a robust insoluble network is an attractive route to improving their functional performance, longevity, and processability. In this chapter, thiol-ene click chemistry is explored to form robust, device-compatible cross-linked films of a conjugated polymer (CP). Poly(dialkyl fluorene)s are a class of material that has been extensively investigated for use in polymer light-emitting diode (PLED) applications due to their deep blue emission, chemical and thermal stability, ease of functional tuning at the bridging 9-position, and high photoluminescent and electroluminescent yields.(*1-3*) One drawback of poly(fluorene)s is the exhibition of a broad green emission band between 500 and 550 nm which has been attributed to the formation of aggregates and/or the generation of ketone defects over time and under annealing conditions.(*4-7*) Cross-linking of CP films has been shown in the literature to provide more stable emission, presumably due to polymer chains being "locked" into position, significantly reducing their tendency to re-align during annealing or device operation.(*8*) Cross-linking also allows for the formation of dual-layer devices where the robust cross-linked layer will not be dissolved during solution processing of a second layer. Additionally, cross-linking enables the incorporation of a wide range of chemical functionality that can be imbedded in the polymer during curing.

Several methods can be found in the literature describing the cross-linking of CP films. The thermally-intiated free-radical autopolymerization of styrene is widely known, and there is already a considerable amount of work exploiting this chemistry to cross-link 4-phenyethenyl

* Portions of this chapter have been reprinted with permission from Davis, Maegerlein, Carter, *J. Am. Chem. Soc. 133*, 20546 (2011). Copyright 2011 American Chemical Society.

end-capped CPs such as poly(fluorene)s,(*9-11*) poly(phenylene vinylene)s,(*12*) triarylamines,(*13, 14*) and heteroleptic iridium complexes.(*15*) Examples of these styrene-functionalized CPs previously used for thermal cross-linking are shown in Figure 2.1.

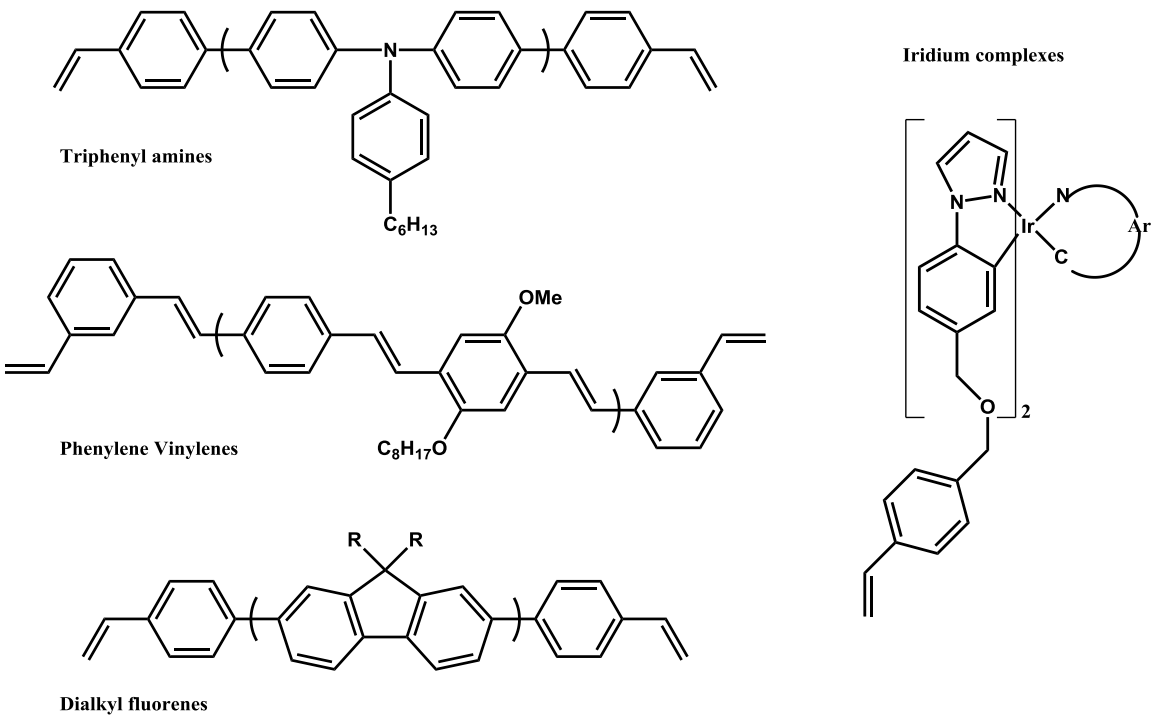

Figure 2.1: Examples of previously studied thermally cross-linkable conjugated polymers.

While the thermal autopolymerization chemistry is attractive as it requires no additional cross-linking reagents and no side products are anticipated, curing requires an oxygen-free environment at elevated temperatures (above 150 °C) and reaction times up to several hours. To circumvent these concerns, several different UV-initiated cross-linking chemistries have been investigated with various CPs allowing for curing at lower temperatures and with shorter reaction times. UV-initiated curing gives the added benefit for photo-patterning, providing the potential for the fabrication of materials with more complex architectures. One popular example found in the literature is the acrylate group, readily polymerized by a radical mechanism which can be initiated photochemically.(*16, 17*) Oxetanes, strained four-member cyclic ethers that can undergo cationic ring-opening polymerization, have similarly been used as

cross-linkable functional groups provided a suitable initiator is added,(*18*) and bromine-terminated side chains have been employed to cross-link poly(thiophene)s.(*19*) Examples of free-radical sensitive monomers and pre-polymers used in the systhesis of these systems are shown in Figure 2.2. While UV-initiated cross-linking removes the need for high heat and long reaction times, the curing procedures require some mechanism for initiation. Generally this is achieved by adding a photo-acid or –radical generator (PAG/PRG) to the reaction mixture which acts as an initiator upon UV exposure. It is easy to imagine that this small molecule additive may result in deleterious effects including residual initiator and/or undesired side products.

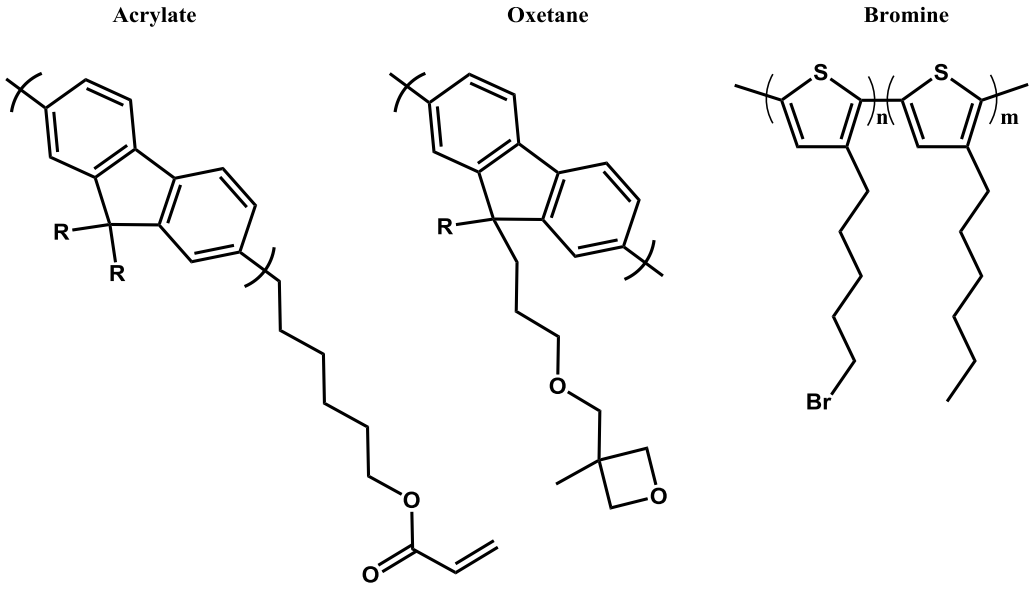

Figure 2.2: Examples of previously studied photo-curable conjugated molecules.

This chapter describes the investigation of a previously unexplored cross-linking chemistry for CPs that takes advantage of the low curing temperatures and quick processing time provided by UV-curing but proceeds by click chemistry to avoid the problems related to systems utilizing photo-acid/base generators or uncontrolled radical initiators. Thiol-ene click chemistry has grown tremendously in popularity over the past few years and has been shown to posses various advantages such as rapid reaction rates, minimal oxygen inhibition, and high

yields.(*20-26*) Because the initiation proceeds by UV-induced homolytic cleavage of the S-H bond, thiol-ene chemistry is advantageous for CP cross-linking as it does not require high temperatures such as those needed for the thermal initiation of 4-phenylethenyl groups and mitigates potential issues with residual photointiator additives. Furthermore, thiol-ene chemistry is well-suited to patterning by photolithography as shown by Hagberg et al.(*27*) Specifically under investigation here is the use of thiol-ene chemistry to photochemically cross-link a thin film of 4-phenylethenyl end-capped poly(dihexyl fluorene) (xDHF). Additionally, cross-linked PLED devices are fabricated to demonstrate the use of this chemistry in active devices.

2.2 Experimental Section

2.2.1 Materials

4-bromostyrene, 2,7-dibromo-9,9-dihexyl-9H-fluorene (DBDHF), 2,2'-bipyridyl (BPY), 1,5-cyclooctadiene (COD), tetrahydrofuran (THF), pentaerythritol tetrakis-(3-mercaptopropionate), and Poly(3,4-ethylenedioxythiophene) poly(styrenesulfonate) (PEDOT:PSS) were purchased from Sigma-Aldrich Company. DBDHF was recrystallized from ethanol prior to use. The active Ni-(0) coupling reagent, bis(1,5-cyclooctadiene)nickel(0) [$Ni(COD)_2$], was purchased from Strem Chemicals and handled under inert atmosphere. Anhydrous toluene and dimethylformamide (DMF), stored under nitrogen over molecular sieves, were purchased from Sigma Aldrich Company. All reagents were used as received unless otherwise noted. Silicon substrates were purchased from University Wafers. Indium tin oxide (ITO)-coated glass was purchased from Thin Film Devices, Inc (sheet resistance 20 Ω/sq). All reactions were run under dry N_2 unless otherwise noted.

2.2.2 Instrumentation

All nuclear magnetic resonance (NMR) spectra were acquired on a Bruker AF 300 (300 MHz) spectrometer and internally referenced via residual solvent signal [$CHCl_3$: ^1H) 7.26 ppm; 13C) 77.00 ppm]. All chemical-shift values are given in ppm. Gel permeation chromatography (GPC) was performed in THF at room temperature with 1.0 mL/min elution rate. A Waters R403 differential refractometer and three PLgel columns (105, 104, and 103 Å) calibrated with narrow molecular weight polystyrene standards were used. Differential scanning calorimetry (DSC) was performed on a Thermal Analysis (TA) Q-2000 in T-zero aluminum pans using modulated DSC at 3 °C/min. Thermal gravimetric analysis was performed using a Perkin-Elmer TGS-2, under nitrogen atmosphere with a heating rate of 10 °C/min.

Film thicknesses were measured by contact profilometry using a Dektak 150 profilometer. UV-Vis spectra were recorded in 1cm path-length quartz cuvettes. Fluorescence measurements were taken on a Perkin-Elmer LS-50B. Infrared spectroscopy of polymer films were performed on a Nicolet 6700 FT-IR spectrometer with a Harrick grazing angle ATR accessory (GATR).

2.2.3 Microwave Reactor

Microwave heating was performed in a SmithCreator™ single-mode microwave cavity producing continuous radiation at a frequency of 2.45 GHz (Personal Chemistry, Inc). Reactions were conducted under nitrogen in 35 mL, heavy-walled pyrex glass reaction vials sealed with silicone caps fitted with a silicone septum. Reaction mixtures were stirred internally with a magnetic stir bar during the irradiation.

2.2.4 Polymerization of Styrene End-capped 2,7-dibromo-9,9-dihexyl-9*H*-fluorene (xDHF)

Cross-linkable, end-capped homopolymer (xDHF) was synthesized by the nickel (0)-mediated polymerization of 2,7-dibromo-9,9-dihexyl-9*H*-fluorene (DBDHF) and 4-bromostyrene via microwave heating. DBDHF (300 mg, 0.609 mmol, 1 equiv.) and 2,2'-dipyridyl (257 mg, 1.645 mmol, 2.87 equiv.) were added to a 35 mL microwave vial. In a glove box, $Ni(COD)_2$ (409 mg, 1.487 mmol, 2.44 equiv.) and a stirbar were added to the vial which was then sealed. 4-bromostyrene (12.2 µL, 0.06 mmol, 0.125 equiv.), COD (191 µL, 1.554 mmol, 2.55 equiv.), and 15 mL dry toluene/DMF (3:1 v/v) were injected and the vial was degassed and backfilled with nitrogen three times. The reaction was heated in a microwave at 100 °C for 30 min after 30 sec of pre-stirring. After reaction, the polymer solution was filtered through a syringe filter (0.45 µm) and precipitated by adding dropwise into 300 mL methanol and concentrated HCl (98:2 v/v). The crude polymer was dissolved in minimal THF and reprecipitated into methanol. The recovered light yellow precipitated was dried overnight under vacuum (170mg, 81% yield). ^{1}H NMR (300 MHz, $CDCl_3$) δ 7.86-7.68 (40H, aromatic); 6.84, 5.86, 5.32 (dd 1H, d 1H, d1H, vinyl endcaps); 2.11, 1.14, 0.80 (24H, 72H, 60H, alkyl chain). DP via ^{1}H NMR = 13; M_n via GPC 10400; PDI 2.31.

2.2.5 Film Coating and Cross-linking

Silicon wafers were solvent rinsed sequentially with hexanes, acetone, THF, water, and 2-propanol, then dried under a stream of nitrogen. Subsequently, the substrate was soaked in a piranha bath (5:1 concentrated sulfuric acid:30% hydrogen peroxide) at 100 °C for 30 minutes, rinsed thoroughly with DI water, and dried under nitrogen. xDHF solutions were made by dissolving 15 mg polymer in 500 µL $CHCl_3$ then adding 500 µL toluene. In the case of thermally cross-linkable films, no further reagents were added. In the case of UV-curable films, the

tetrafunctional cross-linker, pentaerythritol tetrakis-(3-mercaptopropionate), was added in a stoichometric amount (1:2 vinyl:thiol) as a solution in toluene. Solutions were spin-coated onto the cleaned wafers at 2000 rpm for 60 seconds. Thermal cross-linking was carried out on a hotplate at 200 °C for 45 min under a nitrogen atmosphere to form an insoluble layer. UV cross-linking was accomplished at 85 °C for 5 min in a nitrogen atmosphere under 365 nm light unless noted otherwise, forming an insoluble layer. All films were rinsed with THF and dried under a stream of nitrogen to ensure all uncross-linked material was removed from the surface.

2.2.6 Device Fabrication

Polymer light emitting diodes (PLEDs) were fabricated using xDHF as the active emitting layer. ITO-coated glass was first solvent cleaned and subsequently treated with O_2 plasma for 3 minutes. Poly(ethylene-dioxythiophene)/poly(styrene sulfonate) (PEDOT/PSS) (1.3wt% in H_2O, Aldrich) was then spin-coated at 4000 RPM and dried under N_2 at 150°C for 30 minutes. Solutions of xDHF were then spun from a mixed solution of chloroform and toluene containing pentaerythritol tetrakis-(3-mercaptopropionate) tetra-functional cross-linker, such that the ratio of S-H groups to xDHF vinyl groups was 2:1 to ensure complete cross-linking. UV cross-linked devices were then heated to 85°C under N_2 and exposed to a 365 nm UV light source for 5 min. Thermally cross-linked devices were cured at 200°C under N_2 for 1 hour. All cross-linked devices were then rinsed with THF and dried under vacuum overnight. As spun devices were simply placed under vacuum overnight directly following spin-coating. In order to ensure all devices had comparably thick active layers, spin-coating speeds for the active layer solution was varied for each treatment to account for losses in thickness during curing. Devices were completed by the thermal evaporation of 15 nm Ca cathodes capped with 100 nm Al at pressure $<10^{-5}$ Torr

with active areas of 0.15 cm^2. Devices were tested in air using a Kiethley 2602 Sourcemeter and a calibrated Ocean Optics USB4000 UV–vis spectrometer.

Patterned PLEDs were fabricated using a photo-mask during UV curing of the xDHF layer to selectively cross-link xDHF circles. Substrates were rinsed in THF to remove uncrued xDHF, and a solution of poly(fluorene-co-benzothiadiazole) in chloroform was subsequently spun on the substrates. Drying, cathode deposition, and testing were completed as above.

2.3 Results and Discussion

2.3.1 Synthesis

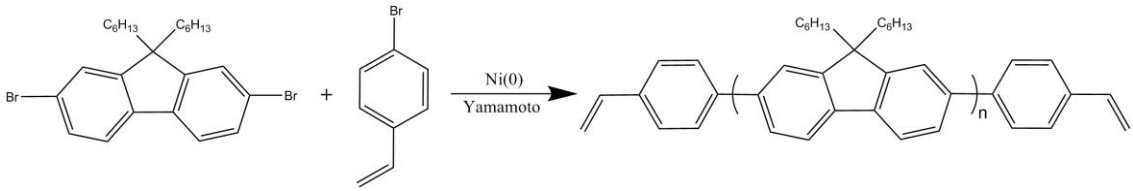

Figure 2.3: Synthesis of xDHF via Yamamoto coupling.

xDHF was synthesized by conventional Yamamoto coupling of 2,7-dibromo-9,9-dihexyl-9H-fluorene with the addition of 4-bromostyrene as an end-capping species with good yield (81%) (Figure 2.3). ^{1}H NMR of synthesized xDHF (Figure 2.4) showed the desired product with clearly visible vinylic proton resonances (δ = 5.3, 5.9, 6.8 ppm) from the end-groups. Molecular weight and degree of polymerization (DP) of xDHF was calculated by taking the ratio of these vinylic proton signals to the methylene proton of the 9-position hexyl chain α to the fluorene backbone [fluorene–(**CH_2**)-$(CH_2)_4$-CH_3] and were found to be Mn = 4500 kDa and DP = 13. The considerably larger molecular weight of Mn = 10400 determined from gel permeation chromatography (GPC) can be explained by the rigid nature of poly(fluorene) compared to polystyrene standards. The relatively low molecular weight was chosen to allow for a greater cross-linking density (since cross-linking occurs at the chain ends) as well as to limit

polydispersity which is known to adversely affect PLED performance.(*28*) Furthermore, the modest glass transition temperature T_g of xDHF at 85°C (by differential scanning calorimetry) as well as its high thermal stability are factors that prove advantageous for cross-linking by arguments of increased chain mobility as discussed later.

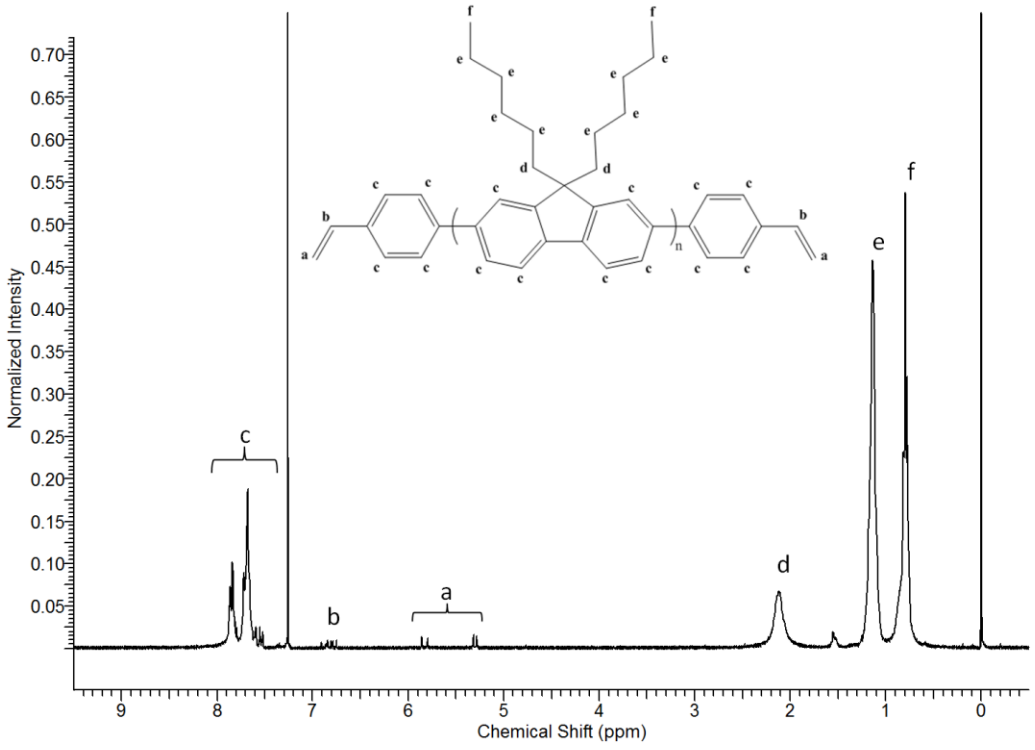

Figure 2.4: ^{1}H NMR spectrum of xDHF showing terminal vinyl signals used for end-capping confirmation and calculation of molecular weight.

2.3.2 Cross-Linking of xDHF Films

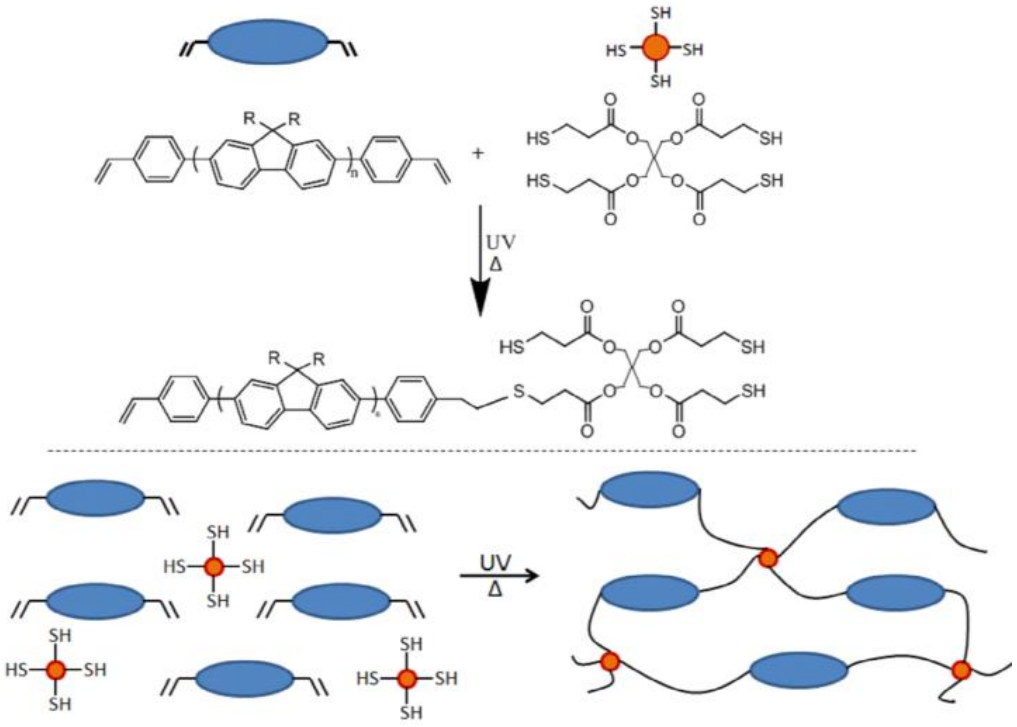

Figure 2.5: Schematic showing a thiol-ene click reaction between the vinyl group of end-capped poly(9,9-dihexyl fluorene) (xDHF) and one thiol group of pentaerythritol tetrakis(3-mercaptopropionate) (SH-4), with full cross-linking illustrated below.

The overall thiol-ene reaction scheme enabling cross-linking of xDHF is illustrated in Figure 2.5. Cross-linking of xDHF films was achieved by spin-coating a solution containing both xDHF and a tetra-functional thiol cross-linker, pentaerithritol tetrakis(3-mercaptopropionate) (SH-4). An excess of SH-4 (thiol:vinyl = 2:1) was used to ensure that the maximum number of vinyl end groups could find a cross-linker during the thiol-ene click reaction. Upon exposure of the film to UV light, homolytic cleavage of the S-H bond followed by radical reaction with a vinyl end group of xDHF resulted in a cross-linked film. Curing was simple and reproducible via exposure to UV light for as little as 1 min. at the polymer's T_g of 85°C. These conditions are notably milder than thermal cross-linking previously reported for 4-phenylethenyl end-capped

poly(fluorene)s.(*9-11*) Extent of cross-linking was monitored qualitatively by a combination of FTIR, film thickness measurements, differential scanning calorimetry (DSC) and film insolubility.

Figure 2.6 shows the FTIR spectra of the xDHF films before and after cross-linking, where the vinyl C-H peaks at 908 cm^{-1} and 988 cm^{-1} as well as the S-H peak of free thiol at 2577 cm^{-1} are all observed to decrease in intensity following curing. This clearly corresponds to a successful click event where a C-S-C linkage is formed between SH-4 and xDHF vinyl end groups.

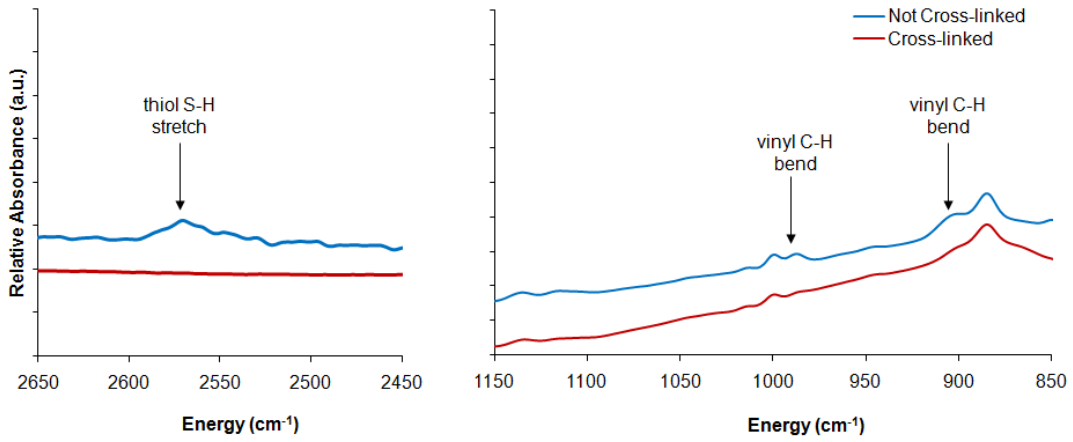

Figure 2.6: FTIR spectra of xDHF films before and after UV cross-linking. The reduction of the vinyl C-H bending peaks and thiol S-H stretching peak is indicative of successful cross-linking through the vinyl end groups of xDHF.

Following successful cross-linking, films were observed to be insoluble in solvents that were good for the pre-cured resin (e.g., THF, $CHCl_3$). However, decreased film thicknesses were observed both immediately after curing and again when rinsed with solvent. Thus, initial decrease in thickness following curing must be due to both shrinkage during network formation, as well as the loss of some non-cross-linked material. Film thicknesses after cross-linking and solvent rinsing are shown in Figure 2.7 as a function of substrate temperature during curing. Reduced film thicknesses observed with decreasing temperature are indicative of material loss due to reduced extent of cross-linking. As the films are heated below T_g (85 °C) during curing, chain mobility is reduced such that the xDHF end-groups are less likely to encounter an active

thiol cross-linker during the brief UV exposure. Curing at 75 °C resulted in a cross-linked film that was roughly half as thick as one cured at 85 °C, and curing at 65 °C showed no measurably cross-linked xDHF film. Curing at temperatures above 85 °C did not significantly increase final film thickness, suggesting that the full extent of cross-linking can be achieved at T_g of the polymer. All processing was well below the polymer's decomposition temperature of 450 °C as measured by thermogravimetric analysis.

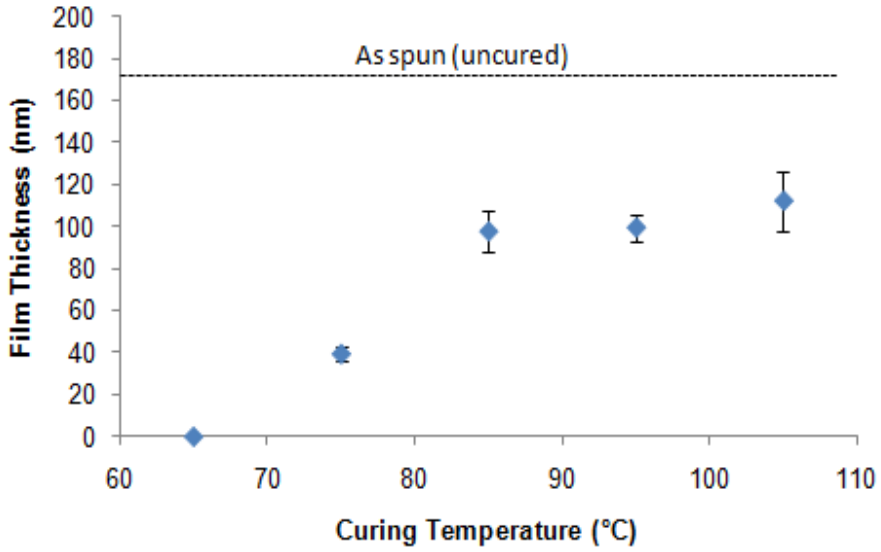

Figure 2.7: Thicknesses of xDHF films as a function of curing temperature. Dashed line shows the initial film thickness as spun from $CHCl_3$ at 2000 RPM.

Cross-linking of xDHF was additionally investigated using photo calorimetry and modulated DSC. Photo calorimetry results (Figure 2.8) show how rapid the UV-initiated reaction occurs, with completion in only 6 seconds upon exposure to 365 nm light (6 mW/cm^2) with the sample held at an isotherm of 85 °C. This is consistent with the very rapid rates of thiol-ene polymerization previously reported.(*24-26*) Curing with 254 nm light, which more efficiently cleaves the S-H thiol bond, would likely lead to even more effective cross-linking. The inset of Figure 2.8 shows high temperature modulated DSC results for a previously UV-cross-linked sample (solid line) and pristine xDHF (dashed line). The exotherm near 150 °C for the pristine

xDHF confirms cross-linking achieved by the auto-initiation of xDHF end-capping groups. The lack of a similar exotherm for the UV-cured xDHF provides further evidence that all accessible cross-linking sites have reacted during UV curing. As evidenced by FT-IR data, it appears that some residual vinyl functionality does exist in the cured xDHF films. Again, the most reasonable conclusion is that once incorporated into the cross-linked network, these unreacted vinyl groups lack the necessary mobility to reach similarly unreacted end groups.

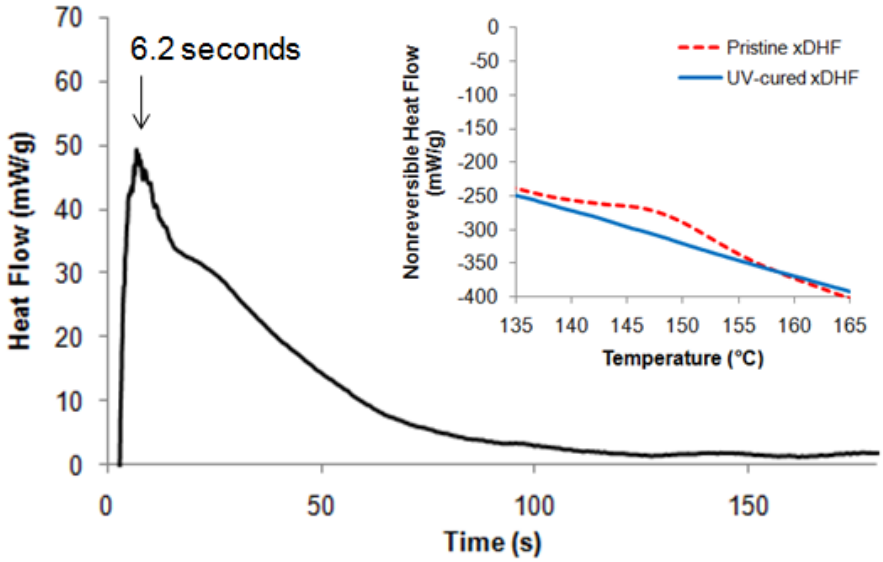

Figure 2.8: Photo DSC response of xDHF with cross-linking thiol upon exposure to 365 nm UV light. Inset: High temperature modulated DSC response of pristine xDHF (dashed line) and UV-cured xDHF (solid line).

The UV-vis absorption and photoluminescence (PL) of the xDHF polymer are shown in Figure 2.9. Both UV-vis absorption and PL were found to red-shift from solution state to solid film, as would be expected upon the formation of lower energy states in the aggregated solid state. Furthermore, UV cross-linking of the xDHF film was not found to adversely affect emissive behavior, with cured and uncured films showing an identical peak emission at 424 nm. In fact, UV curing of the spun films seems to somewhat suppress lower energy emissions, likely due to xDHF chains being locked into a rigid matrix preventing rearrangement to lower energy aggregate states. In order to confirm the advantageous effects of thiol-ene cross-linking on

emissive color stability, various xDHF films were examined under high temperature annealing conditions (Figure 2.10). When annealed in nitrogen for 1 hr at 150 °C, as spun films of pristine xDHF and xDHF mixed with SH-4 both show increasing green emission near 520 nm. Thus the presence of the unreacted small molecule cross-linker is not alone sufficient to inhibit aggregation. Thermally cross-linked films (with no added thiol cross-linker) show a large peak at 520 nm both before and after annealing. Since thermal cross-linking necessitated heating of a pristine xDHF above 150 °C, introduction of lower energy aggregates during the curing procedure is inevitable. Thus it is not surprising that a large amount of green emission is observed in the pre-annealed film. By comparison, UV-initiated thiol-ene cross-linked films show no increased green emission even after high temperature annealing. The low curing temperature coupled with formation of a rigid cross-linked matrix is thus effective at preventing aggregation, consistent with other studies of poly(fluorene) networks.(*9-11*)

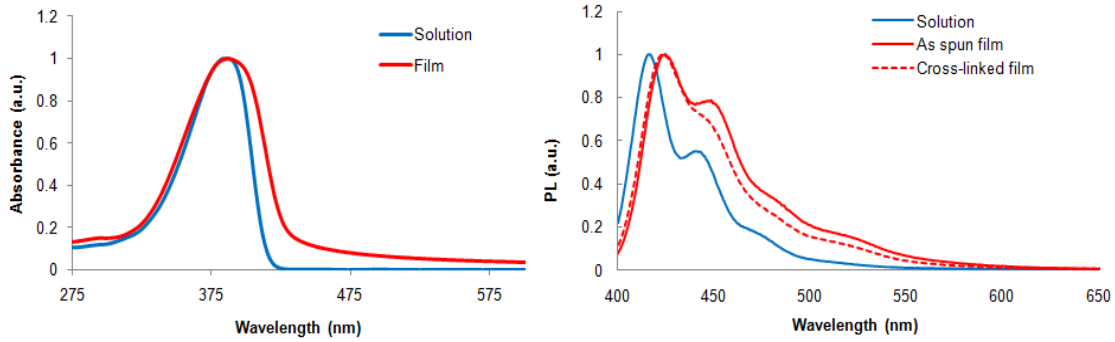

Figure 2.9: UV-vis absorption (left) and photoluminescence (PL) of xDHF in both the solution and solid state. PL is also shown for the thiol-ene cross-linked xDHF film.

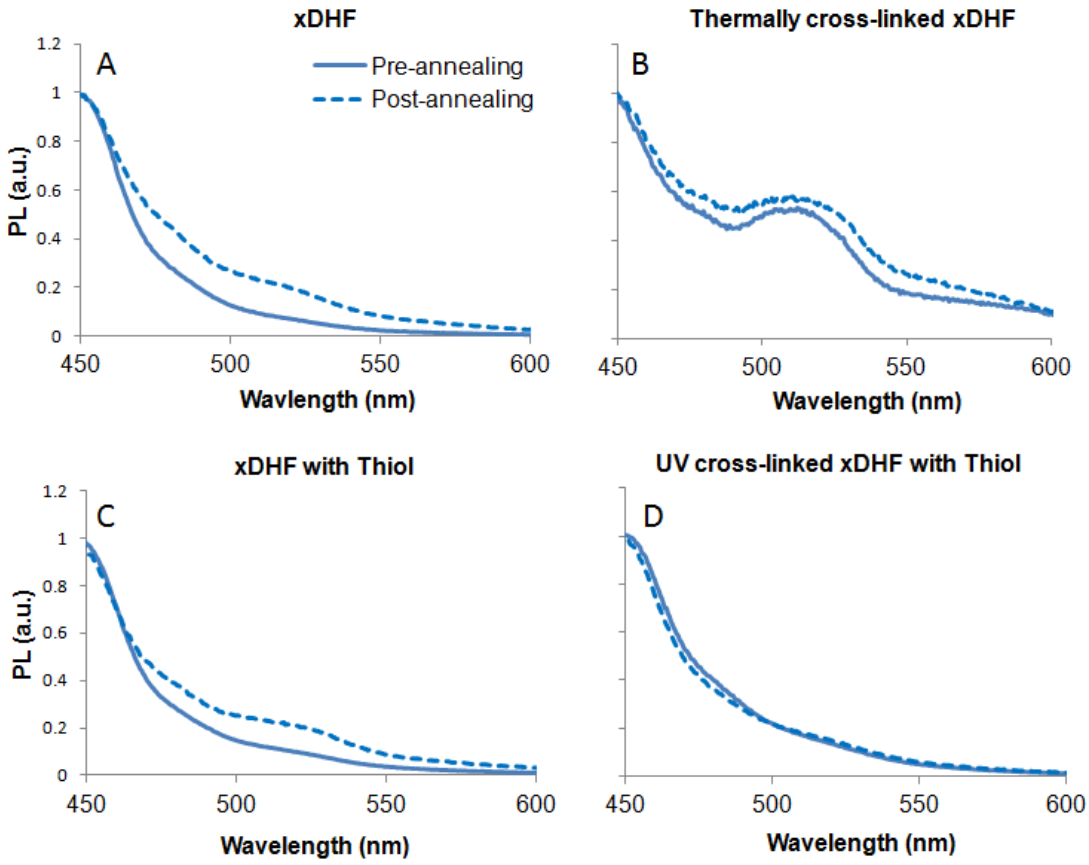

Figure 2.10: Photoluminescence of various xDHF films before (solid lines) and after (dashed lines) annealing at 150 °C under N_2. Spectra are shown for (A) as-spun xDHF, (B) xDHF thermally pre-cured at 200 °C, (C) xDHF film cast with added thiol (no curing), and (D) xDHF film with added thiol pre-cured under UV.

2.3.3 Light Emitting Diodes and Patterned Structures

Thiol-ene cross-linking chemistry is additionally shown to be fully compatible with organic electronic devices. Figure 2.11 and Figure 2.12 show the current density-voltage-luminance (J-V-L) and electroluminescence (EL) behavior of PLEDs fabricated using xDHF as an active layer. Devices were compared using xDHF either directly as spun, cross-linked via UV exposure as described above, or cross-linked thermally at elevated temperatures without added SH-4 (under N_2 by autoinitiation of styrenic end groups).

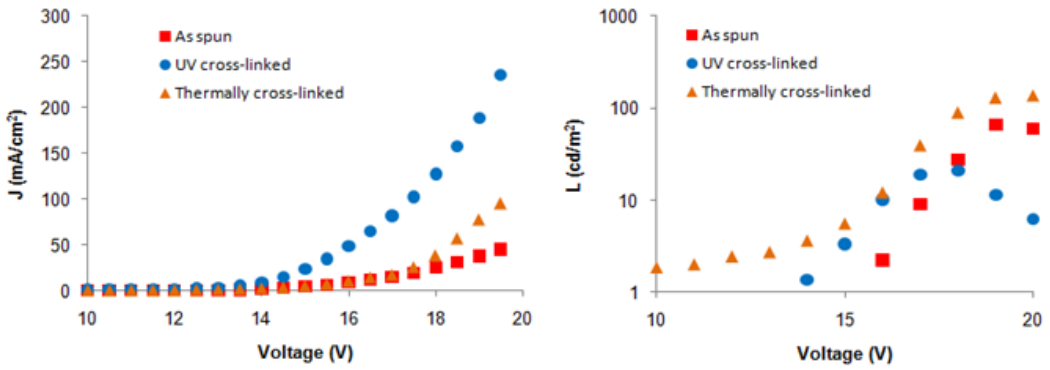

Figure 2.11: Current density (J) and luminance (L) response for PLEDs with xDHF as the active layer as a function of operating voltage. Devices were fabricated with either as spun xDHF, thermally cross-linked xDHF, or UV-initiated thiol-ene cross-linked xDHF.

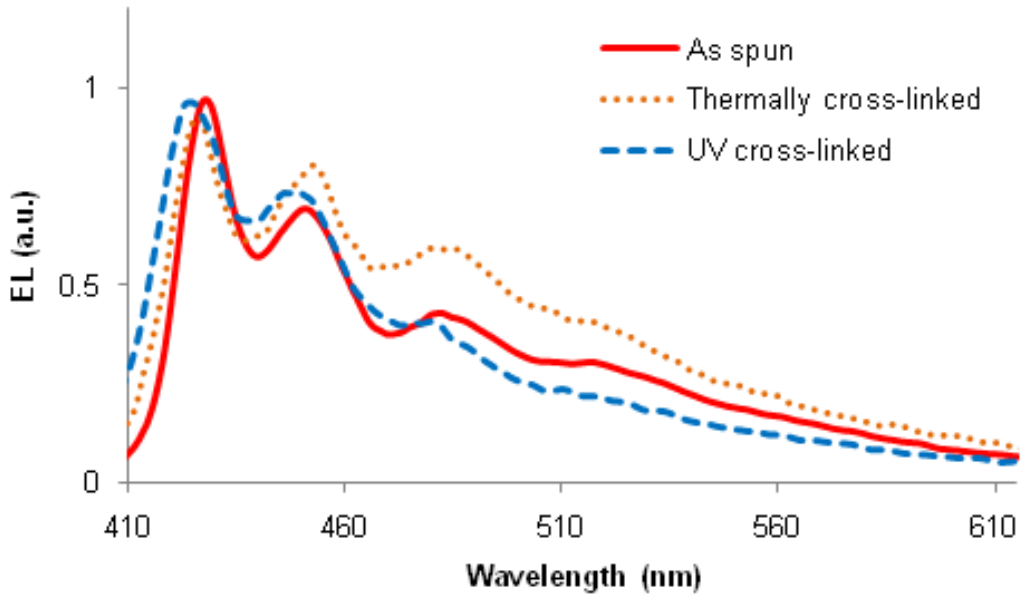

Figure 2.12: Electroluminescence (EL) profiles of various PLEDs using xDHF as the emissive layer. Devices were fabricated with either as spun xDHF, thermally cross-linked xDHF, or UV-initiated thiol-ene cross-linked xDHF. PLED structure was ITO/PEDOT:PSS/xDHF/Ca/Al in all cases.

J-V-L behavior of the PLEDs shows that cross-linking does not significantly affect turn-on voltages of the devices, with all devices turning on near 15 V, a somewhat high operating voltage, but one that is consistent among tested devices. The UV cross-linked xDHF PLEDs were

found to display comparable brightness to as spun or thermally cross-linked devices, especially at lower operating voltages. Device performance would no doubt be improved with further optimization of film and cathode thicknesses. Relatedly, it is possible that higher molecular weight xDHF would also improve device performance. However, this would potentially come at the cost of poorer curing properties due to dilution of the reactive vinyl end groups.

The EL profiles retain the same general lineshape following curing, suggesting that thiol-ene cross-linking does not degrade emissive color. One difference between devices is particularly noteworthy: devices fabricated via thiol-ene cross-linking do not show the increased secondary peak emission that is evident with thermal cross-linking, similar to the above photoluminescent behavior. This undesired green emission has long been reported in poly(fluorene) emission,(*4-6*) and it is not surprising that the high temperature of thermal curing at 200 °C increases its intensity due to the formation of low energy aggregates and/or fluorenone defects. The more moderate temperatures required for UV-initiated thiol-ene chemistry allow for cross-linking of the active film without introduction of this undesired green emission.

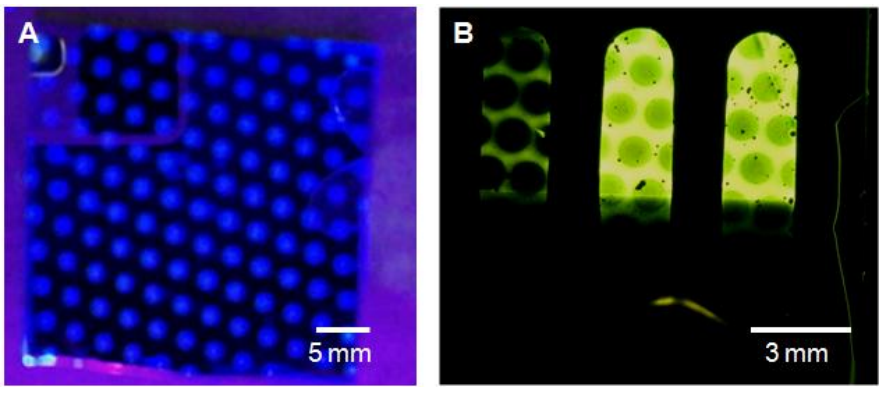

Figure 2.13: Image of a photo-patterned xDHF film on Si (A) and PLED (B) with the device structure ITO/PEDOT:PSS/xDHF(circles)/PFBT/Ca/Al. For PLEDs, emission from only the PFBT regions was observed at lower voltages (left device), while emission across the entire device was seen at larger operating voltages (right two devices).

Finally, the opportunity for using UV curable xDHF as a photo-patternable active layer was demonstrated in both a thin film of xDHF on a silicon wafer and in a multicolor PLED (Figure 2.13) using an arbitrary photo-mask to create patterned CP films. Figure 2.13A shows the resulting fluorescent pattern after cross-linking on Si, where the bright blue regions are areas of cross-linked polymer visibly fluorescing under UV light. Dark regions were masked (and thus not cross-linked) during curing, and the uncured xDHF was easily rinsed away with THF, leaving no emissive polymer. The ability to use a photo-mask to create any desired CP pattern is a significant advantage of the thiol-ene chemistry over thermally activated cross-linking systems.

Using the same photo-mask, circular patterns of xDHF were fabricated on an ITO substrate and a bi-layer device was created via the subsequent spin-coated deposition of poly(dihexylfluorene-co-benzothiadiazole) (PFBT) from chloroform. The preservation of the xDHF patterns after an additional processing step in chloroform (a good solvent for uncured xDHF) further proves their robustness. It is interesting to note that at low operating voltages (< 15 V), electroluminescence was observed only in the PFBT-coated regions (left device, Figure 2.13B). With increased operational voltage (> 15 V), the entire device was seen to emit (right devices, Figure 2.13B). Since single-layer xDHF devices were observed to turn on at approximately 15 V, this behavior is primarily due to differences in energy levels between xDHF and PFBT. As measured by cyclic voltammetry, HOMO/LUMO levels of xDHF were found to be 5.39 and 2.42 eV respectively compared to PFBT HOMO/LUMO energies of 5.9 and 3.2 eV.(*29*) Given the 2.9 eV work function of the calcium cathode, we expect a lower energy barrier for charge carrier injection into the PFBT layer than the xDHF layer. This could explain the partial emission we observed below 15 V.

2.4 Conclusions

The work in this chapter demonstrated the use of UV-initiated thiol-ene cross-linking of 4-phenylethenyl end-capped poly(dihexyl fluorene). This is the first reported use of thiol-ene click chemistry to form cross-linked emissive CP networks. Characteristic of click chemistry, network formation is simple and rapid, with curing accomplished in a matter of seconds at modest temperatures that are not detrimental to emissive color. Furthermore, cross-linking was shown to enhance color stability at high temperature. Additionally, cross-linked CP films are fully compatible with electroluminescent devices, and their performance is comparable to uncured devices. Photo-curing of these films provides the advantage of patternability, and it was shown that an arbitrary pattern can be generated in the xDHF layer by use of a photo-mask (results unachievable with thermally cross-linkable chemistries). This allows for a new chemical avenue toward pixilated multicolor displays. Chapter 3 of this work will investigate this chemistry as applied to lower band gap copolymers, and Chapters 4 and 5 will investigate the effects of alternative cross-linked network architectures on the physical and optoelectronic properties of poly(fluorene) networks.

2.5 References

1. M. Fukuda, K. Sawada, K. Yoshino, Fusible Conducting Poly(9-alkylfluorene) and Poly(9,9-dialkylfluorene) and Their Characteristics, *Jpn. J. Appl. Phys.* **28**, L1433 (1989).

2. Q. Pei, Y. Yang, Efficient Photoluminescence and Electroluminescence from a Soluble Polyfluorene. *J. Am. Chem. Soc.* **118**, 7416-7417 (1996).

3. U. Scherf, D. Neher, in *Advances in Polymer Science*. (Springer, New York, 2008), vol. 212.

4. L. Romaner, A. Pogantsch, P. S. de Freitas, U. Scherf, M. Gaal, E. Zojer, E. J. W. List, The Origin of Green Emission in Polyfluorene-Based Conjugated Polymers: On-Chain Defect Fluorescence, *Adv. Func. Mater.* **13**, 597-601 (2003).

5. K.-H. Weinfurtner, H. Fujikawa, S. Tokito, Y. Taga, Highly efficient pure blue electroluminescence from polyfluorene: Influence of the molecular weight distribution on the aggregation tendency, *Appl. Phys. Lett.* **76**, 2502 (2000).

6. V. N. Bliznyuk, S. A. Carter, J. C. Scott, G. Klärner, R. D. Miller, D. C. Miller, Electrical and Photoinduced Degradation of Polyfluorene Based Films and Light-Emitting Devices, *Macromolecules* **32**, 361-369 (1999).

7. X. Gong, K. I. Parameswar, D. Moses, C. B. Guillermo, A. J. Heeger, S. S. Xiao, Stabilized Blue Emission from Polyfluorene-Based Light-Emitting Diodes: Elimination of Fluorenone Defects, *Adv. Func. Mater.* **13**, 325-330 (2003).

8. W. Zhao, T. Cao, J. M. White, On the Origin of Green Emission in Polyfluorene Polymers: The Roles of Thermal Oxidation Degradation and Crosslinking, *Adv. Func. Mater.* **14**, 783-790 (2004).

9. J. P. Chen, G. Klaerner, J. Lee, D. Markiewicz, V. Y. Lee, R. D. Miller, J. C. Scott, Efficient, blue light-emitting diodes using cross-linked layers of polymeric arylamine and fluorene, *Synth. Met.*, 129-135 (1999).

10. G. Klärner, J.-I. Lee, V. Y. Lee, E. Chan, J.-P. Chen, A. Nelson, D. Markiewicz, R. Siemens, J. C. Scott, R. D. Miller, Cross-linkable Polymers Based on Dialkylfluorenes, *Chem. Mater.* **11**, 1800-1805 (1999).

11. L. D. Bozano, K. R. Carter, V. Y. Lee, R. D. Miller, R. Dipietro, J. C. Scott, Electroluminescent devices based on cross-linked polymer blends, *J. Appl. Phys.* **94**, 3061 (2003).

12. H. Sun, Z. E. Liu, Y. Hu, L. Wang, D. Ma, X. Jing, F. Wang, Crosslinkable Poly(p-phenylenevinylene) Derivative, *J. Polym. Sci. A: Polym. Chem.* **42**, 2124-2129 (2004).

13. G. K. Paul, J. Mwaura, A. A. Argun, P. Taranekar, J. R. Reynolds, Cross-Linked Hyperbranched Arylamine Polymers as Hole-Transporting Materials for Polymer LEDs, *Macromolecules* **39**, 7789-7792 (2006).

14. Y.-H. Niu, M. S. Liu, J.-W. Ka, A. K. Jen, Thermally crosslinked hole-transporting layers for cascade hole-injection and effective electron-blocking / exciton-confinement in phosphorescent polymer light-emitting diodes, *Appl. Phys. Lett.* **88**, 23 (2006).

15. B. B. Ma, B. J. Kim, D. A. Poulsen, S. J. Pastine, J. M. J. Fre, Multifunctional Crosslinkable Iridium Complexes as Hole Transporting / Electron Blocking and Emitting Materials for Solution-Processed Multilayer Organic Light-Emitting Diodes, *Adv. Func. Mater.* **19**, 1024-1031 (2009).

16. E. Scheler, I. Bauer, P. Strohrigl, Synthesis and Photopatterning of Fluorene Based Reactive Mesogens, *Macromolecular SYmposia* **254**, 203-209 (2007).

17. E. Scheler, P. Strohriegl, Tailoring fluorene-based oligomers for fast photopatterning, *J. Mater. Chem.* **19**, 3207-3212 (2009).

18. M. S. Bayerl, T. Braig, O. Nuyken, D. C. Muller, M. Groβ, K. Meerholz, Crosslinkable hole-transport materials for preparation of multilayer organic light emitting devices by spin-coating, *Macromolecular Rapid Comm.* **20**, 224-228 (1999).

19. H. J. Kim, A. R. Han, C. H. Cho, H. Kang, H. H. Cho, M. Y. Lee, J. M. J. Frechet, J. H. Oh, B. J. Kim, Solvent-Resistant Organic Transistors and Thermally Stable Organic Photovoltaics Based on Cross-linkable Conjugated Polymers, *Chem. Mater.* **24**, 215-221 (2012).

20. T. Posner, Beiträge zur Kenntniss der ungesättigten Verbindungen. II. Ueber die Addition von Mercaptanen an ungesättigte Kohlenwasserstoffe, *Berichte der deutschen chemischen Gesellschaft* **38**, 646 (1905).

21. T. Kaneko, On the Simple Synthesis of Methionol (γ-Methlmercapto-propyl Alcohol), *J. Chem. Soc. Jpn.* **59**, 1139 (1938).

22. N. B. Cramer, J. P. Scott, C. N. Bowman, Photopolymerizations of Thiol−Ene Polymers without Photoinitiators, *Macromolecules* **35**, 5361-53-65 (2002).

23. R. K. Iha, K. L. Wooley, A. M. Nystrom, D. J. Burke, M. J. Kade, C. J. Hawker, Applications of Orthogonal "Click" Chemistries in the Synthesis of Functional Soft Materials, *Chem. Rev.* **109**, 5620-5686 (2009).

24. A. B. Lowe, Thiol-ene "click" reactions and recent applications in polymer and materials synthesis, *Polym. Chem.* **1**, 17-36 (2010).

25. C. E. Hoyle, C. N. Bowman, Thiol-Ene Click Chemistry, *Angew. Chem. Int. Ed.* **49**, 1540-1573 (2010).

26. C. E. Hoyle, A. B. Lowe, C. N. Bowman, Thiol-click chemistry: a multifaceted toolbox for small molecule and polymer synthesis, *Chem. Soc. Rev.* **39**, 1355-1387 (2010).

27. E. C. Hagberg, M. Malkoch, Y. Ling, C. J. Hawker, K. R. Carter, Effects of Modulus and Surface Chemistry of Thiol-Ene Photopolymers in Nanoimprinting, *Nano Letters* **7**, 233-237 (2007).

28. T. A. Skotheim, J. R. Reynolds, *Handbook of Conducting Polymers*. (CRC Press, Boca Raton, FL, 2007).

29. A. J. Campbell, D. D. C. Bradley, H. Antoniadis, Dispersive electron transport in an electroluminescent polyfluorene copolymer measured by the current integration time-of-flight method, *Appl. Phys. Lett.* **79**, 2133 (2001).

CHAPTER 3

APPLICATIONS FOR END-CHAIN CROSS-LINKABLE CONJUGATED POLYMERS[†]

3.1 Introduction

Cross-linked films of conjugated polymers (CPs) have been a topic of considerable interest in the past few decades.(1-6) The attractiveness of CPs as highly processable semiconducting materials for light-emitting, solar energy harvesting, and electronic applications largely stems from their solution processibility.(7-10) This property allows for easy spin-coating, spraying, and inking of films directly onto a variety of rigid and flexible substrates. However, the same ease of solution processing leads to difficulties in building multilayer and patterned devices, which can greatly improve device performance.(11, 12) Covalent cross-linking of CP films offers one solution to this problem.(13) By making the semiconducting layers robust and solvent-resistant after processing, a path is opened for more complicated fabrication processing. Additionally, the "locking" of polymer chains into position has been shown to improve certain electronic characteristics by significantly reducing their tendency to re-align during device operation.(14) Cross-linking also enables the incorporation of a wide range of chemical functionality that can be imbedded in the polymer during curing.

Figure 3.1 shows an example using cross-linkable CPs with varying emissive color for multilayer solution-processed light emitting diodes, where the effect of layer order plays a dramatic role in determining the final observed device color.(*15*) For this reason, it is clearly desirable to have a wide range of cross-linkable CPs so that processing order is not limited by which materials can be made insoluble by cross-linking.

[†] Portions of this chapter have been reprinted with permission from Koyuncu, Davis, Carter, *Chem. Mater. 24*, 4410 (2012). Copyright 2012 American Chemical Societry.

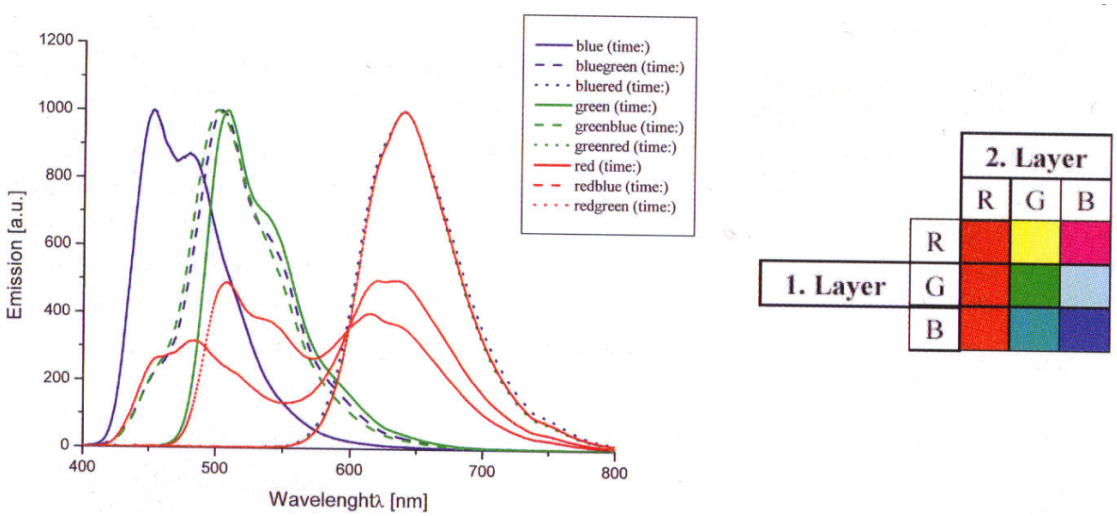

Figure 3.1: Effect of layering order on the observed color of cross-linked multilayer polymer light emitting diodes. Figure reproduced with permission from Klaus Meerholz in *Organic Light Emitting Devices. Synthesis, Properties and Applications.,* p. 309, 2006. Copyright Wiley-VCH Verlag GmbH & Co. KGaA.(*15*)

This chapter aims to investigate thiol-ene cross-linked CPs with variable band gaps and emissive colors by the introduction of heterocycles in the CP backbone. Chapter 2 described the first use of thiol-ene click chemistry to form electroluminescent networks from a poly(dihexyl fluorene) homopolymer.(*16*) However, with only a blue-emitting cross-linkable polymer, fine tuning of devices' energy levels by mixing or layering with other CPs was very limited. The thiol-ene literature has clearly established that the electron withdrawing or donating effects of heteroatoms and extended conjugation can greatly affect the rates and efficiencies of the photo-induced thiol-ene click reaction.(*17*) These same heteroatoms, when incorporated into aromatic rings, are perhaps the most popular method for tuning the band gaps and optoelectronic properties of CPs.(*18, 19*) For this reason, this chapter details the concerns of achieving effective thiol-ene cross-linking with CPs incorporating heterocycles for optoelectronic tuning. Emission from newly synthesized and cross-linked polymers incorporating heterocycles is shown to cover the entire visible range, with device performances equal to non-cross-linked devices.

3.2 Experimental Section

3.2.1 Materials

4-Bromostyrene, 9,9-dioctyl-9H-fluorene-2,7-diboronic acid bis(1,3-propanediol) ester, 2,1,3-benzothiadiazole, 1H-benzotriazole, tetrahydrofuran (THF), (4-vinylphenyl)boronic acid, tetrakis(triphenylphosphine)palladium(0) ($Pd(PPh_3)_4$), sodium carbonate (Na_2CO_3), hydrobromic acid (HBr), bromine (Br_2), sodium borohydride ($NaBH_4$), selenium dioxide (SeO_2), 1-bromohexane, potassium tert-butoxide ($(CH_3)_3COK$) and poly(3,4-ethylenedioxythiophene)/poly(styrene sulfonate) (PEDOT:PSS) were purchased from Sigma-Aldrich Company. All reagents were used as received unless otherwise noted. Silicon substrates were purchased from University Wafers. Indium tin oxide (ITO)-coated glass was purchased from Thin Film Devices, Inc. (sheet resistance 20 Ω/sq). All reactions were run under dry N_2 unless otherwise noted. The monomers, 4,7-dibromo-2,1,3-benzothiadiazole,(*20*) 4,7-dibromo-2,1,3-benzoselenadiazole,(*21, 22*) and 4,7-dibromo-2-hexyl-2H-1,2,3-benzotriazole(*23*) were prepared by previously published procedures.

3.2.2 Instrumentation

All nuclear magnetic resonance (NMR) spectra were acquired on a Bruker Avance 400 (400MHz) spectrometer and internally referenced via residual solvent signal [$CHCl_3$: ^{1}H 7.26 ppm; ^{13}C 77.00 ppm]. All chemical-shift values are given in ppm. Gel permeation chromatography (GPC) was performed in THF at room temperature with 1.0 mL/min elution rate. A Waters R403 differential refractometer and three PL gel columns (105, 104, and 103 Å) calibrated with narrow molecular weight polystyrene standards were used. Differential scanning calorimetry (DSC) was performed on a Thermal Analysis (TA)Q-2000 in T-zero aluminum pans using modulated DSC at a heating rate of 3 °C/min. Thermal gravimetric analysis was performed

using a Perkin-Elmer TGS-2, under nitrogen atmosphere with a heating rate of 10 °C/min. Film thicknesses were measured by contact profilometry using a Dektak 150 profilometer. UV-Vis spectra were recorded in 1-cm path length quartz cuvettes by using a Shimatszu UV 3600 spectrophotometer. Fluorescence measurements were taken on a PTI QM-30 spectrophotometer. CV measurements were taken on BAS Epsilon electrochemical workstation. These measurements were carried out under argon atmosphere, and the electrochemical cell included an Ag wire as reference electrode, Pt wire as counter electrode and glassy carbon as working electrode immersed in 0.1 M tetrabutylammonium hexafluorophosphate ($TBAPF_6$) as the supporting electrolyte.

Photo calorimetry was performed using the above TA Q-2000 instrument with a TA photocalorimeter accessory (PCA) using a 365 nm UV source. Photo calorimetry response was measured at a constant temperature of 90 °C with 6 mW/cm^2 exposure intensity (identical to thin film curing conditions). The instrument was calibrated by running a model UV-initiated thiol-ene reaction of 9-vinylcarbazole with pentaerythritol tetrakis(3-mercaptopropionate). Extent of reaction calculated from heat flow in the photo calorimeter agreed with extent of reaction found by NMR measurement of the model system following curing.

3.2.3 Synthesis of Styrene End-Capped Tunable Band Gap Polymers (xPFN, xPFS, xPFSe)

The synthetic pathway for the cross-linkable conjugated copolymers is shown in Figure 3.1. The copolymers were synthesized utilizing 9,9-dioctyl-9H-fluorene-2,7-diboronic acid bis(1,3-propanediol) ester in the presence of dibromo benzodiazole-based heterocycles using conventional Suzuki coupling polymerization. For example, dibromo monomer (1 mol equivalent), 9,9-dioctyl-9H-fluorene-2,7-diboronic acid bis(1,3-propanediol) ester (1 mol equivalent), and $Pd(PPh_3)_4$ (5 mol%) were added into a degassed mixture of aqueous sodium

carbonate (K_2CO_3, 2M in H_2O) and THF (4:1 THF:water). The mixture was refluxed at 80 °C for 12 h under nitrogen. 4-Bromostyrene (0.123 mol equivalent) was added to the reaction as an end-capping reagent and refluxed 4 hours. Finally, 4-vinylphenyl boronic acid (0.123 mol equivalent) was added as the second end-capping reagent and stirred for another 4 hours. At the end of the reaction, the reaction mixture was cooled to room temperature, filtered, and poured into a large volume of methanol. The precipitated polymer was filtered again and dried in a vacuum oven. For final purification, soxhlet extraction was performed with methanol and then chloroform for 24 h.

xPFN: ^{1}H NMR (400 MHz, $CDCl_3$) δ 8.24-7.31 (C-H, aromatic); 6.76, 5.84, 5.28 (dd 1H, d 1H, d1H, vinyl end-caps); 4.85 (N-CH2); 2.24-0.79 (C-H, alkyl chain).

xPFS: ^{1}H NMR (400 MHz, $CDCl_3$) δ 8.42-7.40 (C-H, aromatic); 6.79, 5.86, 5.32 (dd 1H, d 1H, d1H, vinyl end-caps); 2.13-0.75 (C-H, alkyl chain).

xPFSe:^{1}1H NMR (400 MHz, $CDCl_3$) δ 8.08-7.33 (C-H, aromatic); 6.86, 5.88, 5.34 (dd 1H, d 1H, d1H, vinyl end-caps); 2.11-0.80 (C-H, alkyl chain).

3.2.4 Cross-Linking of Conjugated Polymer Thin Films

Cross-linking was achieved using a solution of the cross-linkable polymer and tetra-functional cross-linker pentaerythritol tetrakis(3-mercaptopropionate) at a molar ratio of 2:1 thiol:vinyl functional groups as determined by ^{1}H NMR. Solutions were prepared at 10 mg/mL of polymer in a 1:1 mixture of $CHCl_3$ and toluene. Solutions were then spin-coated on silicon substrates at 2000 rpm for 60 seconds and illuminated by a handheld UV lamp (365 nm, 6 mW/cm2) for 2 minutes under N_2 atmosphere at 90°C. The resulting films were then rinsed with $CHCl_3$ to remove uncured material.

3.2.5 Device Fabrication and Characterization

Polymer light emitting diodes (PLEDs) were fabricated on indium-tin-oxide (ITO)-coated glass using the cross-linkable polymers with general device structure of ITO/PEDOT:PSS (20 nm)/polymer(s)/Ca (30 nm)/Al (100 nm). ITO was first cleaned by sonication in three sequential solvents (water, acetone, isopropanol), followed by 2 minutes of O_2 plasma treatment. A mixture of PEDOT:PSS and a small amount of DMSO (1 wt%) was spin-coated on the ITO at 4000 RPM, and the substrates were baked at 150°C for 1 hr. Polymer solutions with pentaerythritol tetrakis(3-mercaptopropionate) (composition same as above section) were then immediately spin-coated on the substrates at 3000 RPM. They were then either placed immediately under vacuum in the case of non-cured devices, or they were cross-linked as described above, rinsed with $CHCl_3$, and then placed under vacuum (cured devices). Cross-linked devices were then illuminated by a handheld UV lamp for 2 minutes under N_2 atmosphere at 90°C and rinsed with chloroform. For multilayer devices, additional polymer layers were spin-coated over the previously cured layer, illuminated by UV with the same conditions, and rinsed with $CHCl_3$. Coated substrates were then placed in vacuum overnight. Non-cross-linked substrates were simply placed under vacuum with no UV or rinsing treatment. Devices were completed by the thermal evaporation of calcium (30 nm) and aluminum (100 nm) at pressure $<10^{-5}$ Torr. Devices were tested in air using a Kiethley 2602 Sourcemeter and a calibrated Ocean Optics USB4000 UV–Vis spectrometer.

3.3 Results and Discussion

3.3.1 Synthesis

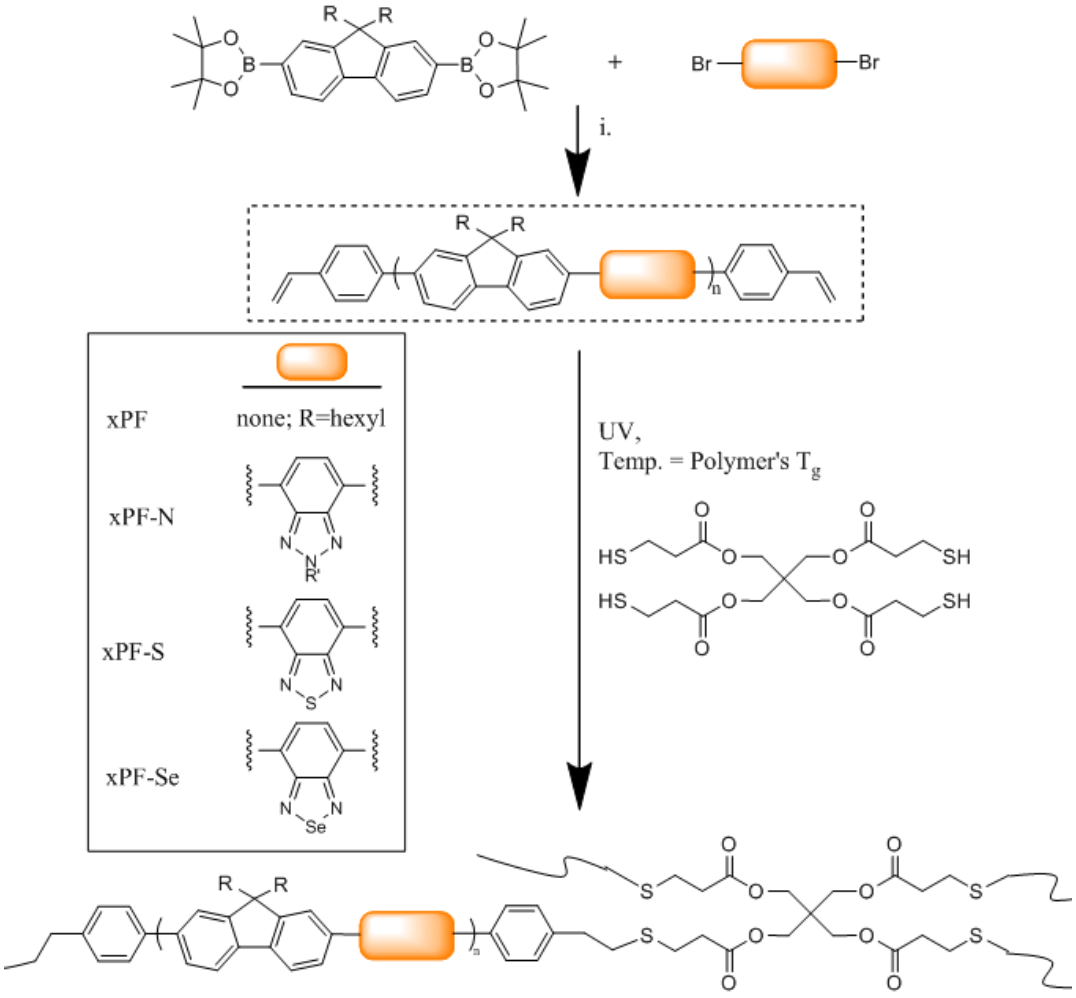

Figure 3.2: Synthetic schemes for creating thiol-ene cross-linkable conjugated polymers with tunable band gaps (dashed box) and subsequent cross-linking conditions to form conjugated networks. i.) $Pd(PPh_3)_4$, K_2CO_3, H_2O/THF, reflux 12 hr; 4-bromostyrene, reflux 4 hr; 4-vinyl phenyl boronic pinacol ester, reflux 4 hr. R = octyl; R' = hexyl, unless noted otherwise.

Figure 3.2 shows the thiol-ene cross-linking scheme similar to that described in Chapter 2 for building conjugated polymers networks with tunable band gaps. In this instance, donor-acceptor copolymers were synthesized using standard Suzuki cross-coupling polymerization and end-capped with styrenic units. For comparison, styrene end-capped poly(dihexyl fluorene) homopolymer (xPF) was synthesized as previously described.(*16*)

A major advantage of this synthetic approach is its relative simplicity. New monomers do not need to be arduously synthesized. Instead, conventional boronic ester-functionalized dialkyl fluorene and dibromo benzodiazole-based heterocyclic monomers used in standard coupling polymerizations can be directly employed. In these experiments, the dibromo benzodiazole-based heterocycles were chosen for their ease of tuning the polymers' band gap by simple substitution at the 2-position. Pd-catalyzed Suzuki coupling polymerizations were used to synthesize all reported polymers, with vinyl end-group functionality installed by adding 4-bromostyrene and 4-vinylphenyl boronic acid at the end of the reaction. This route should be compatible with all similar metal-catalyzed coupling polymerizations (e.g., Suzuki, Sonogashira, etc.).

Physical properties of the polymers are summarized in Table 3.1. The structure and molecular weight of uncured polymers were determined from ^{1}H NMR and gel permeation chromatography (GPC). ^{1}H NMR of synthesized poly(fluorene)-based tunable band gap polymers exhibited the desired products with clearly visible vinylic proton resonances (δ = 5.30, 5.86, 6.79 ppm) from the end-groups. Molecular weight and degree of polymerization (DP) of polymers were calculated by taking the ratio of these vinylic proton signals to the methylene proton of the 9-position octyl chain α to the fluorene backbone [-(**CH_2**)-$(CH_2)_6$-CH_3], similar to the previous chapter. Comparing M_n calculated from ^{1}H NMR and GPC, the degree of polymerization determined by GPC is larger (Table 3.1). This discrepancy can be explained by the rigid nature of the tunable band gap polymers compared to that of the polystyrene GPC standards. The molecular weight was purposely kept low to allow for greater cross-linking density (since cross-linking occurs at the chain ends). Upon adding acceptor molecules, the T_g of the polymers decreases moderately (compared to the fluorene homopolymer). The values were measured as 85°C, 80°C, 68°C, and 73°C for xPF, xPFN, xPFS and xPFSe respectively. The enhanced molecular

mobility along the chain axes arising from the varying heteroatom sizes likely increases the chain mobility and decreases T_g values. Thus S- and Se- containing polymers exhibit different glass transitions determined by the bulkiness of the pendant group.

Table 3.1: Physical properties of synthesized 4-phenylethenyl end-capped polymers. [a]Degree of polymerization (DP) calculated from NMR data. [b]Decomposition temperature reported for 5% weight loss by thermogravimetic analysis.

Polymer	GPC			DP[a]	T_g (°C)	Decomposition Temp. (°C)[b]
	M_n (10^3 g/mol)	M_w (10^3 g/mol)	PDI			
xPF	10.4	24.0	2.31	13	85	419
xPFN	4.7	12.1	2.55	5	80	400
xPFS	6.1	11.8	1.92	8	68	386
xPFSe	2.8	6.6	2.37	3	73	359

3.3.2 Optical and Electrochemical Properties.

Table 3.2: Electrochemical and optical characteristics of synthesized cross-linkable polymers. [a]PF data reproduced from previous report on thiol-ene cross-linkable poly(dihexyl fluorene).(*16*) *Calculated by the subtraction of the optical band gap from the HOMO level.

Polymer	Reduction Onset Potential (V)	Oxidation Onset Potential (V)	HOMO (eV)	LUMO (eV)	Electrochem. Band Gap (eV)	Optical Band Gap (eV)
xPF[a]	-	1.26	-5.54	-2.71*	-	2.83
xPFN	-1.52	1.27	-5.55	-2.79	2.76	2.60
xPFS	-1.17	1.41	-5.69	-3.11	2.58	2.48
xPFSe	-1.03	1.45	-5.73	-3.25	2.48	2.29

A summary of the optical and electrochemical band gaps of the polymers in this chapter is shown in Table 3.2, as determined from both UV-Vis (Figure 3.3) and cyclic voltammetry (CV) (Figure 3.4) data. Table 3.2 shows successful control over the band gap of the various semiconducting polymers achieved by the substitution on the heterocyclic ring. The optical band gap (E_g) values were calculated from their low energy absorption edges (λ_{onset}) where $E_g = 1241/\lambda_{onset}$.(*24*) LUMO energy levels were calculated by the addition of the optical band gap to the HOMO level. Electrochemical HOMO and LUMO energy levels of the polymers were

calculated according to the inner reference ferrocene redox couple E°(Fc/Fc+) = +0.52 V (vs. Ag wire) in dichloromethane by using the formula $E_{HOMO} = -e(E_{ox} - E_{Fc}) + (-4.8\ eV)$ where E_{ox} is the measured potential of oxidation onset and E_{Fc} is the ferrocene redox potential.(*25*)

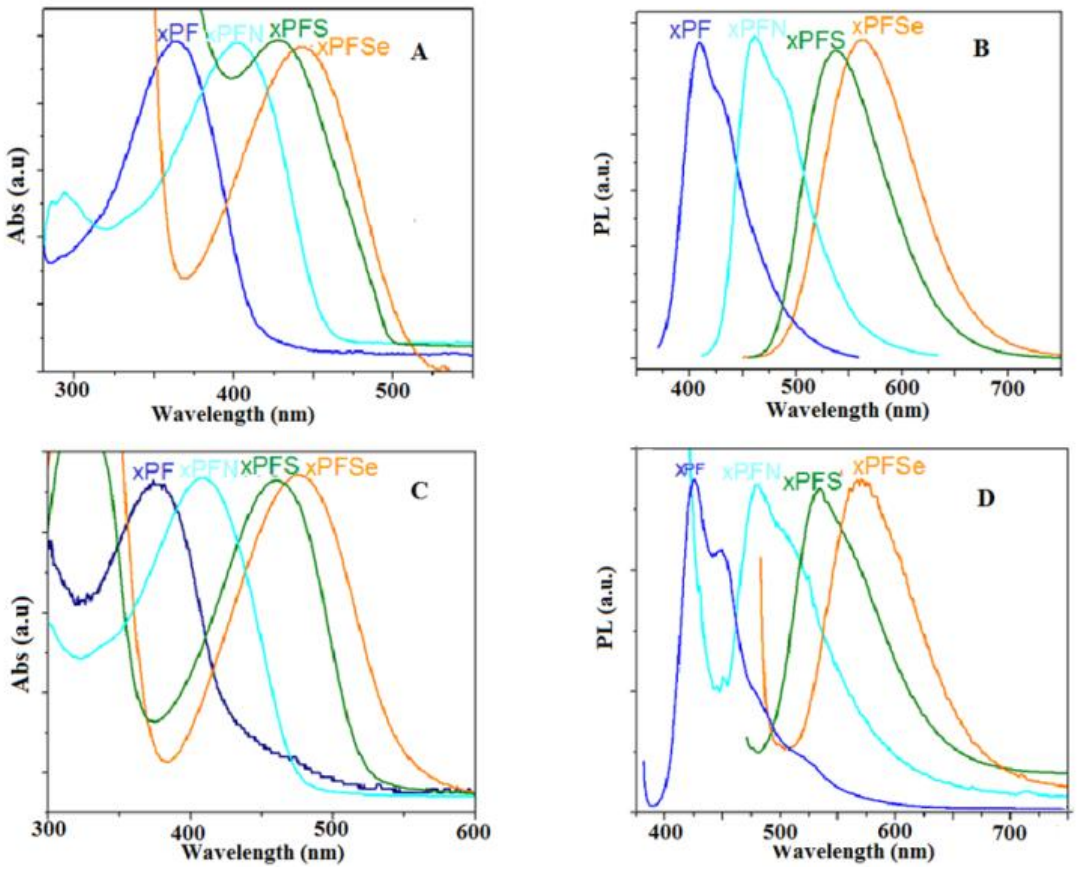

Figure 3.3: UV-Vis and photoluminescence of the 4-phenylethenyl end-capped conjugated polymers in solution (A,B) and thin film (C,D) states.

The UV-Vis absorption and photoluminescence (PL) of the pristine polymers are shown in Figure 3.3 both for solution and thin film states. The acceptor moieties on the polymer chain influenced the absorption bands of the polymers significantly, as confirmed by CV measurements. The broad featureless peak absorption wavelength λ_{max} originates from the intramolecular charge transfer interaction between the electron donor fluorene and all electron acceptor moieties.(*21, 26*) Due to the formation of fluorene-donor and benzodiazole-acceptor conjugated structure, characteristically broad charge transfer bands were observed at 402 nm,

427 nm, and 441 nm respectively for xPFN, xPFS and xPFSe in the UV-Vis absorption spectra. A greater red shift was observed in the charge transfer band of xPFSe in comparison to xPFN and xPFS due to the weaker electron-withdrawing character of selenium.(*27-29*) Similar results were obtained from the fluorescence measurements. Excitation at the polymers' absorption maxima (λ_{max}= 402 nm for xPFN, λ_{max}= 427 nm for xPFS, and λ_{max}= 441 nm for xPFSe) resulted in strong emission bands peaking at 460 nm, 537 nm and 562 nm with Stokes' shifts of 58 nm, 110 nm and 121 nm, respectively. While benzotriazole-based xPFN polymer showed cyan emission color, the benzothiadiazole and benzoselenadiazole based polymers showed yellow-green and orange emission colors, respectively. UV-Vis and photoluminescence of the synthesized polymers are in agreement with literature data for the same polymer structures without 4-phenylenthenyl end-capping.(*26, 30, 31*) Thus, starting with the blue emission of poly(fluorene), color was tuned across the visible spectrum by the substitution of different acceptor moieties. Additionally, typical red shifting was observed on the polymer coated films in both UV-Vis absorption and PL measurements due to solid state aggregation and π-π stacking effects.

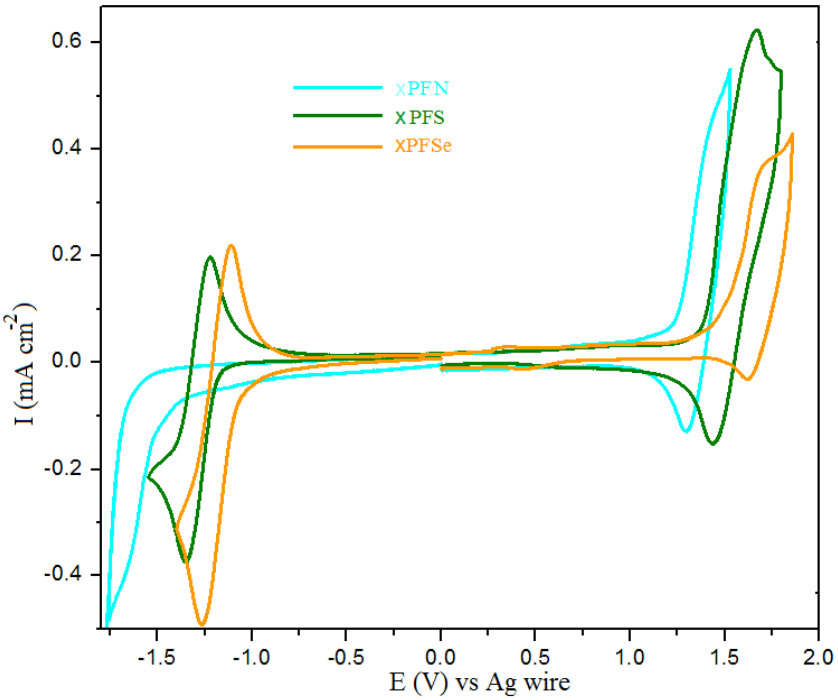

Figure 3.4: Cyclic voltammograms of the 4-phenylethenyl end-capped conjugated polymers.

As expected, the electrochemistry measurements shown in Figure 3.4 are in agreement with the UV-vis data above. The role of the acceptor units on the redox behavior of poly(fluorene)-based doner/acceptor systems were investigated by cyclic voltammetry measurements in 0.1 M tetrabutylammonium hexafluorophosphate ($TBAPF_6$) dissolved in methylene chloride. It was found that these systems exhibited both anodic and cathodic redox behaviors. During anodic scans, xPFN, xPFS and xPFSe exhibited semi-reversible oxidation waves with onset potentials observed at 1.27 and 1.41 and 1.45 V, respectively. The higher oxidation potential of xPFSe was attributed to higher electron attraction as compared to xPFS and xPFN.

During cathodic scans, the reduction potentials were strongly influenced by the electron-withdrawing character of the heteroatoms of the acceptor moieties. xPFS and xPFSe had good reversible reduction couples at -1.35/-1.22V and -1.27/-1.12V while xPFN showed an irreversible peak at -1.86V. The larger observed negative peak potential for the formation of radicalic anions of xPFN can be ascribed to higher electron density of the acceptor group when

compared to xPFS and xPFSe. These results clearly suggested that the acceptor moiety in xPFN, xPFS and xPFSe polymers play a key role in tuning the polymers' redox behavior and the interaction between donor and acceptor components of the system.

3.3.3 Thin Film Thiol-Ene Cross-Linking

Illustration of thin film cross-linking chemistry is shown in Figure 3.2. Briefly, thiol-ene cross-linking of 4-phenylethenyl functionalized polymers was accomplished by first spin coating a thin film (ca. 50 nm) from a solution containing both the cross-linkable polymer and tetra-functional thiol cross-linker pentaerythritol tetrakis(3-mercaptopropionate). After spin-coating the film was then heated to just above its T_g in order to promote chain mobility(*16*) and exposed to 365 nm UV light at 6 mW/cm^2 for 2 minutes. Cross-linking was confirmed qualitatively by rinsing the cured films with chloroform or THF (both are good solvents for the uncured polymers). The thiol-ene cross-linked polymer films were found to be insoluble in these solvents. Furthermore, FT-IR measurements confirmed thiol-ene reaction with reduction in both the vinyl C-H and thiol S-H signals. As observed previously with xPF,(*16*) thiol-ene cross-linking did not significantly affect the UV-Vis and photoluminescent characteristics of the polymers.

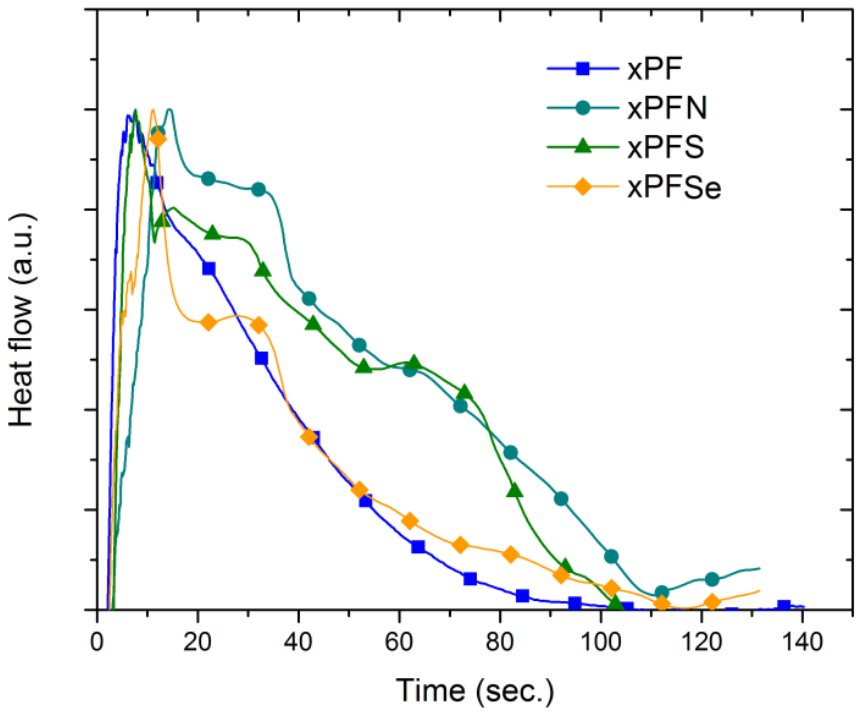

Figure 3.5: Photo calorimetry response of the thiol-ene cross-linking of the conjugated polymers during UV curing. Lamp turn-on is at t=0 seconds.

Thiol-ene network formation was also monitored using photo calorimetry, shown in Figure 3.5. Upon UV exposure, all network-forming systems reached peak heat flow (maximum polymerization rate) in less than 20 seconds, which corresponds well with the known timescale of UV-initiated thiol-ene reactions.(*32-36*) The similarity of curing kinetics between these conjugated polymers and previously known non-conjugated thiol-ene systems suggests that a rigid conjugated molecule does not hinder thiol-ene reaction. The slight differences in curing time can be attributed to the dynamics of each individual system (i.e. different molecular weight, T_g, etc.). Curing appeared to be independent of the individual polymer matrices' absorption of 365 nm light considering their varied absorption to the exposure wavelength (see Figure 3.3). The photo calorimetry curves are not entirely smooth, which can be attributed to measurement artifacts due to the difficulty in accurately measuring the small heat flows of the considerably low mass thin film samples.

Calculating the heat evolved during photo reaction and comparing it to the known heat of reaction for thiol-ene polymerizations revealed that all networks here reached less than 10% total thiol-ene conversion. The presence of residual vinyl and thiol signals in FT-IR measurements corroborates this observation. Low thiol-ene conversion is a topic for future investigations, which we initially suspect is due to the solid-state, solvent free conditions of thiol-ene reaction. As discussed here, regardless of the low conversion, cross-linked films were still found to be solvent resistant and amenable for device applications.

3.3.4 Polymer Light-Emitting Diodes

Polymer light emitting diodes (PLEDs) were fabricated from the 4-phenylethenyl functionalized polymers with the general structure ITO/PEDOT:PSS (20 nm)/polymer/Ca (30 nm)/Al (100 nm). Figure 3.6 shows the electroluminescence (EL) spectra of PLEDs with a single cross-linked emissive polymer layer along with photographs of the cross-linked single-layer devices during operation. A wide range of the color space was accessible using just the four cross-linkable polymers synthesized in this report. Thiol-ene cross-linking was not found to affect the PLEDs' emissive colors, showing negligible changes in EL spectra from non-cross-linked PLEDs fabricated using the analogous polymers (Figure 3.7).

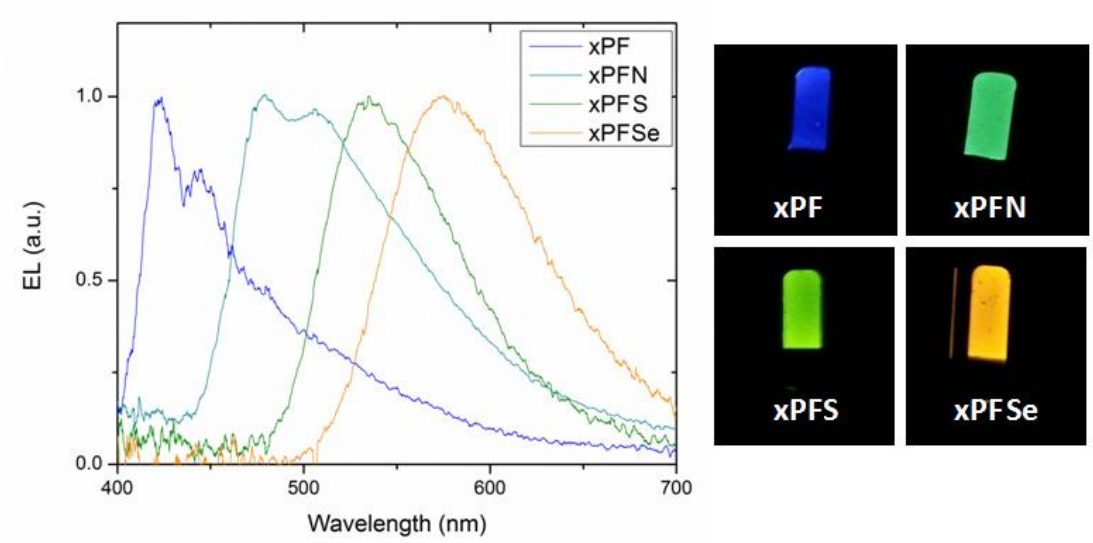

Figure 3.6: Electroluminescence (EL) spectra and photographs of PLEDs consisting of single layer cross-linked polymers.

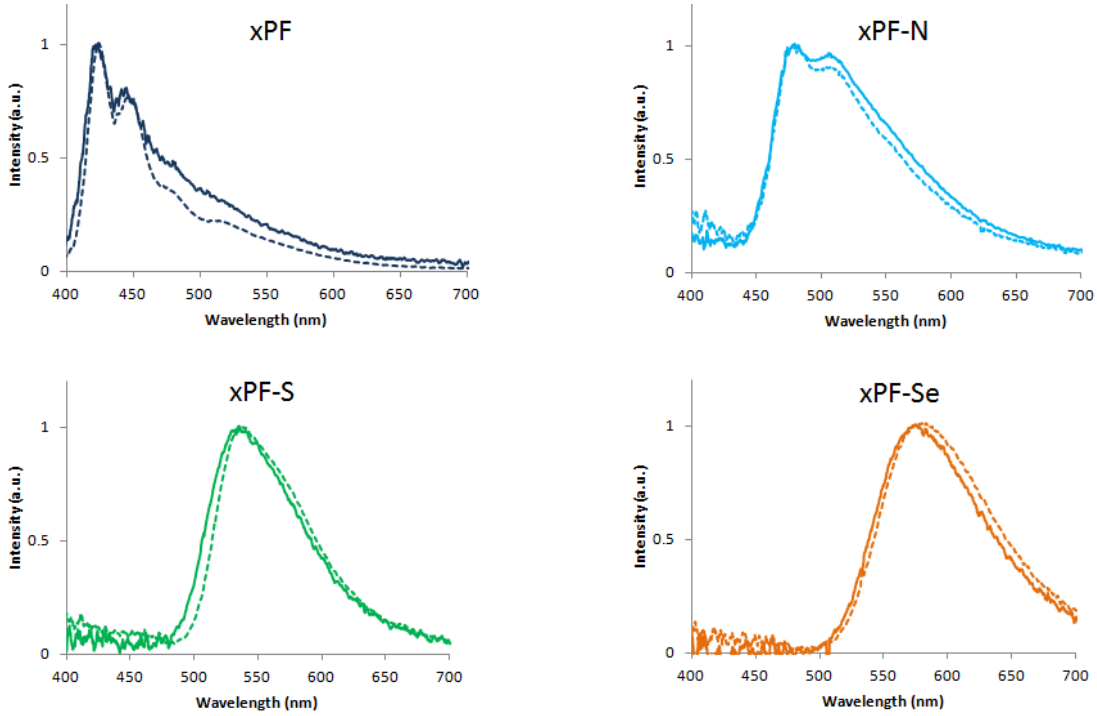

Figure 3.7: Comparison of electroluminescence (EL) spectra between cross-linked (solid) and non-cross-linked (dashed) PLEDs.

Current density-voltage-luminance (J-V-L) response of the same single layer PLEDs is shown in Figure 3.8. All devices required 8 V or less to turn on. Briefly, xPFN and xPFS gave the best performances (lowest turn-on voltage and highest brightness), likely due to the close

alignment of their LUMO levels (3.1 and 2.8 eV, respectively) with the work function of the calcium cathode (2.9 eV). Their greater affinity for electron transport also likely improved current density and brightness. We observe that xPF and xPFN PLEDs have nearly identical performance before and after thiol-ene cross-linking, but xPFS and xPFSe devices appear to be affected by cross-linking. Both xPFS and xPFSe devices show increased current density when cross-linked, with minimal changes in brightness.

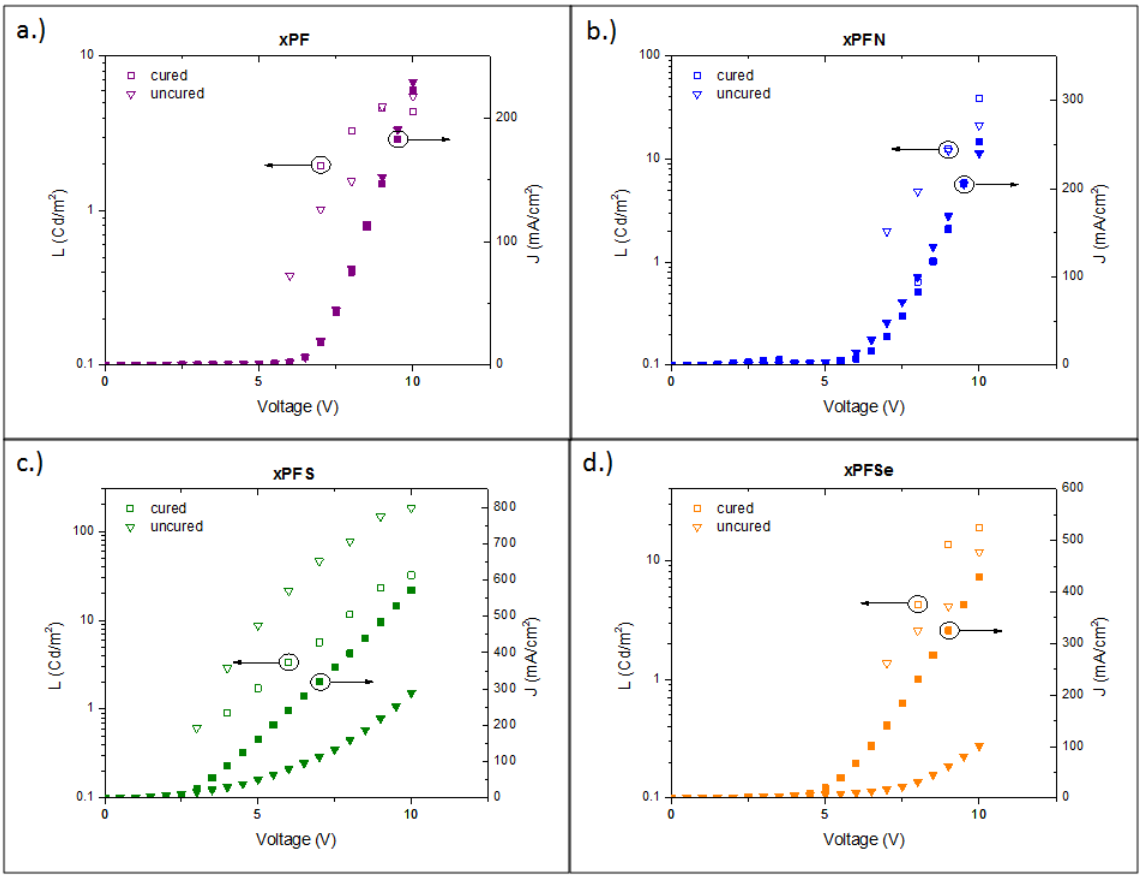

Figure 3.8: Comparison of J-V-L behavior between cross-linked (squares) and non-cross-linked (triangles) PLEDs fabricated from a) xP-F b) xPF-N, c) xPF-S, and d) xPF-Se.

The wide range of band gaps now available as cross-linkable semiconducting moieties offered the capability to fabricate more complex device architectures. To exploit this opportunity, the robust electroluminescent films were used to build multilayer devices by solution processing. Blending of multiple emissive species is one way to achieve white and

multicolor emission in PLEDs. However, blended active layers often result in energy transfer to the low energy emissive states (usually the emitter with the smallest band gap) which can lead to bathochromic shifts in electroluminescence or even complete quenching of emission. A multilayered emissive architecture would alleviate this problem by separating different emitting species, reducing charge transfer processes.(*37-39*)

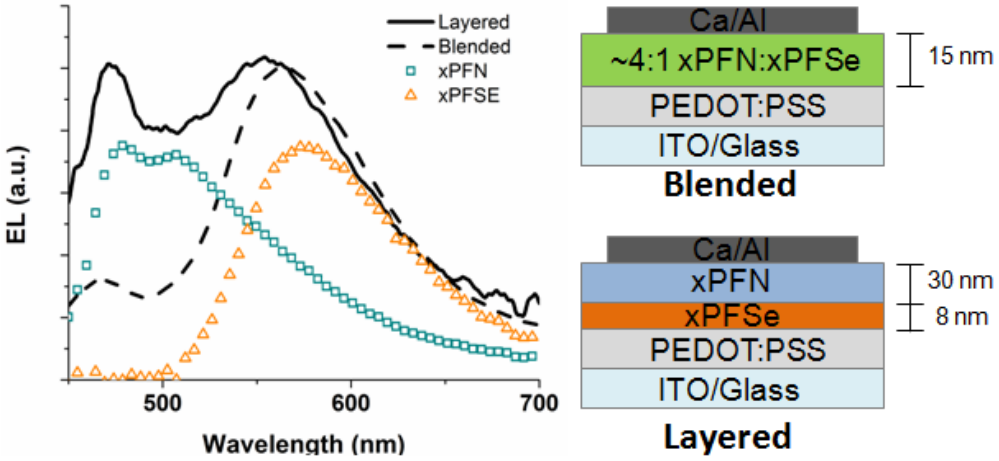

Figure 3.9: Electroluminescence spectra of multilayer and blended PLEDs incorporating xPFN and xPFSe (see text for device structures). EL spectra for single layer xPFN and xPFSe PLEDs are also shown.

Figure 3.9 shows the electroluminescence of solution-processed PLEDs fabricated by both layering and blending xPFN (cyan emitter) with xPFSe (orange emitter), along with schematics of the two device structures. The spectra of single layer xPFN and xPFSe PLEDs are also overlaid. The layered device was fabricated by spin-coating and then cross-linking xPFSe, with subsequent solution deposition and curing of xPFN. This approach is not possible without cross-linking due to the pristine polymers' similar solubilities. The blended system was spin cast from $CHCl_3$ with approximately 4:1 weight ratio of xPFN:xPFSe to mimic the content of xPFN and xPFSe in the layered devices (where thickness of the xPFN layer was approximately 4 times thicker than the xPFSe layer).

Emissive colors are summarized in Table 3.3. As expected, a cross-linked blend of the two emitters (structure: ITO/PEDOT:PSS/xPFN+xPFSe (15 nm)/Ca/Al) shows that the emission is dominated by energy transfer to xPFSe, with only a small secondary peak observable near 475 nm. In contrast, the device fabricated from cross-linked bilayers (structure: ITO/PEDOT:PSS/xPFSe(8 nm)/xPFN(30 nm)/Ca/Al) shows dramatically increased emission near 475 nm, indicating reduced charge transfer from xPFN to xPFSe. CIE 1931 chromaticity for the layered system (0.306, 0.348) confirms that it is a much better white emitter than the blend system (0.374, 0.481) at equivalent driving current. And while both designs are clearly not optimized, the cross-linked layered PLED also achieved better luminance efficiencies at higher brightness values. This data clearly shows the advantage offered by the solution-processed bilayer system achieved by thiol-ene cross-linking, which gives a total color profile unattainable by mixing. This has serious implications for new chemical routes to process high-complexity device structures such as white emitting PLEDs.

Table 3.3: Turn-on voltage, emission peaks, and CIE 1931 color parameters of PLED devices operated at 100 mA/cm^2.

Device	Turn-on Voltage (V)	$\lambda_{EL,\ peak}$ (nm)	CIE_x	CIE_y
ITO/PEDOT:PSS/**xPF**/Ca/Al	7	425, 445	0.147	0.125
ITO/PEDOT:PSS/**xPFN**/Ca/Al	6	478, 507	0.144	0.343
ITO/PEDOT:PSS/**xPFS**/Ca/Al	3	536	0.404	0.574
ITO/PEDOT:PSS/**xPFSe**/Ca/Al	5	572	0.529	0.413
ITO/PEDOT:PSS/**xPFSe/xPFN**/Ca/Al (layered)	6	472, 553	0.306	0.348
ITO/PEDOT:PSS/**xPFSe+xPFN**/Ca/Al (blended)	7	470, 561	0.374	0.481

3.4 Conclusions

In conclusion, a series of tunable band gap conjugated polymers was synthesized for use in thiol-ene click cross-linking reactions. Thiol-ene click chemistry was used to obtain cross-linked tunable band gap polymers giving the ability to tune the band gap as well as the emission

colors. The fabricated devices gave PLEDs ranging in color from blue to orange with moderately low turn on voltages. Multilayer devices were prepared and demonstrated effective color separation and improved color characteristics compared to blends or copolymers. In subsequent chapters, the effect of various cross-linking architectures on the conjugated networks' optoelectronic properties will be explored through thiol-ene compatible side-chains on poly(fluorene) derivates.

3.5 References

1. G. Klärner, J.-I. Lee, V. Y. Lee, E. Chan, J.-P. Chen, A. Nelson, D. Markiewicz, R. Siemens, J. C. Scott, R. D. Miller, Cross-linkable Polymers Based on Dialkylfluorenes, *Chem. Mater.* **11**, 1800-1805 (1999).

2. L. D. Bozano, K. R. Carter, V. Y. Lee, R. D. Miller, R. Dipietro, J. C. Scott, Electroluminescent devices based on cross-linked polymer blends, *J. Appl. Phys.* **94**, 3061 (2003).

3. E. Scheler, I. Bauer, P. Strohrigl, Synthesis and Photopatterning of Fluorene Based Reactive Mesogens, *Macromolecular Symposia* **254,** 203-209 (2007).

4. M. S. Bayerl, T. Braig, O. Nuyken, D. C. Muller, M. Groβ, K. Meerholz, Crosslinkable hole-transport materials for preparation of multilayer organic light emitting devices by spin-coating, *Macromolecular Rapid Comm.* **20**, 224-228 (1999).

5. A. Charas, L. Alcacer, A. Pimentel, J. P. Conde, J. Morgado, Observation of field-effect in a cross-linked polyfluorene semiconductor, *Chem. Phys. Lett.* **455**, 189-191 (2008).

6. H. J. Kim, A. R. Han, C. H. Cho, H. Kang, H. H. Cho, M. Y. Lee, J. M. J. Frechet, J. H. Oh, B. J. Kim, Solvent-Resistant Organic Transistors and Thermally Stable Organic Photovoltaics Based on Cross-linkable Conjugated Polymers, *Chem. Mater.* **24**, 215-221 (Jan 10, 2012).

7. A. C. Grimsdale, K. L. Chan, R. E. Martin, P. G. Jokisz, A. B. Holmes, Synthesis of Light-Emitting Conjugated Polymers for Applications in Electroluminescent Devices, *Chem. Rev.* **109**, 897-1091 (2009).

8. M. Helgesen, R. Sondergaard, F. C. Krebs, Advanced materials and processes for polymer solar cell devices, *J. Mater. Chem.* **20**, 36-60 (2010).

9. Y. G. Wen, Y. Liu, Recent Progress in n-Channel Organic Thin-Film Transistors, *Adv. Mater.* **22**, 1331-1345 (2010).

10. P. M. Beaujuge, J. R. Reynolds, Color Control in π-Conjugated Organic Polymers for Use in Electrochromic Devices, *Chem. Rev.* **110**, 268-320 (2010).

11. G. E. Jabbour, Y. Kawabe, S. E. Shaheen, J. F. Wang, M. M. Morrell, B. Kippelen, N. Peyghambarian, Highly efficient and bright organic electroluminescent devices with an aluminum cathode, *Appl. Phys. Lett.* **71**, 1762 (1997).

12. W. Zhao, T. Cao, J. M. White, On the Origin of Green Emission in Polyfluorene Polymers: The Roles of Thermal Oxidation Degradation and Crosslinking, *Adv. Func. Mater.* **14**, 783-790 (2004).

13. R. Q. Png, P.-J. Chia, J.-C. Tang, B. Liu, S. Sivaramakrishnan, High-performance polymer semiconducting heterostructure devices by nitrene-mediated photocrosslinking of alkyl side chains, *Nature Mater.* **9**, 152-158 (2010).

14. T. Posner, Beiträge zur Kenntniss der ungesättigten Verbindungen. II. Ueber die Addition von Mercaptanen an ungesättigte Kohlenwasserstoffe, *Berichte der deutschen Chemischen Gesellschaft* **38**, 646 (1905).

15. K. Meerholz, C.-D. Muller, O. Nuyken, in *Organic Light Emitting Devices. Synthesis, Properties and Applications.,* K. Mullen, U. Scherf, Eds. (Wiley-VCH Verlag GmbH & Co., Weinheim, 2006).

16. A. R. Davis, J. A. Maegerlein, K. R. Carter, Electroluminescent Networks via Photo "Click" Chemistry, *J. Am. Chem. Soc.* **133**, 20546-20551 (2011).

17. C. E. Hoyle, T. Y. Lee, T. Roper, Thiol-enes: Chemistry of the past with promise for the future *J. Polym. Sci. Part A: Polym. Chem.* **42**, 5301-5338 (2004).

18. G. R. Hutchison, M. A. Ratner, T. J. Marks, Accurate Prediction of Band Gaps in Neutral Heterocyclic Conjugated Polymers, *J. Phys. Chem. A* **106**, 10596-10605 (2002).

19. Y.-J. Cheng, S.-H. Yang, C.-S. Hsu, Synthesis of conjugated polymers for organic solar cell applications, *Chem. Rev.* **109**, 5868-5923 (2009).

20. K. Pilgram, M. Zupan, R. Skiles, Bromination of 2,1,3-Benzothiadiazoles, *J. Heterocyclic Chem.* **7**, 629-633 (1970).

21. T. Yasuda, T. Imase, T. Yamamoto, Synthesis, Characterization, and Optical and Electrochemical Properties of New 2,1,3-Benzoselenadiazole-Based CT-Type Copolymers *Macromolecules* **38**, 7378-7385 (2005).

22. F. B. Koyuncu, E. Sefer, S. Koyuncu, E. Ozdemir, A new low band gap electrochromic polymer containing 2,5-bis-dithienyl-1H-pyrrole and 2,1,3-benzoselenadiazole moiety with high contrast ratio, *Polymer* **52**, 5772-5779 (2011).

23. T. Yasuda, T. Imase, S. Sasaki, T. Yamamoto, Synthesis, Solid Structure, and Optical Properties of New Thiophene-Based Alternating π-Conjugated Copolymers Containing 4-Alkyl-1,2,4-triazole or 1,3,4-Thiadiazole Unit as the Partner Unit *Macromolecules* **38**, 1500-1503 (2005).

24. A. O. Patil, A. J. Heeger, F. Wudl, Optical-Properties of Conducting Polymers *Chemical Reviews* **88**, 183-200 (1988).

25. G. Yu, Y. Yang, Y. Cao, Q. Pei, C. Zhang, A. J. Heeger, Measurement of the energy gap in semiconducting polymers using the light-emitting electrochemical cell, *Chem. Phys. Lett.* **259**, 465-468 (1996).

26. M. L. Sun, Q. L. Niu, R. Q. Yang, B. Du, R. S. Liu, W. Yang, J. B. Peng, Y. Cao, Fluorene-based copolymers for color-stable blue light-emitting diodes *European Polym. J.* **43**, 1916-1922 (2007).

27. H. A. Saadeh, L. Lu, F. He, J. E. Bullock, W. Wang, B. Carsten, L. Yu, Polyselenopheno[3,4-b]selenophene for Highly Efficient Bulk Heterojunction Solar Cells, *ACS Macro Letters* **1**, 361-365 (2012).

28. A. Patra, Y. H. Wijsboom, G. Leitus, M. Bendikov, Tuning the Band Gap of Low-Band-Gap Polyselenophenes and Polythiophenes: The Effect of the Heteroatom, *Chem. Mater.* **23**, 896-906 (2011).

29. U. Salzner, J. B. Lagowski, P. G. Pickup, R. A. Poirier, Comparison of geometries and electronic structures of polyacetylene, polyborole, polycyclopentadiene, polypyrrole, polyfuran, polysilole, polyphosphole, polythiophene, polyselenophene and polytellurophene, *Synth. Met.* **96**, 177-189 (1998).

30. A. J. Campbell, D. D. C. Bradley, H. Antoniadis, Dispersive electron transport in an electroluminescent polyfluorene copolymer measured by the current integration time-of-flight method, *Appl. Phys. Lett.* **79**, 2133 (2001).

31. R. Q. Yang, R. Y. Tian, Q. Hou, W. Yang, Y. Cao, Synthesis and optical and electroluminescent properties of novel conjugated copolymers derived from fluorene and benzoselenadiazole *Macromolecules* **36**, 7453-7460 (Oct 7, 2003).

32. R. K. Iha, K. L. Wooley, A. M. Nystrom, D. J. Burke, M. J. Kade, C. J. Hawker, Applications of Orthogonal "Click" Chemistries in the Synthesis of Functional Soft Materials, *Chem. Rev.* **109**, 5620-5686 (2009).

33. N. B. Cramer, J. P. Scott, C. N. Bowman, Photopolymerizations of Thiol−Ene Polymers without Photoinitiators, *Macromolecules* **35**, 5361-5365 (2002).

34. A. B. Lowe, Thiol-ene "click" reactions and recent applications in polymer and materials synthesis, *Polym. Chem.* **1**, 17-36 (2010).

35. C. E. Hoyle, C. N. Bowman, Thiol-Ene Click Chemistry, *Angew. Chem. Int. Ed.* **49**, 1540-1573 (2010).

36. C. E. Hoyle, A. B. Lowe, C. N. Bowman, Thiol-click chemistry: a multifaceted toolbox for small molecule and polymer synthesis *Chem. Soc. Rev.* **39**, 1355-1387 (2010).

37. M. Berggren, O. Inganäs, G. Gustafsson, J. Rasmusson, M. R. Andersson, T. Hjertberg, O. Wennerström, Light-emitting diodes with variable colours from polymer blends *Nature* **372**, 444-446 (1994).

38. S. E. Shaheen, B. Kippelen, N. Peyghambarian, J.-F. Wang, J. D. Anderson, E. A. Mash, P. A. Lee, N. R. Armstrong, Y. Kawabe, Energy and charge transfer in organic light-emitting diodes: A soluble quinacridone study, *J. Appl. Phys.* **85**, 7939 (1999).

39. A. Können, N. Riegel, H.-W. Jonas, M. Kremer, H. Lademann, D. C. Müller, K. Meerholz, Organic LEDs: The Simple Way to Solution-Processed Multilayer OLEDs – Layered Block-Copolymer Networks by Living Cationic Polymerization, *Adv. Mater.* **21**, 879-884 (2009).

CHAPTER 4

SYNTHESIS OF SIDE-CHAIN CROSS-LINKABLE POLY(FLUORENE)S AND THEIR NETWORK FORMATION

4.1 Introduction

A growing amount of research has explored cross-linking conjugated polymers (CPs) in order to promote or arrest particular structural changes in CP thin films, as discussed in Chapters 1-3. A number of applicable chemistries have been investigated, including thermally-initiated end-groups,(*1-6*) electropolymerizable conjugated moieties,(*7-9*) and photo-initiated side-groups and end-groups such as acrylates,(*10, 11*) oxetanes,(*12*) and azides(*13*). While these efforts have demonstrated a number of device-level property improvements, none offer a facile route for systemically controlling and probing network connectivity. Thermally cross-linked systems offer little if any control over the timing of reaction initiation and thus offer systems with ill-defined cross-links. In most UV curable systems proceeding by radical initiation and propagation, side reactions from the radical chemistry can leave residual small molecules and side products with indeterminate connectivity or termination. Since the semiconducting nature of these materials so acutely depends on their packing and morphology, there is clearly a hole in the existing literature regarding the precise control of network architecture and its effect on the charge transport properties of cross-linked conjugated molecules.

Studies detailed in Chapters 2 and 3 have explored the uses of thiol-ene chemistry for cross-linking conjugated polymer networks and have shown that the thiol-ene photo-click reaction does not inhibit electroluminescent CP device performance and is fully compatible with a range of CP structures.(*14, 15*) The thiol-ene reaction is particularly advantageous over other photo-curing chemistries owing to its rapid and efficient conversion at relatively mild

temperatures, tolerance to impurities and other functional groups, and initiator-free reaction when exposed to the proper wavelength of light.(*16-19*) Furthermore, thiol-ene cross-linking results in chemically well-defined connections, and the availability of a large variety of thiol-cross-linkers enables a range of potential architectures for any given vinyl-functionalized molecule. Owing to its high efficiency and selectivity, the thiol-ene reaction is thus an ideal candidate to explore the influences specific network architectures in cross-linked CP thin films.

This chapter details the synthesis of new poly(fluorene) derivatives with vinyl-terminated side-chains of variable lengths which are solution processed with multi-functional thiol cross-linkers and cured under UV irradiation. Using FTIR, contact profilometry, and photo calorimetry measurements, the choice of cross-linker and polymer architectures and their effects on network formation in the semiconducting cross-linked poly(fluorene) thin films are explored.

4.2 Experimental Section

4.2.1 Materials

5-bromo-1-penetene was purchased from Alfa Aesar. 11-bromo-1-undecene, tetrabutylammonium bromide, 9,9-dihexylfluorene-2,7-diboronic acid bis(1,3-propanediol) ester, potassium tert-butoxide, tetrakis(triphenylphosphine) palladium(0), and Aliquat 336 were purchased from Aldrich Chemical Company. Solvents, sodium hydroxide, and silica were purchased from Fischer Scientific. All chemicals were used as-received without further purification. Reactions were carried out under N_2 in conventional glassware unless noted otherwise.

4.2.2 Instrumentation

All nuclear magnetic resonance (NMR) spectra were acquired on a Bruker Avance 400 (400MHz) NMR spectrometer and internally referenced via residual solvent signal [$CHCl_3$ ^1H 7.26 ppm; ^{13}C 77.00 ppm]. All chemical-shift values are given in ppm. Gel permeation chromatography (GPC) was performed with an Agilent 1260 system in THF at 40 °C with 1.0 mL/min elution rate. A refractive index detector, 5 µm guard column, three PL gel columns (2 Agilent Mixed-C 5 µm columns and 1 Agilent Mixed-D 5 µm column), and narrow molecular weight polystyrene standards were used. Differential scanning calorimetry (DSC) was performed on a Thermal Analysis (TA) Q-2000 in T-zero aluminum pans using modulated DSC at a heating rate of 3 °C/min. Film thicknesses were measured by contact profilometry using a Dektak 150 profilometer. UV-Vis spectra were recorded in 1-cm path length quartz cuvettes by using Shimatszu UV 3600 spectrophotometer. Fluorescence measurements were taken on a Perkin-Elmer LS-50B. Infrared spectroscopy of polymer films were performed on a Nicolet 6700 FT-IR spectrometer with a Harrick grazing angle ATR accessory (GATR).

4.2.3 Synthesis of 9,9-dialkenyl-2,7-dibromofluorene Monomers

Di-alkenyl side-chain functionality was installed on 2,7-dibromofluorene by typical nucleophilic substitution at the fluorene 9-position with bromoalkenes. Specifically, the dipentenyl and diundecenyl monomers were synthesized using 5-bromo-1-pentene and 11-bromo-1-undecene.

General reaction: 2,7-dibromofluorene (2.5 g, 7.7 mmol) previously synthesized by established procedures(*20*) was dissolved in 50 mL of a 1:1 mixture of toluene and 50% aqueous NaOH in a condenser-equipped 150mL round bottom flask. Tetrabutylammonium bromide (0.2 g, 0.65 mmol) was also added as a phase transfer reagent. The bromoalkene (14.4 mmol) was

then added dropwise, with the solution turning to a deep purple color. The solution was heated to reflux under N_2 and reacted for 17h. Upon cooling, the product was extracted using ethyl acetate. The organic phase was then neutralized and washed with 1M HCl, whereupon it turned yellow in color, and was further washed with brine. Collection of the organic phase and evaporation of solvent yielded a dark orange oil. Product was purified by column chromatography using 9:1 hexane:ethyl acetate as an eluent, and solvent was removed by evaporation.

9,9-Dipentenyl-2,7-dibromofluorene

Product was isolated as a viscous yellow oil after purification by column chromatography and initial solvent removal. Extended drying under vacuum yielded off-white solid crystals (2.87 g, 81% yield). ^{1}H NMR (400 MHz, $CDCl_3$) δ 7.44-7.30 (m, 6H, aromatic), 5.56 (m, 2H, vinyl), 4.88 (m, 2H, vinyl), 4.84 (m, 2H, vinyl), 1.94-1.82 (m, 8H, alkyl), 0.69 (m, 4H, alkyl) ppm. ^{13}C NMR (100 MHz, $CDCl_3$) δ 152.1 (aromatic), 139.1 (aromatic), 138.3 (vinyl), 130.3 (aromatic), 126.2 (aromatic), 121.6 (aromatic), 121.2 (aromatic), 114.7 (vinyl), 55.5 (quaternary), 39.6, 33.8, 22.9 ppm.

9,9-Diundecenyl-2,7-dibromofluorene

Product was isolated as a viscous yellow oil after purification by column chromatography and recrystallized from methanol to yield off-white solid crystals (4.11 g, 85% yield). ^{1}H NMR (400 MHz, $CDCl_3$) δ 7.60-7.30 (m, 6H, aromatic), 5.85-5.75 (m, 2H, vinyl), 5.0-4.90 (m, 4H, vinyl), 2.03-1.89 (m, 8H, alkyl), 1.35-1.05 (m, 24H, alkyl), 0.57 (b, 4H, alkyl) ppm. ^{13}C NMR (100 MHz, $CDCl_3$) δ 152.5 (aromatic), 139.3 (aromatic), 139.1 (vinyl), 130.2 (aromatic), 126.2

(aromatic), 121.5 (aromatic), 121.1 (aromatic), 114.1 (vinyl), 55.6 (quaternary), 40.2, 33.8, 29.8, 29.5, 29.4, 29.2, 29.1, 28.9, 23.6 ppm.

4.2.4 Synthesis of Dialkenyl/Dihexyl Alternating Poly(fluorene)s (xPF-5 and xPF-11)

Alternating poly(fluorene) copolymers xPF-5 and xPF-11 were synthesized by microwave-assisted Suzuki-Miyauara cross-coupling of 9,9-dialkenyl-2,7-dibromofluorenes and 9,9-dihexylfluorene-2,7-diboronic acid bis(1,3-propanediol) ester. Fine-tuning of reaction conditions, as informed by Hunt and co-workers(*21*) and summarized in Table 4.1, was required to minimize unwanted Heck coupling side products.

General procedure: 9,9-Dialkenyl-2,7-dibromofluorene (0.3 mmol), 9,9-dihexylfluorene-2,7-diboronic acid bis(1,3-propanediol) ester (0.3 mmol), potassium tert-butoxide (1.8 mmol), sodium chloride (0.85 mmol), and $Pd(PPh_3)_4$ (0.015 mmol) were added along with a stir bar to a 10 mL microwave vial and capped under Ar atmosphere. A N_2-sparged 3: 1 mixture of tetrahydrofuran and water (4 mL) with a few drops of phase-transfer reagent Aliquat 336 was then added to the vial, and the contents were stirred until all solids were dissolved. The solution was subsequently degassed by a freeze-pump-thaw procedure and allowed to warm back to room temperature. The vial was then heated and held at 60 °C in a microwave reactor for 1.5h. The product was precipitated by pouring into stirring acidic methanol, yielding the crude polymer. After filtering, the polymer was purified by dissolving in $CHCl_3$ and reprecipitating from MeOH. Final products were then filtered and vacuum-dried.

Di-pentenyl/Dihexyl Poly(fluorene) (xPF-5)

xPF-5 was obtained as an off-white powder (160 mg) in 85 % yield. ^{1}H NMR (400 MHz, $CDCl_3$) δ 7.85-7.28 (m, 12H, aromatic); 5.64 (m, 2H, vinyl), 4.91-4.87 (m, 4H, vinyl); 2.15 (b, 8H,

alkyl); 1.91 (b, 4H, alkyl); 1.14-0.79 (b, 30H, alkyl). M_n via GPC in tetrahydrofuran: 8.4 kg/mol vs PS standards (DP=11), PDI: 2.6.

Di-undecenyl/Dihexyl Poly(fluorene) (xPF-11)

xPF-11 was obtained as an off-white powder (223 mg) in 93% yield. ^{1}H NMR (400 MHz, $CDCl_3$) δ 7.90-7.60 (m, 12H, aromatic); 5.79 (m, 2H, vinyl), 5.05-4.81 (m, 4H, vinyl); 2.30-1.85 (m, 11H, alkyl); 1.40-0.65 (b, 45H, alkyl) ppm. M_n via GPC in tetrahydrofuran: 9.4 kg/mol vs PS standards (DP=12), PDI: 2.5.

4.2.5 General Procedure for Thin Film Cross-Linking

Cross-linkable poly(fluorene) derivatives were dissolved in chloroform at a concentration 20 mg/mL. A volume of stock solution containing multifunctional thiol in toluene (10 mg/mL) was then added to achieve the desired thiol:vinyl molar ratio, and a balance of toluene was finally added to achieve a final polymer concentration of 10 mg/mL. This ensured that the processing solutions were comparable for any given thiol:vinyl loading. These solutions were then spin-coated at 3000 RPM on clean glass substrates. Spun films were then placed under a quartz cover dish and covered with a N_2 blanket. Substrates were heated above their glass transition temperature, held for 5 min., and cured via exposure to 254 nm UV light via handheld lamp (1.5 mW/cm^2) for 2 min. Cured films were then rinsed with $CHCl_3$ and dried under vacuum.

4.2.6 Photo Calorimetry

Photo calorimetry was performed with a TA Q-2000 instrument with a TA photocalorimeter accessory (PCA) using a broad-band UV source. Solutions of poly(fluorene)s and thiol as prepared above were drop cast into aluminum T-zero DSC pans and dried in the

dark. Photo calorimetry response was measured during curing at a constant temperature of 90 °C with 1 mW/cm^2 exposure intensity. Calibration of the instrument was confirmed by running a model UV-initiated thiol-ene reaction of 9-vinylcarbazole with pentaerythritol tetrakis(3-mercaptopropionate) until completion and comparing heat evolved to theoretical thiol-ene reaction enthalpies.

4.3 Results and Discussion

4.3.1 Synthesis of Cross-linkable Poly(fluorene)s

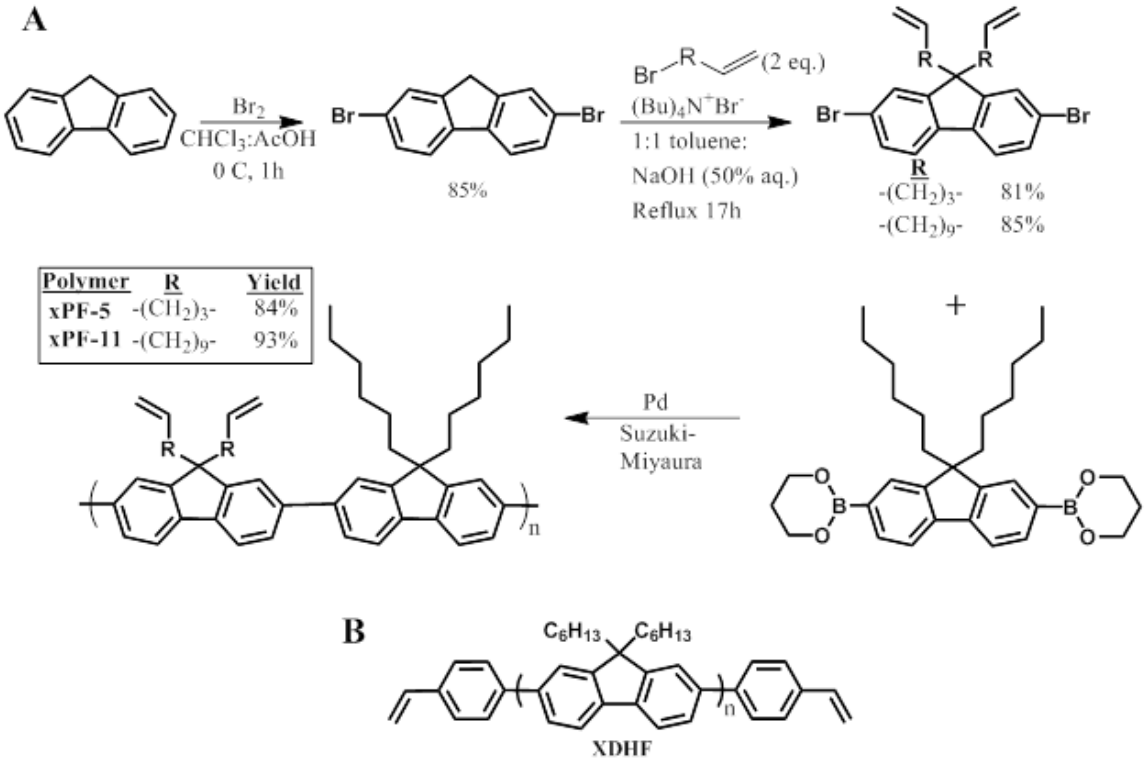

Figure 4.1: (A) Synthetic route for side-chain cross-linkable poly(fluorene) derivatives xPF-5 and xPF-11. (B) Structure of previously synthesized end-chain cross-linkable poly(dihexyl fluorene) XDHF.

To access control of network structure and connectivity, poly(fluorene)s were synthesized which could be cross-linked through alkenyl side-chains of varying lengths (Figure 4.1). In general, dialkenyl functionality was installed on the 2,7-dibromofluorene monomer by

typical nucleophilic substitution reaction at the fluorene 9-position. Yields were good with no mono-functional defects observed by NMR after column purification (typical spectra shown in Figures 4.2 and 4.3). Polymerization of this monomer with a diboronic acid-based dihexylfluorene via Suzuki-Miyaura cross coupling afforded the desired side-chain functionalized copolymers. However, it is important to note that special considerations were necessary to avoid unwanted Pd-catalyzed Heck coupling between the dibromo and dialkenyl monomer functionalities. Informed by results from Hunt and co-workers on competing cross-coupling reactions,(*21*) cross-coupling reactions using lower temperatures in a THF/H_2O mixture with KO^tBu base plus added NaCl salt consistently produced linear polymer with respectable molecular weights. Subsequent ^1H NMR confirmed that the alkenyl groups were present after polymerization. A more thorough summary of unsuccessful polymerization conditions can be found in Table 4.1

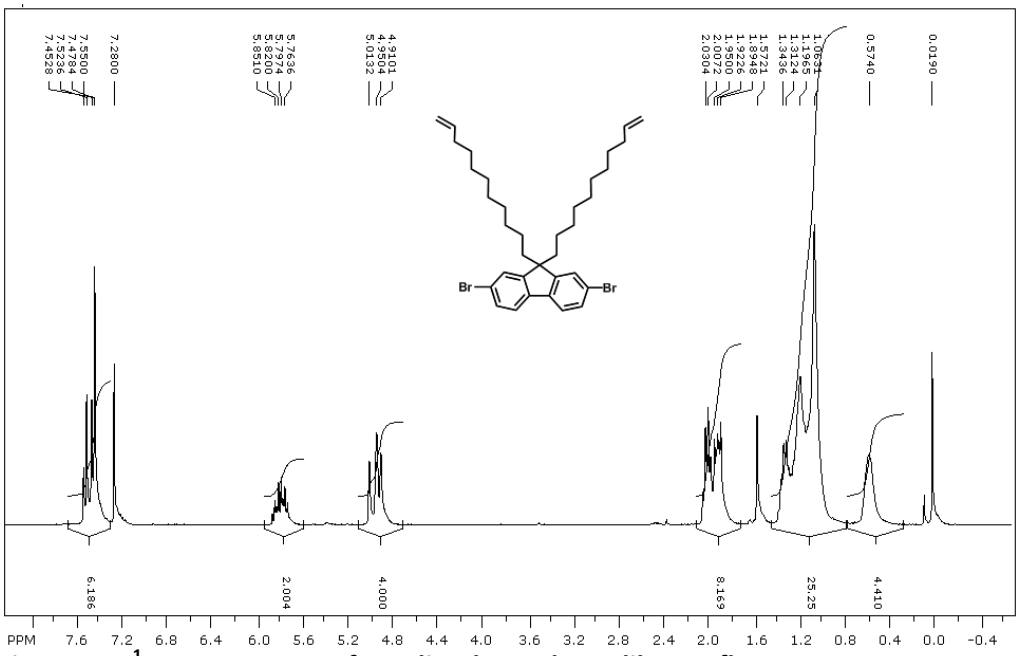

Figure 4.2: ^1H NMR spectra of 9,9-diundecenyl-2,7-dibromofluorene monomer.

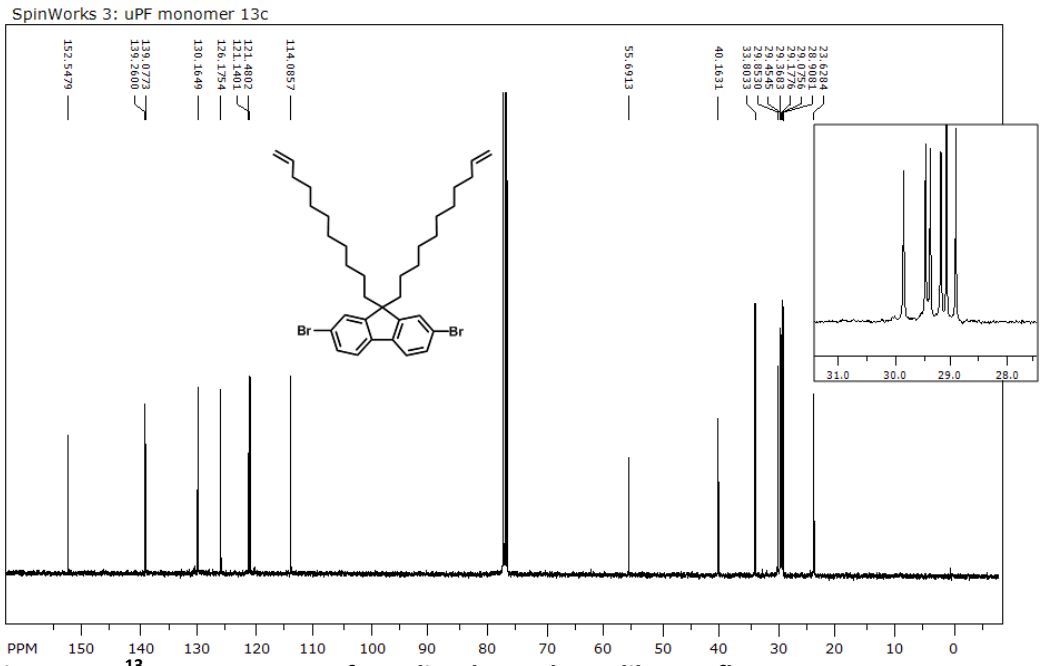

Figure 4.3: ^{13}C NMR spectra of 9,9-diundecenyl-2,7-dibromofluorene monomer.

Table 4.1: Reaction conditions explored for optimizing Suzuki vs Heck cross-coupling reactions in with di-alkenyl dibromofluorene monomers. Procedures (proc.): 1) 1:1 toluene:H_2O + Na_2CO_3; 2) 1:1 THF/H_2O + KO_tBu + NaCl.

Monomer /method	Proc.	Temp. (°C)	Time (hr)	M_n (g/mol)	Đ	Fluorenes (DP)	Yield
xPF-11, microwave	1	110	2	--	--	--	0%
xPF-11, oil bath	1	100	48	--	--	2 (DP 1)	0%
xPF-5, oil bath (slow addition)	1	100	6	--	--	2 (DP 1)	0%
xPF-5, microwave	1	100	0.5	--	--	2 (DP 1)	0%
xPF-5, microwave	2	60	1	5300	1.71	16 (DP 8)	66%
xPF-5, microwave	2	60	1.5	9200	2.10	30 (DP 15)	84%
xPF-11, microwave	2	60	1.5	9400	2.42	24 (DP 12)	93%

Polymer sizes and glass transition temperatures, $T_{g,}$ obtained from differential scanning calorimetry (DSC) are reported in Table 4.2. The polymers are all of comparable size with chain lengths above the conjugation length of poly(fluorene)s. It is useful to note that the T_g of the polymer systems decreases as the length of the alkene side chain is increased. As reported previously,(*14*) thiol-ene photo-curing of poly(fluorene) thin films is only successful when performed at temperatures above the polymer's T_g. Therefore, the data here suggests that careful tuning of the polymer T_g by side-chain length could allow for conjugated polymers which are photo-curable at even more modest temperature conditions than previously explored.

Table 4.2: Summary of number average molecular weight M_n, dispersity $Đ$, and glass transition temperatures T_g of synthesized polymers.

Polymer	M_n (g/mol)	Number Avg. Fluorene units per chain	$Đ$	T_g (°C)
XDHF	10400	31	2.3	85
xPF-5	8400	26	2.6	98
xPF-11	9400	23	2.5	45

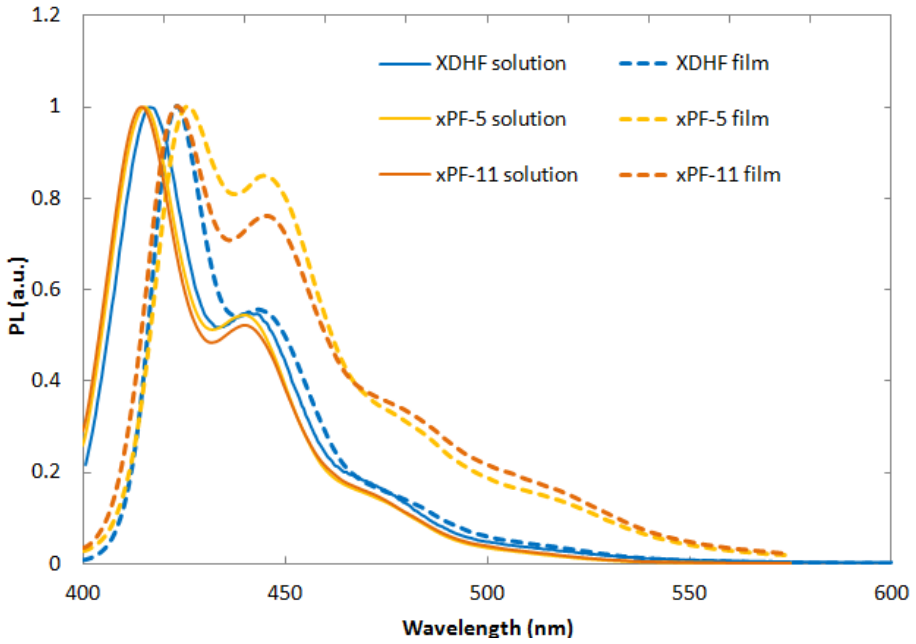

Figure 4.4: Solution and solid state photoluminescence (PL) of cross-linkable poly(flourene) derivatives, excited at 365 nm.

Photoluminescence (PL) of the vinyl-functionalized poly(fluorene)s at 365 nm excitation is shown in Figure 4.4. Previously synthesized homopolymer XDHF, with a fully dihexyl functionalized backbone, is shown for comparison.(*14*) All polymers show effectively indistinguishable emissive behavior in dilute $CHCl_3$ solution as expected from their identical conjugated fluorene backbones. The PL spectra all broaden and red-shift when measured in the thin film state, and significant differences between the polymers' PL become evident. The alkenyl side-chain copolymers show increased intensity from the lower energy PL peak at 450 nm compared to styrene end-capped XDHF, possibly due to electronic interactions of the conjugated backbone with the unsaturated alkene side chains. This secondary peak emission increases in intensity as the alkene side chain length increases from xPF-5 to xPF-11. The precise reason for this increase is unknown, but it could be a result of increased planarization of the molecules arising from the reduced steric needs of the shorter side chains in the solid state. This would relate well to reported helical conformations of dialkyl fluorene homopolymers and the

observed dependencies of the secondary emission peak on stresses during processing and on intramolecular, rather than intermolecular, excitation events.(*22, 23*)

4.3.2 Photocured Network Architecture and Kinetics

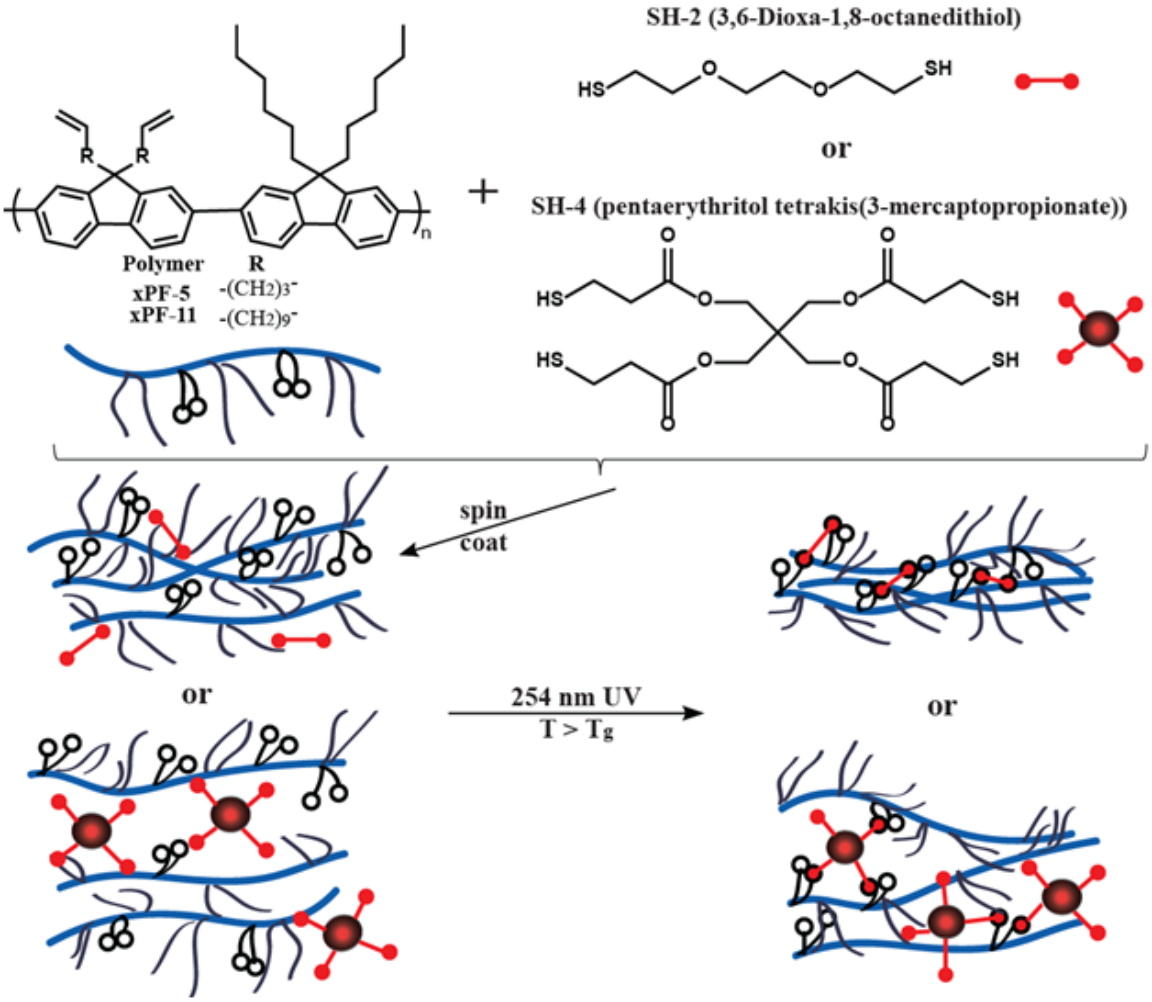

Figure 4.5: Illustration of the alkene-functionalized polymers and thiol cross-linkers used for fabricating thiol-ene cross-linked semiconducting networks. After spin coating from mixed chloroform/toluene solutions, thin films of polymer and cross-linker could be photo-cured by exposure to 254 nm at temperatures above their T_g.

With the side-chain functionalized polymers synthesized, a number of variables were available for tuning network connectivity: polymer side-chain length, thiol cross-linker functionality, and relative thiol:vinyl molar loading in the spin-coated thin films. Figure 4.5

illustrates the general procedure for fabricating cross-linked semiconducting thin films. Homogenous solutions containing both cross-linkable polymer and thiol cross-linker could be spin coated as uniform films approximately 20-50 nm in thickness with no observed evidence of phase separation. Exposed films were entirely insoluble to all solvents after UV radiation exposure at 254 nm for as few as 120 seconds under a N_2 blanket at temperatures above the polymer T_g. This proved particularly advantageous with xPF-11 systems, whose low T_g (47 °C) allowed for photo-curing below 60 °C. All attempts to cross-link films at temperatures below their respective T_g were unsuccessful.

FTIR measurements of the final cured, reacted networks provided further insight into the cross-linked nature of the semiconducting thin films (Fig. 4.6). The vinyl C-H absorption at 905 cm^{-1} proves to be the most useful analytical signal to gauge thiol-ene reactivity, since these thin films have relatively low thiol loading (generally less than 1 mg). Thus changes and disappearance of the 2550 cm^{-1} S-H thiol mode are difficult to conclusively analyze since the thiol S-H absorption is known to be particularly weak.(*24, 25*).

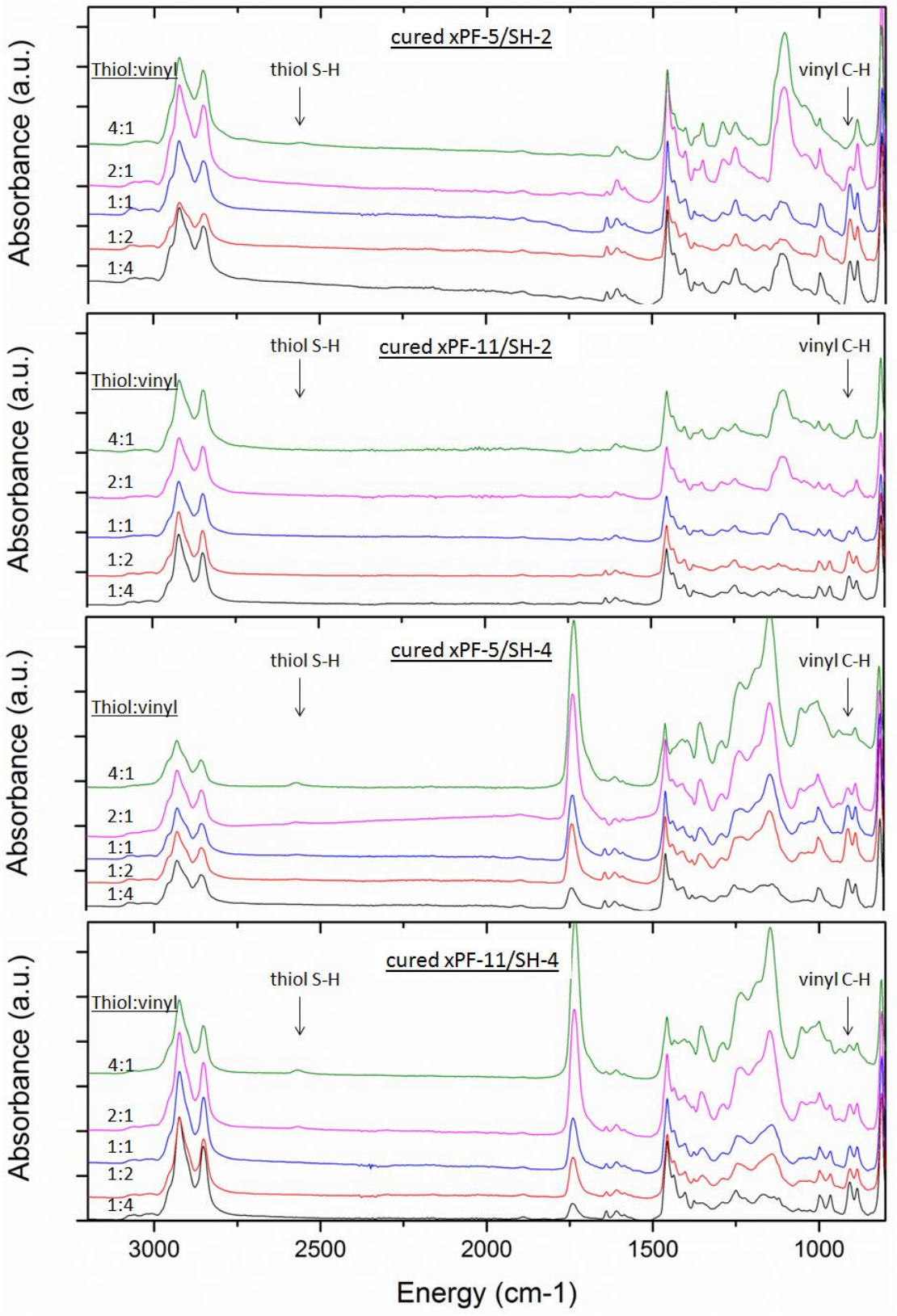

Figure 4.6: FTIR spectra of fully cured xPF-5 and xPF-11 networks.

First, the effect of SH-2 versus SH-4 on vinyl group reaction is explored. The vinyl peaks for both xPF-5 and xPF-11 are reduced much more readily when cross-linked with the di-functional SH-2 cross-linker than with SH-4, suggesting that the SH-2 thiols remain considerably more reactive during network formation than the SH-4 thiols. This makes intuitive sense, as unreacted thiols in the bulky tethered SH-4 likely become inaccessible as the network starts forming. Conversely, the flexible non-tethered SH-2 thiols can continue to react after the network begins to vitrify. In both systems cured with SH-2, IR absorption from the vinyl group is greatly diminished as the thiol:vinyl loading is increased beyond 1:1. This is not the case with SH-4, where even an abundance of thiols results in residual vinyl groups after curing. Furthermore, residual weak thiol signal (while quantitatively difficult to assess) can still be seen at smaller cross-linker loadings with SH-4 where the same signal has disappeared in the SH-2 cross-linked samples with the same molar amount of thiol loading (e.g. 1:2 thiol:vinyl ratio for xPF-5 cured with SH-4 and SH-2).

Comparison of the short side-chain xPF-5 and long side-chain xPF-11 also sheds light on the nature of the final poly(fluorene) networks. Greater residual vinyl groups appear to be present in xPF-5 compared to xPF-11 after network formation with di-functional SH-2. This can be assumed to be the result of the solubilizing hexyl chains within each repeat unit, which effectively screen the shorter pentenyl groups of xPF-5 from reacting once chain mobility is reduced during curing. It is more difficult to assess any differences when xPF-5 and xPF-11 are cured with tetra-functional SH-4, where the residual vinyl signals do not appear to react particularly differently. There is evidence of reduced conversion in xPF-5 versus xPF-11 as seen in the residual weak S-H band. Residual thiol is only observable beyond 2:1 thiol:vinyl molar loading in xPF-11, but in xPF-5 there appears to be a small presence of unreacted thiol at 1:1

thiol:vinyl molar loading. This would indicate a similar trend as SH-2-cured samples, where the shorter xPF-5 reactive side-chains leave more unreacted thiols in the final network.

Photo DSC was additionally used to probe the effect of the initial thiol:vinyl ratio and thiol functionality on the kinetics of network formation. Solutions of cross-linkable poly(fluorene)s and either tetra-functional pentaerythritol tetrakis(3-mercapopropionate) (SH-4) or di-functional 3,6-dioxa-1,8-octanedithiol (SH-2) thiol cross-linkers were drop cast into DSC sample pans and dried in the dark. Low sample masses (less than 3mg) and thin films were used to mimic device processing conditions.

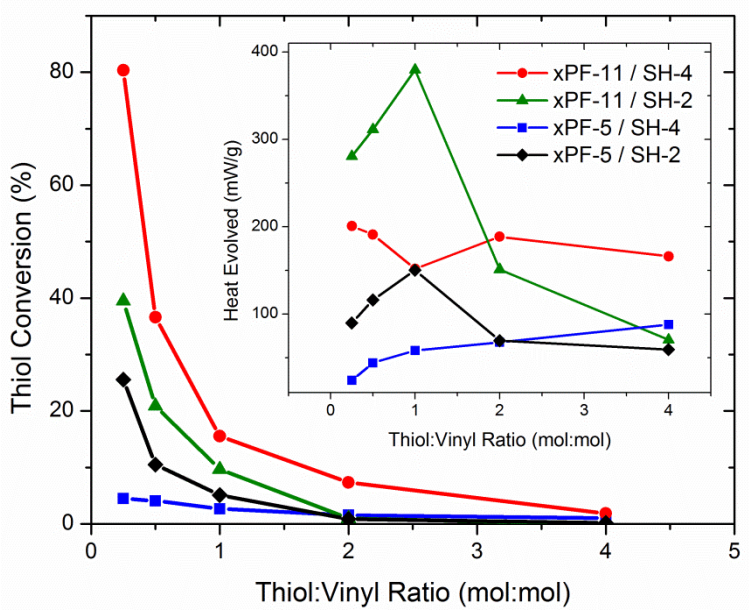

Figure 4.7: Extent of thiol conversion after 20 min. exposure to 1mW/cm^2 UV exposure as measured by heat evolved during photo DSC curing. Inset shows total measured heat evolved during 20 min. of photo-curing (254 nm at 1 mW/cm^2).

Figure 4.7 shows the extent of thiol conversion after 20 min. of photo-curing at 1 mW/cm^2 UV intensity as measured by photo calorimetry. Percent conversion was calculated from the total heat evolved during the photo calorimetry experiment as compared to calculation of quantitative reaction enthalpies informed by literature (~70 kJ/mol for a thiol and terminal aliphatic -ene).(*26*) The largest thiol conversions occur with the xPF-11 systems, which are all

consistently higher than those in xPF-5 networks. This result is in agreement with the IR data above, intuitively explained by the longer, more flexible undecenyl side-chains of xPF-11 which can continue to encounter reactive thiols as the network vitrifies. Curiously, we observe that in all cases the thiol conversion is reduced by half for every doubling of thiol concentration in the film. That is, it appears once a fixed, initial amount of thiol reacts with vinyl groups, rapid network vitrification inhibits the further conversion of excess reactive groups. Such a regular and systematic inverse dependence of conversion on loading suggests that vitrification of these conjugated thiol-ene networks occurs very rapidly.

Influences of the thiol cross-linker structure on network curing can be seen by the total heats of curing (Fig. 4.7, inset). In particular, heat evolved from the SH-4 cross-linked system continually increases (with xPF-5) or initially increases and then plateaus (with xPF-11) as the thiol content increases. The increase in cuing enthalpy at thiol:ene ladings greater than 1:1 in xPF-5 suggests the system becomes highly constrained and is dependent on a thiol proximity when the film is cast (i.e. within reach of a short pentenyl side-chain as the network vitrifies, which increases as more thiol is added). The xPF-11 film shows fairly constant reaction enthalpies as thiol content is increased, as the longer side-chains are not similarly inhibited. Both situations arise from the tethered nature of SH-4 which presumably leaves many free thiols inaccessible once the initial thiol-ene reactions begin. In contrast, reaction enthalpies with di-functional SH-2 cross-linker markedly decrease beyond 1:1 thiol:vinyl molar loading which implies that excess cross-linker can serve to inhibit reaction in this case since the non-tethered more flexible SH-2 encourages greater and more thorough initial reaction.

It is worth noting that all measured reaction enthalpies are considerably lower than theoretical thiol-ene reaction enthalpies for this system. This is likely due to required experimental constraints. Low sample masses (less than 3 mg) and thin films were used to

mimic device processing conditions, leading to very small reaction enthalpies, which are further complicated by environmental heating from the UV light source during photo calorimetry operation. Thus, comparison of measured heat flow between experimental samples is likely more insightful than comparisons with theoretical thiol-ene reaction enthalpies.

In all cases and thiol loadings, insoluble cross-linked films remained after curing and rinsing with chloroform. Insolubility and network vitrification are no doubt enhanced by the rigidity and inherently modest solubility of the conjugated polymer backbones, which lock into a high molecular weight insoluble film once just a few cross-links occur within the amorphous alkyl regions between chains.

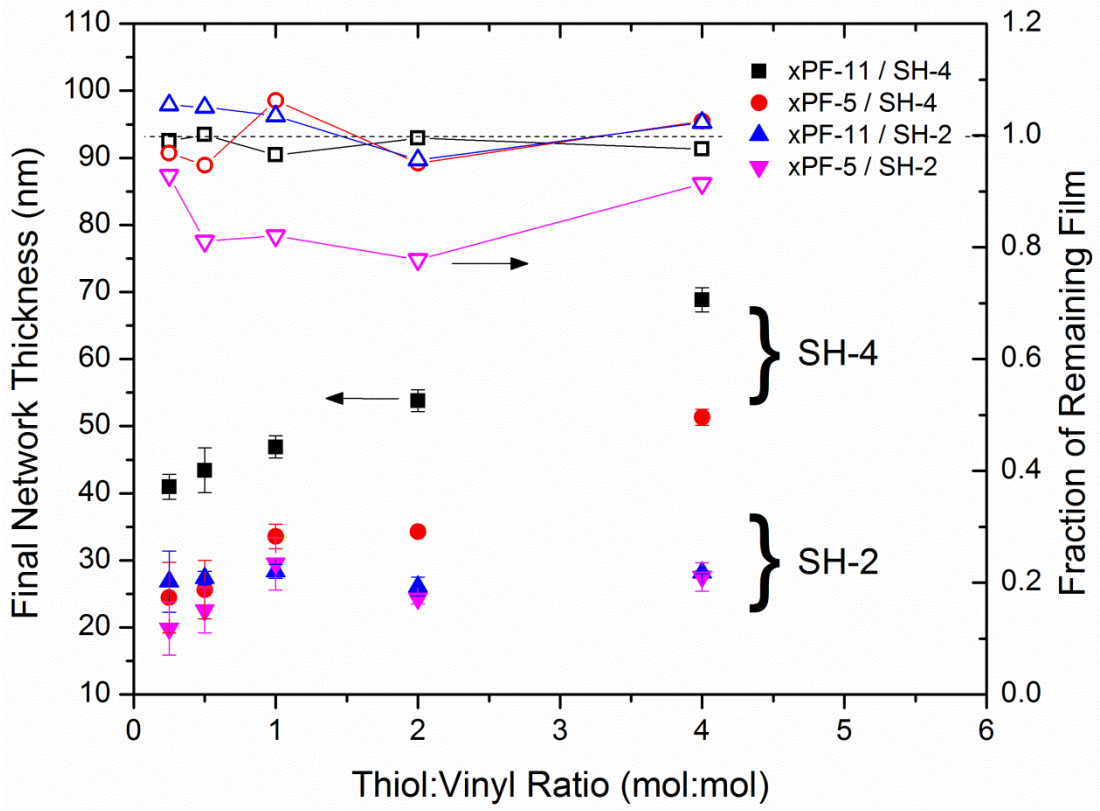

Figure 4.8: Thickness of processed poly(fluorene) networks (solid symbols) and fraction of remaining film compared to as-spun film thickness (open symbols), measured as functions of thiol functionality and loading.

Figure 4.8 shows contact profilometry measurements of processed film thicknesses following photo reaction, solvent rinsing, and vacuum drying. It is clear that the bulky SH-4 tetra-thiol provides significant volumetric contribution to the polymer film, while the SH-2 di-thiol does not. Both xPF-5 and xPF-11 cured films increase linearly in thickness as a function of SH-4 content, while cured polymer networks remain effectively constant in thickness as more di-thiol is added. Comparing the cured, solvent-rinsed network thickness (following subsequent drying) to the pre-cured film thicknesses (Fig. 4.8, right axis) reveals effectively no loss of material or network contraction in most cases. The one notable exception is for the xPF-5/di-thiol network, which shows considerable shrinkage of approximately 20%. These results imply an increasingly dense conjugated polymer network as more di-thiol as added.. This behavior can be rationalized by considering the di-thiol cross-linker reacting with the short pentenyl side-chains. Since these side-chains are shorter than the adjacent co-monomer's dihexyl side-chains, it is likely that during curing the conjugated polymer segments are pulled closer and tighter than their as-coated morphology dictated by the hexyl side-chains.

The combination of FTIR, photo calorimetry, and profilometry data all support the conclusion that choice of side-chain length and cross-linker geometry can be used to tune thin film network architecture. A short flexible di-thiol like SH-2 results in a denser, more completely reacted conjugated network, while the tetra-functional SH-4 cross-linker can lead to a less connected and more dilute (yet still vitrified and fully insoluble) poly(fluorene) network.

4.3.3 Network Photoluminescence

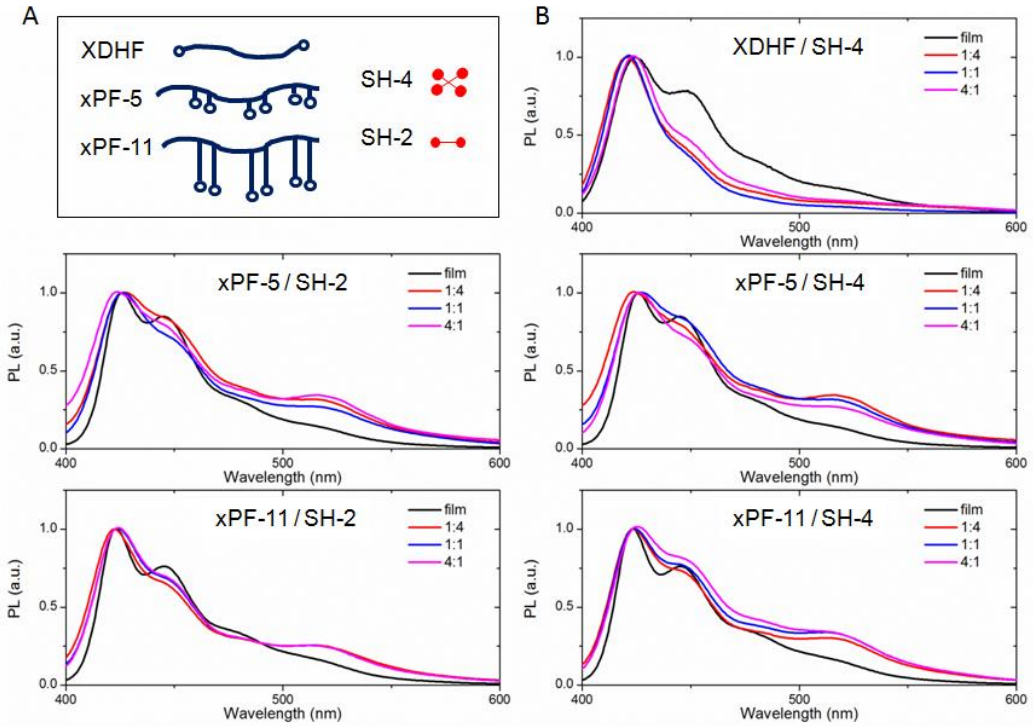

Figure 4.9: (A) Schematic cartoon representation of the salient details of each network component (end-chain vs short side-chain vs long side-chain reactivity, and thiol functionality). (B) Photoluminescence (PL) of poly(fluorene) films before and after network formation with dithiol SH-2 and tetrathiol SH-4 as a function of vinyl:thiol (mol:mol) loading, indicated in legends.

Figure 4.9 shows the photoluminescence (PL) of the as-spun poly(fluorene) films (without thiol) and the photo-cured networks as prepared and illustrated in Figure 4.5. Subtle changes in the PL spectra show how network connectivity can affect the optoelectronic properties of the final conjugated network. As thiol content increases with the shorter side-chain xPF-5, the secondary PL peak at 450 nm broadens and disappears, and the green emission mode at 520 nm (commonly attributed to emission from deleterious oxidative fluorene defects, enhanced by polymer packing and interchain communication between defect sites(*27-29*)) changes as well. Curiously, the change of these two peaks depends on thiol functionality. With the bulky SH-4, both peaks decrease in intensity as more thiol is added, perhaps indicative of

reduced interchain electronic communication or backbone planarization. By contrast, xPF-5 films cross-linked with SH-2 do not follow a clear trend in PL intensity changes, possibly due to more complex optoelectronic interactions dictated by the more tightly constrained network (as discussed above).

The longer side-chain xPF-11 PL shows little dependence on thiol loading, especially with the di-functional SH-2 thiol, perhaps owing to the longer cross-linkable side chains which can flex through the curing network without distorting the conjugated packing. Likewise, the end-functional XDHF PL spectra show a marked change upon thiol cross-linking with SH-4 compared to an as-spun film, but otherwise the system shows only a weak dependence on thiol loading.

Regardless of network connectivity, cross-linking of these materials unambiguously leads to a reduction in the vibronic character in the PL spectra. This could be advantageous to device fabrication design, as mentioned previously regarding unwanted low-energy emissions in poly(fluorene) materials. Thus, the cross-linked emissive behavior shown here could be useful in eliminating unwanted low-energy emissions or non-radiative relaxation modes in electroluminescent devices. These observed effects on PL spectra show that cross-linking content and network architecture via thiol functionality can be used to fine-tune emissive behavior. Since photo induced emission is a relatively localized event in the film, we expect these subtle morphological changes to play a much more significant role in current carrying devices such as PLEDs and thin film transistors where interchain charge transport is a crucial aspect of device operation. The observed PL changes here are quite subtle, and future work will more closely examine the role cross-linking architecture plays in optoelectronic behavior.

4.4 Conclusions

This chapter has described the photo-initiated thiol-ene curing of conjugated poly(fluorene) networks using polymers with a variety of cross-linkable alkenyl side-chains and multi-functional thiol cross-linkers. Through a combination of photo calorimetry, IR, and thickness measurements, the thiol-ene reaction has been identified as a new, molecular-level handle for pushing and pulling polymer chains beyond their as-spun state. Large, bulky cross-linkers like SH-4 allow for volumetric dilution of the network, while shorter flexible cross-linkers allow for pulling polymer chains closer together than their as-spun morphology, particularly when coupled with short reactive polymer side-chains. These results can be easily generalized to a range of cross-linkers and polymer architectures. In the next chapter, changes in solid state photoluminescence will be exploited to further identify the subtle effects of conjugated network architecture on the materials' optoelectronic behavior.

4.5 References

1. G. Klärner, J.-I. Lee, V. Y. Lee, E. Chan, J.-P. Chen, A. Nelson, D. Markiewicz, R. Siemens, J. C. Scott, R. D. Miller, Cross-linkable Polymers Based on Dialkylfluorenes, *Chem. Mater.* **11**, 1800-1805 (1999).

2. L. D. Bozano, K. R. Carter, V. Y. Lee, R. D. Miller, R. Dipietro, J. C. Scott, Electroluminescent devices based on cross-linked polymer blends, *J. Appl. Phys.* **94**, 3061 (2003).

3. J. P. Chen, G. Klaerner, J. Lee, D. Markiewicz, V. Y. Lee, R. D. Miller, J. C. Scott, Efficient, blue light-emitting diodes using cross-linked layers of polymeric arylamine and fluorene, *Synth. Met.* **107**, 129-135 (1999).

4. H. Sun, Z. E. Liu, Y. Hu, L. Wang, D. Ma, X. Jing, F. Wang, Crosslinkable Poly(p-phenylenevinylene) Derivative, *J. Polym. Sci. A: Polym. Chem.* **42**, 2124-2129 (2004).

5. G. K. Paul, J. Mwaura, A. A. Argun, P. Taranekar, J. R. Reynolds, Cross-Linked Hyperbranched Arylamine Polymers as Hole-Transporting Materials for Polymer LEDs, *Macromolecules* **39**, 7789-7792 (2006).

6. Y.-H. Niu, M. S. Liu, J.-W. Ka, A. K. Jen, Thermally crosslinked hole-transporting layers for cascade hole-injection and effective electron-blocking / exciton-confinement in phosphorescent polymer light-emitting diodes, *Appl. Phys. Lett.* **88**, 093505 (2006).

7. C. Xia, X. Fan, M.-k. Park, R. C. Advincula, Ultrathin Film Electrodeposition of Polythiophene Conjugated Networks through a Polymer Precursor Route *Langmuir* **17**, 7893-7898 (2001).

8. A. Baba, K. Onishi, W. Knoll, R. C. Advincula, Investigating Work Function Tunable Hole-Injection/Transport Layers of Electrodeposited Polycarbazole Network Thin Films, *J. Phys. Chem. B* **108**, 18949-18955 (2004).

9. R. Ponnapati *et al.*, Conjugated Polymer Network Films of Poly(p-phenylene vinylene) with Hole-Transporting Carbazole Pendants: Dual Photoluminescence and Electrochromic Behavior, *ACS Appl. Mater. & Interfaces* **4**, 1211-1218 (2012).

10. E. Scheler, I. Bauer, P. Strohrigl, Synthesis and Photopatterning of Fluorene Based Reactive Mesogens, *Macromolecular Symposia* **254**, 203-209 (2007).

11. E. Scheler, P. Strohriegl, Tailoring fluorene-based oligomers for fast photopatterning, *J. Mater. Chem.* **19**, 3207-3212 (2009).

12. M. S. Bayerl, T. Braig, O. Nuyken, D. C. Muller, M. Groβ, K. Meerholz, Crosslinkable hole-transport materials for preparation of multilayer organic light emitting devices by spin-coating, *Macromolecular Rapid Comm.* **20**, 224-228 (1999).

13. H. J. Kim, A. R. Han, C. H. Cho, H. Kang, H. H. Cho, M. Y. Lee, J. M. J. Frechet, J. H. Oh, B. J. Kim, Solvent-Resistant Organic Transistors and Thermally Stable Organic Photovoltaics Based on Cross-linkable Conjugated Polymers, *Chem. Mater.* **24**, 215-221 (2012).

14. A. R. Davis, J. A. Maegerlein, K. R. Carter, Electroluminescent Networks via Photo "Click" Chemistry, *J. Am. Chem. Soc.* **133**, 20546-20551 (2011).

15. F. B. Koyuncu, A. R. Davis, K. R. Carter, Emissive Conjugated Polymer Networks with Tunable Band-Gaps via Thiol–Ene Click Chemistry, *Chem. Mater.* **24**, 4410-4416 (2012).

16. C. E. Hoyle, A. B. Lowe, C. N. Bowman, Thiol-click chemistry: a multifaceted toolbox for small molecule and polymer synthesis, *Chem. Soc. Rev.* **39**, 1355-1387 (2010).

17. C. E. Hoyle, C. N. Bowman, Thiol-Ene Click Chemistry, *Angew. Chem. Int. Ed.* **49**, 1540-1573 (2010).

18. A. B. Lowe, Thiol-ene "click" reactions and recent applications in polymer and materials synthesis, *Polym. Chem.* **1**, 17-36 (2010).

19. R. K. Iha, K. L. Wooley, A. M. Nystrom, D. J. Burke, M. J. Kade, C. J. Hawker, Applications of Orthogonal "Click" Chemistries in the Synthesis of Functional Soft Materials, *Chem. Rev.* **109**, 5620-5686 (2009).

20. L. A. Carpino, Convenient Preparation of (9-Fluorenyl)methanol and Its 2,7-Dihalo Derivatives, *J. Org. Chem.* **45**, 4250-4252 (1980).

21. A. R. Hunt, S. K. Stewart, A. Whiting, Heck versus Suzuki Palladium Catalyzed Cross-Coupling of a Vinyl Borate Ester with Aryl Halides, *Tetrahedron Lett.* **34**, 3599-3602 (1993).

22. M. Grell, D. D. C. Bradley, G. Ungar, J. Hill, K. S. Whitehead, Interplay of Physical Structure and Photophysics for a Liquid Crystalline Polyfluorene, *Macromolecules* **32**, 5810-5817 (1999).

23. G. Lieser *et al.*, Ordering, Graphoepitaxial Orientation, and Conformation of a Polyfluorene Derivative of the “Hairy-Rod” Type on an Oriented Substrate of Polyimide, *Macromolecules* **33**, 4490-4495 (2000).

24. R. M. Silverstein, G. C. Bassler, in *Spectrometric Identification of Organic Compounds*. (John Wiley & Sons, Inc., New York, 1967), pp. 99-100.

25. J. Coates, in *Encyclopedia of Analytical Chemistry,* R. A. Meyers, Ed. (John Wiley & Sons, Inc., Chichester, 2000), pp. 10815-10837.

26. T. M. Roper, C. E. Hoyle, D. H. Magers, in *Photochemistry and UV curing: New Trends,* J. P. Fouassier, Ed. (Research Signpost, Kerala, India, 2006), pp. 253-264.

27. X. Gong, K. I. Parameswar, D. Moses, C. B. Guillermo, A. J. Heeger, S. S. Xiao, Stabilized Blue Emission from Polyfluorene-Based Light-Emitting Diodes: Elimination of Fluorenone Defects, *Adv. Func. Mater.* **13**, 325-330 (2003).

28. A. P. Kulkarni, X. Kong, S. A. Jenekhe, Fluorenone-Containing Polyfluorenes and Oligofluorenes: Photophysics , Origin of the Green Emission and Efficient Green Electroluminescence, *J. Phys. Chem. B* **108**, 8689-8701 (2004).

29. V. N. Bliznyuk, S. A. Carter, J. C. Scott, G. Klärner, R. D. Miller, D. C. Miller, Electrical and Photoinduced Degradation of Polyfluorene Based Films and Light-Emitting Devices, *Macromolecules* **32**, 361-369 (1999).

CHAPTER 5

FLUORENONE INORPORATION INTO CROSS-LINKABLE POLY(FLUORENE)S FOR ASSESSING NETWORK OPTOELECTRONICS

5.1 Introduction

Cross-linking of conjugated polymers into semiconducting networks has been investigated via numerous chemical routes in order to open new possibilities for solvent processing, luminescent color stability, and morphological control.(*1-6*) The previous chapters have shown the thiol-ene photo-click reaction to be especially attractive for fabricating semiconducting electroluminescent polymer networks owing to the reaction's high speed and efficiency, functional group tolerance, and initiator-free reaction.(*7, 8*) This high fidelity reaction has allowed for discrete control over poly(fluorene) network connectivity in cross-linked thin films which is difficult to achieve via other cross-linking chemistries. While many studies have tracked the influence of monomer and polymer connectivity on the formation and macro-scale properties of thiol-ene networks,(*9-12*) no reports have attempted to couple conjugated cross-linked architecture with optoelectronic and charge transport properties.

This chapter turns to the fluorenone moiety as a new diagnostic handle. Fluorenone, with a ketone at the 9-position of an aromatic fluorene unit, has been observed to act as a low-energy charge trapping and recombination site when present in poly(fluorene) systems, showing a characteristic broad green photo- and electro-luminescence around 520 nm. The specific effects of fluorenone defects on the optoelectronic properties of poly(fluoene)s have been extensively studied through both the environmental oxidation of poly(fluorene) by heat(*13*) and light(*14, 15*) as well through deliberate incorporation of fluorenone molecules into model polymers and oligomers during synthesis.(*13, 16-18*) The referenced studies have shown that

even a few molar percent of fluorenone present in poly(fluorene) is enough to suppress those polymers' usual blue luminescence and introduce a dominant green emission. Figure 5.1 shows how the relative amount of fluorenone in the copolymer poly(dialkyl fluorene-*co*-fluorenone) increases low energy green emission and decreases high energy fluorene emission. A range of compelling data (including but not limited to Figure 5.1) supports the argument that low-energy fluorenone emission arises from isolated on-chain defect emission, but at the same time, relative intensity of this emission is unquestionably influenced by defect concentration and polymer packing in the solid state where excitation energy can much more efficiently transfer from high-energy fluorenes to the low-energy fluorenone species.(*15, 16*) Recent work in this field from Rathnayake and co-workers (shown in Figure 5.2) is especially applicable to variably cross-linked poly(fluorene) networks, since they demonstrate that fluorenone emission is sensitive to the concentration and relative dilution of the conjugated molecules.(*18*) These studies indicate that fluorenone emission is considerably affected by how readily excited states along the poly(fluorene) backbone can find and migrate to a fluorenone moiety. Thus changes in the relative amounts of green fluorenone and blue poly(fluorene) emission intensity are excellent indicators of relative fluorenone concentration and chain packing.

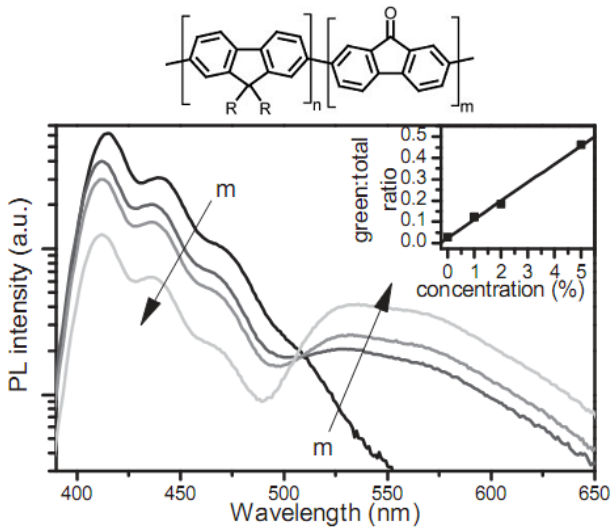

Figure 5.1: Effect of increasing fluorenone content on the solution photoluminescence (PL) spectra in a poly(fluorene-*co*-fluorenone) copolymer. Reprinted with permission from Becker , *Adv. Func. Mater.,* 16, 364-370 (2006). Copyright 2006 Wiley-VCH.

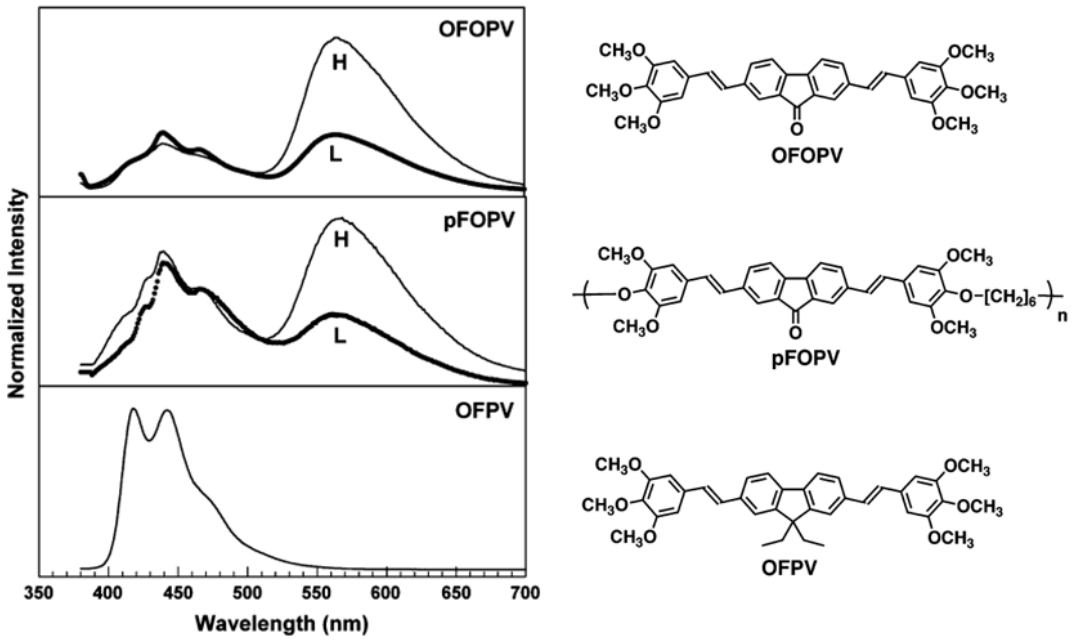

Figure 5.2: Effect of fluorenone incorporation in conjugated small molecules and polymers on photoluminescence spectra at high (H) and low (L) concentration in solution. Adapted with permission from Rathnayake, *Chem. Mater.*, 19, 3265-3270 (2007). Copyright 2007 American Chemical Society.

The above literature reports have inspired the current work which uses fluorenone emission as a diagnostic handle in cross-linked poly(fluorene) networks, where the intensity of

the low energy fluorenone emission serves as a colorimetric network connectivity sensor. This chapter describes the synthesis of thiol-ene cross-linkable poly(fluorene)s similar to those reported previously.(*19*) The notable synthetic difference is the deliberate inclusion of a small amount of fluorenone into the backbone of the poly(fluorene) derivatives. These polymers prove to be highly useful in characterizing the effect of cross-linked network architecture on interchain charge communication within the conjugated network. Insight from this characterization is then used to inform the design of improved-efficiency optoelectronic devices.

5.2 Experimental Section

5.2.1 Materials

2,7-dibromo-9-fluorenone, 9,9-dihexylfluorene-2,7-diboronic acid bis(1,3-propanediol) ester, potassium tert-butoxide, tetrakis(triphenylphosphine) palladium(0), and Aliquat 336 were purchased from Aldrich Chemical Company. Solvents, sodium hydroxide, and silica were purchased from Fischer Scientific. All chemicals were used as-received without further purification. Reactions were carried out under N_2 in conventional glassware unless noted otherwise.

5.2.2 Instrumentation

All nuclear magnetic resonance (NMR) spectra were acquired on a Bruker Avance 400 (400MHz) NMR spectrometer and internally referenced via residual solvent signal [$CHCl_3$ ^{1}H 7.26 ppm; ^{13}C 77.00 ppm]. All chemical-shift values are given in ppm. Gel permeation chromatography (GPC) was performed with an Agilent 1260 system at 40 °C with tetrahydrofuran (THF) as the eluent with 1.0 mL/min elution rate. A refractive index detector, 5 µm guard column, three PL gel columns (2 Agilent Mixed-C 5 µm columns and 1 Agilent Mixed-D

5 µm column), and narrow molecular weight polystyrene standards were used. Differential scanning calorimetry (DSC) was performed on a Thermal Analysis (TA) Q-2000 in T-zero aluminum pans using modulated DSC at a heating rate of 3 °C/min. Film thicknesses were measured by contact profilometry using a Dektak 150 profilometer. UV-Vis spectra were recorded in 1-cm path length quartz cuvettes by using a Shimatszu UV 3600 spectrophotometer. Fluorescence measurements were taken on a Perkin-Elmer LS-50B. Infrared spectroscopy of polymer films was performed on a Nicolet 6700 FT-IR spectrometer with a Harrick grazing angle ATR accessory (GATR).

5.2.3 Synthesis of 9,9-dialkenyl-2,7-dibromofluorene Monomers

9,9-dipentenyl- and 9,9-diundecenyl-2,7-dibromofluorene monomers were synthesized as reported in Chapter 4 and a companion study.(*19*) In brief, 2,7-dibromofluorene (2.5 g, 7.7 mmol) was dissolved in 50 mL of a 1:1 mixture of toluene and 50% aqueous NaOH in a condenser-equipped 150mL round bottom flask along with tetrabutylammonium bromide (0.2 g, 0.65 mmol) as a phase transfer reagent. The desired bromoalkene (14.4 mmol) was then added, and the solution was heated to reflux under N_2 and reacted for 17h. After cooling, the product was extracted using ethyl acetate. The organic phase was then neutralized and washed with 1M HCl, whereupon it turned yellow in color, and was further washed with brine. Collection of the organic phase and evaporation of solvent yielded a dark orange oil. Product was purified by column chromatography using 9:1 hexane:ethyl acetate as an eluent, and solvent was removed by evaporation.

5.2.4 Polymerization of Fluorenone-Containing Alkene/Alkyl Side-Chain Poly(fluorene) Copolymers (xPF/O-5 and xPF/O-11)

General procedure: 9,9-Dialkenyl-2,7-dibromofluorene (0.293 mmol), 2,7-dibromo-9-fluorenone (0.007 mmol), 9,9-dihexylfluorene-2,7-diboronic acid bis(1,3-propanediol) ester (0.3 mmol), potassium tert-butoxide (1.8 mmol), sodium chloride (0.85 mmol), and $Pd(PPh_3)_4$ (0.015 mmol) were added along with a stir bar to a 10 mL microwave vial and capped under Ar atmosphere. An N_2-sparged 3: 1 mixture of tetrahydrofuran and water (4 mL) with a few drops of phase-transfer reagent Aliquat 336 was then added to the vial, and the contents were stirred until all solids were dissolved. The solution was subsequently degassed by a freeze-pump-thaw procedure and allowed to warm back to room temperature. The vial was then heated and held at 60 °C in a microwave reactor for 1.5h. The product was then precipitated by pouring into stirring acidic methanol, yielding the crude polymer. After filtering, the polymer was purified by dissolving in $CHCl_3$ and reprecipitating from MeOH. Final products were then filtered and vacuum-dried.

Di-pentenyl/Dihexyl Fluorenone-Containing Poly(fluorene) (xPF/O-5)

xPF/O-5 was obtained as a yellow-white powder (116 mg) in 61% yield. ^{1}H NMR (400 MHz, $CDCl_3$) δ 7.86-7.65 (m, 12H, aromatic); 5.65 (m, 2H, vinyl), 4.94-4.89 (m, 4H, vinyl); 2.16 (b, 6H, alkyl); 1.94 (b, 4H, alkyl); 1.15 (b, 10H, alkyl), 0.91-0.080 (b, 12H, alkyl) ppm. M_n via GPC in tetrahydrofuran: 9.4 kg/mol vs PS standards (DP=15), PDI: 2.9.

Di-undecenyl/Dihexyl Fluorenone-Containing Poly(fluorene) (xPF/O-11)

xPF/O-11 was obtained as a yellow-white powder (210 mg) in 88% yield. ^{1}H NMR (400 MHz, $CDCl_3$) δ 7.86-7.70 (m, 12H, aromatic); 5.78 (m, 2H, vinyl), 5.00-4.94 (m, 4H, vinyl); 2.13-1.92 (b, 15H, alkyl); 1.30-1.15 (b, 40H, alkyl); 0.98-0.81 (b, 20H, alkyl) ppm. M_n via GPC in tetrahydrofuran: 7.9 kg/mol vs PS standards (DP=10), PDI: 2.6.

5.2.5 Polymerization of Alkene/Alkyl Side-Chain Poly(fluorene) Copolymers (xPF-5 and xPF-11)

Fluorenone-free alkene/alkyl side-chain copolymers xPF-5 and xPF-11 were synthesized as reported in Chapter 4 and a companion study.(*19*)

5.2.6 General Procedure for Thin Film Cross-Linking

Cross-linkable poly(fluorene) derivatives were dissolved in chloroform at a concentration 20 mg/mL. A volume of stock solution of multifunctional thiol in toluene (10 mg/mL) was then added to achieve the desired thiol:vinyl molar ratio, and a balance of toluene was finally added to achieve a polymer concentration of 10 mg/mL. These solutions were then spin-coated at 3000 RPM on clean glass substrates. Coated substrates were then heated above the polymers' glass transition temperature under a N_2 blanked, held for 5 min., and cured via exposure to 254 nm UV light via handheld lamp (1.5 mW/cm^2) for 2 min. through a quartz cover dish. Cured films were then rinsed with $CHCl_3$ and dried under vacuum.

5.2.7 Device Fabrication and Measurement

Polymer Light Emitting Diodes (PLEDs)

PLEDs were fabricated with the general architecture of ITO/ Poly(ethylene-dioxythiophene):poly(styrene sulfonate) (PEDOT:PSS)/emissive polymer/Ca/Al. ITO-coated glass was first solvent cleaned via sonication and subsequently treated with O_2 plasma for 3 minutes. PEDOT/PSS (1.3wt% in H_2O, Aldrich) was then spin-coated at 4000 RPM and dried under N_2 at 150°C for 30 minutes. Solutions of cross-linkable polymers were then spun from a mixed solution of chloroform and toluene containing thiol cross-linker (either tetra-functional SH-4 or di-functional SH-2) at prescribed vinyl:thiol mol:mol ratios and cross-linked as described above. As spun and uncured devices were simply placed under vacuum overnight directly following

spin-coating. In order to ensure all devices had comparably thick active layers, spin-coating speeds for the active layer solution was varied for each treatment to account for losses in thickness during curing. Devices were completed by the thermal evaporation of 15 nm Ca cathodes capped with 100 nm Al at pressure <10^{-5} Torr with active areas of 0.15 cm^2. Devices were tested in air using a Kiethley 2602 Sourcemeter and a calibrated Ocean Optics USB4000 UV–vis spectrometer.

Thin Film Transistors

Top-contact thin film transistors were fabricated on highly doped Si/SiO_2 (200nm) substrates. The Si substrates were sequentially cleaned using H_2O, acetone, and IPA, and they were then exposed to O_2-plasma for 2 min. to further clean the surface and install reactive hydroxyl groups. Plasma-treated films were then placed in a vapor chamber with octadecyltrichlorosilane (OTS) for 8hr at 80°C to improve final device performance. Upon removal from OTS vapor, substrates were rinsed with toluene and dried under N_2. Polymer solutions containing thiol cross-linkers were spin-coated at 3000 RPM and cured as described above. Au source/drain were deposited by thermal evaporation through a shadow mask (L=80μm, W=2400μm) at pressure less than 10^{-5} Torr. All devices were subsequently measured under vacuum.

Field effect hole mobilities were extracted from IV measurements in the saturation regime using the conventional relationship:

$$I_D = \frac{W}{2L}\mu_{sat}C_i(V_G - V_{th}),$$

where I_D is the saturated drain current, W is the device channel width, L is the device channel length, μ_{sat} is the saturation-regime hole mobility, C_i is the film capacitance per unit area, V_G is the applied gate voltage, and V_{th} is the threshold voltage.

5.3 Results and Discussion

5.3.1 Synthesis of Cross-Linkable Fluorenone-Containing Poly(fluorene)s

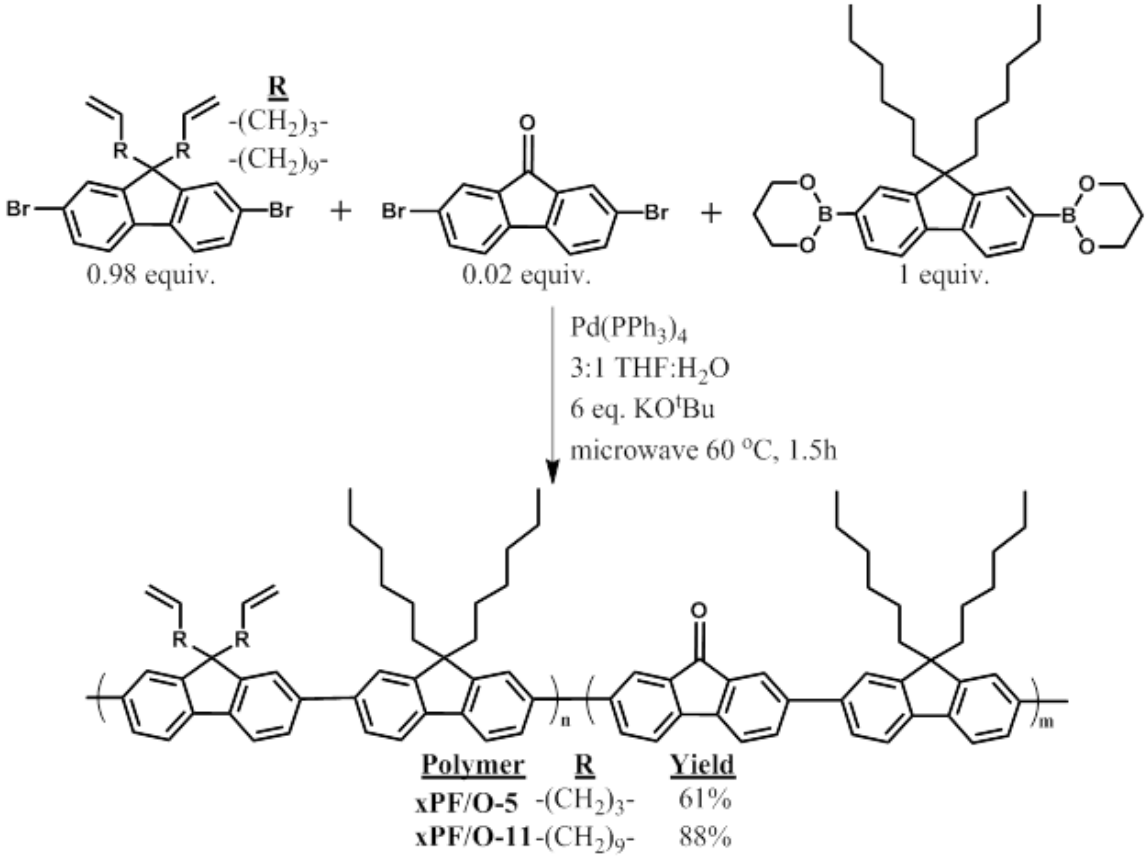

Figure 5.3: Synthesis of fluorenone-containing poly(fluorene)s xPF/O-5 and xPF/O-11 via Suzuki-Miyaura cross-coupling.

The synthesis of thiol-ene cross-linkable poly(fluorene) derivatives by copolymerization of alkenyl side-chain fluorene and di-hexyl fluorene monomers has been introduced previously in Chapter 4. This chemistry is easily adapted to the synthesis of poly(fluorene)s containing fluorenone in the conjugated backbone by including 1 mol% of 2,7-dibromo-9-fluorenone in the monomer feed, as shown in Figure 5.3. These new poly(fluorene) derivatives could be photo-chemically cross-linked through either short pentenyl side-chains (xPF/O-5) or longer undecenyl side-chains (xPF/O-11). Pristine polymers without fluorenone incorporation (xPF-5 and xPF-11) were synthesized as described previously. In both fluorenone-free and fluorenone-containing

polymers, optimized Suzuki-Miyauara reaction conditions as informed by previous studies(*19, 20*) were employed to minimize Heck coupling of the alkenes with the aryl bromide monomers which, uncontrolled, yielded self-cross-linked, insoluble, unusable materials.

Table 5.1: Summary of polymer size, dispersity *Đ,* and glass transition temperature T_g of alkene/alkyl side-chain poly(fluorene)s both with and without fluorenone incorporation.

Polymer	M_n (kg/mol)	Number Avg. Fluorene units per chain	*Đ*	T_g (°C)
xPF-5	8.4	26	2.6	108
xPF-11	9.4	23	2.5	45
xPF/O-5	9.4	30	2.9	99
xPF/O-11	7.9	20	2.6	46

Table 5.1 summarizes the physical size properties of the polymers as obtained from Suzuki-Miyauara coupling. All polymers were of comparable size, with a number average of 20-30 continuous fluorene units in the conjugated polymer backbone. These numbers are all well above the conjugation length of poly(dialkyl fluorene)s (~10 fluorene units),(*21*) allowing for meaningful comparison of the optoelectronic behavior between different polymers. Assuming an equal reactivity of the dialkenyl dibromofluorene (0.98 equiv.) and dibromofluorenone monomers (0.02 equiv.) during polymerization, these degrees of polymerization statistically result in approximately one fluorenone unit per four or five poly(fluorene) molecules. The low amount of fluorenone incorporated was chosen for two reasons: first, so that the strong fluorenone emission and charge trapping would not wholly overwhelm high-energy fluorene emission, and second, so that most poly(fluorene) chains would *not* have fluorenone present. This is crucial in using fluorenone as a colorimetric sensor for network connectivity so that the enhancement or inhibition of interchain electronic communication arising from network connectivity could be observed (i.e., fluorescence can occur from both high energy fluorene and low energy fluorenone, instead of simply from the charge trapping fluorenone). The low loading

of fluorenone (overall 1 mol% relative to di-functional fluorene units) is not assessable by NMR, however FTIR absorption spectra (Figure 5.4) and the photoluminescence spectra discussed in the following sections unambiguously confirm successful incorporation of fluorenone into the polymers. The differences in glass transition temperature (T_g) values can most likely be attributed to the slight variation in molecular weights and dispersities between polymer samples.

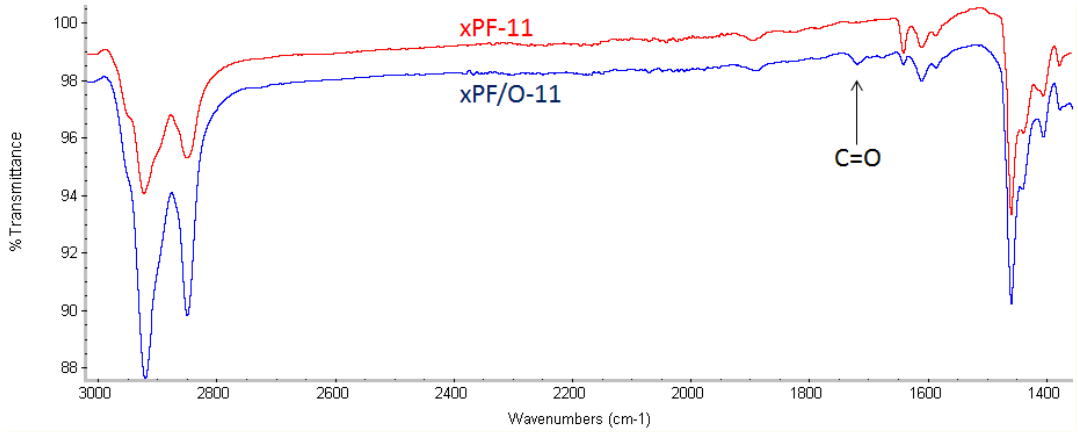

Figure 5.4: FTIR of pristine xPF-11 and fluorenone-containing xPF/O-11. Successful incorporation of fluorenone into the polymer is evidenced by the carbonyl peak at 1710 cm^{-1} seen only in the xPF/O-11 sample.

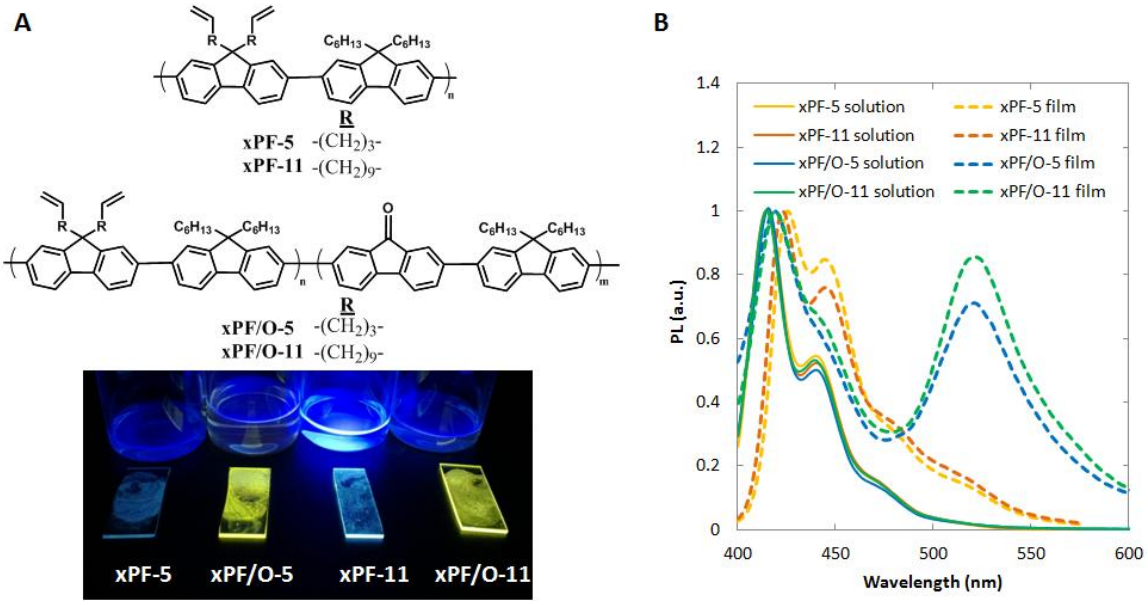

Figure 5.5: (A) Structures and digital photograph of pristine alkene/alkyl copolymers (xPF-5 and xPF-11) and fluorenone-containing alkene/alkyl copolymers (xPF/O-5 and xPF/O-11). Photo shows the materials' observed fluorescence when exposed to 365 nm UV light as solutions in $CHCl_3$ and as thin films. (B) Associated photoluminescence (PL) spectra of pristine copolymers (xPF-5 and xPF-11) and the fluorenone-containing copolymers (xPF/O-5 and xPF/O-11) under 365 nm photo excitation.

Figure 5.5A shows the structure of fluorenone-free and fluorenone-containing copolymers, along with a photograph of their fluorescence when photo excited at 365 nm. The dramatic effect of just 1 mol% of fluorenone n the monomer feed on the resulting polymer's photoemission is clearly seen by eye in the thin film samples. The fluorenone-free xPF-5 and xPF-11 polymers and the fluorenone-containing xPF/O-5 and xPF/O-11 polymers all fluoresce bright blue in the solution state, characteristic of high-energy fluorene backbone emission. In contrast, the fluorenone-containing xPF/O-5 and xPF/O-11 show dramatically distinct green fluorescence in the solid state, while the fluorenone-free xPF-5 and xPF-11 retain their characteristic blue fluorescence. This lower energy green emission in the solid state is a clear indication of successful fluorenone incorporation during synthesis.

The solution state photoluminescence (PL) spectra in Figure 5.5B reveal effectively identical emission for all species regardless of fluorenone content. Only in the aggregated solid

state does the green emission from the fluorenone species become evident, confirming visual evidence. While the solid state PL spectra are dramatically affected by fluorenone incorporation, UV-vis absorption spectra with the same polymers show effectively no difference (Figure 5.6). These observations suggest that photoexcitation occurs along the π-π^* transition in polyfluorene and low energy green emission occurs only via energy transfer to the fluorenone following photo excitation of the high energy fluorene backbone. This agrees with excitation data from Kulkarni and co-workers who only observe fluorenone π-π^* absorption at 450 nm with high fluorenone content (10 mol%), yet observe low energy green PL at all dilute fluorenone loadings.(16) In the dilute solution state, the fluorenone-free poly(fluorene) chains dominate the PL spectra owing to their statistical abundance. In the solid state, efficient interchain electronic communication facilitates the migration of excitation energy to the infrequent low-energy fluorenone groups. This sensitivity of photoemissive color to interchain contact is the basis of using fluorenone as an optoelectronic connectivity sensor in the following experiments.

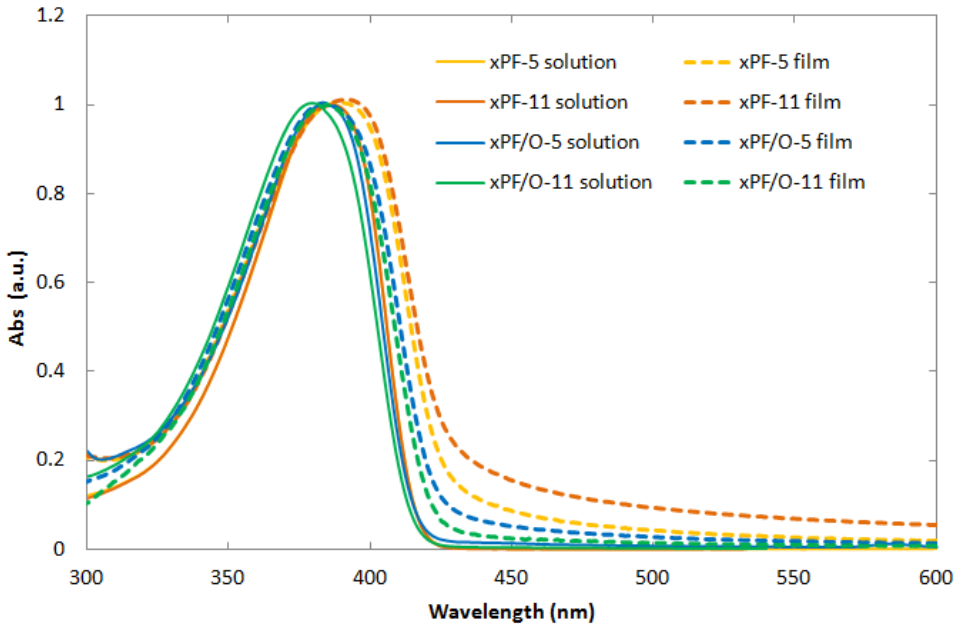

Figure 5.6: UV-vis absorption spectra of fluorenone-containing xPF/O-5 and xPF/O-11 compared to their fluorenone-free counterparts xPF-5 and xPF-11. Solution measurements were made in chloroform, and thin film measurements were made from films spin-coated from chloroform.

5.3.2 Network Formation and Optical Properties

Given the considerable changes in xPF/O-5 and xPF/O-11 PL spectra between dilute and aggregated states, PL measurements were next investigated as a colorimetric detector of interchain electronic communication in cross-linked conjugated polymers with varying network architecture. Photo-curing and thin film network formation were achieved as described in Chapter 2-4. In general, thiol-ene compatible conjugated polymers were spin-coated from a solution containing a thiol cross-linker (structures are shown in Figure 5.7). Spun thin films were then cured under N_2 by exposure to 254 nm UV light at temperatures above their T_g. PL spectra of the cured semiconducting networks were then measured.

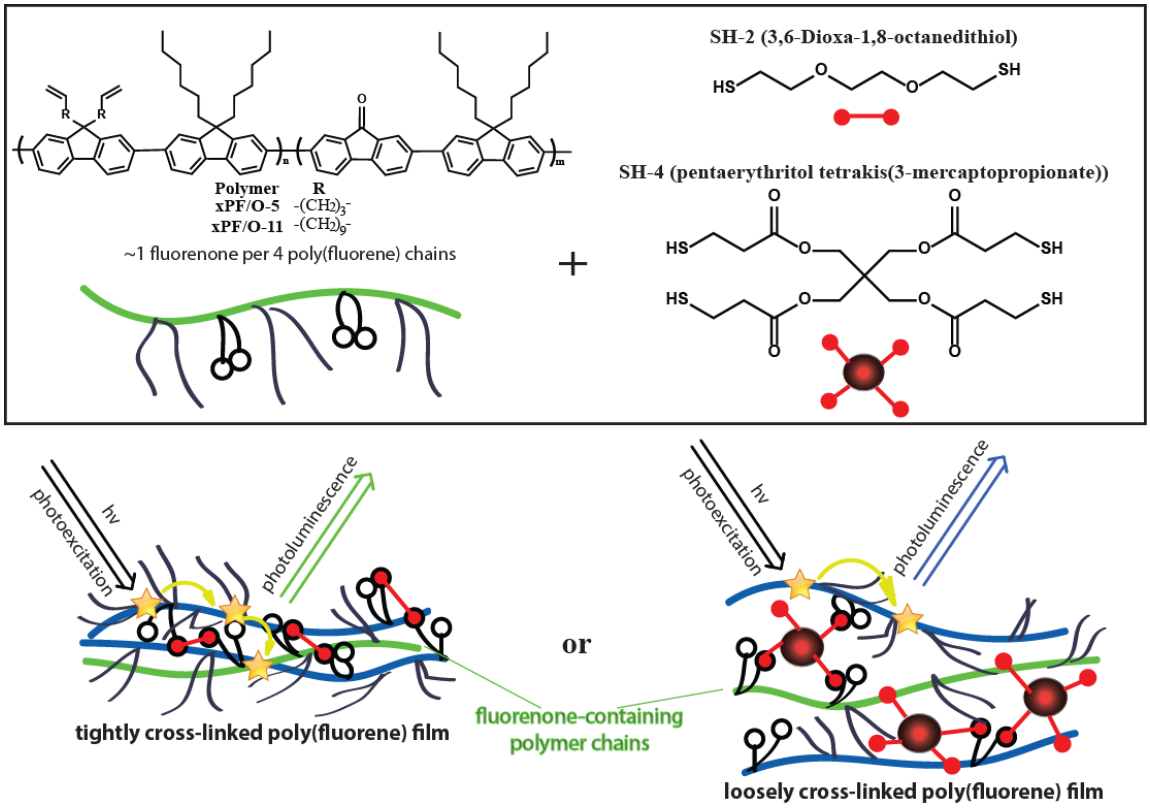

Figure 5.7: Illustration showing how network density and connectivity could affect electronic communication in cross-linked poly(fluorene) networks. Fluorenone-containing chains are represented in green, and fluorenone-free chains are represented in blue. Photo excitation of a tightly bound network allows for efficient migration of an excited species to a fluorenone moiety with subsequent photo emission. A diluted loosely bound network prohibits such effective charge trapping and recombination.

Figure 5.7 illustrates the principle of using network connectivity to affect the facility of interchain electronic communication in conjugated polymer networks. By using a short, flexible cross-linker like the di-functional thiol 3,6-dioxa-1,8-octanedithiol (SH-2), the network can be cross-linked with high density and contraction, while a bulkier tethered tetra-function thiol like pentaerythritol tetrakis(3-mercaptopropionate) (SH-4) provides significant volumetric contribution to the network and can act as a diluents as described in Chapter 4. By incorporating fluorenone-containing poly(fluorene)s into the cross-linked network (illustrated in green), photoluminescence from either the low-energy fluorenone sites or high energy poly(fluorene) backbone could be correlated with network architecture.

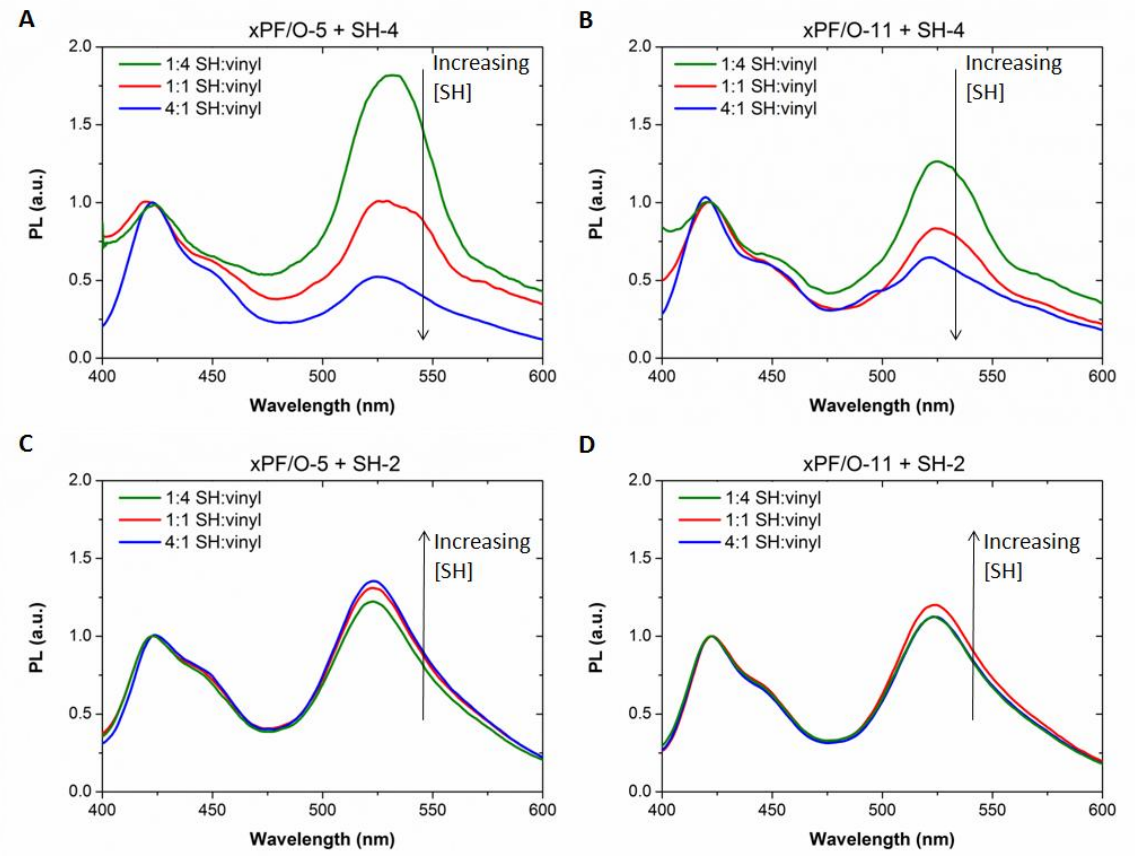

Figure 5.8: Photoluminescence (PL) of fluorenone-containing dipentenyl xPF/O-5 (A,C) and diundecenyl xPF/O-11 (B,D) cross-linked films as a function of thiol content for tetra-functional and di-functional thiol cross-linkers. Excitation wavelength for all samples was 365 nm.

Figure 5.8 shows photoluminescence (PL) spectra of short side-chain xPF/O-5 and long side-chain xPF/O-11 polymer networks cured with the two different thiol cross-linkers, demonstrating how the fluorenone emission can be used as colorimetric indicator of network architecture. The strong emission at 520 nm arising from fluorenone incorporation is clearly evident in all network configurations. The relative intensity of this emissive mode compared to the blue poly(fluorene) PL emission between 400 and 450 nm serves as metrology tool for assessing network density and interchain communication in the conjugated networks.

Comparing the PL spectra from the tetra-thiol- to the di-thiol-cured systems most clearly shows the effect of network architecture on the conjugated materials' optoelectronic properties. As the amount of tetra-thiol is increased, the fluorenone PL emission in the xPF/O-5 and xPF/O-11 networks greatly decreases, indicating increasingly poor interchain charge communication similar to the dilute solution state poly(fluorene)s in Figure 5.5. By contrast, the networks cured with the shorter, linear di-thiol shows the exact opposite behavior. Fluorenone PL emission increases as more cross-linker is added, suggesting more tightly packed poly(fluorene) chains with better interchain electronic communication. While this increase is slight and not as dramatic as the changes observed in the tetra-thiol-cured networks, it clearly opposes the phenomenon occurring in the tetra-thiol networks.

The short side-chain xPF/O-5 networks (Fig. 5.8A,C) display considerably greater PL sensitivity overall than the long side-chain xPF/O-11 networks (Fig. 5.8B,D), whether cured with either SH-2 or SH-4. This is an intuitive result of the longer flexible undecenyl side-chains being able to conform and distort through the network during curing, leading to less influence on the conjugated poly(fluorene) backbone. In contrast, the pentenyl side-chains are shorter than adjacent di-hexyl side-chains in the xPF-5 copolymer, and so they more efficiently push and pull the conjugated backbone when reacted into the thiol-ene network.

Unexpectedly, a curious increase of the low-energy fluorenone emission in the polymer thin films occurs upon addition of any amount thiol-cross-linker compared to as-spun films without any added thiol. The exact cause of this increased low-energy emission is still an open question, possibly arising from hydrogen-bonding interactions between the thiols and ketone of the fluorenone groups leading to subtle and complex morphological changes.

The PL data here encouragingly suggest that clever choice of cross-linker in a photo-cured conjugated polymer network can be used to tune the desired optoelectronic properties from a single cross-linkable semiconducting polymer. A larger more rigid cross-linker, such as SH-4, can be used to discourage chain packing and crystallization, as would be advantageous in amorphous polymer applications. A smaller more flexible cross-linker, such as SH-2, can be used to the opposite effect, pulling conjugated polymer chains closer together to encourage facile charge transport, as would be desired in a polymer thin film transistor.

5.3.3 Cross-Linked Poly(fluorene) Semiconducting Devices

Cross-linked polymer light emitting diodes (PLEDs) were fabricated from the systems described above to investigate how the network's structural influence on optoelectronics might translate to device design. PLEDs were fabricated with xPF-5 owing to the greater sensitivity of the pentenyl side-chain system to cross-linker structure as seen in Figure 5.8. Current density and luminance of a number of devices are shown in Figure 5.9 and reveal performance behavior that can indeed be tuned by cross-linking architecture. In particular, the more tightly connected network, xPF-5 cured with the short linear SH-2 di-thiol, resulted in devices which were twice as bright with three times the luminous efficiency compared to as-spun xPF-5 devices containing no cross-linker. In contrast, xPF-5 network devices cured with the bulky SH-4 cross-linker showed poor performance with low cross-linker loading or did not work at all at high cross-

linker loading. In all cases, the cross-linked devices showed an increase in blue emission and shifted overall toward white electroluminescence (Figure 5.10).

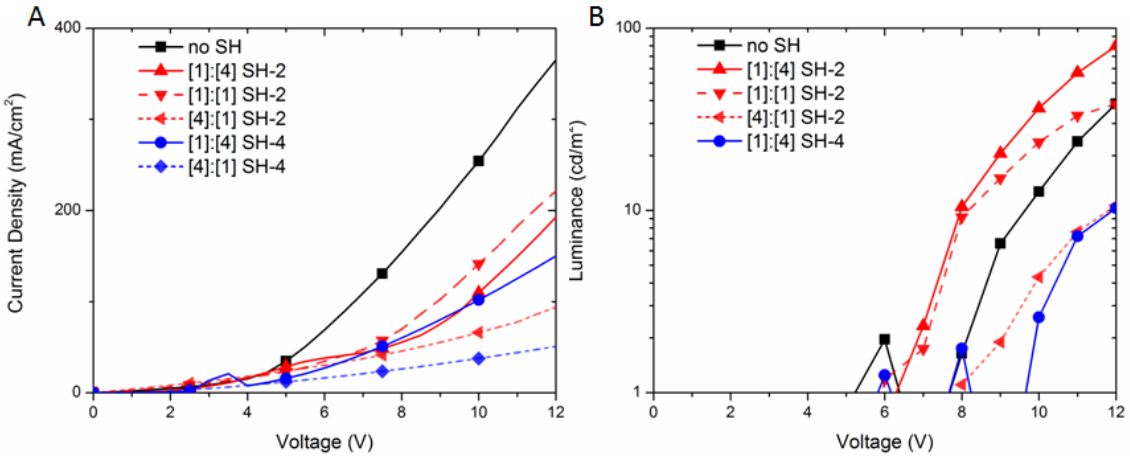

Figure 5.9: Current density-voltage (A) and luminance-voltage (B) output of best performing xPF-5 PLEDs.

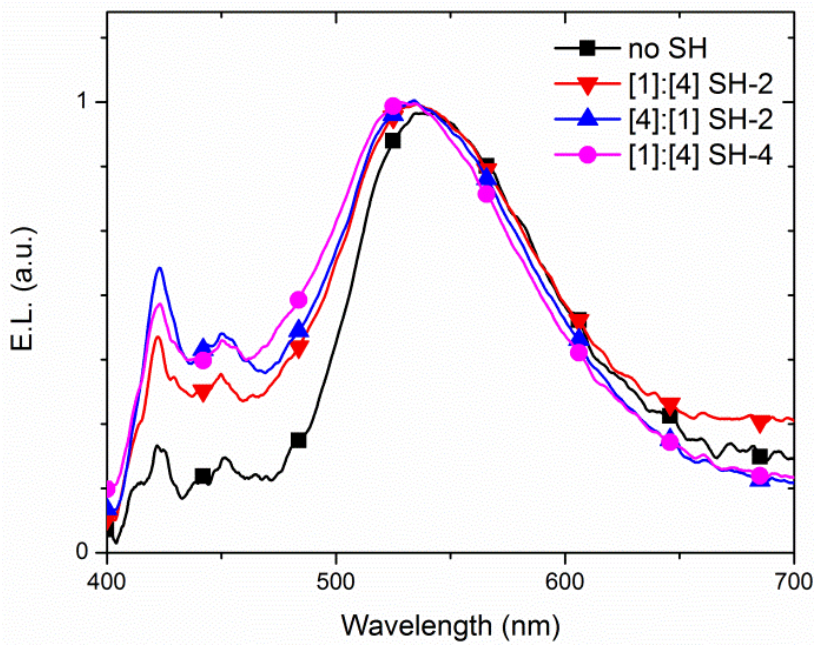

Figure 5.10: Electroluminescence (EL) spectra of xPF-5 PLEDs cross-linked with varying network architecture indicated in legend.

Close examination of the current density-voltage (J-V) and luminance-voltage (L-V) behavior of the cured xPF-5 PLEDs provide even further insight into the effect of network architecture on charge transport and recombination. PLEDs incorporating as spun films of xPF-5 without any thiol show higher overall current density than any device incorporating thiol. In

these cases the lack of insulating thiol cross-linker increases current flow through xPF-5 chains to some degree and improves charge mobility. However despite decreasing current density, devices cured with SH-2 at modest thiol loading (up to 1:1 molar vinyl:thiol) consistently display brighter luminance and lower turn-on voltages than the un-cured, thiol-free devices. A summary of device performance over multiple samples is listed in Table 5.2.

As more thiol is loaded into the thin film, device performance becomes less consistent (although the best performing cross-linked devices still outperform films without thiol as well as films incorporation un-cured thiols). Addition of too much SH-2 leads to a significant reduction in both current density and device brightness. Cross-linked devices cured with the tethered SH-4 thiol show similarly reduced performance at even low loading (1:4 molar thiol:vinyl) or devices that produced no visible electroluminescence at high loading (4:1 molar thiol:vinyl). Both cases are clearly the result of incorporating too much insulating material into the semiconducting poly(fluorene) network.

Table 5.2: Performance summary of thiol-ene cross-linked pentenyl side-chain poly(fluorene) xPF-5 in light emitting diodes.

xPF-5 Device	Turn On Voltage (V)	Brightness at 12 V (cd/m^2)	Max. Efficiency (10^{-2} cd/A)
No SH	7.5	33 ± 7	0.9 ± 0.1
SH-2 [1]:[4]	6.5	56 ± 3	2.9 ± 0.8
SH-2 [1]:[1]	7.0	23 ± 13	1.0 ± 0.6
SH-2 [4]:[1]	8.5	11 ± 6	1.1 ± 0.4
SH-4 [1]:[4]	9.5	10 ± 3	0.6 ± 0.1
SH-4 [4]:[1]	n/a	n/a	n/a

The mechanism for the devices' performance improvement when cured with SH-2 could be due to a few factors. Aggregates and excimers are generally considered to reduce PLED emissive performance via self-quenching, and work by Rathnayake and co-workers has shown that addition of an insulating, dilatory matrix can improve PLED brightness.(*22*) However, PL

measurements in Figure 5.8 suggest increased aggregation and excited state energy transfer despite the improved performance of those PLEDs. Clearly chain packing and aggregation are not unequivocally detrimental to PLEDs. Some studies have demonstrated that "weak" aggregates can indeed improve and blue-shift electroluminescent properties as charge transport is enhanced in the conjugated polymer thin films without compromising photo-emissive emission.(*23, 24*) This is particularly compelling since the referenced studies cite the benefit of long amorphous side chains, similar to those in the poly(fluorene) systems here. It is also possible that the insulating nature of the thiol cross-linker improves the balance of hole and electron mobilities which would further contribute to luminescent enhancements as long as the insulating component (i.e., thiol loading) is not too great.

Cross-linked xPF-5 was additionally incorporated into thin film transistors (TFTs) to serve as a hole-conducting layer under field effect operation, with results summarized in Table 5.3. Devices did not show as pronounced performance improvement and variation as the PLEDs, likely due to the typically lackluster performance of the highly amorphous poly(fluorene)s in TFTs in general. However, field-effect behavior was clearly recorded in cross-linked films. As with the PLEDs, adding an excess of the bulky SH-4 tetra-thiol resulted in significant degradation of electronic properties due to the large content of insulating material. These results confirm that modest thiol incorporation does not inhibit charge transport, and we are looking forward to exploring thiol-ene influence on higher mobility, more crystalline conjugated polymer devices.

Table 5.3: Performance of variably cross-linked xPF-5 in thin film transistors.

Cured xPF-5 with cross-linker thiol:vinyl loading (mol:mol)	Turn-On Voltage (V)	On/Off Drain Current Ratio	Field Effect Hole Mobility (10^{-7} cm^2/V s)
None	-29.0	34.5	0.3
SH-4 [1]:[4]	-28.5	29.2	0.6
SH-4 [4]:[1]	0.6	4.8	1
SH-2 [1]:[4]	-25.5	17.2	0.3
SH-2 [4]:[1]	-27.7	39.2	0.2

These operational device results clearly show how the thiol-ene reaction can be used as a molecular-level handle with the same conjugated polymer to push and pull polymer chains beyond their as-spun morphologies. While these devices are far from optimized and clearly do not yet show performance worthy of commercialization, these results are exciting since they reveal network architecture to be a new molecular handle on device performance. The results optimistically suggest that thiol-ene and similar high-fidelity cross-linking chemistries can be used to tune conjugated film structure and morphology in ways that are impossible to accomplish through other annealing routes.

5.4 Conclusions

In this chapter, a small amount of the low-energy emissive fluorenone species was incorporated into the backbone of thiol-ene curable poly(fluorene)s as a colorimetric detector to assess the effect of cross-linked conjugated network architecture on the optoelectronic properties of variously scaffolded poly(fluorene) networks. By tracking the characteristic, highly packing-dependent green emission of fluorenone, it was shown that the thiol-ene reaction can be used a powerful handle on molecular packing which in turn influences the interchain electronic communication in conjugated polymer thin films. Chain packing and charge transport was found to decrease in networks cured with a bulky tetrathiol, while a shorter linear dithiol resulted in a tight, contracted network which increased electronic communication and excited state trapping at the fluorenone recombination sites. Driven by brightness improvements in electroluminescent devices, these results offer a fully generalizable approach to influencing optoelectronic properties of conjugated systems using thiol-ene click chemistry to fine-tune their packing and electronic communication.

5.5 References

1. L. D. Bozano, K. R. Carter, V. Y. Lee, R. D. Miller, R. Dipietro, J. C. Scott, Electroluminescent devices based on cross-linked polymer blends *J. Appl. Phys.* **94**, 3061 (2003).

2. M. S. Bayerl, T. Braig, O. Nuyken, D. C. Muller, M. Groβ, K. Meerholz, Crosslinkable hole-transport materials for preparation of multilayer organic light emitting devices by spin-coating, *Macromolecular Rapid Comm.* **20**, 224-228 (1999).

3. J. P. Chen, G. Klaerner, J. Lee, D. Markiewicz, V. Y. Lee, R. D. Miller, J. C. Scott, Efficient , blue light-emitting diodes using cross-linked layers of polymeric arylamine and fluorene, *Synth. Met.* **107**, 129-135 (1999).

4. G. Klärner, J.-I. Lee, V. Y. Lee, E. Chan, J.-P. Chen, A. Nelson, D. Markiewicz, R. Siemens, J. C. Scott, R. D. Miller, Cross-linkable Polymers Based on Dialkylfluorenes, *Chem. Mater.* **11**, 1800-1805 (1999).

5. G. K. Paul, J. Mwaura, A. A. Argun, P. Taranekar, J. R. Reynolds, Cross-Linked Hyperbranched Arylamine Polymers as Hole-Transporting Materials for Polymer LEDs, *Macromolecules* **39**, 7789-7792 (2006).

6. E. Scheler, I. Bauer, P. Strohrigl, Synthesis and photopatterning of fluorene based reactive mesogens, *Macromolecular Symposia* **254**, 203-209 (2007).

7. A. R. Davis, J. A. Maegerlein, K. R. Carter, Electroluminescent Networks via Photo "Click" Chemistry, *J. Am. Chem. Soc.* **133**, 20546-20551 (2011).

8. F. B. Koyuncu, A. R. Davis, K. R. Carter, Emissive Conjugated Polymer Networks with Tunable Band-Gaps via Thiol–Ene Click Chemistry, *Chem. Mater.* **24**, 4410-4416 (2012).

9. N. B. Cramer, J. P. Scott, C. N. Bowman, Photopolymerizations of Thiol-Ene Polymers without Photoinitiators, *Macromolecules* **35**, 5361-5365 (2002).

10. C. E. Hoyle, C. N. Bowman, Thiol-Ene Click Chemistry, *Angew. Chem. Int. Ed.* **49**, 1540-1573 (2010).

11. C. E. Hoyle, A. B. Lowe, C. N. Bowman, Thiol-click chemistry: a multifaceted toolbox for small molecule and polymer synthesis, *Chem. Soc. Rev.* **39**, 1355-1387 (2010).

12. R. K. Iha, K. L. Wooley, A. M. Nystrom, D. J. Burke, M. J. Kade, C. J. Hawker, Applications of Orthogonal "Click" Chemistries in the Synthesis of Functional Soft Materials, *Chem. Rev.* **109**, 5620-5686 (Nov, 2009).

13. L. Romaner, A. Pogantsch, P. S. de Freitas, U. Scherf, M. Gaal, E. Zojer, E. J. W. List, The Origin of Green Emission in Polyfluorene-Based Conjugated Polymers: On-Chain Defect Fluorescence, *Adv. Func. Mater.* **13**, 597-601 (2003).

14. V. N. Bliznyuk, S. A. Carter, J. C. Scott, G. Klärner, R. D. Miller, D. C. Miller, Electrical and Photoinduced Degradation of Polyfluorene Based Films and Light-Emitting Devices, *Macromolecules* **32**, 361-369 (1999).

15. X. Gong, K. I. Parameswar, D. Moses, C. B. Guillermo, A. J. Heeger, S. S. Xiao, Stabilized Blue Emission from Polyfluorene-Based Light-Emitting Diodes: Elimination of Fluorenone Defects, *Adv. Func. Mater.* **13**, 325-330 (2003).

16. A. P. Kulkarni, X. Kong, S. A. Jenekhe, Fluorenone-Containing Polyfluorenes and Oligofluorenes: Photophysics , Origin of the Green Emission and Efficient Green Electroluminescence, *J. Phys. Chem. B* **108**, 8689-8701 (2004).

17. K. Becker, J. M. Lupton, J. Feldmann, B. S. Nehls, F. Galbrecht, D. Q. Gao, U. Scherf, On-Chain Fluorenone Defect Emission from Single Polyfluorene Molecules in the Absence of Intermolecular Interactions, *Adv. Func. Mater.* **16**, 364-370 (2006).

18. H. P. Rathnayake, A. Cirpan, F. E. Karasz, M. Y. Odoi, N. I. Hammer, M. D. Barnes, P. M. Lahti, Luminescence of Molecular and Block Copolymeric 2,7-Bis(phenylethenyl)-fluorenones; Identifying Green-Band Emitter Sites in a Fluorene-Based Luminophore, *Chem. Mater.* **19**, 3265-3270 (2007).

19. A. R. Davis, K. C. Carter, Cross-Linked Poly(fluorene) Networks with Varying Network Connectivity by Thiol-Ene Photo Chemistry, *submitted*.

20. A. R. Hunt, S. K. Stewart, A. Whiting, Heck versus Suzuki Palladium Catalyzed Cross-Coupling of a Vinyl Borate Ester with Aryl Halides, *Tetrahedron Lett.* **34**, 3599-3602 (1993).

21. G. Klaerner, R. D. Miller, Polyfluorene Derivatives: Effective Conjugation Lengths from Well-Defined Oligomers, *Macromolecules* **31**, 2007-2009 (1998).

22. H. P. Rathnayake, A. Cirpan, P. M. Lahti, F. E. Karasz, Optimizing LED Properties of 2,7-Bis(phenylethenyl)fluorenes, *Chem. Mater.* **18**, 560-566 (2006).

23. Y. Shi, J. Liu, Y. Yang, Device performance and polymer morphology in polymer light emitting diodes: The control of thin film morphology and device quantum efficiency, *J. Appl. Phys.* **87**, 4254 (2000).

24. Y.-H. Niu, Q. Hou, Y. Cao, Thermal annealing below the glass transition temperature: A general way to increase performance of light-emitting diodes based on copolyfluorenes, *Appl. Phys. Lett.* **81**, 634 (2002).

CHAPTER 6

PHOTO GRAFTING VINYL-CONTAINING POLY(FLUORENE)S ONTO THIOL-FUNCTIONALIZED SURFACES[‡]

6.1 Introduction

Over the past two decades, the structural and chemical details of organic/organic and organic/inorganic interfaces in organic electronic devices have been found to have immense impact on device performance.(*1-3*) This has led to considerable research into surface modification techniques that improve ordering at the interface, beneficially shift metal work functions, or improve device longevity. These effects have been observed through the use of self-assembled monolayers (SAMs)(*4-6*) or with thin interlayer materials such as zwitterionic species,(*7*) conjugated polyelectrolytes,(*8, 9*) or inorganic materials(*10*).

[‡] Portions of this chapter have been reprinted with permission from Davis, Carter, *Langmuir* (2014, accepted). Copyright 2014 American Chemical Societry.

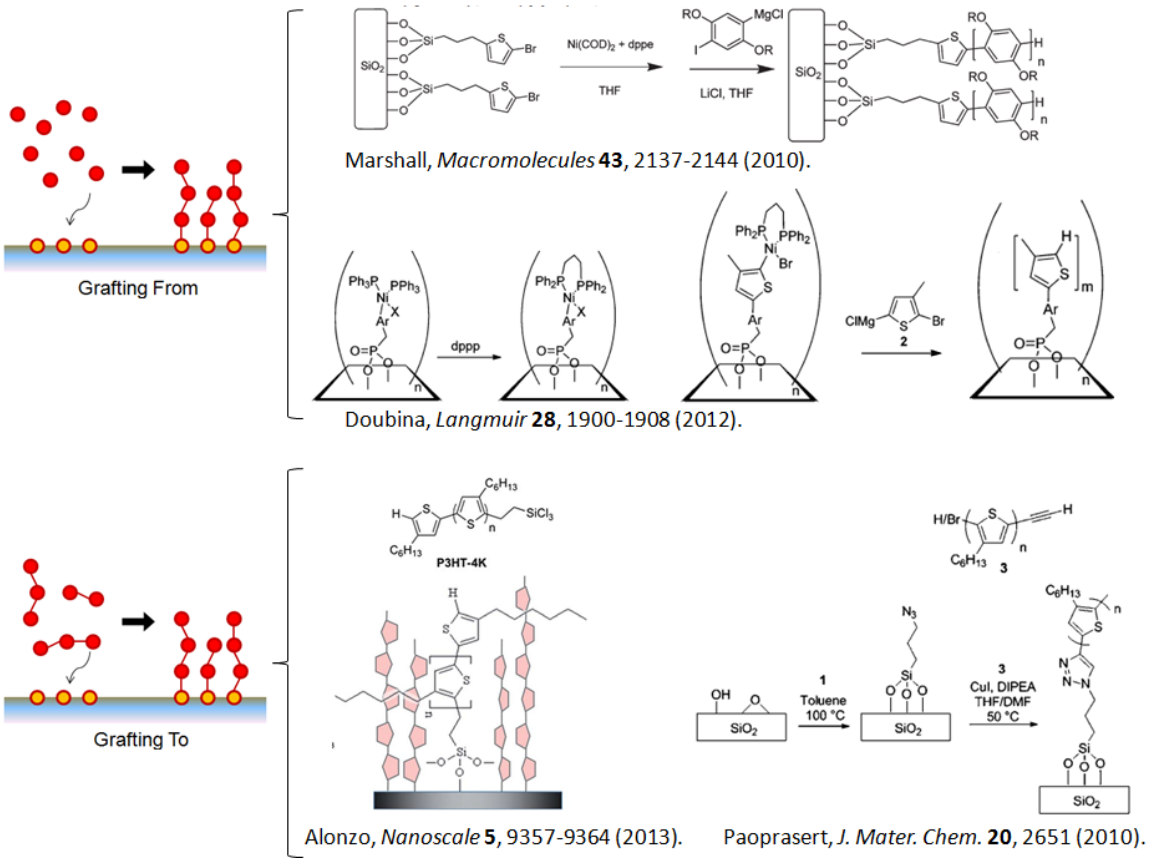

Figure 6.1: Illustration of grafting-from and grafting-to processes, with examples of conjugated polymer grafting selected from published literature. Adapted with permission from (as indicated in figure): Marshall, *Macromolecules* 43, 2127-2144 (2010). Copyright 2010 American Chemical Society; Doubina, *Langmuir* 28, 1900-1908 (2020). Copyright 2012 American Chemical Society; Alonzo, *Nanoscale* 5, 9357-9364 (2013). Copyright 2013 Royal Society of Chemistry; Paoprasert, *J. Mater. Chem.* 20, 2651-2658 (2010). Copyright 2010 Royal Society of Chemistry.

For this reason, the covalent bonding of semiconducting polymers directly to inorganic and organic surfaces is of particular interest due to a potentially high degree of control over surface ordering and chemistry. Figure 6.1 shows examples of "grafting from" and "grafting to" approaches from published studies where conjugated polymers were attached to surfaces via popular grafting chemistries. Particular "grafting from" success with poly(fluorene) has been achieved via Yamamoto polymerization from a surface bound monomer(*11*) and polyacetylene via tungsten-catalyzed microwave polymerization from an acetylene-functionalized surface.(*12*) Additional grafting-from surface-initiated polymerization success has been seen with the growth

of polyvinylcarbazole brushes via free radical polymerization(*13*) as well as poly(thiophene) and poly(phenylene) brushes via Kumada-type polymerizations.(*14-19*) Typically, high coverage of conjugated polymers on surfaces via "grafting to" – either by bonding along the polymer chain or by bonding as a brush from the chain end – is difficult due to their relatively rigid nature. Furthermore, very few studies quantitatively report grafting densities, and previous experience from the Carter laboratory and others have often yielded patchy, non-uniform surface coverage of conjugated polymers through either grafting method.(*14, 17*) There has been modest but increasing success in recent years using "grafting to" approaches, primarily employing reactive silanes or alkyne-azide chemistry, to attach conjugated polymer chains directly to a reactive surface.(*20-23*)

Inspired by the successes of alkyne-azide click chemistry compared to the general difficulties of conjugated polymer grafting, the thiol-ene reaction could provide an efficient route to functionalize surfaces with conjugated polymers. As detailed in previous chapters, photo-initiated thiol-ene chemistry is highly efficient and tolerant of impurities, giving the reaction a wide range of applicability and interest.(*24-27*) The efficiency of this reaction may be useful in accomplishing the historically difficult task of grafting conjugated polymers to surfaces. Chapters 2-5 have demonstrated that conjugated polymers can easily be functionalized to include alkene moieties, and these polymers were shown to be amenable to rapid initiator-free cross-linking reactions with multi-functional thiols to form robust electronically-active networks.(*28, 29*) Expanding on this work, this chapter describes the successful photo-induced thiol-ene surface grafting of end-group and side-chain functionalized conjugated poly(fluorene)s and investigates the effect of that surface tethering on their optoelectronic properties.

6.2 Experimental Section

6.2.1 Materials

All materials were purchased from Sigma-Aldrich Company and used without further purification unless otherwise noted. $Pd(PPh_3)_4$ and $Ni(COD)_2$ were purchased from Strem Chemicals and handled under inert atmosphere. Silicon substrates (B-doped, 0.01-0.018 ohm-cm, 200nm thermally grown SiO_2) were purchased from University Wafers.

6.2.2 Instrumentation

All nuclear magnetic resonance (NMR) spectra were acquired on a Bruker AF 400 MHz spectrometer and internally referenced via residual solvent signal [$CHCl_3$: ^1H) 7.26 ppm; ^{13}C NMR) 77.00 ppm]. All chemical shift values are given in ppm. Gel permeation chromatography (GPC) was performed with an Agilent 1260 system at 40 °C with tetrahydrofuran (THF) as the eluent with 1.0 mL/min elution rate. A refractive index detector, 5 µm guard column, three PL gel columns (2 Agilent Mixed-C 5 µm columns and 1 Agilent Mixed-D 5 µm column), and narrow molecular weight polystyrene standards were used. Differential scanning calorimetry (DSC) was performed on a Thermal Analysis (TA) Q-2000 in T-zero aluminum pans using modulated DSC at 3°C/min.

Fluorescence measurements were taken on a Perkin-Elmer LS-50B using a front surface attachment for thin film measurements. Infrared spectroscopy of polymer films were performed on a Nicolet 6700 FT-IR spectrometer with a Harrick grazing angle ATR accessory (GATR).

6.2.3 Synthesis of 2,7-dibromo-9,9-dipentenyl-9H-fluorene

The side-chain vinyl functionalized monomer, 2,7-dibromo-9,9,dipentenyl-9H-fluorene, was synthesized from 2,7-dibromo fluorene as described in Chapter 4. 2,7-dibromofluorene (2.5

g, 7.72 mmol) and tetrabutylammonium bromide (0.21 g, 0.085 mmol) were dissolved 50 mL of 1:1 mixture of toluene and 50% NaOH. The solution was sparged with N_2 and stirred for 5 min. Bromopentene (2.3 g, 15.4 mmol) was slowly added dropwise and the solution was observed to turn deep purple. Reaction was refluxed for 17 hr. The organic phase was extracted with ethyl acetate, neutralized, and washed with 1M HCl and brine, where the solution turned deep yellow in color. Solvent was removed by evaporation to yield a dark yellow oil which was purified by column chromatography (9:1 hexane:ethyl acetate; difunctional product R_f = 0.84). Final product was crystallized from MeOH as an off-white solid in 81% yield (2.87 g). ^{1}H NMR (400 MHz, $CDCl_3$) δ 7.44-7.30 (m, 6H, aromatic), 5.56 (m, 2H, vinyl), 4.88 (m, 2H, vinyl), 4.84 (m, 2H, vinyl), 1.94-1.82 (m, 8H, alkyl), 0.69 (m, 4H, alkyl) ppm. ^{13}C NMR (400 MHz, $CDCl_3$) δ 152.1 (aromatic), 139.1 (aromatic), 138.3 (vinyl), 130.3 (aromatic), 126.2 (aromatic), 121.6 (aromatic), 121.2 (aromatic), 114.7 (vinyl), 55.5 (quaternary), 39.6, 33.8, 22.9 ppm.

6.2.4 Polymerization of Side-Chain Functionalized Poly(fluorene) (pPF)

Alternating 9,9-dihexyl/dipentenyl poly(fluorene) copolymer pPF was synthesized by conventional Pd-catalyzed Suzuki-Miyaura coupling as described in Chapter 4. 2,7-dibromo-9,9-dipenetenyl-9H-fluorene (301 mg, 0.65 mmol) and 9,9-dihexylfluorne-2,7-diboronic acid bis(1,3-propanediol) ester (328 mg, 0.65 mmol) were added to a round bottom flask containing $Pd(PPh_3)_4$ (22 mg, 0.02 mmol) under Ar. Solids were dissolved in 10mL 3:1 mixture of toluene:2M potassium carbonate with a few drops of Aliquat 336 added as a phase transfer agent, and the reaction flask was placed under vacuum and backfilled with N_2 (x3). Reaction was refluxed for 48 hours, turning dark purple and beginning to fluoresce under UV after 1 hr. Product was isolated in 60% yield as a light yellow powder following precipitation from acidic methanol. ^{1}H NMR (400 MHz, $CDCl_3$) δ 7.85-7.28 (m, 12H, aromatic); 5.64 (m, 2H, vinyl), 4.91-

4.87 (m, 4H, vinyl); 2.15 (b, 8H, alkyl); 1.91 (b, 4H, alkyl); 1.14-0.79 (b, 30H, alkyl). M_n via GPC in tetrahydrofuran: 3.5 kg/mol vs PS standards (DP=6), PDI: 2.7.

6.2.5 Polymerization of Styrene End-Capped Poly(fluorene) (xPF)

End-capped poly(dihexyl fluorene) xPF was synthesized as previously reported.(*28*) Briefly, 2,7-dibromo-9,9-dihexyl-9H-fluorene was polymerized via Ni(0)-mediated Yamamoto coupling with 0.125 equiv. of 4-bromostyrene added as an end-capping agent. Product was isolated in good yield as a grey powder after precipitation from acidic methanol. DP = 13 via ^{1}H NMR; M_n via GPC 10400; PDI 2.31.

6.2.6 Mercaptosilanization

Highly doped Si substrates with 200nm of thermally grown SiO_2 were sequentially rinsed with water, acetone, and isopropanol. Substrates were then treated with O_2 plasma for 2 min and immediately immersed in 5 vol.% 3-mercaptopropyltriethoxysilane in anhydrous toluene. Si substrates were allowed to react for 4 hr at 40 °C. Functionalized surfaces were then removed, rinsed with toluene and ethanol, and dried under N_2.

6.2.7 Thiol-Ene Surface Grafting of Poly(fluorene) Derivatives

Solutions of xPF and pPF in $CHCl_3$ (5 mg/mL) were spin-coated on thiol-functionalized Si substrates at 3000 RPM. The polymer-coated surfaces were then placed under N_2 at 100 °C and exposed to 254 nm light for 2 min. through a quartz cover dish. UV exposed films were then rinsed in $CHCl_3$ for 30 seconds to reveal the surface grafted polymer layer. For photo-patterning, an arbitrary photomask was placed over the spin-coated films prior to UV exposure.

6.2.8 Device Fabrication

Top-contact thin film transistors were fabricated on highly doped Si/SiO_2 (200 nm) substrates. The substrates were sequentially cleaned using H_2O, acetone, and IPA, and they were then exposed to O_2-plasma for 2 min. to clean the surface and install reactive hydroxyl groups. Surfaces were functionalized with 3-mercaptopropyltriethoxysilane as above. pPF was then spin-coated at 3000 RPM (5 mg/mL $CHCl_3$ solution) and either grafted as described above or placed under vacuum for non-grafted devices. Au source/drain were then deposited by thermal evaporation via shadow mask (W/L=30) at pressures $<10^{-5}$ Torr. Octadecyltrichlorosilane (OTS) functionalized devices were prepared by vapor treating the plasma-cleaned Si/SiO_2 substrates with OTS in a sealed vessel for 8 hr. After OTS exposure, substrates were rinsed with toluene and dried under N_2, pPF was coated as above, and electrodes were evaporated. All devices were measured under vacuum.

6.3 Results and Discussion

6.3.1 Synthesis of Thiol-Ene Compatible Poly(fluorene)s

Polymers investigated for thiol-ene grafting were poly(fluorene) derivatives with vinyl functionality installed either as styrene-type units at the chain ends or as terminal alkenes at the 9-position in the fluorene repeat unit In order to assess the effects of surface connectivity on film properties. End-functionalized poly(dihexyl fluorene) (xPF) was synthesized via Yamamoto coupling as previously reported and described in Chapter 2.(*28*) Side chain-functionalized polymer of alternating dipentenyl-dihexyl fluorene (pPF) was synthesized via Suzuki-Miyaura co-polymerization of 2,7-dibromo-9,9-dipentenylfluorene and a 9,9-dihexylfluorene boronic ester as detailed in Chapter 4, shown in Figure 6.2.

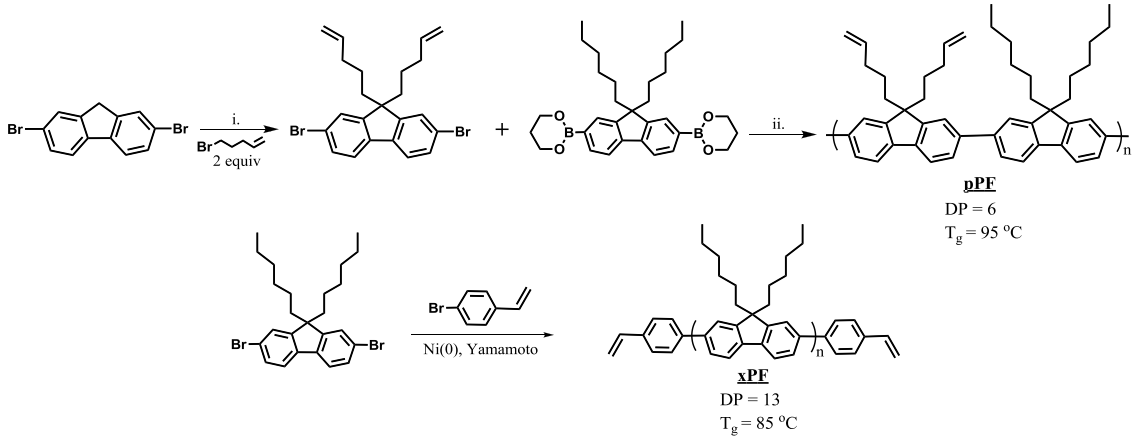

Figure 6.2: Synthesis of alkene-functionalized poly(fluorene) derivatives for surface grafting via thiol-ene reaction. Reaction conditions: i.) Tetrabutylammonium bromide (0.01 equiv.), 50 mL 1:1 toluene: 50% aqueous NaOH. Reflux 17h. ii.) $Pd(PPh_3)_4$ (0.03 equiv.), 10mL 3:1 toluene:2M aqueous K_2CO_3, Aliquat 336. Reflux 48h.

Lower molecular weight pPF (3.5 kg/mol) than described previously was easily isolated, with ^{1}H NMR similarly showing good preservation of vinyl functionality. The lower molecular weight was chosen to allow for improved grafting density. For xPF, the relative amount of 4-bromostyrene end-capping agent added to the reaction was chosen so that both xPF and pPF averaged approximately 12 fluorene units per chain.

6.3.2 Thiol-Ene Surface Grafting

Treatment of Si substrates with O_2 plasma is known to afford a hydrophilic surface rich in hydroxyl groups.(*30, 31*) Subsequent condensation reaction of these surfaces in dilute solutions of (3-mercaptopropyl)triethoxysilane yields the desired surface functionalized with free thiol reactivity as described by Pallavicini and co-workers.(*32*) It is likely that the thiol-functionalized layer is not a perfect monolayer as it is notably difficult to prevent trialkoxy silanes from forming multilayers on hydroxylated Si surfaces. However, surfaces appear clean and pristine by eye following silane reaction, and AFM measurements reveal a surface clean of islanding and other multilayer artifacts. Furthermore, surface contact angles below 90° are

characteristic of surface-bound free thiols,(*33*) and so these surfaces are sufficiently functionalized for grafting needs.

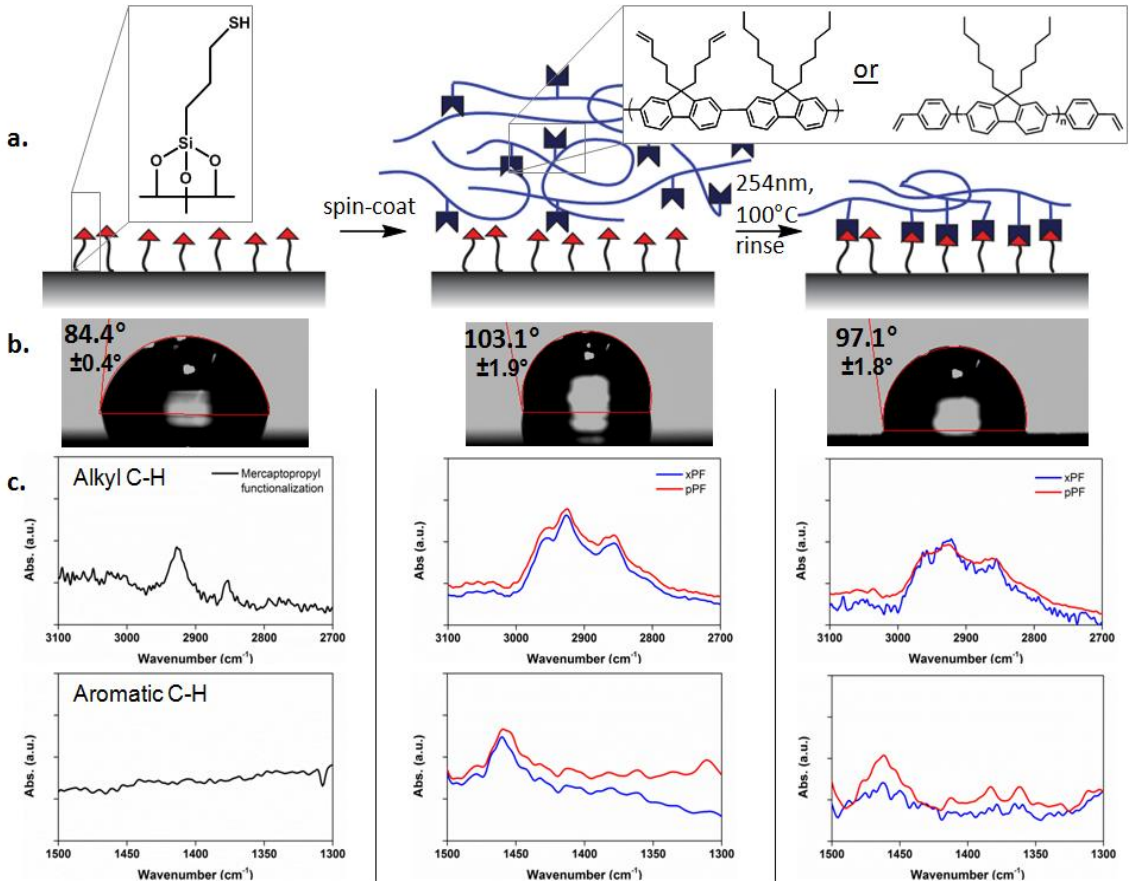

Figure 6.3: (a) Schematic representation of grafting process. (b) Water contact angle measurements for (left to right): pristine thiol-treated wafers; as-spun polymer; cured polymer after rinsing in $CHCl_3$. (c) Grazing-angle FT-IR measurements of alkyl C-H stretch (top) and aromatic C-H modes (bottom) for pristine thiol-treated wafers, as-spun polymer, and cured polymer after rinsing in $CHCl_3$.

Figure 6.3 follows the photo-induced initiator-free grafting procedure as illustrated in Figure 6.3a with characterization at each step by contact angle (Figure 6.3b) and grazing-angle FT-IR (Figure 6.3c). Briefly, alkene-containing poly(fluorene)s were spin-coated from chloroform onto thiol-functionalized wafers. Coated wafers were then cured by exposure to 254 nm UV light for 2 min under nitrogen atmosphere at 100°C (above the polymers' glass transition temperatures: xPF T_g=85 °C, pPF T_g=95 °C as measured by DSC).

Success of the grafting reaction was first confirmed by static water contact angle (Fig. 6.3b) which increased from 84.4° for the thiol-treated Si substrate to 103.1° following polymer spin-coating, consistent with a hydrophobic polymer coating. After UV exposure and rinsing in $CHCl_3$, no film could be observed by eye on the substrate. However, subsequently measured contact angles of the cured and rinsed surfaces decreased only slightly to 97.1°, indicating a thin hydrophobic polymer coating remained bound to the surface.

Grazing angle FT-IR measurements (Fig. 6.3c) revealed two sharp C-H bands at 2920 cm^{-1} and 2850 cm^{-1} from the symmetric alkyl C-H stretch in the mercaptopropyl layer after surface functionalization. Direct observation of the thiol S-H band was not possible due to the thin surface coverage and the known weakness of the S-H absorption.(*34, 35*) A broadening of the alkyl C-H band occurs after polymer coating and is consistent with polymers' long alkyl side chains compared to the propyl group of the mercaptopropyl layer. This broad band remains even after continuously soaking the films in solvent over 3 days. Additional aromatic signals between 1500-1300 cm^{-1} behave similarly and are also indicative of surface-bound poly(fluorene).

Confirmation of the thiol-ene reaction was also evident from the vinyl IR signals of the poly(fluorene) films (Figure 6.4). The vinyl C-H absorption at 910 cm^{-1} is clearly evident in spun and UV-exposed poly(fluorene) films since numerous unreacted vinyl groups remain in the bulk (the second expected vinyl signal near 990 cm^{-1} is lost in the intense Si-O-Si band). After rinsing, this peak has fully disappeared indicating that the vinyl functionalities of the surface-bound poly(fluorene)s have been significantly reduced during reaction. This suggests that the abundance of free thiol groups on the Si surface are sufficient to consume all of the vinyl functionality of the poly(fluorene) chains ultimately bound to the substrate. Given the short reaction time, this further suggests that the extent of thiol-ene grafting is limited by the amount

of vinyl groups which are present at the surface rather than being limited by the presence of thiols.

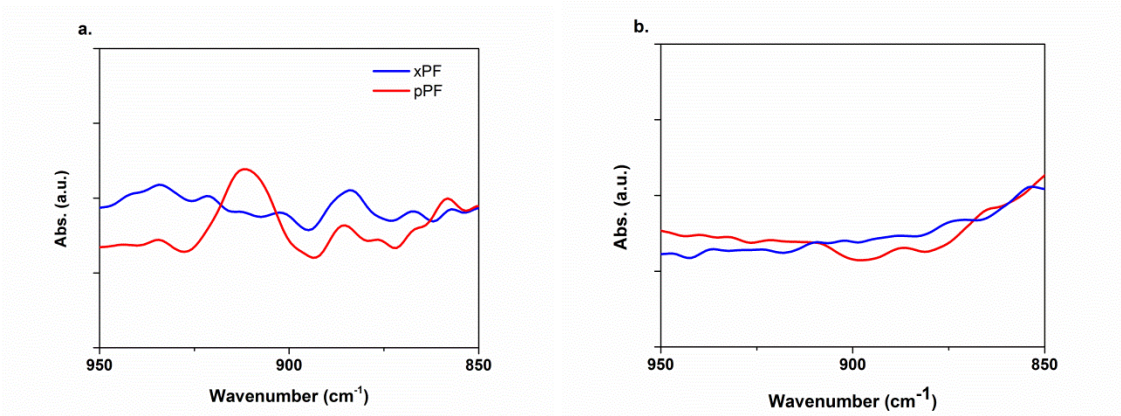

Figure 6.4: Grazing-angle FT-IR showing the vinyl C-H peaks for (a) spun and UV-exposed xPF and pPF films, and (b) UV-exposed and rinsed grafted xPF and pPF films.

6.3.3 Effects of Surface Grafting on Optoelectronic Properties of Poly(fluorene)s

Figure 6.5 shows photoluminescence (PL) measurements at various stages of the grafting process for both xPF and pPF, normalized to the as-spun film PL. Characteristic poly(fluorene) emission is seen at ~420 nm for as-spun and cured films. This peak remains with weakened intensity after solvent rinsing and does not disappear even after soaking the substrate in a good solvent for 3 days. These observations further supports the presence of a robust, surface bound poly(fluorene) film. The presence of physically adsorbed polymer on the substrate can be discounted since no appreciable PL response is observed after rinsing as-spun films without UV curing. Neither is any appreciable PL observed when the curing procedure is performed on alkene-free poly(dihexyl fluorene) on the thiol-functionalized surfaces, clearly indicating the necessity of alkenes for successful grafting.

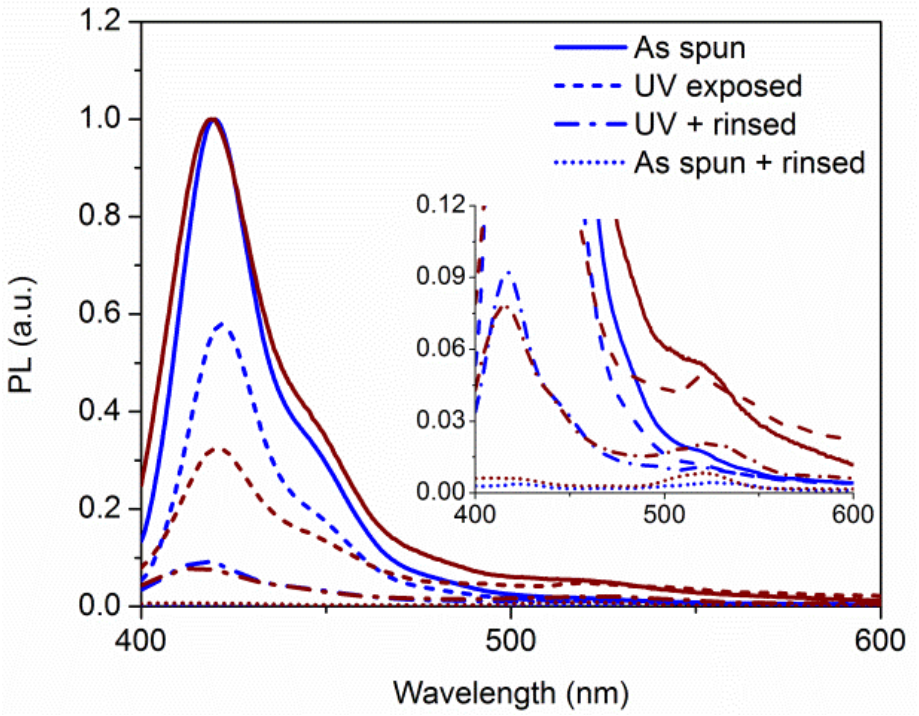

Figure 6.5: Photoluminescence (PL) of surfaces after various processing steps for xPF (blue) and pPF (red).

Peak PL emissions of xPF is slightly red-shifted after exposure to UV but before rinsing away uncured material, as expected from the annealing-like processing temperature of 100 °C. Similar red-shifting is not observed for pPF, likely due to the side-chain grafts which greatly limit chain mobility once formed. The PL of both end-chain and side-chain grafted poly(fluorene) films is blue-shifted compared to the as-spun films, with grafted xPF blue-shifting 3 nm (420 nm to 417 nm) and grafted pPF blue-shifting 5 nm (421 nm to 416 nm). It is only after removal of the non-grafted polymer does the blue-shift in PL become apparent, implying that only the surface-grafted chains contribute to the blue-shifted signal. In all cases, PL of grafted polymer was blue-shifted back to values observed in dilute solution as well (Table 6.1). These reductions in peak emission wavelength are comparable to the 1-10 nm shifts reported when reducing the number of conjugated polymer repeat units to just below the critical conjugation length,(*36*) and the polymers reported here are just at the edge of their own critical conjugation length. This

data then indicates that covalently bonding the poly(fluorene) chains to a rigid substrate must lead to some distortion of the polymer backbone, reducing its effective conjugation length.

Table 6.1: Peak photoluminescence (PL) emission wavelengths for solutions and surfaces excited at 365nm.

System	xPF peak PL λ (nm)	pPF peak PL λ (nm)
Dilute solution ($CHCl_3$)	417	416
As-spun	420	421
UV exposed and cured	422	421
Cured and rinsed	417	416

Table 6.2: Summary of thicknesses, grafting coverage, and amounts of polymer removed from surface-grafted xPF and pPF sample. [a]Rinsing is accomplished with washing in $CHCl_3$ for 30 seconds. [b]Soaking is accomplished by fully immersing pre-rinsed grafted films in $CHCl_3$ for 3 days.

Polymer	Thickness via AFM (nm)		Grafting Coverage (10^{13} chains/cm^2)	Extracted unbound polymer (10^{-13} mol)	
	As-spun	Grafted (post-rinse)	via AFM	Rinsing[a]	Soaking[b]
xPF	**10**	**6**	**8.1**	**4.2**	**14.7**
pPF	**11**	**3**	**2.8**	**4.3**	**16.3**

Table 6.2 summarizes the thicknesses of spun films and the resultant solvent-rinsed grafted layers, as well as calculated surface coverage and amount of polymer removed from the grafted coatings. For xPF and pPF respectively, approximately half and one-third of the as-spun film thickness remains as an insoluble grafted film after processing as measured by AFM. These grafted film thicknesses correlate to surface grafting densities of 8.1×10^{13} xPF chains/cm^2 and 6.7×10^{13} pPF chains/cm^2, calculated in a similar manner described by Paoprasert and co-workers.(*23*) The grafted poly(fluorene) films have similarly low overall thickness as the cited report owing to limitations in grafting to chemistries. Since both xPF and pPF are highly photoluminescent, grafting densities can alternatively be estimated by comparing PL intensity to calibrated concentrations of each polymer (Figure 6.6). Doing so yields modest surface densities of 1.1×10^{11} cm^{-2} and 2.5×10^{10} cm^{-2} for xPF and pPF respectively. These numbers clearly

underestimate surface density since they are calibrated against dilute solution PL, and solid state emission will at least partially quench in the aggregated state. Regardless, the measurements offer a useful lower bound on grafted xPF and pPF surface density and additionally confirm that xPF achieves a greater grafting density than pPF.

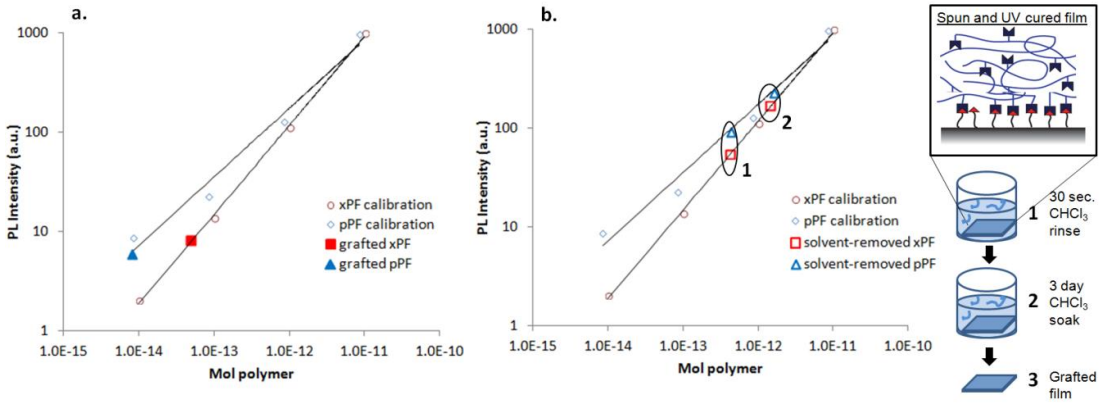

Figure 6.6: Determination of poly(fluorene) surface grafting density (a) and residual uncured polymer (b) from photoluminescence (PL) calibration curves.

Both calculations agree that end-chain grafted xPF achieves nearly four times the surface packing of side-chain grafted pPF. Indeed, given the two polymers' comparable size, the thicker films of xPF suggest a more brush-like grafting compared to pPF which is likely bound to the thiol-functionalized substrate as a mat instead of brushes, reducing overall grafting density and blocking the surface from additional thiol-ene reactions after grafting first begins. This particular grafting architecture can also explain the trends in blue-shifted PL observed in Figure 2. Repeated surface tethering along the backbone of pPF may distort the conjugated backbone slightly, giving rise to its more pronounced PL blue-shift despite lower overall grafting density.

Table 6.2 also reports the amount of non-crosslinked material removed from the surface-bound networks via rinsing and soaking with chloroform (illustrated in Figure 6.6). For both xPF and pPF, roughly four times as much material was removed from the cured films via extended soaking as from the initial rinse. This is likely due to significant interpenetration of uncured polymer into the surface-grafted layer as it is only during extended solvent soaking that

the non-grafted material is dissolved and removed. One would expect that a majority of ungrafted polymer would be removed by an initial rinse if there was not significant interpenetration. This is clearly not the case and could have interesting implications for the design of electronic devices with surface-bound layers which can interact effectively with the bulk conjugated polymer due to interpenetrating chains.

6.3.4 Applications of Surface Grafted Poly(fluorene)s.

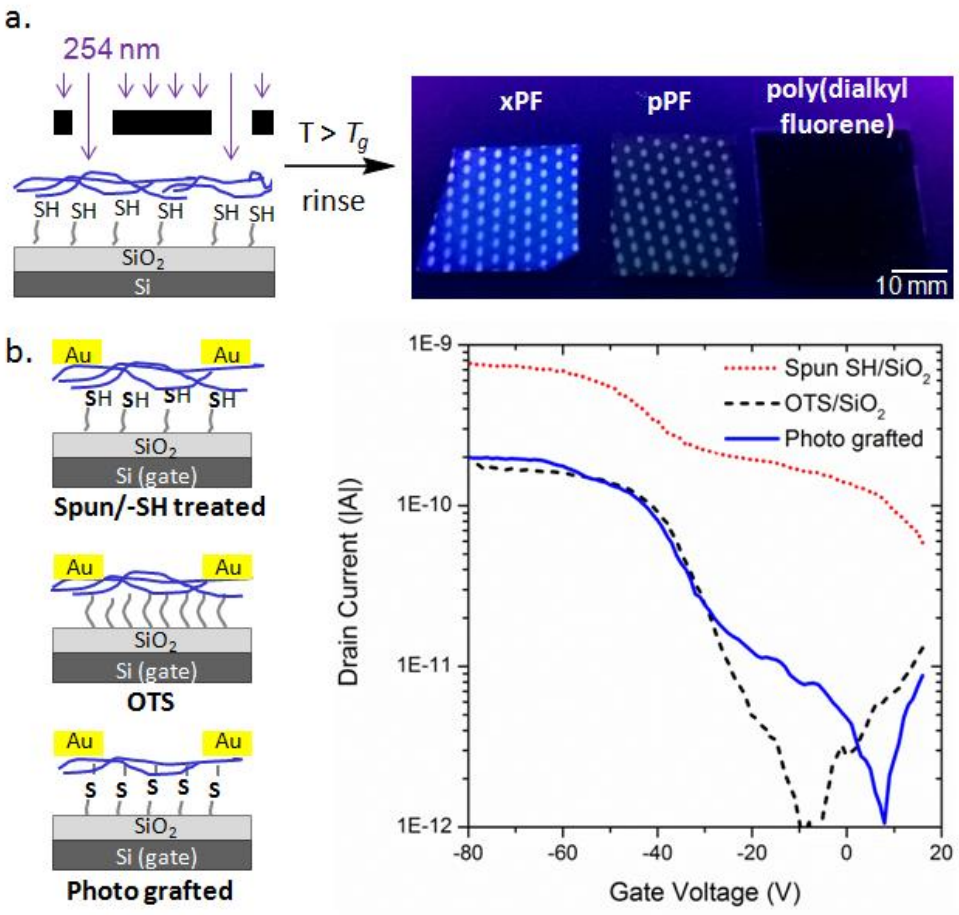

Figure 6.7: Demonstration of thiol-ene surface grafting for (a) photo patterning and (b) thin film transistor applications compared to additional device processing conditions.

Use of thiol-ene surface grafting is now feasible as an additional tool for surface and device processing, with examples shown in Figure 6.7. Due to the efficient photo-initiation of

the thiol when exposed to 254 nm UV light, use of a shadow mask during photo curing of xPF and pPF films on thiol functionalized Si wafers provides for clean replication of an arbitrary pattern (Figure 6.7a). The initiator-free reaction and short wavelength suggests this process would be amenable for efficient high resolution spatial grafting of conjugated polymers without any residual small molecules, which would be beneficial for semiconducting devices. Also shown is a thiol-functionalized substrate which was coated with conventional poly(dihexyl fluorene) without reactive end capping or side chain functionality, exposed to UV curing conditions, and rinsed with chloroform. As mentioned previously, this control easily demonstrates the need for both a reactive alkene and thiol for effective thiol-ene photo-grafting.

Figure 6.7b shows a proof of concept regarding how surface grafting could be used to modify or control electronic device performance. A thiol-functionalized Si/SiO_2 substrate with surface grafted pPF was fabricated into a thin film transistor (TFT) architecture by thermal evaporation of Au source and drain electrodes. For comparison, similar devices were fabricated using bulk pPF films spun on thiol-functionalized Si/SiO_2 without any photo-curing (i.e., leaving unreacted thiols) as well as bulk pPF films processed on octadecyltrichlorosilane (OTS) treated Si/SiO_2 which is a ubiquitous modification technique for improving organic TFT performance. Measurements were averaged over at least three devices in each configuration, and typical outputs are shown in Figure 6.7. While the current-voltage (IV) behavior does not follow ideal field-effect behavior in any of the devices, clear differences between the configurations are immediately evident in the IV curves. The photo-grafted devices were found to perform comparably to those fabricated on OTS treated substrates. Thus surface grafting potentially offers an attractive alternative to standard performance-improving OTS surface treatments,(*5, 37*) giving similar improvements in carrier mobility and on/off drain current ratios. The particularly low hole mobilities (on the order of 10^{-7} to 10^{-6} cm^2/V s) are not surprising for

homopolymers of dialkyl fluorenes which are rarely reported in the literature and generally show low charge mobility due to the polymer's considerably amorphous character.(*38*) However, direct comparison of these mobilities is still insightful for examining the role of surface chemistry on charge transport. Films of pPF processed but not cured on free thiol-functionalized surfaces fared much worse. No clear gating of current was observed, and charge mobilities were consistently the lowest of all tested devices. An import insight for any future thiol-ene based electronic devices is obtained by observing the detrimental effect of free thiol on charge transport along a thin film interface. These poor performances are likely due to the highly polarizable and dynamic S-H bond, and the evidence here shows that reacting those groups via thiol-ene chemistry can provide beneficial improvements in device electronics. Future expansions on this work could involve extending the thiol-ene grafting reaction to more crystalline, higher mobility conjugated polymers.

6.4. Conclusions

In this chapter, thiol-ene chemistry is used to graft semiconducting polymers to surfaces, rapidly forming uniform thin films of surface-bound conjugated polymers. End-chain reactive polymers can achieve grafting densities nearly four times as large as side-chain reactive polymers at the cost of a reduction in effective conjugation length, likely due to deformation of the polymer backbone during grafting. The highly efficient thiol-ene click reaction allows for spatial grafting and control of surface morphology that rivals the beneficial effects of standard alkyl-silane surface modification approaches in organic thin film transistors. The results raise hope that this approach could be another avenue to lead to improved control of polymer ordering at electrode interfaces for understanding and enhancing electronic device performance.

6.5 References

1. W. Salaneck, K. Seki, A. Kahn, J.-J. Pireaux, *Conjugated Polymer And Molecular Interfaces: Science and Technology For Photonic And Optoelectronic Application*. (M. Dekker, New York, 2002).

2. W. Salaneck, S. Stafstrom, J.-L. Bredas, *Conjugated polymer surfaces and interfaces. Electronic and chemical structure for polymer light emitting devices*. (Cambridge University Press, Cambridge, 1996).

3. K. M. Coakley, M. D. McGehee, Conjugated Polymer Photovoltaic Cells, *Chem. Mater.* **16**, 4533-4542 (2004).

4. I. H. Campbell, J. D. Kress, R. L. Martin, D. L. Smith, N. N. Barashkov, J. P. Ferraris, Controlling charge injection in organic electronic devices using self-assembled monolayers, *Appl. Phys. Lett.* **71**, 3528 (1997).

5. S. C. Lim, S. H. Kim, J. H. Lee, M. K. Kim, D. J. Kim, T. Zyung, Surface-treatment effects on organic thin-film transistors *Synth. Met.* **148**, 75-79 (2005).

6. B. de Boer, A. Hadipour, M. M. Mandoc, T. van Woudenbergh, P. W. M. Blom, Tuning of Metal Work Functions with Self-Assembled Monolayers, *Adv. Mater.* **17**, 621-625 (2005).

7. Z. A. Page, V. V. Duzhko, T. Emrick, Conjugated Thiophene-Containing Polymer Zwitterions: Direct Synthesis and Thin Film Electronic Properties, *Macromolecules* **46**, 344-351 (2013).

8. H. Wu, F. Hunag, Y. Mo, W. Yang, D. Wang, J. Peng, Y. Cao, Efficient Electron Injection from a Bilayer Cathode Consisting of Aluminum and Alcohol-/Water-Soluble Conjugated Polymers, *Adv. Mater.* **16**, 1826-1830 (2004).

9. J. H. Seo, A. Gutacker, B. Walker, S. Cho, A. Garcia, R. Yang, T.-Q. Nguyen, A. J. Heeger, G. C. Bazan, Improved injection in n-type organic transistors with conjugated polyelectrolytes, *J. Am. Chem. Soc.* **131**, 18220-18221 (2009).

10. L. Hung, C. Tang, M. Mason, Enhanced electron injection in organic electroluminescence devices using an Al/LiF electrode, *Appl. Phys. Lett.* **70**, 152 (1997).

11. I. W. Moran, S. B. Jhaveri, K. R. Carter, Patterned layers of a semiconducting polymer via imprinting and microwave-assisted grafting, *Small* **4**, 1176-1182 (2008).

12. S. B. Jhaveri, K. R. Carter, Disubstituted polyacetylene brushes grown via surface-directed tungsten-catalyzed polymerization, *Langmuir* **35**, 8288-8290 (2007).

13. T. M. Fulghum, P. Taranekar, R. C. Advincula, Grafting Hole-Transport Precursor Polymer Brushes on ITO Electrodes: Surface-Initiated Polymerization and Conjugated Polymer Network Formation of PVK, *Macromolecules* **41**, 5681-5687 (2008).

14. N. Marshall, S. K. Sontag, J. Locklin, Substituted Poly(p-phenylene) Thin Films via Surface-Initiated Kumada-Type Catalyst Transfer Polycondensation, *Macromolecules* **43**, 2137-2144 (2010).

15. N. Doubina, J. L. Jenkins, S. A. Paniagua, K. A. Mazzio, G. A. MacDonald, A. K-.Y. Jen, N. R. Armstrong, S. R. Marder, C. K. Luscombe, Surface-initiated synthesis of poly(3-methylthiophene) from indium tin oxide and its electrochemical properties, *Langmuir* **28**, 1900-1908 (2012).

16. S. K. Sontag, N. Marshall, J. Locklin, Formation of conjugated polymer brushes by surface-initiated catalyst-transfer polycondensation, *Chem. Comm.* **23**, 3354-3356 (2009).

17. N. Khanduyeva, V. Senkovskyy, T. Beryozkina, M. Horecha, M. Stamm, C. Uhrich, M. Riede, K. Leo, A. Kiriy, Surface engineering using Kumada catalyst-transfer polycondensation (KCTP): preparation and structuring of poly(3-hexylthiophene)-based graft copolymer brushes, *J. Am. Chem. Soc.* **131**, 153-161 (2009).

18. S. K. Sontag, G. R. Sheppard, N. M. Usselman, N. Marshall, J. Locklin, Surface-confined nickel mediated cross-coupling reactions: characterization of initiator environment in Kumada catalyst-transfer polycondensation, *Langmuir* **27**, 12033-12041 (2011).

19. V. Senkovskyy, N. Khanduyeva, H. Komber, U. Oertel, M. Stamm, D. Kuckling, A. Kiriy, Conductive Polymer Brushes of Regioregular Head-to-Tail Poly(3-alkylthiophenes) via Catalyst-Transfer Surface-Initiated Polycondensation, *J. Am. Chem. Soc.* **129**, 6626-6632 (2007).

20. J. Alonzo, W. M. Kochemba, D. L. Pickel, M. Ramanathan, Z. Sun, D. Li, J. Chen, B. G. Sumpter, W. T. Heller, S. M. Kilbey, Assembly and organization of poly(3-hexylthiophene) brushes and their potential use as novel anode buffer layers for organic photovoltaics *Nanoscale* **5**, 9357-9364 (2013).

21. D. Meng, J. Sun, S. Jiang, Y. Zeng, Y. Li, S. Yan, J. Geng, Y. Huang, Grafting P3HT brushes on GO sheets: distinctive properties of the GO/P3HT composites due to different grafting approaches *J. Mater. Chem.* **22**, 21583-21591 (2012).

22. L. Zhao, X. Pang, R. Adhikary, J. W. Petrich, Z. Lin, Semiconductor Anisotropic Nanocomposites Obtained by Directly Coupling Conjugated Polymers with Quantum Rods, *Angew. Chem. Int. Ed.* 50, 3958-3962 (2011).

23. P. Paoprasert, J. W. Spalenka, D. L. Peterson, R. E. Ruther, R. J. Hamers, P. G. Evans, P. Gopalan, Grafting of poly(3-hexylthiophene) brushes on oxides using click chemistry, *J. Mater. Chem.* **20**, 2651-2658 (2010).

24. C. E. Hoyle, C. N. Bowman, Thiol-Ene Click Chemistry, *Angew. Chem. Int. Ed.* **49**, 1540-1573 (2010).

25. C. E. Hoyle, A. B. Lowe, C. N. Bowman, Thiol-click chemistry: a multifaceted toolbox for small molecule and polymer synthesis, *Chem. Soc. Rev.* **39**, 1355-1387 (2010).

26. A. B. Lowe, Thiol-ene "click" reactions and recent applications in polymer and materials synthesis, *Polym. Chem.* **1**, 17-36 (2010).

27. R. K. Iha, K. L. Wooley, A. M. Nystrom, D. J. Burke, M. J. Kade, C. J. Hawker, Applications of Orthogonal "Click" Chemistries in the Synthesis of Functional Soft Materials, *Chem. Rev.* **109**, 5620-5686 (Nov, 2009).

28. A. R. Davis, J. A. Maegerlein, K. R. Carter, Electroluminescent Networks via Photo "Click" Chemistry, *J. Am. Chem. Soc.* **133**, 20546-20551 (2011).

29. F. B. Koyuncu, A. R. Davis, K. R. Carter, Emissive Conjugated Polymer Networks with Tunable Band-Gaps via Thiol-Ene Click Chemistry, *Chem. Mater.* **24**, 4410-4416 (2012).

30. M. Owen, T. Gentle, T. Orbeck, D. Williams, in *Polymer Surface Dynamics,* J. Andrade, Ed. (Plenum Press, New York, 1988), pp. 101-110.

31. M. Morra, E. Occhiello, R. Marola, F. Garbassi, P. Humphrey, D. Johnson, On the aging of oxygen plasma-treated polydimethylsiloxane surface, *J. Colloid and Interface Sci.* **137**, 11-24 (1990).

32. P. Pallavicini, G. Dacarro, M. Galli, M. Patrini, Spectroscopic evaluation of surface functionalization efficiency in the preparation of mercaptopropyltrimethoxysilane self-assembled monolayers on glass *J. Colloid and Interface Sci.* **332**, 432-438 (2009).

33. J.-J. Chen, K. N. Struk, A. B. Brennan, Surface Modification of Silicate Glass Using 3-(Mercaptopropyl)trimethoxysilane for Thiol-Ene Polymerization, *Langmuir* **27**, 13754-13761 (2011).

34. L. Duan, S. J. Garrett, An Investigation of Rigid p-Methylterphenyl Thiol Self-Assembled Monolayers on Au(111) Using Reflection-Absorption Infrared Spectroscopy and Scanning Tunneling Microscopy, *J. Phys. Chem. B* **105**, 9812-9816 (2001).

35. J. Coates, in *Encyclopedia of Analytical Chemistry* R. Meyers, Ed. (John Wiley & Sons Ltd, Chichester, 2000), pp. 10815-10837.

36. L. O'Neill, H. J. Byrne, Structure-Property Relationships for Electron-Vibrational Coupling in Conjugated Organic Oligomeric Systems, *J. Phys. Chem. B* **109**, 12685-12690 (2005).

37. A. Facchetti, M.-H. Yoon, T. J. Marks, Gate Dielectrics for Organic Field-Effect Transistors: New Opportunities for Organic Electronics, *Adv. Mater.* **17**, 1705-1725 (2005).

38. H. Kajii, K. Koiwai, Y. Hirose, Y. Ohmori, Top-gate-type ambipolar organic field-effect transistors with indium–tin oxide drain/source electrodes using polyfluorene derivatives, *Org. Elec.* **11**, 509-513 (2010).

CHAPTER 7

SPATIAL IMAGING OF CHARGE DENSITY IN CONJUGATED POLYMER FILMS USING MODULATION-AMPLIFIED REFLECTANCE SPECTROSCOPY (MARS)[§]

7.1 Introduction

Semiconducting polymers have enabled the development of a remarkable new class of optoelectronic devices, including flexible solar cells, roll-to-roll electronics, and organic transistors. However, charge transport in conjugated molecules is a complex phenomenon that remains an open scientific question with a range of mechanistic theories, slowing the commercial development of organic optoelectronics(*1-5*). Development of charge-carrier visualization tools for organic semiconductors is essential both for fundamental explorations of carrier transport in organic thin films and for smartly engineering high efficiency organic devices.

Chapter 1 summarized the unique properties of conjugated organic molecules that allow for optical observations and outlined some of the recent developments in charge visualization tools and their practical disadvantages. Recent charge modulated spectroscopy studies have tracked electronic interactions and carrier formation in conjugated organic molecules by probing the optical changes that occur when a charge-carrying species is formed (*6-17*). A handful of complementary experiments have shown that these and similar tools can provide spatial mapping of electronic and charge-related phenomena (*18-23*). However, these techniques generally rely on indirectly detecting carrier density, probe rastering, or modulation of an elastic polymer dielectric. None of these efforts provide a rapid, large-area, high resolution method of visualizing charge carrying species in organic materials and devices. In this chapter, a novel modulated reflectance spectroscopy technique is described and used to spatially and temporally

[§] Portions of this chapter have been reprinted with permission from Davis, Pye, Katz, Hudgings, Carter, *Adv. Mater.* (2014, accepted). Copyright 2014 Wiley-VCH.

examine carrier transport in large area thin film devices, carrier depletion in strongly biased organic devices, and the interaction of carriers with the inevitability of device defects.

7.2 Experimental Section

7.2.1 Materials

Regioregular poly(3-hexylthiophene) (P3HT) was purchased from Rieke Metals, Inc. and used as received. Si substrates (resistivity = 0.01-0.08 Ω-cm) with 200 nm thick SiO_2 layer were purchased from University Wafers. Octadecyltrichlorosilane was used as received from Sigma-Aldrich.

7.2.2 Device Fabrication and Testing

Top-contact thin film transistors were fabricated on Si/SiO_2 (200 nm) substrates. The substrates were sequentially cleaned using H_2O, acetone, and IPA, and they were then exposed to O_2-plasma for 2 min. to further clean the surface and install reactive hydroxyl groups. Substrates were then vapor treated with octadecyltrichlorosilane (OTS) in a sealed vessel for 8hr to improve final device performance. After OTS exposure, substrates were rinsed with toluene and dried under N_2. P3HT was spun from $CHCl_3$ solutions (3mg/mL) at 3000 RPM, and devices were immediately dried under vacuum overnight. Films were annealed at 150°C for 30 min. in an Ar-filled glovebox, and Au source/drain were deposited by thermal evaporation through a shadow mask (L=80μm, W=2400μm). All devices were subsequently measured under ambient conditions.

7.2.3 CCD Measurement and Processing

In the experimental setup for measuring ΔR/R, the tested device is placed in a standard optical microscope and illuminated at nearly normal incidence using commercial LED light sources. Light reflected from the device surface is imaged by a connected CCD camera. To obtain a change in reflectance during operation, the device is modulated with frequency *f*, and the CCD camera is phase-locked and modulated at 4*f*. This allows for 'four bucket' lock-in processing of reflected light, where four images are captured during each oscillation period and are used to extrapolate modulation amplitude ΔR, dc image (base reflectivity) R_0, and relative phase. Figure 7.1 illustrates the phase-locked signal input to the device and CCD camera for four bucket processing, and Equations 7.1-7.8 detail the mathematical processing of CCD output for mapping direct reflectivity (R_0), normalized change in reflectivity ($\Delta R/R_0$), and relative phase change (ϕ) in tested devices. Typical processed measurement outputs are shown in Figure 7.2. Reference 24 (Farzaneh et al.) contains a more detailed description of the optical processing(*24*) and advantages of four bucket processing.

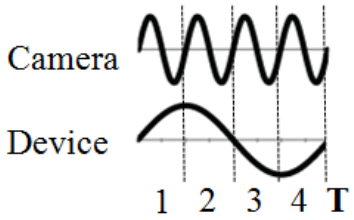

Figure 7.1: Illustration of the phase-locked modulated electrical input to device and CCD camera (with period *T*) allowing for four-bucket processing.

Equation 7.1: Reflectance intensity over first quarter of modulation period.

$$I_1 = \int_0^{T/4} R(x,y,t)dt$$

Equation 7.2: Reflectance intensity over second quarter of modulation period.

$$I_2 = \int_{T/4}^{T/2} R(x,y,t)dt$$

Equation 7.3: Reflectance intensity over third quarter of modulation period.

$$I_3 = \int_{T/2}^{3T/4} R(x,y,t)dt$$

Equation 7.4: Reflectance intensity over fourth quarter of modulation period.

$$I_4 = \int_{3T/4}^{T} R(x,y,t)dt$$

Equation 7.5: Change in reflectivity during on/off modulation.

$$\Delta R(x,y) = \frac{4\pi}{\sqrt{2}T}\sqrt{(I_1 - I_3)^2 + (I_2 - I_4)^2}$$

Equation 7.6: Baseline reflectivity of tested device.

$$R_0(x,y) = \frac{2}{T}(I_1 + I_2 + I_3 + I_4)$$

Equation 7.7: Normalized change in reflectivity during on/off modulation.

$$\frac{\Delta R(x,y)}{R_0(x,y)} = \sqrt{2}\pi\frac{\sqrt{(I_1 - I_3)^2 + (I_2 - I_4)^2}}{I_1 + I_2 + I_3 + I_4}$$

Equation 7.8: Phase shift of reflectivity during device testing.

$$\varphi(x,y) + \psi = \frac{2}{\pi} arctan\frac{I_1 + I_2 - I_3 - I_4}{I_1 - I_2 - I_3 + I_4}$$

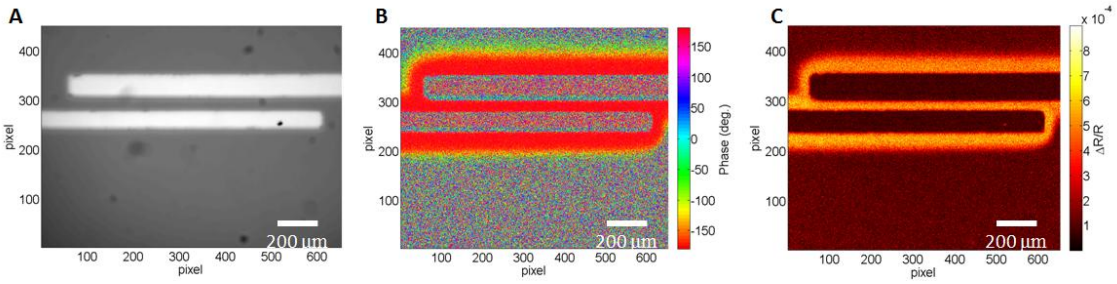

Figure 7.2: Output following a typical MARS measurements, showing (A) dc signal direct reflectivity (R_0), (B) relative phase (ϕ), and (C) $\Delta R/R_0$ signal for modulated gate voltage (square wave, 0 V to -20 V) with grounded top electrodes.

7.3 Results and Discussion

7.3.1 Modulation-Amplified Reflectance Spectroscopy (MARS)

To explore charge mapping in organic thin film transistors (TFTs), a modulation-amplified reflectance spectroscopy (MARS) imaging technique is developed for high resolution, two dimensional mapping of charge carrier density (Figure 7.3A). In a MARS measurement, a modulated voltage is applied across one pair of transistor electrodes, either the gate-source electrodes or the drain-source electrodes, while the other pair is held at a constant voltage. All biases are applied relative to a grounded source electrode. An external LED (10 mW, 740nm) constantly illuminates a top contact, hole carrying Si(gate)/SiO_2/poly(3-hexylthiophene) (P3HT) TFT, and the reflected light is recorded with a CCD camera phase-locked to the voltage modulation as shown in Figure 7.1 to obtain a two-dimensional mapping of differential reflectivity $\Delta R/R$. Pixel-by-pixel lock-in amplification provides very high signal resolution ($\Delta R/R \sim 10^{-4}$; typical processing output is shown in Fig. 7.2). Using this technique, two-dimensional amplitude and phase images of $\Delta R/R$ across the surface of the TFT can be obtained in under 10 minutes, with a theoretical spatial resolution up to 250 nm(*24*).

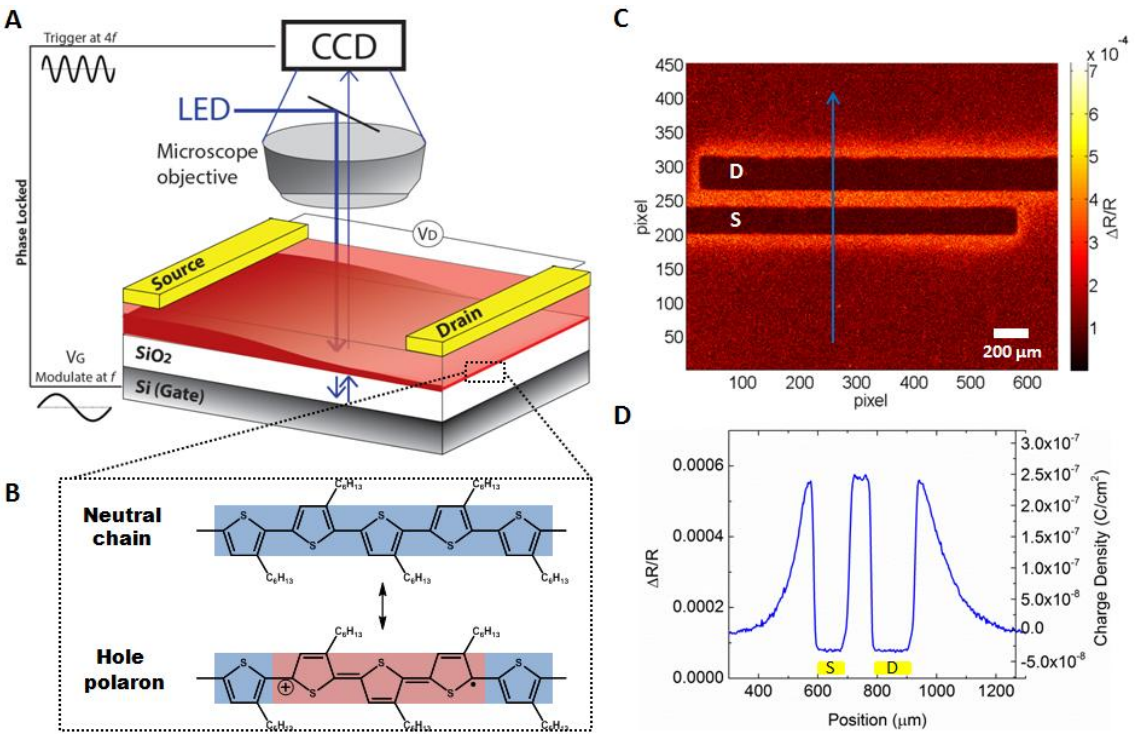

Figure 7.3: (A) Experimental setup for MARS imaging of TFTs. (B) Schematic of hole polaron formation in P3HT. (C) ΔR/R spatial map and (D) line trace under modulated gate bias (V_G = 10 Hz square wave, 0V to -20V; V_D=0V). Probe LED = 740 nm at 10 mW.

Figure 7.3B shows the localized structural change associated with hole polaron formation in P3HT that gives rise to the measured ΔR/R contrast. Illumination by probe LED at 740 nm is known from transmission experiments to strongly interact with this charge carrying mode (*10, 11*). While this technique images the net reflected light from the test structures, the ΔR/R contrast arises from the variable absorption of the LED light as transmitted through the P3HT and reflected off the Si substrate back into the CCD camera (Figure 7.4). This reflection mode allows for imaging standard devices fabricated with no special geometric or transmittance considerations as needed for typical differential transmission measurements(*18*). Furthermore, the measured differential reflectivity spectrum for devices biased off versus in the hole accumulation regime (Figure 7.5) is consistent in sign and shape with prior differential transmission measurements (*10, 11*), confirming observation of charge carrying states.

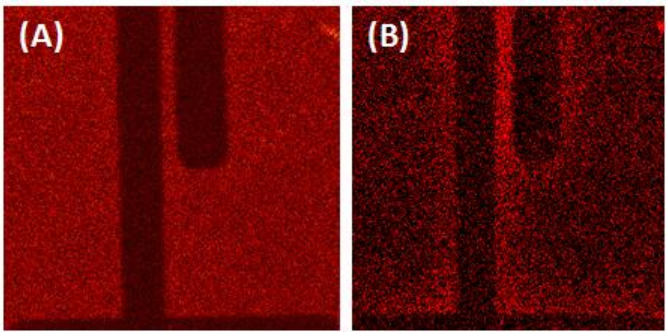

Figure 7.4: ΔR/R for a P3HT TFT built on a transparent ITO gate/PMMA dielectric substrates. No signal contrast is seen when placed above a light absorbent stage (A), compared to contrast observed when placed on a reflective stage (B). Signal in (B) is significantly attenuated compared to Si/SiO_2 devices due to the thicker dielectric layer (~1 μm) and longer light path which goes through both the semitransparent ITO and PMMA layers before reflecting off the back stage. Contrast in (A) and (B) have been enhanced through image processing to aid in visualization.

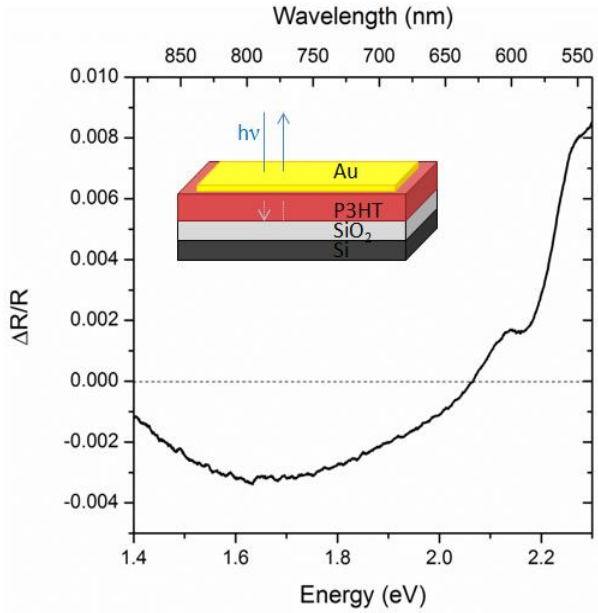

Figure 7.5: Differential reflection spectrum of a capacitor-like P3HT device (structure: Si/SiO_2/P3HT/Au) with semi-transparent 15 nm Au top electrode. Spectrum shows the change in device reflectance when the back Si electrode is biased off (0V) and on (-20V, for hole accumulation in P3HT) relative to grounded top Au electrode. Negative ΔR/R below 2.0 eV owes to increased polaron absorption and positive ΔR/R above 2.0 eV owes to neutral state bleaching.

Further experimental evidence (Figures 7.6-7.10) confirms that imaging contrast indeed arises from changes in the distribution of charge-carrying species. As expected for a hole transporting material, modulating V_G at negative voltages (inducing hole transport) induces clear uniform signal, while modulating at positive voltages (inducing electron transport) results in no

distinct signal (Figure 7.6). Replacement of the gold source and drain electrodes with a low work function metal like aluminum results in an order of magnitude lower ΔR/R signal with a corresponding drop in drain current (Figure 7.7). This reflects the larger barrier for hole injection into P3HT from Al than from Au. As expected, no ΔR/R signal is observed if the P3HT layer is replaced with an insulating polymer, nor is a signal observed during device modulation if the probe LED is turned off, negating the possibility that light is being emitted from the polymer layer (Figure 7.8). Signal strength is also drastically reduced when measuring the same device if it has been left exposed to ambient atmosphere for a period of days (Figure 7.9). The fact that ΔR/R signal strength is strongly correlated with factors which are known to affect drain current (gate voltage, electrode metal choice, presence of a semiconducting layer, prolonged device exposure to atmosphere, and chemical modification of the dielectric interface via monolayer formation discussed below) points to charge carrier density as the primary contrast agent, which is particularly confirmed in Figure 7.10 where peak ΔR/R signal intensity at varying operating voltages correlates very strongly with the measured TFT drain current.

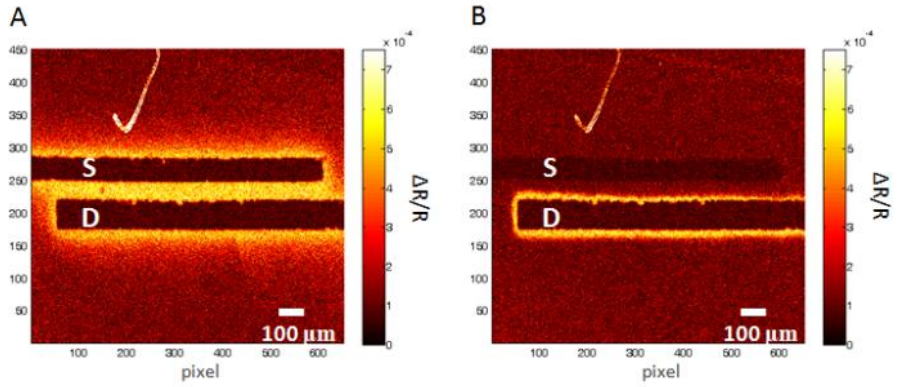

Figure 7.6: ΔR/R map of P3HT TFT under (A) hole formation (V_G = square wave -20V to -40V) and (B) electron formation (V_G = square wave +20V to +40V) conditions. The non-zero ΔR/R signal for the positively modulated V_G is observed only around one electrode and likely arises from edge effect artifacts due to the large magnitude of the gate-source bias.

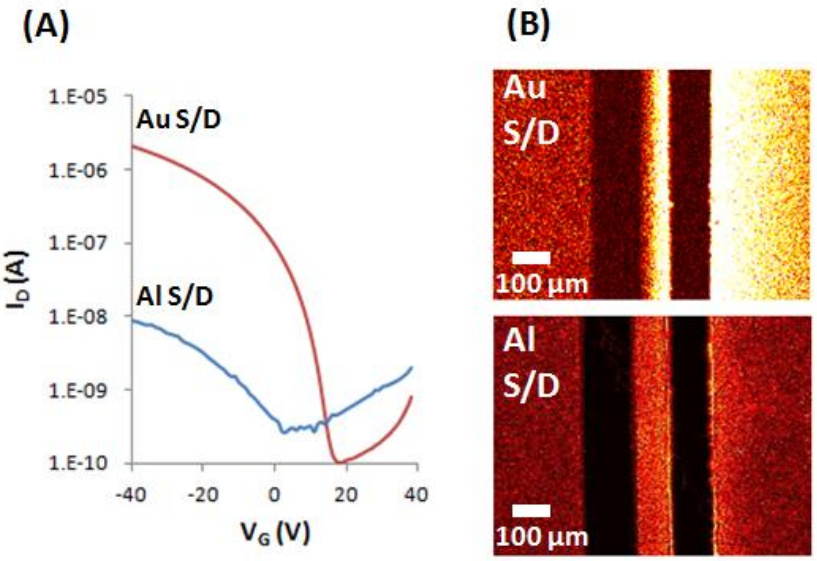

Figure 7.7: Effect of replacing Au source (S) and drain (D) electrodes with Al electrodes . Drain current (A) and ΔR/R intensity (B) (modulated V_D = square wave, 0V to -20V; constant V_G=-10V) both decrease by approximately an order of magnitude when Al is used instead of Au, primarily due to the energy barrier associated with charge injection.

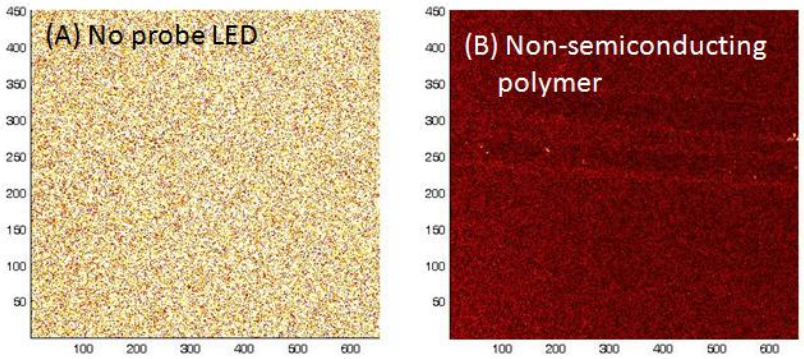

Figure 7.8: ΔR/R signal with no probe LED (A) and a non-semiconducting polymer (polystyrene) replacing P3HT (B) (modulated V_G = square wave, 0V to -20V; constant V_D=0V).

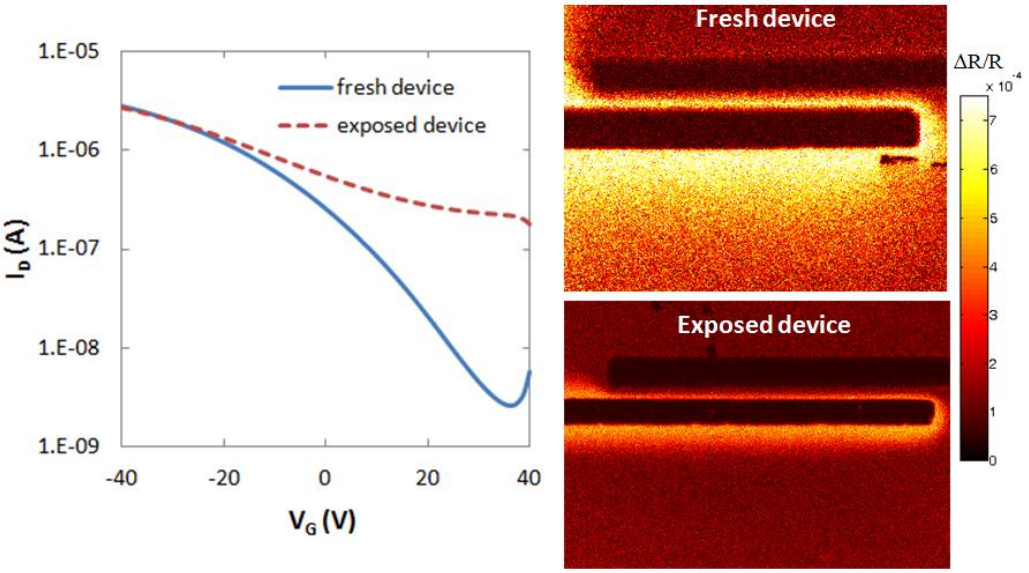

Figure 7.9: IV curves and ΔR/R measurements (modulated V_D = square wave, 0V to -20V; constant V_G=0V) for a freshly prepared device and a device left exposed to ambient conditions for 7 days.

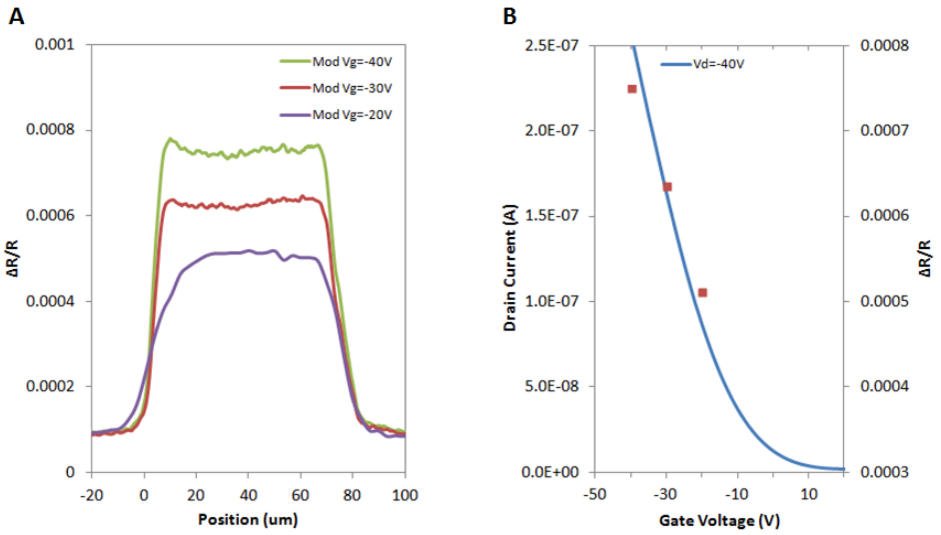

Figure 7.10: (A) In-channel line traces of ΔR/R at varying modulated gate voltages. (B) Comparison of peak in-channel ΔR/R signal (symbols) overlaid with device IV behavior (line) as a function of gate voltage.

7.3.2 Mapping Charge Density in Semiconducting Polymer Thin Films

The charge density maps obtained by MARS are in excellent agreement with both conventional bulk current-voltage (IV) characterization and TFT theory. Strong spatial ΔR/R contrast is observed as the gate voltage is negatively modulated with the source and drain

grounded (Figure 7.3C-D). The symmetric signal distribution is consistent with the expectation that a negative gate bias applied to a hole-transporting TFT while the source and drain are grounded should form a uniformly distributed injected hole layer at the semiconductor/dielectric interface. Additionally, ΔR/R increases linearly with the modulation depth of the gate voltage (Figure 7.10), in agreement with a simple capacitive model of charge formation(*18*) where the total charge density Q across the dielectric interface can be approximated by $Q = C_i(V_G-V_{th})$ where C_i is the areal capacitance, V_G is the applied gate voltage, and V_{th} is the threshold voltage. This allows for translating the measured ΔR/R intensity to an approximate total charge density in the P3HT film, whose values on the order of 0.1 $\mu C/cm^2$ compare favorably to literature (*3, 6, 20*). A particularly interesting feature that has not been previously reported is the large charge density measured beyond the electrodes outside of the channel arising from the paddle gate extending beyond the electrode-defined channel.

The ability of MARS to monitor the linear and saturation regimes of transistor operation is clearly demonstrated in Figure 7.11. In the linear regime with a DC drain bias $|V_D|$ well below the magnitude of the gate voltage modulation $|V_G|$, the charge distribution and drain current both respond linearly to changes in $|V_D|$. As $|V_D|$ exceeds $|V_G|$, the charge distribution ceases changing and reaches a saturated shape (Figure 7.11A) concurrently with drain current saturation, consistent with literature understanding of TFT behavior (*25, 26*). In Figure 7.11B, the slope of the measured ΔR/R distribution across the channel starting from the source to the in-channel ΔR/R minimum is plotted versus $|V_D|$. This characterization of the carrier distribution shape closely follows the measured IV transfer curves, directly increasing with drain voltage magnitude at low $|V_D|$, and then saturating at larger $|V_D|$ as current saturates.

As expected, the charge distribution begins to decrease from the source electrode toward the drain as the magnitude of the drain voltage is increased. However, regardless of

$|V_D|$, charge densities increase and spatially converge as they approach the drain electrode within the channel. Line traces from a larger area MARS mapping shown in Figure 7.11C clarify this phenomenon: as $|V_D|$ increases, charge density decreases rapidly to zero adjacent to the drain outside of the TFT channel, while the region outside the grounded source is relatively independent of drain bias. Given this constant plateau of charge density adjacent to the drain solely within the channel (which additionally was found to *increase* with $|V_D|$ for thick-film top contact devices), we qualitatively conclude that within the channel we are observing slow-moving space-charge limited carriers as they are pulled through the bulk of the P3HT and extracted from the channel.

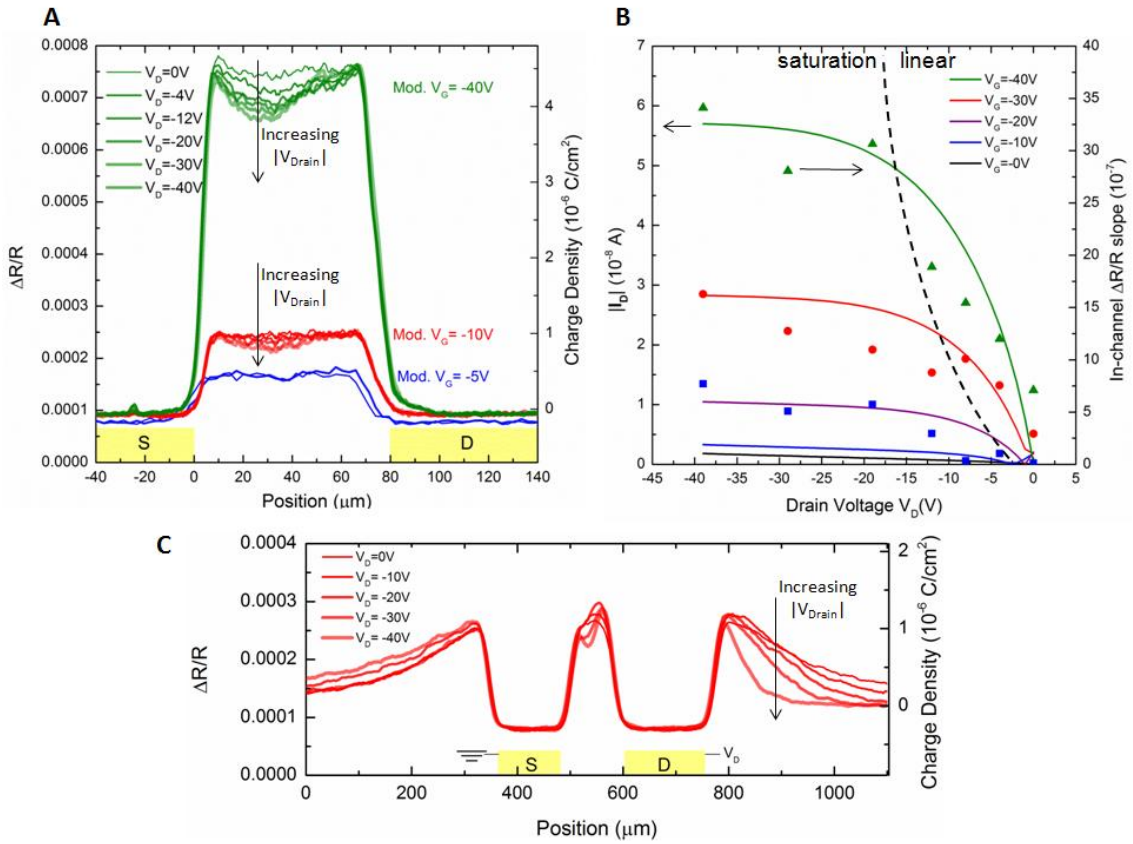

Figure 7.11: (A) ΔR/R line traces across the channel of a P3HT TFT under various operating conditions. (B) Slope of ΔR/R in the channel shown as a function of V_D and overlaid with the device's output current. Dashed line shows a rough guide to the eye, delineating linear and saturation regimes. (C) Expanded view of a large-area MARS line trace of an operational TFT showing the region outside the source-drain channel.

7.3.3 Time-Resolved Mapping of Charge Density

MARS is further capable of temporal charge density mapping since it is a lock-in amplified technique, enabling exploration of a wide range of organic electronic behavior that is not accessible using conventional bulk IV curve measurements. Figure 7.12 shows the ΔR/R signal spreading outside the conductive channel as V_G is modulated from 2 Hz up to 12.5 Hz (square wave, 0 to -20V). As expected, the carrier signal spreads farther laterally along the semiconductor/dielectric interface as frequency is decreased, corresponding to increased migration time across the surface. To a first approximation, the electrostatic drift distance *d* was calculated to be $d^2 = \mu \cdot V \cdot t$ (dashed theory line in Figure 7.12) where μ is the hole mobility

extracted from saturation-regime IV curves ($3.4 \cdot 10^{-4}$ $cm^2/V\,s$), V is the applied bias, and t is time ($1/f$) (*25*). Field effect hole mobilities were extracted from IV measurements in the saturation regime using the conventional relationship:

Equation 9: Saturation-regime drain current in a thin film transistor.

$$I_D = \frac{W}{2L}\mu_{sat}C_i(V_G - V_{th})^2,$$

where I_D is the saturated drain current, W is the device channel width, L is the device channel length, μ_{sat} is the saturation-regime hole mobility, C_i is the film capacitance per unit area, V_G is the applied gate voltage, and V_{th} is the threshold voltage.

Plotting the full-width half-maximum distance of ΔR/R spread as a function of f reveals good agreement with the predicted electrostatic drift at frequencies above 8Hz (i.e., $1/f$ timescales faster than 125 ms). The increasing deviation at longer times could be due to the cumulative effects of local traps, grain boundaries, and defects inhibiting efficient carrier mobility.

Additionally, the time resolved spatial imaging allows us to empirically evaluate carrier mobility using the same electrostatic drift relationship referenced above. Instead of fixing the mobility value to the calculated saturation-regime field effect mobility, we can set the mobility μ as a free variable and find the best fit of the electrostatic drift equation to the data in Figure 7.12. Doing so yields a hole mobility of $2.4 \cdot 10^{-4}$ $cm^2/V \cdot s$, which is lower (but still in decent agreement) compared to the value extracted from current-voltage data. This lower value again suggests that charge transport over long distances is being hindered by defects and grain boundaries. By measuring the charge diffusion over varying length scales and time frames, MARS offers a powerful visual and empirical tool for assessing carrier mobilities which compliments traditional calculations.

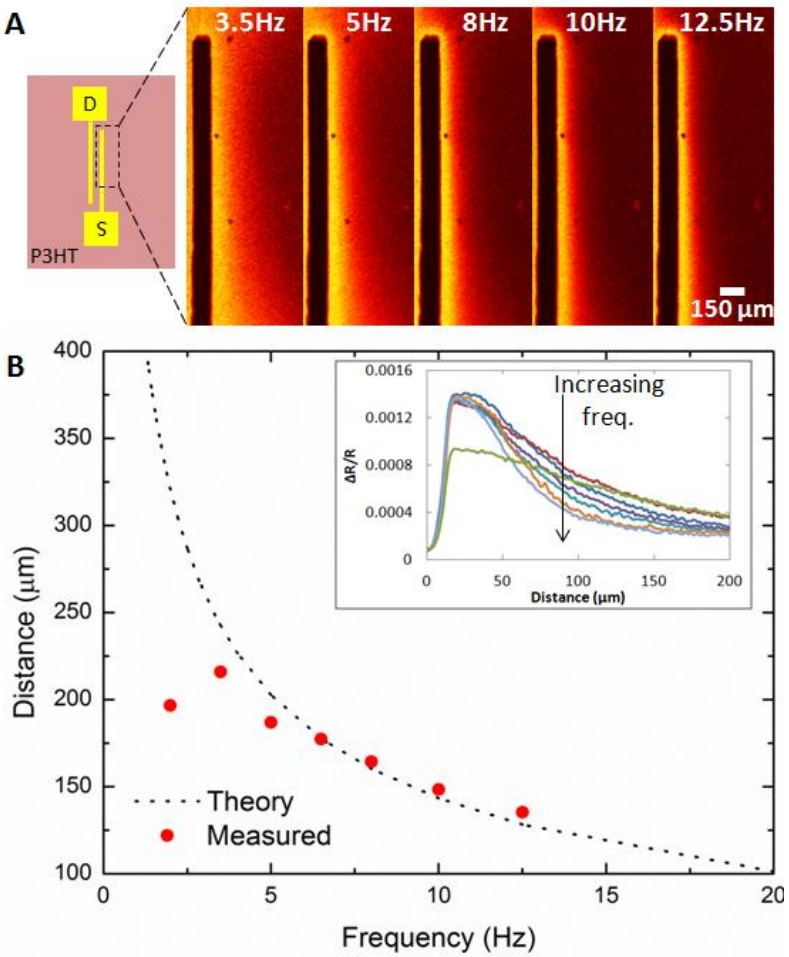

Figure 7.12: Frequency dependence of MARS signal in TFTs with modulated V_G. (A) Spatial map of ΔR/R signal outside of a grounded Au electrode with increasing modulation frequency *f*. (B) Plot of ΔR/R FWHM distance as a function of *f*. Dashed line indicates expected carrier spread from electrostatic drift (see text). ΔR/R line traces are shown in the inset. Testing: V_G = square wave 0V to -20V, V_D=0V.

7.3.4 Imaging defects in organic thin film devices

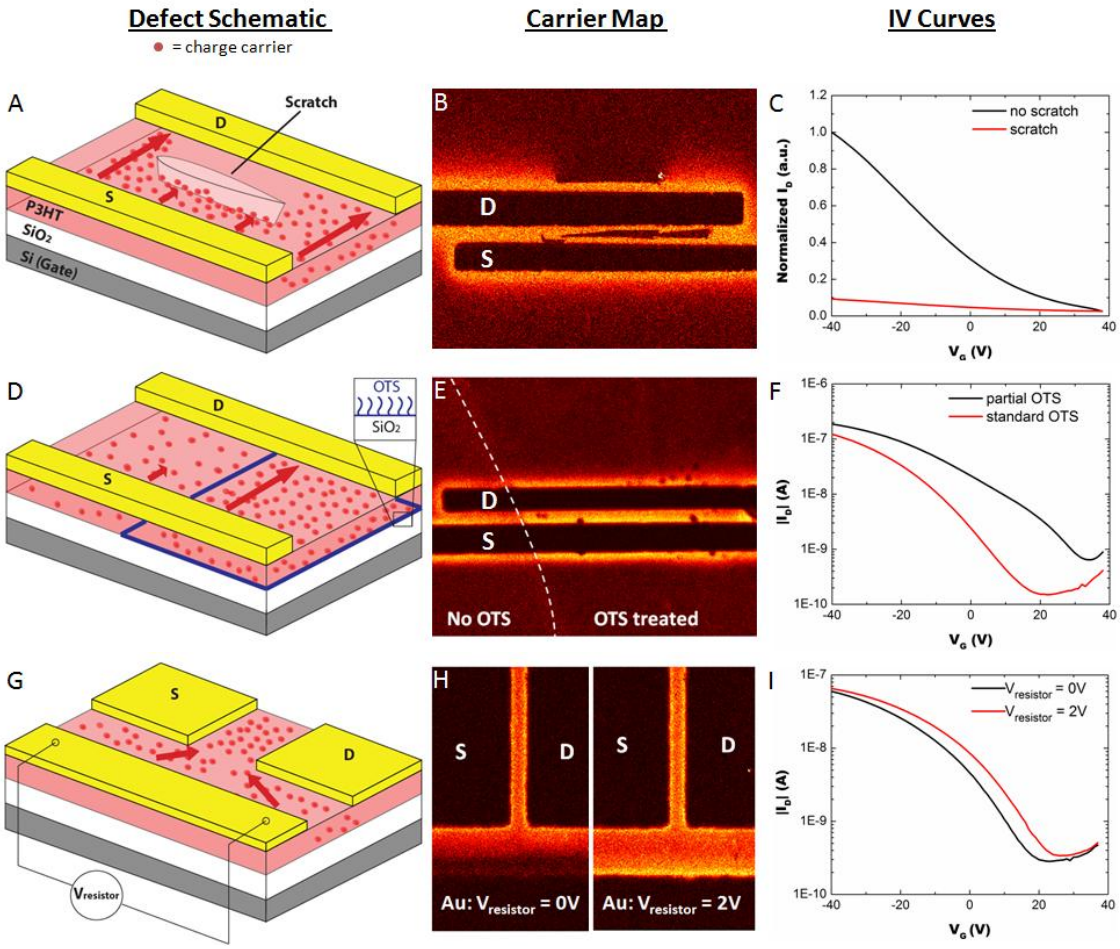

Figure 7.13: Schematic drawings (A,D,G), ΔR/R mapping (B,E,H), and IV curves with V_{Drain} = -40V (C,F,I) for various device defects. Represented are physical defects via scratching (A-C), surface chemical defects via non-uniform OTS treatment (D-F), and electrical (crosstalk) defects from an adjacent, non-isolated thin film Au resistor (G-I). Dark spots in (E) are physical artifacts not related to chemical treatment.

To investigate how carriers spatially interact with device architecture and defects, three types of artifacts were deliberately introduced into sample transistors shown in Figure 7.13: a physical defect (Figure 7.13A-C), a surface treatment defect (Figure 7.13D-F), and an electrical "crosstalk" defect (Figure 7.13G-I). In Figure 7.13B, the effect of a scratch on the P3HT is most visible outside the channel where the defect clearly screens the direct flow of carriers from the electrodes out across the dielectric interface, with the far side of the scratch remaining dark. A scratch within the channel is also clearly identified by a lack of ΔR/R signal. Because both the

source and drain are grounded as $|V_G|$ is modulated, signal appears on both sides of the scratch within the channel. The IV curve (Figure 7.13C) confirms that little current flows through a channel when scratched.

Chemical treatment of substrate surfaces with self-assembling molecules like octadecyltrichlorosilane (OTS) before organic semiconductor deposition is known to affect polymer morphology and device performance(*27*). We fabricated a partially treated surface to mimic a surface treatment defect (Figure 7.13D-F) in which half of the SiO_2 surface of the channel was masked when vapor treated with OTS during fabrication. Noticeably weaker MARS signal is revealed in the region lacking OTS, indicative of reduced carrier density. It is important to note that the ΔR/R map is sensitive enough to detect subtle surface differences between fully and partially OTS-treated surfaces that are difficult to interpret from IV measurement data alone. Spatial mapping of the carrier distribution clearly reveals that these differences are due to heterogeneity within the chemically treated TFT channel.

Finally, the effect of electrical fields generated by neighboring structures was examined in order to simulate crosstalk-type events between poorly-isolated devices in integrated designs (Figure 7.13G-I). A rectangular-shaped Au pad was deposited adjacent to the source and drain and then independently biased as a simple resistor (Figure 7.13G). Imaging of the modulated TFT with the Au resistor turned “on” (+2V, 2mA) shows clear crosstalk between the devices with increased spread of carriers throughout the semiconducting P3HT in contrast to the “off” resistor (0V, 0mA) (Figure 7.13H). The only observable difference in bulk electrical characterization is a very subtle increase in threshold voltage by 5V (Figure 7.13I), likely due to the positive electric field of the resistor interacting with the gate across the dielectric. With no other appreciable change in IV behavior, this small shift in threshold voltage could be nearly impossible to interpret without the visual clues offered by MARS.

7.4 Conclusions

MARS imaging takes advantage of the optical changes associated with the presence of charged species in organic semiconductors in a powerful way, allowing for rapid two-dimensional spatial mapping of charge densities in a thin semiconducting polymer film. The ability to track carrier saturation, dynamically image charge distributions, and map the influence of device artifacts, such as the first ever visualization of charge buildup at the drain owing to the access resistance of a top contact architecture, allows for facile exploration of organic charge transport phenomena which will aid in answering many of the still open questions surrounding the precise nature of charge transport in organic materials.

7.5 References

1. A. Heeger, N. Sariciftci, E. Namdas, *Semiconducting and Metallic Polymers*. (Oxford University Press, Oxford, 2010).

2. J. Zaumseil, H. Sirringhaus, Electron and ambipolar transport in organic field-effect transistors, *Chem. Rev.* **107**, 1296-1323 (2007).

3. G. Horowitz, Organic thin film transistors: From theory to real devices, *J. Mater. Res.* **19**, 1946-1962 (2004).

4. H. Sirringhaus, Device Physics of Solution-Processed Organic Field-Effect Transistors, *Adv. Mater.* **17**, 2411-2425 (2005).

5. H. Sirringhaus, P. J. Brown, R. H. Friend, M. M. Nielsen, K. Bechgaard, B. M. W. Lengeveld-Voss, A. J. H. Spiering, R. A. J. Janssen, E. W. Meijer, P. Herwig, D. M. de Leeuw, Two-dimensional charge transport in self-organized, high-mobility conjugated polymers, *Nature* **401**, 685-688 (1999).

6. T. Manaka, S. Kawashima, M. Iwamoto, Evaluation of Carrier Density in Organic Field-Effect Transistor by Charge Modulated Spectroscopy, *Jpn. J. Appl. Phys.* **50**, 04DK12 (2011).

7. T. Manaka, S. Kawashima, M. Iwamoto, Charge modulation spectroscopy for probing ambipolar carrier injection into pentacene field effect transistors, *Phys. Procedia* **14**, 209-212 (2011).

8. A. Horvath, H. Bassler, G. Weiser, Electroabsorption in Conjugated Polymers, *Physica Status Solidi* **173**, 755-764 (1992).

9. A. Horvath, G. Weiser, G. Baker, S. Etemad, Influence of disorder on the field-modulated spectra of polydiacetylene films, *Phys. Rev. B* **51**, 2751-2758 (1995).

10. P. Brown, H. Sirringhaus, M. Harrison, M. Shkunov, R. Friend, Optical spectroscopy of field-induced charge in self-organized high mobility poly(3-hexylthiophene), *Phys. Rev. B* **63**, 125204 (2001).

11. P. Brown, D. Thomas, A. Köhler, J. Wilson, J.-S. Kim, C. Ramsdale, H. Sirringhaus, R. Friend, Effect of interchain interactions on the absorption and emission of poly(3-hexylthiophene) *Phys. Rev. B* **67**, 064204 (2003).

12. W. H. Lee, S. Y. Chuang, H. L. Chen, W. F. Su, C. H. Lin, Exploiting optical properties of P3HT:PCBM films for organic solar cells with semitransparent anode, *Thin Solid Films* **518**, 7450-7454 (2010).

13. J.-F. Chang, H. Sirringhaus, M. Giles, M. Heeney, I. McCulloch, Relative importance of polaron activation and disorder on charge transport in high-mobility conjugated polymer field-effect transistors, *Phys. Rev. B* **76**, 205204 (2007).

14. A. Sadakata, K. Osada, D. Taguchi, T. Yamamoto, M. Fukuzawa, T. Manaka, M. Iwamoto, Probing interfacial charge accumulation in ITO/α-NPD/Alq3/Al diodes under two electroluminescence operational modes by electric-field induced optical second-harmonic generation, *J. Appl. Phys.* **112**, 083723 (2012).

15. Y. Harima, Y. Ishiguro, K. Komaguchi, I. Imae, Y. Ooyama, Optical absorption spectrum of pentacene cation radicals measured by charge-modulation spectroscopy, *Chem. Phys. Lett.* **495**, 228-231 (2010).

16. J. W. Spalenka, E. M. Mannebach, D. J. Bindl, M. S. Arnold, P. G. Evans, Spectral resolution of states relevant to photoinduced charge transfer in modified pentacene/ZnO field-effect transistors, *Appl. Phys. Lett.* **99**, 193304 (2011).

17. L. Zhang, D. Taguchi, T. Manaka, M. Iwamoto, Direct probing of selective electron and hole accumulation processes along the channel of an ambipolar double-layer field-effect transistor by optical modulation spectroscopy, *Appl. Phys. Lett.* **100**, 103301 (2012).

18. Z. Q. Li, G. M. Wang, N. Sai, D. Moses, M. C. Martin, M. Di Ventra, A. J. Heeger, D. N. Basov, Infrared imaging of the nanometer-thick accumulation layer in organic field-effect transistors, *Nano Lett.* **6**, 224-228 (2006).

19. T. Manaka, E. Lim, R. Tamura, M. Iwamoto, Direct imaging of carrier motion in organic transistors by optical second-harmonic generation, *Nature Photonics* **1**, 581-584 (2007).

20. C. Sciascia, M. Celebrano, M. Binda, D. Natali, G. Lanzani, J. R. Cabanillas-Gonzalez, Electric field and charge distribution imaging with sub-micron resolution in an organic Thin-Film Transistor, *Org. Elec.* **13**, 66-70 (2012).

21. H. Matsui, T. Hasegawa, Visualization of accumulated charge density in operating organic thin-film transistors *Appl. Phys. Lett.* **95**, 223301 (2009).

22. T. Manaka, S. Kawashima, M. Iwamoto, Charge modulated reflectance topography for probing in-plane carrier distribution in pentacene field-effect transistors, *Appl. Phys. Lett.* **97**, 113302 (2010).

23. N. M. Gabor, J. C. W. Song, Q. Ma, N. L. Nair, T. Taychatanapat, K. Watanabe, T. Taniguchi, L. S. Levitov, P. Jarillo-Herrero, Hot carrier-assisted intrinsic photoresponse in graphene, *Science* **334**, 648-652 (2011).

24. M. Farzaneh, K. Maize, D. Lüerßen, J. A. Summers, P. M. Mayer, P. E. Raad, K. P. Pipe, A. Shakouri, R. J. Ram, J. A. Hudgings, CCD-based thermoreflectance microscopy: principles and applications, *J. Phys. D: Appl. Phys.* **42**, 143001 (2009).

25. S. M. Sze, in *Physics of Semiconductor Devices*. (John Wiley & Sons, Inc., New York, 1969), pp. 505-566.

26. P. Stallinga, in *Electrical Characterization of Organic Electronic Materials and Devices* (John Wiley & Sons, Inc. New York, 2009), pp. 189-279.

27. S. C. Lim, S. H. Kim, J. H. Lee, M. K. Kim, D. J. Kim, T. Zyung, Surface-treatment effects on organic thin-film transistors, *Synth. Met.* **148**, 75-79 (2005).

CHAPTER 8

CONCLUSIONS AND OUTLOOK

The work presented in this dissertation demonstrates how polymeric properties and architectures can be used in new ways to control and visualize the electronic properties of conjugated polymer materials and devices. The photo-initiated thiol-ene reaction is shown to be an excellent route to controlling the architecture of cross-linked conjugated polymer networks, owing to the reaction's high efficiency, fidelity, and tolerance to a wide range of impurities and functional groups. By tuning the architecture of the cross-linker and the reactive polymer side chains, the network spacing and interchain communication can easily be controlled, with visual fluorescent evidence illuminating the subtle but highly impactful changes in charge communication. Furthermore, the unique nature of charge formation and transport along a polymeric backbone was used to directly visualize and map charge densities across an operating semiconducting device using commercially available, off-the shelf hardware and optics. These achievements are clear illustrations of how the polymeric nature of semiconducting polymers can be used in powerfully advantageous ways.

Conjugated polymers are ultimately polymers. To treat them as historical semiconducting materials, with regards to either device architecture, chemistry, or charge transport behavior, is to unreasonably abandon decades of knowledge on polymer materials and to discount potential handles for improving their application uses. These materials may never reach the vaunted properties of silicon, germanium, or related alloys, but those inorganic semiconductors cannot be cross-linked, processed, or morphologically tuned in any comparable way to polymers. Combining the best elements of both the semiconducting and polymeric properties of conjugated polymers will likely be the most meaningful approach to realizing useful and commercializable semiconducting polymer materials.

BIBLIOGRAPHY

S. Allard, M. Forster, B. Souharce, H. Thiem, U. Scherf, "Organic semiconductors for solution-processable field-effect transistors (OFETs)." Angewandte Chemie (International ed. in English) vol. 47 (2008): 4070-4098.

J. Alonzo *et al.*, "Assembly and organization of poly(3-hexylthiophene) brushes and their potential use as novel anode buffer layers for organic photovoltaics." Nanoscale vol. 5 (2013): 9357-9364.

T. Arai, M. Tanaka, H. Kawakami, "Porphyrin-containing electrospun nanofibers: positional control of porphyrin molecules in nanofibers and their catalytic application." ACS applied materials & interfaces vol. 4 (2012): 5453-5457.

D. Aspnes, J. Rowe, "Resonant nonlinear optical susceptibility: Electroreflectance in the low-field limit." Physical Review B vol. 5 (1972): 4022-4030.

A. Baba, K. Onishi, W. Knoll, R. C. Advincula, "Investigating Work Function Tunable Hole-Injection/Transport Layers of Electrodeposited Polycarbazole Network Thin Films." The Journal of Physical Chemistry B vol. 108 (2004): 18949-18955.

A. Babel, S. a. Jenekhe, "Alkyl chain length dependence of the field-effect carrier mobility in regioregular poly(3-alkylthiophene)s." Synthetic Metals vol. 148 (2005): 169-173.

Z. Bao, J. Locklin, *Organic Field-Effect Transistors*. (CRC Press, Boca Raton, FL, 2007).

H. Bässler, "Charge Transport in Disordered Organic Photoconductors a Monte Carlo Simulation Study." Physica Status Solidi B vol. 175 (1993): 15-56.

M. S. Bayerl *et al.*, "Crosslinkable hole-transport materials for preparation of multilayer organic light emitting devices by spin-coating." Macromolecular Rapid Communications vol. 20 (1999): 224-228.

P. M. Beaujuge, J. R. Reynolds, "Color Control in pi-Conjugated Organic Polymers for Use in Electrochromic Devices." Chemical Reviews vol. 110 (2010): 268-320.

K. Becker *et al.*, "On-Chain Fluorenone Defect Emission from Single Polyfluorene Molecules in the Absence of Intermolecular Interactions." Advanced Functional Materials vol. 16 (2006): 364-370.

J. M. Behrendt *et al.*, "Hybrid inorganic–organic composite nanoparticles from crosslinkable polyfluorenes." Journal of Materials Chemistry C vol. 1 (2013): 3297.

M. Berggren *et al.*, "Light-emitting diodes with variable colours from polymer blends." Nature vol. 372 (1992): 444-446.

V. N. Bliznyuk *et al.*, "Electrical and Photoinduced Degradation of Polyfluorene Based Films and Light-Emitting Devices." Macromolecules vol. 32 (1999): 361-369.

L. D. Bozano *et al.*, "Electroluminescent devices based on cross-linked polymer blends." Journal of Applied Physics vol. 94 (2003): 3061-3068.

C. Brabec, V. Dyakonov, U. Scherf, *Organic Photovoltaics - Materials, Deice Physics, and Manufacturing Technologies*. (John Wiley & Sons, Hoboken, NJ, 2008).

J.-L. Brédas, D. Beljonne, V. Coropceanu, J. Cornil, "Charge-Transfer and Energy-Transfer Processes in π-Conjugated Oligomers and Polymers: A Molecular Picture." Chemical Reviews vol. 104 (2004): 4971-5004.

P. Brown, H. Sirringhaus, M. Harrison, M. Shkunov, R. Friend, "Optical spectroscopy of field-induced charge in self-organized high mobility poly(3-hexylthiophene)." Physical Review B vol. 63 (2001): 125204.

P. Brown *et al.*, "Effect of interchain interactions on the absorption and emission of poly(3-hexylthiophene)." Physical Review B vol. 67 (2003): 1-16.

L. Bürgi, T. J. Richards, R. H. Friend, H. Sirringhaus, "Close look at charge carrier injection in polymer field-effect transistors." Journal of Applied Physics vol. 94 (2003): 6129.

A. J. Campbell, D. D. C. Bradley, H. Antoniadis, "Dispersive electron transport in an electroluminescent polyfluorene copolymer measured by the current integration time-of-flight method." Applied Physics Letters vol. 79 (2001): 2133-2135.

I. H. Campbell *et al.*, "Controlling charge injection in organic electronic devices using self-assembled monolayers." Applied Physics Letters vol. 71 (1997): 3528-3530.

M. Campoy-Quiles *et al.*, "Morphology evolution via self-organization and lateral and vertical diffusion in polymer:fullerene solar cell blends." Nature materials vol. 7 (2008): 158-164.

L. A. Carpino, "Convenient Preparation of (9-Fluorenyl)methanol and Its 2,7-Dihalo Derivatives." Journal of Organic Chemistry vol. 45 (1980): 4250-4252.

M. L. Chabinyc *et al.*, "Short channel effects in regioregular poly(thiophene) thin film transistors." Journal of Applied Physics vol. 96 (2004): 2063.

J.-F. Chang, H. Sirringhaus, M. Giles, M. Heeney, I. McCulloch, "Relative importance of polaron activation and disorder on charge transport in high-mobility conjugated polymer field-effect transistors." Physical Review B vol. 76 (2007): 1-12.

J.-F. Chang *et al.*, "Enhanced Mobility of Poly(3-hexylthiophene) Transistors by Spin-Coating from High-Boiling-Point Solvents." Chemistry of Materials vol. 16 (2004): 4772-4776.

A. Charas, L. Alcácer, A. Pimentel, J. P. Conde, J. Morgado, "Observation of field-effect in a cross-linked polyfluorene semiconductor." Chemical Physics Letters vol. 455 (2008): 189-191.

C.-C. Chen, M.-Y. Chiu, J.-T. Sheu, K.-H. Wei, "Photoresponses and memory effects in organic thin film transistors incorporating poly(3-hexylthiophene)/CdSe quantum dots." Applied Physics Letters vol. 92 (2008): 143105.

J.-J. Chen, K. N. Struk, A. B. Brennan, "Surface modification of silicate glass using 3-(mercaptopropyl)trimethoxysilane for thiol-ene polymerization." Langmuir vol. 27 (2011): 13754-13761.

J. P. Chen *et al.*, "Efficient , blue light-emitting diodes using cross-linked layers of polymeric arylamine and fluorene." Synthetic Metals vol. (1999): 129-135.

Y.-J. Cheng, S.-H. Yang, C.-S. Hsu, "Synthesis of conjugated polymers for organic solar cell applications." Chemical reviews vol. 109 (2009): 5868-5923.

R. Chesterfield, J. McKeen, C. D. Frisbie, "Organic thin film transistors based on N-alkyl perylene diimides: charge transport kinetics as a function of gate voltage and temperature." Journal of Physical Chemistry B vol. 108 (2004): 19281-19292.

J.-C. Chiang, A. G. MacDiarmid, "'Polyanilin': Protonic acid doping of the emeraldine form to the metallic regime." Synthetic Metals vol. 13 (1986): 193-205.

K. M. Coakley, M. D. McGehee, "Conjugated Polymer Photovoltaic Cells." Chemistry of Materials vol. 16 (2004): 4533-4542.

J. Coates, in *Encyclopedia of Analytical Chemistry,* R. A. Meyers, Ed. (John Wiley & Sons, Inc., Chichester, 2000), pp. 10815-10837.

N. B. Cramer, J. P. Scott, C. N. Bowman, "Photopolymerizations of thiol-ene polymers without photoinitiators." Macromolecules vol. 35 (2002): 5361-5365.

R. Das, P. Harrop, “Printed, Organic & Flexible Electronics: Forecasts, Players & Opportunities 2013-2023” (IDTechEx, 2013).

A. R. Davis, K. C. Carter, "Cross-Linked Poly(fluorene) Networks with Varying Network Connectivity by Thiol-Ene Photo Chemistry. " *submitted*.

A. R. Davis, J. A. Maegerlein, K. R. Carter, "Electroluminescent Networks via Photo "Click" Chemistry." Journal of the American Chemical Society vol. 133 (2011): 20546-20551.

B. de Boer, A. Hadipour, M. M. Mandoc, T. van Woudenbergh, P. W. M. Blom, "Tuning of Metal Work Functions with Self-Assembled Monolayers." Advanced Materials vol. 17 (2005): 621-625.

N. Doubina *et al.*, "Surface-initiated synthesis of poly(3-methylthiophene) from indium tin oxide and its electrochemical properties." Langmuir vol. 28 (2012): 1900-1908.

L. Duan, S. J. Garrett, "An Investigation of Rigid p-Methylterphenyl Thiol Self-Assembled Monolayers on Au(111) Using Reflection-Absorption Infrared Spectroscopy and Scanning Tunneling Microscopy." Journal of Physical Chemistry B vol. 105 (2001): 9812-9816.

S. Ege, *Organic Chemistry Structure and Reactivity*. (Houghton Mifflin Company, New York, 2004).

A. Facchetti, "π-Conjugated Polymers for Organic Electronics and Photovoltaic Cell Applications." Chemistry of Materials vol. 23 (2011): 733-758.

A. Facchetti, M.-H. Yoon, T. J. Marks, "Gate Dielectrics for Organic Field-Effect Transistors: New Opportunities for Organic Electronics." Advanced Materials vol. 17 (2005): 1705-1725.

M. Farzaneh *et al.*, "CCD-based thermoreflectance microscopy: principles and applications." Journal of Physics D: Applied Physics vol. 42 (2009): 143001.

B. Friedel, C. R. McNeill, N. C. Greenham, "Influence of Alkyl Side-Chain Length on the Performance of Poly(3-alkylthiophene)/Polyfluorene All-Polymer Solar Cells." Chemistry of Materials vol. 22 (2010): 3389-3398.

M. Fukuda, K. Sawada, K. Yoshino, "Fusible Conducting Poly(9-alkylfluorene) and Poly(9,9-dialkylfluorene) and Their Characteristics." Japanese Journal of Applied Physics vol. 28 (1989): L1433.

T. M. Fulghum, P. Taranekar, R. C. Advincula, "Grafting Hole-Transport Precursor Polymer Brushes on ITO Electrodes: Surface-Initiated Polymerization and Conjugated Polymer Network Formation of PVK." Macromolecules vol. 41 (2008): 5681-5687.

G. Fytas, H. Nothofer, U. Scherf, D. Vlassopoulos, G. Meier, "Structure and dynamics of nondilute polyfluorene solutions." Macromolecules vol. 35 (2002): 481-488.

N. M. Gabor *et al.*, "Hot carrier-assisted intrinsic photoresponse in graphene." Science vol. 334 (2011): 648-652.

C. Gärditz, a. Winnacker, F. Schindler, R. Paetzold, "Impact of Joule heating on the brightness homogeneity of organic light emitting devices." Applied Physics Letters vol. 90 (2007): 103506.

W. D. Gill, "Drift mobilities in amorphous charge-transfer complexes of trinitrofluorene and poly-n-vinylcarbazole." Journal of Applied Physics vol. 43 (1972): 5033-5040.

M. Giulianini, E. R. Waclawik, J. M. Bell, N. Motta, "Temperature and electric field dependent mobility in poly(3-hexylthiophene) diodes." Journal of Applied Physics vol. 108 (2010): 014512.

X. Gong *et al.*, "Stabilized Blue Emission from Polyfluorene-Based Light-Emitting Diodes: Elimination of Fluorenone Defects." Advanced Functional Materials vol. 13 (2003): 325-330.

M. Grell *et al.*, "Chain geometry, solution aggregation and enhanced dichroism in the liquid-crystalline conjugated polymer poly(9,9-dioctylfluorene)." Acta Polymerica vol. 49 (1998): 439-444.

M. Grell, D. D. C. Bradley, G. Ungar, J. Hill, K. S. Whitehead, "Interplay of Physical Structure and Photophysics for a Liquid Crystalline Polyfluorene." Macromolecules vol. 32 (1999): 5810-5817.

A. C. Grimsdale, K. L. Chan, R. E. Martin, P. G. Jokisz, A. B. Holmes, "Synthesis of Light-Emitting Conjugated Polymers for Applications in Electroluminescent Devices." Chemical Reviews vol. 109 (2009): 897-1091.

S. Haas, H. Matsui, T. Hasegawa, "Field-modulation spectroscopy of pentacene thin films using field-effect devices: Reconsideration of the excitonic structure." Physical Review B vol. 82 (2010): 161301.

E. C. Hagberg, M. Malkoch, Y. B. Ling, C. J. Hawker, K. R. Carter, "Effects of modulus and surface chemistry of thiol-ene photopolymers in nanoimprinting." Nano Letters vol. 7 (2007): 233-237.

Y. Harima, Y. Ishiguro, K. Komaguchi, I. Imae, Y. Ooyama, "Optical absorption spectrum of pentacene cation radicals measured by charge-modulation spectroscopy." Chemical Physics Letters vol. 495 (2010): 228-231.

A. Heeger, N. Sariciftci, E. Namdas, *Semiconducting and Metallic Polymers*. (Oxford University Press, Oxford, 2010).

M. Helgesen, R. Sondergaard, F. C. Krebs, "Advanced materials and processes for polymer solar cell devices." Journal of Materials Chemistry vol. 20 (2010): 36-60.

V. Ho, B. W. Boudouris, R. a. Segalman, "Tuning Polythiophene Crystallization through Systematic Side Chain Functionalization." Macromolecules vol. 43 (2010): 7895-7899.

G. Horowitz, in *Organic Field-Effect Transistors,* Z. Bao, J. Locklin, Eds. (CRC Press, Boca Raton, FL, 2007).

G. Horowitz, "Organic thin film transistors: From theory to real devices." Journal of Materials Research vol. 19 (2004): 1946-1962.

A. Horvath, H. Bassler, G. Weiser, "Electroabsorption in COnjugated Polymers." Physica Status Solidi vol. 173 (1992): 755-764.

A. Horvath, G. Weiser, G. Baker, S. Etemad, "Influence of disorder on the field-modulated spectra of polydiacetylene films." Physical Review B vol. 51 (1995): 2751-2758.

C. E. Hoyle, C. N. Bowman, "Thiol-Ene Click Chemistry." Angewandte Chemie-International Edition vol. 49 (2010): 1540-1573.

C. E. Hoyle, T. Y. Lee, T. Roper, "Thiol-enes: Chemistry of the past with promise for the future." Journal of Polymer Science Part A: Polymer Chemistry vol. 42 (2004): 5301-5338.

C. E. Hoyle, A. B. Lowe, C. N. Bowman, "Thiol-click chemistry: a multifaceted toolbox for small molecule and polymer synthesis." Chemical Society Reviews vol. 39 (2010): 1355-1387.

A. J. Huber, D. Kazantsev, F. Keilmann, J. Wittborn, R. Hillenbrand, "Simultaneous IR Material Recognition and Conductivity Mapping by Nanoscale Near-Field Microscopy." Advanced Materials vol. 19 (2007): 2209-2212.

L. Hung, C. Tang, M. Mason, "Enhanced electron injection in organic electroluminescence devices using an Al/LiF electrode." Applied Physics Letters vol. 70 (1996): 152-154.

A. R. Hunt, S. K. Stewart, A. Whiting, "Heck versus Suzuki Palladium Catalyzed Cross-Coupling of a Vinyl Borate Ester with Aryl Halides." Tetrahedron Letters vol. 34 (1993): 3599-3602.

G. R. Hutchison, M. a. Ratner, T. J. Marks, "Accurate Prediction of Band Gaps in Neutral Heterocyclic Conjugated Polymers." The Journal of Physical Chemistry A vol. 106 (2002): 10596-10605.

R. K. Iha *et al.*, "Applications of Orthogonal "Click" Chemistries in the Synthesis of Functional Soft Materials." Chemical Reviews vol. 109 (2009): 5620-5686.

T. Ito, H. Shirakawa, S. Ikeda, "Polymerization and Formation of Polyacetylene Film." Journal of Polymer Science Part A: Polymer Chemistry vol. 12 (1974): 11-20.

G. E. Jabbour *et al.*, "Highly efficient and bright organic electroluminescent devices with an aluminum cathode." Applied Physics Letters vol. 71 (1997): 1762-1764.

S. Jhaveri, K. Carter, "Disubstituted polyacetylene brushes grown via surface-directed tungsten-catalyzed polymerization." Langmuir vol. 35 (2007): 8288-8290.

H. Jia, S. Gowrisanker, G. K. Pant, R. M. Wallace, B. E. Gnade, "Effect of poly (3-hexylthiophene) film thickness on organic thin film transistor properties." Journal of Vacuum Science & Technology A: Vacuum, Surfaces, and Films vol. 24 (2006): 1228.

H. Kajii, K. Koiwai, Y. Hirose, Y. Ohmori, "Top-gate-type ambipolar organic field-effect transistors with indium–tin oxide drain/source electrodes using polyfluorene derivatives." Organic Electronics vol. 11 (2010): 509-513.

T. Kaneko, Journal of the Chemical Society of Japan vol. 59 (1938): 1139.

N. Khanduyeva *et al.*, "Surface engineering using Kumada catalyst-transfer polycondensation (KCTP): preparation and structuring of poly(3-hexylthiophene)-based graft copolymer brushes." Journal of the American Chemical Society vol. 131 (2009): 153-161.

C. Kim, "Fundamental benefits of the staggered geometry for organic field-effect transistors." Electron Device Letters, … vol. 32 (2011): 1302-1304.

D. H. Kim, Y. Jang, Y. D. Park, K. Cho, "Controlled one-dimensional nanostructures in poly(3-hexylthiophene) thin film for high-performance organic field-effect transistors." The journal of physical chemistry. B vol. 110 (2006): 15763-15768.

H. J. Kim *et al.*, "Solvent-Resistant Organic Transistors and Thermally Stable Organic Photovoltaics Based on Cross-linkable Conjugated Polymers." Chemistry of Materials vol. 24 (2012): 215-221.

B. Kiskan, J. Weber, "Versatile Postmodification of Conjugated Microporous Polymers Using Thiol-yne Chemistry." Macro Letters vol. 1 (2012): 37-40.

V. V. Kislyuk, O. P. Dimitriev, a. a. Pud, J. Lautru, I. Ledoux-Rak, "In-situ conductivity and UV-VIS absorption monitoring of iodine doping-dedoping processes in poly(3-hexylthiophene) (P3HT)." Journal of Physics: Conference Series vol. 286 (2011): 012009.

G. Klaerner, R. Miller, "Polyfluorene Derivatives: Effective Conjugation Lengths from Well-Defined Oligomers." Macromolecules vol. 31 (1998): 2007-2009.

G. Klaerner, R. Miller, "Polyfluorene derivatives: effective conjugation lengths from well-defined oligomers." Macromolecules vol. 9297 (1998): 2007-2009.

G. Klärner *et al.*, "Cross-linkable Polymers Based on Dialkylfluorenes." Chemistry of Materials vol. 11 (1999): 1800-1805.

R. J. Kline *et al.*, "Critical Role of Side-Chain Attachment Density on the Order and Device Performance of Polythiophenes." Macromolecules vol. 40 (2007): 7960-7965.

M. Knaapila *et al.*, "Influence of solvent quality on the self-organization of archetypical hairy rods-Branched and linear side chain polyfluorenes: Rodlike chains versus “beta-sheets” in." Macromolecules vol. 39 (2006): 6505-6512.

A. Können *et al.*, "Organic LEDs: The Simple Way to Solution-Processed Multilayer OLEDs – Layered Block-Copolymer Networks by Living Cationic Polymerization." Advanced Materials vol. 21 (2009): 879-884.

F. B. Koyuncu, A. R. Davis, K. R. Carter, "Emissive Conjugated Polymer Networks with Tunable Band-Gaps via Thiol-Ene Click Chemistry." Chemistry of Materials vol. 24 (2012): 4410-4416.

F. B. Koyuncu, E. Sefer, S. Koyuncu, E. Ozdemir, "A new low band gap electrochromic polymer containing 2,5-bis-dithienyl-1H-pyrrole and 2,1,3-benzoselenadiazole moiety with high contrast ratio." Polymer vol. 52 (2011): 5772-5779.

A. J. C. Kuehne *et al.*, "Sub-Micrometer Patterning of Amorphous- and β -Phase in a Crosslinkable Poly (9 , 9-dioctylfl uorene): Dual-Wavelength Lasing from a Mixed-Morphology Device." Synthesis vol. (2011): 1-7.

A. P. Kulkarni, X. Kong, S. A. Jenekhe, "Fluorenone-Containing Polyfluorenes and Oligofluorenes: Photophysics , Origin of the Green Emission and Efficient Green Electroluminescence." Journal of Physical Chemistry B vol. 108 (2004): 8689-8701.

O. Kwon, M. L. McKee, "Calculations of Band Gaps in Polyaniline from Theoretical Studies of Oligomers." The Journal of Physical Chemistry B vol. 104 (2000): 1686-1694.

F. Laquai, G. Wegner, H. Bässler, "What determines the mobility of charge carriers in conjugated polymers?" Philosophical transactions. Series A, Mathematical, physical, and engineering sciences vol. 365 (2007): 1473-1487.

K. Lee, A. J. Heeger, Y. Cao, "Reflectance spectra of polyaniline." Synthetic Metals vol. 72 (1995): 25-34.

P. I. Lee, S. L. C. Hsu, R. F. Lee, "White-light-emitting diodes from single polymer systems based on polyfluorene copolymers end-capped with a dye." Polymer vol. 48 (2007): 110-115.

W. H. Lee, S. Y. Chuang, H. L. Chen, W. F. Su, C. H. Lin, "Exploiting optical properties of P3HT:PCBM films for organic solar cells with semitransparent anode." Thin Solid Films vol. 518 (2010): 7450-7454.

H. Letheby, "XXIX. - On the production of a blue substance by the electrolysis of sulphate of aniline." Journal of the Chemical Society vol. 15 (1862): 161-163.

D. Li, L. J. Guo, "Micron-scale organic thin film transistors with conducting polymer electrodes patterned by polymer inking and stamping." Applied Physics Letters vol. 88 (2006): 063513.

G. Li *et al.*, ""“Solvent Annealing” Effect in Polymer Solar Cells Based on Poly(3-hexylthiophene) and Methanofullerenes." Advanced Functional Materials vol. 17 (2007): 1636-1644.

T. Li, J. W. Balk, P. P. Ruden, I. H. Campbell, D. L. Smith, "Channel formation in organic field-effect transistors." Journal of Applied Physics vol. 91 (2002): 4312.

Z. Q. Li *et al.*, "Infrared imaging of the nanometer-thick accumulation layer in organic field-effect transistors." Nano letters vol. 6 (2006): 224-228.

G. Lieser *et al.*, "Ordering, Graphoepitaxial Orientation, and Conformation of a Polyfluorene Derivative of the “Hairy-Rod” Type on an Oriented Substrate of Polyimide †." Macromolecules vol. 33 (2000): 4490-4495.

S. C. Lim *et al.*, "Surface-treatment effects on organic thin-film transistors." Synthetic Metals vol. 148 (2005): 75-79.

W. Liu, W. Huang, C.-H. Chen, M. Pink, D. Lee, "Charge Injection and Transport in Metal-Containing Conducting Polymers: Spectroelectrochemical Mapping of Redox Activities." Chemistry of Materials vol. 24 (2012): 3650-3658.

S. Locci, M. Morana, E. Orgiu, a. Bonfiglio, P. Lugli, "Modeling of Short-Channel Effects in Organic Thin-Film Transistors." IEEE Transactions on Electron Devices vol. 55 (2008): 2561-2567.

A. B. Lowe, "Thiol-ene "click" reactions and recent applications in polymer and materials synthesis." Polymer Chemistry vol. 1 (2010): 17-36.

K. Lu *et al.*, "with Oxetane Substituents : Synthesis , Optical , Electrochemical , and Field-Effect Properties." Macromolecules vol. (2009): 3222-3226.

J. M. Lupton, P. Schouwink, P. E. Keivanidis, A. C. Grimsdale, K. Müllen, "Influence of Dendronization on Spectral Diffusion and Aggregation in Conjugated Polymers." Advanced Functional Materials vol. 13 (2003): 154-158.

B. B. Ma, B. J. Kim, D. A. Poulsen, S. J. Pastine, J. M. J. Fréchet, "Multifunctional Crosslinkable Iridium Complexes as Hole Transporting / Electron Blocking and Emitting Materials for Solution-Processed Multilayer Organic Light-Emitting Diodes." Advanced Functional Materials vol. 1460 (2009): 1024-1031.

T. Manaka, S. Kawashima, M. Iwamoto, "Charge modulated reflectance topography for probing in-plane carrier distribution in pentacene field-effect transistors." Applied Physics Letters vol. 97 (2010): 113302.

T. Manaka, S. Kawashima, M. Iwamoto, "Charge modulation spectroscopy for probing ambipolar carrier injection into pentacene field effect transistors." Physics Procedia vol. 14 (2011): 209-212.

T. Manaka, S. Kawashima, M. Iwamoto, "Evaluation of Carrier Density in Organic Field-Effect Transistor by Charge Modulated Spectroscopy." Japanese Journal of Applied Physics vol. 50 (2011): 04DK12.

T. Manaka, E. Lim, R. Tamura, M. Iwamoto, "Direct imaging of carrier motion in organic transistors by optical second-harmonic generation." Nature Photonics vol. 1 (2007): 581-584.

T. Manaka, E. Lim, R. Tamura, D. Yamada, M. Iwamoto, "Probing of the electric field distribution in organic field effect transistor channel by microscopic second-harmonic generation." Applied Physics Letters vol. 89 (2006): 072113.

N. Marshall, S. K. Sontag, J. Locklin, "Substituted Poly(p -phenylene) Thin Films via Surface-Initiated Kumada-Type Catalyst Transfer Polycondensation." Macromolecules vol. 43 (2010): 2137-2144.

D. Marsitzky, J. Murray, J. C. Scott, K. R. Carter, "Amorphous Poly-2 , 7-fluorene Networks." Synthesis vol. (2001): 4285-4289.

H. Matsui, T. Hasegawa, "Visualization of accumulated charge density in operating organic thin-film transistors." Applied Physics Letters vol. 95 (2009): 223301.

K. Meerholz, C.-D. Muller, O. Nuyken, in *Organic Light Emitting Devices. Synthesis, Properties and Applications.,* K. Mullen, U. Scherf, Eds. (Wiley-VCH Verlag GmbH & Co., Weinheim, 2006).

D. Meng *et al.*, "Grafting P3HT brushes on GO sheets: distinctive properties of the GO/P3HT composites due to different grafting approaches." Journal of Materials Chemistry vol. 22 (2012): 21583.

A. Moliton, R. C. Hiorns, "Review of electronic and optical properties of semiconducting π-conjugated polymers: applications in optoelectronics." Polymer International vol. 53 (2004): 1397-1412.

L. M. A. Monzon, K. Rode, M. Venkatesan, J. M. D. Coey, "Electrosynthesis of Iron, Cobalt, and Zinc Microcrystals and Magnetic Enhancement of the Oxygen Reduction Reaction." Chemistry of Materials vol. 24 (2012): 3878-3885.

I. W. Moran, S. B. Jhaveri, K. R. Carter, "Patterned layers of a semiconducting polymer via imprinting and microwave-assisted grafting." Small vol. 4 (2008): 1176-1182.

C. R. Morgan, F. Magnotta, A. D. Ketley, "Thiol / Ene Photocurable Polymers." Journal of Polymer Science Part A: Polymer Chemistry vol. 15 (1977): 627-645.

M. Morra *et al.*, "On the aging of oxygen plasma-treated polydimethylsiloxane surface." Journal of Colloid and Interface Science vol. 137 (1990): 11-24.

C. R. Newman *et al.*, "Introduction to organic thin film transistors and design of n-channel organic semiconductors." Chemistry of Materials vol. 16 (2004): 4436-4451.

T.-Q. Nguyen, R. C. Kwong, M. E. Thompson, B. J. Schwartz, "Improving the performance of conjugated polymer-based devices by control of interchain interactions and polymer film morphology." Applied Physics Letters vol. 76 (2000): 2454.

Y.-H. Niu, Q. Hou, Y. Cao, "Thermal annealing below the glass transition temperature: A general way to increase performance of light-emitting diodes based on copolyfluorenes." Applied Physics Letters vol. 81 (2002): 634.

Y.-H. Niu, M. S. Liu, J.-w. Ka, A. K. Jen, "Thermally crosslinked hole-transporting layers for cascade hole-injection and effective electron-blocking / exciton-confinement in phosphorescent polymer light-emitting diodes." vol. (2006): 23-25.

L. O'Neill, H. J. Byrne, "Structure-Property Relationships for Electron-Vibrational Coupling in Conjugated Organic Oligomeric Systems." Journal of Physical Chemistry B vol. 109 (2005): 12685-12690.

D. Oberhoff, K. P. Pernstich, D. J. Gundlach, B. Batlogg, "Arbitrary density of states in an organic thin-film field-effect transistor model and application to pentacene devices." IEEE Transactions on Electron Devices vol. 54 (2007): 17-25.

M. Owen, T. Gentle, T. Orbeck, D. Williams, in *Polymer Surface Dynamics,* J. Andrade, Ed. (Plenum Press, New York, 1988), pp. 101-110.

Z. A. Page, V. V. Duzhko, T. Emrick, "Conjugated Thiophene-Containing Polymer Zwitterions: Direct Synthesis and Thin Film Electronic Properties." Macromolecules vol. 46 (2013): 344-351.

P. Pallavicini, G. Dacarro, M. Galli, M. Patrini, "Spectroscopic evaluation of surface functionalization efficiency in the preparation of mercaptopropyltrimethoxysilane self-assembled monolayers on glass." Journal of Colloid and Interface Science vol. 332 (2009): 432-438.

P. Paoprasert *et al.*, "Grafting of poly(3-hexylthiophene) brushes on oxides using click chemistry." Journal of Materials Chemistry vol. 20 (2010): 2651.

Y. D. Park *et al.*, "Effect of side chain length on molecular ordering and field-effect mobility in poly(3-alkylthiophene) transistors." Organic Electronics vol. 7 (2006): 514-520.

A. O. Patil, A. J. Heeger, F. Wudl, "Optical-Properties of Conducting Polymers." Chemical Reviews vol. 88 (1988): 183-200.

A. Patra, Y. H. Wijsboom, G. Leitus, M. Bendikov, "Tuning the Band Gap of Low-Band-Gap Polyselenophenes and Polythiophenes: The Effect of the Heteroatom." Chemistry of Materials vol. 23 (2011): 896-906.

G. K. Paul, J. Mwaura, A. A. Argun, P. Taranekar, J. R. Reynolds, "Cross-Linked Hyperbranched Arylamine Polymers as Hole-Transporting Materials for Polymer LEDs." Macromolecules vol. 39 (2006): 7789-7792.

Q. Pei, Y. Yang, "Efficient Photoluminescence and Electroluminescence from a Soluble Polyfluorene." J. Am. Chem. Soc. vol. 118 (1996): 7416.

K. Pilgram, M. Zupan, R. Skiles, "Bromination of 2,1,3-Benzothiadiazoles." Journal of Heterocyclic Chemistry vol. 7 (1970): 629-&.

L. S. C. Pingree, O. G. Reid, D. S. Ginger, "Electrical Scanning Probe Microscopy on Active Organic Electronic Devices." Advanced Materials vol. 21 (2009): 19-28.

A. Pogantsch *et al.*, "Tuning the Electroluminescence Color in Polymer Light-Emitting Devices Using the Thiol-Ene Photoreaction." Advanced Functional Materials vol. 15 (2005): 403-409.

R. Ponnapati *et al.*, "Conjugated polymer network films of poly(p-phenylene vinylene) with hole-transporting carbazole pendants: dual photoluminescence and electrochromic behavior." ACS Applied Materials & Interfaces vol. 4 (2012): 1211-1218.

S. Pons, C. Korzeniewski, R. B. Shirts, A. Bewicks, "Field-induced infrared absorption in metal surface spectroscopy: the electrochemical Stark effect." The Journal of Physical Chemistry vol. 89 (1985): 2297-2298.

T. Posner, "Beiträge zur Kenntniss der ungesättigten Verbindungen. II. Ueber die Addition von Mercaptanen an ungesättigte Kohlenwasserstoffe." Berichte der deutschen chemischen Gesellschaft vol. 38 (1905): 646-657.

L. Qiu *et al.*, "Organic thin-film transistors with a photo-patternable semiconducting polymer blend." Journal of Materials Chemistry vol. 21 (2011): 15637.

H. P. Rathnayake *et al.*, "Luminescence of Molecular and Block Copolymeric Sites in a Fluorene-Based Luminophore." Chemistry of Materials vol. 19 (2007): 3265-3270.

H. P. Rathnayake, A. Cirpan, P. M. Lahti, F. E. Karasz, "Optimizing LED Properties of 2,7-Bis(phenylethenyl)fluorenes." Chemistry of Materials vol. 18 (2006): 560-566.

M. Redecker, D. D. C. Bradley, M. Inbasekaran, E. P. Woo, "Nondispersive hole transport in an electroluminescent polyfluorene." Applied Physics Letters vol. 73 (1998): 1565.

C. Reese, Z. Bao, "Detailed Characterization of Contact Resistance, Gate-Bias-Dependent Field-Effect Mobility, and Short-Channel Effects with Microscale Elastomeric Single-Crystal Field-Effect Transistors." Advanced Functional Materials vol. 19 (2009): 763-771.

R. Reichlin *et al.*, "Optical, x-ray, and band-structure studies of iodine at pressures of several megabars." Physical Review B vol. 49 (1994): 3725-3733.

F. Rohlfing, T. Yamada, T. Tsutsui, "Electroabsorption spectroscopy on tris-(8-hydroxyquinoline) aluminum-based light emitting diodes." Journal of Applied Physics vol. 86 (1999): 4978.

L. Romaner *et al.*, "The Origin of Green Emission in Polyfluorene-Based Conjugated Polymers: On-Chain Defect Fluorescence." Advanced Functional Materials vol. 13 (2003): 597-601.

L. Romaner *et al.*, "The Origin of Green Emission in Polyfluorene-Based Conjugated Polymers: On-Chain Defect Fluorescence." Advanced Functional Materials vol. 13 (2003): 597.

T. M. Roper, C. E. Hoyle, D. H. Magers, in *Photochemistry and UV curing: new trendd,* J. P. Fouassier, Ed. (Research Signpost, Kerala, India, 2006), pp. 253-264.

H. A. Saadeh *et al.*, "Polyselenopheno[3,4-b]selenophene for Highly Efficient Bulk Heterojunction Solar Cells." ACS Macro Letters vol. 1 (2012): 361-365.

A. Sadakata *et al.*, "Probing interfacial charge accumulation in ITO/α-NPD/Alq3/Al diodes under two electroluminescence operational modes by electric-field induced optical second-harmonic generation." Journal of Applied Physics vol. 112 (2012): 083723.

W. Salaneck, K. Seki, A. Kahn, J.-J. Pireaux, *Conjugated Polymer And Molecular Interfaces: Science and Technology For Photonic And Optoelectronic Application*. (M. Dekker, New York, 2002).

W. Salaneck, S. Stafstrom, J.-L. Bredas, *Conjugated polymer surfaces and interfaces. Electronic and chemical structure for polymer light emitting devices*. (Cambridge University Press, Cambridge, 1996).

U. Salzner, J. B. Lagowski, P. G. Pickup, R. A. Poirier, "Comparison of geometries and electronic structures of polyacetylene, polyborole, polycyclopentadiene, polypyrrole, polyfuran, polysilole, polyphosphole, polythiophene, polyselenophene and polytellurophene." Synthetic Metals vol. 96 (1998): 177-189.

N. Sariciftci, A. Heeger, Y. Cao, "Paramagnetic susceptibility of highly conducting polyaniline: Disordered metal with weak electron-electron interactions (Fermi glass)." Physical Review B vol. 49 (1994): 5988-5992.

S. Sax *et al.*, "Efficient blue-light-emitting polymer heterostructure devices: the fabrication of multilayer structures from orthogonal solvents." Advanced materials (Deerfield Beach, Fla.) vol. 22 (2010): 2087-2091.

G. Scarpa, E. Martin, S. Locci, B. Fabel, P. Lugli, "Organic thin-film phototransistors based on poly(3-hexylthiophene)." Journal of Physics: Conference Series vol. 193 (2009): 012114.

E. Scheler, I. Bauer, P. Strohrigl, "Synthesis and photopatterning of fluorene based reactive mesogens." Macromolecular Symposia vol. 254 (2007): 203-209.

E. Scheler, P. Strohriegl, "Tailoring fluorene-based oligomers for fast photopatterning." Journal of Materials Chemistry vol. (2009): 3207-3212.

U. Scherf, D. Neher, in *Advances in Polymer Science*. (Springer, New York, 2008), vol. 212.

B. J. Schwartz, "Conjugated polymers as molecular materials: how chain conformation and film morphology influence energy transfer and interchain interactions." Annual Review of Physical Chemistry vol. 54 (2003): 141-172.

C. Sciascia *et al.*, "Electric field and charge distribution imaging with sub-micron resolution in an organic Thin-Film Transistor." Organic Electronics vol. 13 (2012): 66-70.

C. Sciascia *et al.*, "Sub-Micrometer Charge Modulation Microscopy of a High Mobility Polymeric n-Channel Field-Effect Transistor." Advanced Materials vol. 23 (2011): 5086-5090.

V. Senkovskyy *et al.*, "Conductive polymer brushes of regioregular head-to-tail poly (3-alkylthiophenes) via catalyst-transfer surface-initiated polycondensation." Journal of the American Chemical Society vol. 129 (2007): 6626-6632.

A. F. Senyurt, H. Wei, C. E. Hoyle, S. G. Piland, T. E. Gould, "Ternary Thiol-Ene/Acrylate Photopolymers: Effect of Acrylate Structure on Mechanical Properties." Macromolecules vol. 40 (2007): 4901-4909.

A. F. Senyurt *et al.*, "Physical and Mechanical Properties of Photopolymerized Thiol-Ene/Acrylates." Macromolecules vol. 39 (2006): 39-41.

J. H. Seo *et al.*, "Improved injection in n-type organic transistors with conjugated polyelectrolytes." Journal of the American Chemical Society vol. 131 (2009): 18220-18221.

S. E. Shaheen *et al.*, "Energy and charge transfer in organic light-emitting diodes: A soluble quinacridone study." Journal of Applied Physics vol. 85 (1999): 7935-7945.

Y. Shi, J. Liu, Y. Yang, "Device performance and polymer morphology in polymer light emitting diodes: The control of thin film morphology and device quantum efficiency." Journal of Applied Physics vol. 87 (2000): 4254.

H. Shirakawa, S. Ikeda, "Infrared Spectra of Poly(acetylene)." Polymer Journal vol. 2 (1971): 231-244.

H. Shirakawa, T. Ito, S. Ikeda, "Raman Scattering and Electronic Spectra of Poly(acetylene)." Polymer Journal vol. 4 (1973): 460-462.

H. Shirakawa, E. J. Louis, A. G. MacDiarmid, C. K. Chiang, A. J. Heeger, "Synthesis of electrically conducting organic polymers: halogen derivatives of polyacetylene, (CH) x." Journal of the Chemical Society, Chemical Communications vol. (1977): 578-580.

M. Shur, *Physics of Semiconductor Devices*. (Prentice-Hall, Inc., Englewood Cliffs, NJ, 1990).

R. M. Silverstein, G. C. Bassler, in *Spectrometric Identification of Organic Compounds*. (John Wiley & Sons, Inc., New York, 1967), pp. 99-100.

H. Sirringhaus, "Device Physics of Solution-Processed Organic Field-Effect Transistors." Advanced Materials vol. 17 (2005): 2411-2425.

H. Sirringhaus *et al.*, "Two-dimensional charge transport in self-organized, high-mobility conjugated polymers." Nature vol. 401 (1999): 685-688.

S. K. Sontag, N. Marshall, J. Locklin, "Formation of conjugated polymer brushes by surface-initiated catalyst-transfer polycondensation." Chemical Communications (2009): 3354-3356.

S. K. Sontag, G. R. Sheppard, N. M. Usselman, N. Marshall, J. Locklin, "Surface-confined nickel mediated cross-coupling reactions: characterization of initiator environment in Kumada catalyst-transfer polycondensation." Langmuir vol. 27 (2011): 12033-12041.

J. W. Spalenka, E. M. Mannebach, D. J. Bindl, M. S. Arnold, P. G. Evans, "Spectral resolution of states relevant to photoinduced charge transfer in modified pentacene/ZnO field-effect transistors." Applied Physics Letters vol. 99 (2011): 193304.

P. Stallinga. in *Electrical Characterization of Organic Electronic Materials and Devices* (John Wiley & Sons, Inc. New York, 2009), pp. 189-279.

H. Sun *et al.*, "Crosslinkable Poly (p-phenylenevinylene) Derivative." Polymer vol. 42 (2004): 2124-2129.

M. L. Sun *et al.*, "Fluorene-based copolymers for color-stable blue light-emitting diodes." European Polymer Journal vol. 43 (2007): 1916-1922.

S. M. Sze, in *Physics of Semiconductor Devices*. (John Wiley & Sons, Inc., New York, 1969), pp. 505-566.

H. Tanaka, S.-i. Watanabe, H. Ito, K. Marumoto, S.-I. Kuroda, "Direct observation of the charge carrier concentration in organic field-effect transistors by electron spin resonance." Applied Physics Letters vol. 94 (2009): 103308.

C. W. Tang, S. A. VanSlyke, "Organic electroluminescent diodes." Applied Physics Letters vol. 51 (1987): 913-915.

K. Tashiro, M. Kobayashi, T. Kawai, K. Yoshino, "Crystal structural change in poly(3-alkyl thiophene)s induced by iodine doping as studied by an organized combination of X-ray diffraction, infrared/Raman spectroscopy and computer simulation techniques." Polymer vol. 38 (1997): 2867-2879.

V. Thorsmølle *et al.*, "Morphology Effectively Controls Singlet-Triplet Exciton Relaxation and Charge Transport in Organic Semiconductors." Physical Review Letters vol. 102 (2009): 017401.

S. P. Tiwari, K. a. Knauer, A. Dindar, B. Kippelen, "Performance comparison of pentacene organic field-effect transistors with SiO2 modified with octyltrichlorosilane or octadecyltrichlorosilane." Organic Electronics vol. 13 (2012): 18-22.

A. V. Tunc *et al.*, "Influence of molecular weight on the short-channel effect in polymer-based field-effect transistors." Journal of Polymer Science Part B: Polymer Physics vol. 50 (2012): 117-124.

J. van Herrikhuyzen, A. Syamakumari, A. P. H. J. Schenning, E. W. Meijer, "Synthesis of n-type perylene bisimide derivatives and their orthogonal self-assembly with p-type oligo(p-phenylene vinylene)s." Journal of the American Chemical Society vol. 126 (2004): 10021-10027.

S. Wang, S. Boussaad, S. Wong, N. J. Tao, "High-sensitivity stark spectroscopy obtained by surface plasmon resonance measurement." Analytical chemistry vol. 72 (2000): 4003-4008.

K. Wasapinyokul, W. I. Milne, D. P. Chu, "Photoresponse and saturation behavior of organic thin film transistors." Journal of Applied Physics vol. 105 (2009): 024509.

K.-H. Weinfurtner, H. Fujikawa, S. Tokito, Y. Taga, "Highly efficient pure blue electroluminescence from polyfluorene: Influence of the molecular weight distribution on the aggregation tendency." Applied Physics Letters vol. 76 (2000): 2502.

M. Weis, T. Manaka, M. Iwamoto, "Origin of electric field distribution in organic field-effect transistor: Experiment and analysis." Journal of Applied Physics vol. 105 (2009): 024505.

G. Weiser, "Stark effect of one-dimensional Wannier excitons in polydiacetylene single crystals." Physical Review B vol. 45 (1992): 14076.

Y. G. Wen, Y. Q. Liu, "Recent Progress in n-Channel Organic Thin-Film Transistors." Advanced Materials vol. 22 (2010): 1331-1345.

G. P. Wiederrecht *et al.*, "Visualizing charge movement near organic heterojunctions with ultrafast time resolution via an induced Stark shift." Applied Physics Letters vol. 100 (2012): 113304.

M. W. B. Wilson *et al.*, "Ultrafast dynamics of exciton fission in polycrystalline pentacene." Journal of the American Chemical Society vol. 133 (2011): 11830-11833.

H. Wu *et al.*, "Efficient Electron Injection from a Bilayer Cathode Consisting of Aluminum and Alcohol-/Water-Soluble Conjugated Polymers." Advanced Materials vol. 16 (2004): 1826-1830.

C. Xia, X. Fan, M.-k. Park, R. C. Advincula, "Ultrathin Film Electrodeposition of Polythiophene Conjugated Networks through a Polymer Precursor Route." Langmuir vol. 17 (2001): 7893-7898.

Y. Xia *et al.*, "Printed Sub-2 V Gel-Electrolyte-Gated Polymer Transistors and Circuits." Advanced Functional Materials vol. 20 (2010): 587-594.

M. S. Xu, J. B. Xu, "Real-time visualization of thermally activated degradation of the ITO/CuPC/NPB/Alq 3 stack used in one of the organic light-emitting diodes." Journal of Physics D: Applied Physics vol. 37 (2004): 1603-1608.

Q. Yan, Y. Fan, D. Zhao, "Unusual Temperature-Dependent Photophysics of Oligofluorene-Substituted Tris-Cyclometalated Iridium Complexes." Macromolecules vol. (2011).

R. Q. Yang, R. Y. Tian, Q. Hou, W. Yang, Y. Cao, "Synthesis and optical and electroluminescent properties of novel conjugated copolymers derived from fluorene and benzoselenadiazole." Macromolecules vol. 36 (2003): 7453-7460.

T. Yasuda, T. Imase, S. Sasaki, T. Yamamoto, "Synthesis, solid structure, and optical properties of new thiophene-based alternating pi-conjugated copolymers containing 4-alkyl-1,2,4-triazole or 1,3,4-thiadiazole unit as the partner unit." Macromolecules vol. 38 (2005): 1500-1503.

T. Yasuda, T. Imase, T. Yamamoto, "Synthesis, characterization, and optical and electrochemical properties of new 2,1,3-benzoselenadiazole-based CT-type copolymers." Macromolecules vol. 38 (2005): 7378-7385.

T. Ytterdal, Y. Cheng, T. A. Fjeldly, in *Device Modeling for Analog and RF CMOS Circuit Design*. (2003).

G. Yu *et al.*, "Measurement of the energy gap in semiconducting polymers using the light-emitting electrochemical cell." Chemical Physics Letters vol. 259 (1996): 465-468.

J. Zaumseil, H. Sirringhaus, "Electron and ambipolar transport in organic field-effect transistors." Chemical reviews vol. 107 (2007): 1296-1323.

L. Zhang, D. Taguchi, T. Manaka, M. Iwamoto, "Direct probing of selective electron and hole accumulation processes along the channel of an ambipolar double-layer field-effect transistor by optical modulation spectroscopy." Applied Physics Letters vol. 100 (2012): 103301.

L. Zhang, D. Taguchi, T. Manaka, M. Iwamoto, "Direct probing of the selective electron and hole accumulation at organic/organic interfaces in a triple-layer organic device by time-resolved optical second harmonic generation." Applied Physics Letters vol. 99 (2011): 083301.

L. Zhao, X. Pang, R. Adhikary, J. W. Petrich, Z. Lin, "Semiconductor Anisotropic Nanocomposites Obtained by Directly Coupling Conjugated Polymers with Quantum Rods." Angewandte Chemie vol. 123 (2011): 4044-4048.

W. Zhao, T. Cao, J. M. White, "On the origin of green emission in polyfluorene polymers: The roles of thermal oxidation degradation and crosslinking." Advanced Functional Materials vol. 14 (2004): 783-790.